Understanding Unsteady Flow Dynamics, Temperature, and Dye Distributions of Density Currents in a River-Reservoir System under Different Upstream Releases and Meteorological Scenarios

by

Gang Chen

A dissertation submitted to the Graduate Faculty of
Auburn University
in partial fulfillment of the
requirements for the Degree of
Doctor of Philosophy

Auburn, Alabama
May 7, 2016

Keywords: flow dynamics, water temperature, upstream release, density current, intermittent releases, meteorological condition

Approved by

Xing Fang, Chair, Professor, Civil Engineering
Joel Hayworth, Associate Professor, Civil Engineering
Jose G. Vasconcelos, Associate Professor, Civil Engineering
Jeyhoon (Jay) M. Khodadadi, Professor, Mechanical Engineering
Hanqin Tian, Professor, School of Forestry and Wildlife Sciences

Abstract

Three dimensional hydrodynamic Environmental Fluid Dynamics Code (EFDC) model was applied to simulate flow, temperature and dye distributions in the river-reservoir system. The study is in a river-reservoir system (124.2 km) from SDT (upstream flow boundary) to BLD (downstream water level boundary) in Walker County, AL, USA. The model was calibrated against measured water levels, temperatures, velocities, and flow rates from 2010–2011 data under small constant release (2.83 m^3/s) and large intermittent releases (~140 m^3/s) from an upstream reservoir. Distributions of simulated flow and temperatures and particle tracking at various locations were analyzed which revealed the complex interactions of density currents, dynamic surface waves, and solar heating. Flows in the surface and bottom layers moved in both upstream and downstream directions. If there was small constant release only from Smith Dam, simulated bottom temperatures at Cordova were on average 4.8 ^oC higher than temperatures under actual releases. The momentum generated from large releases pushed bottom density currents advancing towards downstream, but the released water took several days to reach Cordova.

To understand and quantify formation and propagation of density currents which are caused by daily large release of different durations and solar heating, a series of sensitivity model runs were performed under daily repeated large releases (DRLRs) with different durations (2, 4, and 6 hrs) from Smith Dam Tailrace (SDT) when other model

input variables were kept unchanged. The density currents in the river-reservoir system form at different reaches, are destroyed at upstream locations due to the flow momentum of the releases, and form again due to solar heating. DRLRs (140 m^3/s) with longer durations push the bottom cold water further downstream and maintain the bottom water temperature cooler. For the 6-hr DRLR, the momentum effect definitely reaches Cordova (~43.7 km from SDT). There are 48.4%, 69.0%, and 91.1% of time with positive bottom velocity (density currents moving downstream) with average velocity of 0.017, 0.042, and 0.053 m/s at Cordova for the 2-hr, 4-hr, and 6-hr DRLR, respectively. Results show that DRLRs lasting for at least 4 hrs can maintain lower water temperatures at Cordova. When the 4-hr and 6-hr DRLRs repeat more than 6 and 10 days, respectively, bottom temperatures at Cordova become lower than ones for the constant small release (2.83 m^3/s). These large releases overwhelm the mixing effects due to inflow momentum and maintain temperature stratification at Cordova.

Both the duration of large releases and weather conditions affect and control the formation and spread of density currents and then affect the bottom-layer temperatures. A series of model scenario runs were performed to further understand the bottom-layer water temperature changes at downstream corresponding to hypothetical meteorological changes under different release scenarios. The daily drop rate of bottom-layer water temperature under 6-hr DRLRs are 0.3, 0.45 and 0.4 °C/day for 2, 4, 6 days of 2 °C/day air temperature drop. Average bottom temperature at the river intake under 4-hr DRLRs is 2.3 ^oC lower than one under 2-hr DRLRs and only 1.1 ^oC higher than one under 6-hr DRLRs in the whole simulation period. The daily drop rate and dropping duration of bottom temperature are almost same for 2-, 4- and 6-hr DRLRs due to the same drop and

rise pattern for weather conditions. The maximum differences between the constant weather scenario and the 11-day drop and rise weather scenario range from 3.1 to 4.2 °C under different releases. The lower bottom-layer water temperatures at GOUS and the river intake are primarily due to the lower air temperatures and solar radiations during the 11 days and less affected by the release pattern. To identify more efficient release operations should be further studied.

Acknowledgments

I would like to deeply thank to my academic advisor, Dr. Xing Fang, for providing me the opportunity to purse my PhD degree under his guidance. I really appreciate his support, continuous encouragement, patience and guidance he has shown towards me in accomplishing my goals. He is an excellent professional researcher as well a very good human being who will always remain as an inspiration throughout my life.

I am also equally thankful to my graduate committee members; Dr. Joel Hayworth, Dr. Jose G. Vasconcelos, and Dr. Jay Khodadadi; University Reader Dr. Hanqin Tian for their valuable time to review my dissertation and provide the insights and suggestions on my research problems and motivating me which substantially improved my research and study.

I would also like to acknowledge my friends Janesh Devkota, Liping Jiang, Xiaoning Li, Kyle Lusk and Thomas Weems during my research at Auburn University. Thanks for Alabama Power Company to fund a part of my study. I wishes to express my gratitude to the Chinese Scholarship Council for financial support pursuing my graduate study at Auburn University.

Finally, I would like to express my sincere gratitude and appreciation to my wife Lu Xie and my family who have supported me tirelessly throughout my study period. Without your love, care, and encouragement I would not have been capable of

completing this study. I am blessed to be surrounded by such a good support system at home, at school, and at work.

Table of Contents

List of Tables

List of Figures

List of Abbreviations

AU	Auburn University
ADCP	Acoustic Doppler Current Profiler
APC	Alabama Power Company
ASCE	American Society of Civil Engineers
EFDC	Environmental Fluid Dynamics Code
GIS	Geographic Information System
HEC-RAS	Hydrologic Engineering Centers River Analysis System
HSJ	Hydrological Sciences Journal
MSSWF	Sine and Sinusoidal Wave Functions
NAVD	North American Vertical Datum
NOAA	National Oceanographic and Atmospheric Administration
USACE	U.S. Army Corps of Engineers
USEPA	United States Environmental Protection Agency
USGS	United States Geological Survey
UTM	Universal Transverse Mercator
VMS	Velocity Mapping Software

Chapter 1. Introduction

1.1 Background

Water temperature is one of the significant and important water quality characteristics of surface waters (Kothandaraman and Evans 1972). Water temperature affects all biological and chemical reactions and the density of water that influences the transport of water and pollutants in aquatic systems (Thomann and Mueller 1987). Natural processes or human activities such as industrial production, deforestation, and climate change would affect water temperatures (Caissie 2006). Many climate and environmental parameters can also possibly affect water temperature in streams/rivers, for example, solar radiation, relative humidity, wind speed, water depth, groundwater inflow, artificial heat inputs, and thermal conductivity of the sediments (Pilgrim et al. 1998; Johnson et al. 2009). Weather condition is not the only physical parameter influencing water temperature but a very important parameter. Harmeson and Schnepper (1965) and the Texas Water Development Board (1970) indicated graphically that water temperatures in rivers follow closely the pattern of variations in daily mean air temperatures.

The alteration of flow in the river can also be responsible for changes in river water temperature (Morse 1972; Sinokrot and Gulliver 2000). River regulation as a means of water resources management is a common operating procedure all over the

world. To meet hydro-electric power demands, upstream reservoir release is becoming a prominent characteristic for regulated rivers (Petts et al. 1985). The requirement of minimum flow is usually during the warm season of a year, especially during the summer to maintain lower water temperatures downstream (Wunderlich and Shiao 1984; Consultants 1986). Increasing flow release leads to larger flow depths at downstream river, and it is common the release results in rapid stage changes such as more than 1 m (Fang et al. 2013; Chen et al. 2015). Stage changes have been detected more than 100 km downstream of the large dams after the wave attenuation (Petts 1984). Besides the momentum and mixing effect from the upstream large release, atmospheric conditions will continue have a large effect on river temperature after the reservoir release. Due to the solar heating, typically water temperature in a shallow river is much warmer than release temperature of stored water in the reservoir, which makes the variations of river temperature more complex.

A significant number of river-reservoir systems all over the world have large diurnal variations in atmospheric heating rates and develop density currents in the downstream river/reservoir due to colder denser flow releases from an upstream reservoir. A density difference can exist between two fluids because of a difference in temperature, salinity, or concentration of suspended sediment. A density current is kept in motion by the force of gravity acting on differences in density and due to the slope of river and reservoir bottom. Density currents in nature such as turbidity currents typically flow along the bottom of oceans or lakes or reservoirs.

In fluid dynamics, a gravity current is a primarily horizontal flow in a gravitational field that is driven by a density difference, hence gravity currents also sometimes being referred to as density current. In the traditional or classic gravity current, it's driven by the density difference. In natural rivers and reservoirs, with a sloping bottom, the gravity current moves downward (Fig. 1.1). In addition to water temperature difference, it is sometimes caused by the dissolved or suspended solids content. The inflow with larger density also has certain flow momentum and can push through the ambient water with entrainment. When it reaches a balance of forces, it will start to sink beneath the ambient water. The location is referred to as "plunge point". After plunging, underflows can be formed along the river bottom. The plunge phenomenon can be defined as the transitional flow from homogeneous flow to stratified, entraining underflow. The propagation of gravity currents can be divided into three distinct regions, called "homogeneous", "plunge", and "underflow" (Fig. 1.1).

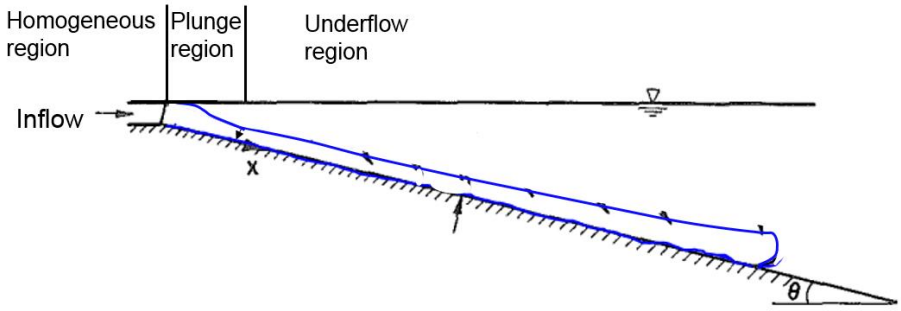

Fig. 1.1 Traditional gravity current

Many laboratory and numerical model studies of density currents have been conducted in the last several decades. Density currents have been studied in situ (Serruya 1974; Smith 1975; Carmack et al. 1979; Fischer and Smith 1983; Alavian and Ostrowski

Jr 1992; Chikita 1992). Because it is quite challenging to study the density currents in the natural systems, the density currents are often investigated in the laboratory (Akiyama and Stefan 1984; Hauenstein and Dracos 1984; Alavian 1986). Most of the previous studies dealt with sloping channels and rectangular cross section. Various simplifying assumptions were made to develop analytical models with laboratory data to understand density currents (Singh and Shah 1971; Savage and Brimberg 1975; Denton 1985; Kranenburg 1993). Fang and Stefan (2000) developed an integral model for a discharge from a river channel over a horizontal or a sloping bottom into a reservoir or a lake to determine dilution up to plunging for density current computations. Using a series of laboratory experiments in a two-layered ambient stratification, Cortes and others (Cortés et al. 2014) developed a theory to predict the partition of the buoyancy flux into the interflow and underflow and how a gravity current splits in two upon reaching the sharp density step.

Two-dimensional (2D) hydrodynamic models were developed to study density current by assuming that the density current does not participate in the dynamics of heating and mixing but the entrainment takes place from the ambient reservoir into the downflow (Imberger and Patterson 1980; Buchak and Edinger 1984; Jokela and Patterson 1985). Gu (2009) used a validated two-dimensional simulation model CE-QUAL-W2 (Cole and Wells 2010) to quantify systematically the effects of inflow and ambient parameters on the behavior of a density-induced contaminant current in various flow regimes in a stratified reservoir through numerical experiments. The k-ε turbulence model has been applied to study density currents plunging into reservoirs (Farrell and Stefan 1986; Fukushima and Watanabe 1990). Bournet (1999) developed the modified k-

ε model with buoyancy effects to describe the characteristics of density currents in terms of plunge point and entrainment in an inclined channel of constant width and then in a diverging channel. Soliman and others (Soliman et al. 2014) developed a 2D multi-phase numerical model for incompressible, immiscible, and variable density fluids based on Navier-Stokes equations. Shlychkov and Krylova (2014) proposed a numerical model for studying the dynamic mixing of sea and river waters in estuary areas, which is based on 2D longitudinal vertical stratified fluid mechanics equations and an equation of salt transport.

Several studies about three-dimensional (3D) gravity currents have been conducted recently using laboratory data and numerical models (Imran et al. 2007; Firoozabadi et al. 2009; An and Julien 2014). In the last several decades, 3D Environmental Fluid Dynamics Code (EFDC) (Hamrick 1992) has been widely used in modeling river, estuarine and coastal hydrodynamics and transport processes. Hamrick and Mills (2000) developed and used the EFDC model to simulate thermal transport and water temperature distributions in Conowingo Pond that was influenced by thermal discharges from the Peach Bottom atomic power plant. In order to quantify numerical and modeled entrainment, Kulis and Hodges (2006) explored the grid resolution required in EFDC to capture gravity current motions in an idealized basin with and without a turbulence closure. Their study was based on the underflow from Oso Bay into Corpus Christi Bay in Texas, USA. Liu and Garcia (2008) used modified 3D EFDC model to simulate the density current and bi-directional flows in the Chicago River system. Xie et al. (2010) used a calibrated 3D EFDC model developed for Yangtze River estuary to study the migration behavior of the movement of fine silt particles in dumped silt.

Lyubimova et al. (2014) used 3D numerical simulations and in situ measurements to study the upstream propagation of vertical stratification of water mineralization, which is observed only under small (200 m^3/s) or moderate (700 m^3/s) seasonal flow rates but absent when flow rates in the rivers is larger than 1400 m^3/s. Do An (2014) used the Flow-3D (Hirt and Nichols 1988) model to simulate the propagation dynamics of density currents under the same conditions as the laboratory experimental setup and focused on the intrusive density flows into a two-layer ambient fluid.

There are many studies about flow in natural systems such as flows from a river into a lake, a reservoir, an ocean, or an estuary. Fatih and Varcin (2012) developed a mathematical model solving nonlinear, unsteady continuity, momentum, energy, and k-ε turbulence equations and applied the model to successfully simulate the formation of density currents and plunging flow in Eğrekkaya Dam Reservoir. Wells and Nadarajah (2009) presented theory and laboratory experiments describing the intrusion depth of a density current into a linearly stratified water column. They concluded that, if the buoyancy flux of a dense current was to double while the stratification in ambient water remained constant, then the intrusion depth would only increase 25%, whereas doubling the stratification would result in a 50% decrease of the intrusion depth. Soliman and others (Soliman et al. 2014) applied the 2D multi-phase numerical model to simulate the density current propagation and salinity intrusion into Ohashi River that connects Nakaumi and Shinji coastal lakes and concluded the further refinement of the model is needed for field study application. Biton and others (Biton et al. 2008) studied density current formation and flow dynamics in the northern Gulf of Eilat, Red Sea, and demonstrated the intrinsic nonlinearity of density currents, which is poorly represented in

the general circulation model, affect properties of simulated density currents. Owens et al. (2012) provided hourly measurements to study stream plunging and used the hydrodynamic and transport model ELCOM (Estuary Lake and Coastal Ocean Model) (Hodges and Dallimore 2006) to simulate the plunging behavior of two tributaries in Onondaga Lake, New York. Cook and Richmond (2004) conducted a field monitoring study and used the Flow-3D (Hirt and Nichols 1988) model to simulate the complex 3D density currents at the Clearwater and Snake River confluence and discovered several predictable stratification patterns that would develop depending upon the discharge ratio and the thermal gradients between the two rivers. Jackson et al. (2008) studied density currents in the Chicago River mostly resulted from salinity differences between the North Branch and the main stem of the Chicago River, whereas temperature difference does not appreciably affect the creation of density currents.

1.2 Study Areas

The study deals with numerical model simulations of flow and temperature in a river-reservoir system in Alabama (AL) that is 124.2 river km long (Fig. 1.1a). The upstream boundary of the study area is Smith Dam Tailrace (SDT, Fig. 1.1b) and the downstream boundary is at the Bankhead Lock& Dam (BLD, Fig. 1.1d). The Dam is about 23.5 m height and 426.7 m long. The river reach from upstream to downstream includes Sipsey Fork (21.9 km), the lower Mulberry Fork (70.6 km), and a reservoir segment (31.7 km) of Bankhead Lake. The Sipsey Fork joints with the upper Mulberry Fork to flow into the lower Mulberry (Fig. 1.1c). Sipsey Fork, the upper and the lower Mulberry Fork are the riverine portions of Bankhead Lake. The Black Warrior River is

formed about 40 km west of Birmingham, AL, by the confluence of the Mulberry Fork and the Locust Fork, which join as arms of Bankhead Lake, a narrow reservoir formed by constructing BLD in 1963. The study area is referred in this study as the Bankhead river-reservoir system (BRRS).

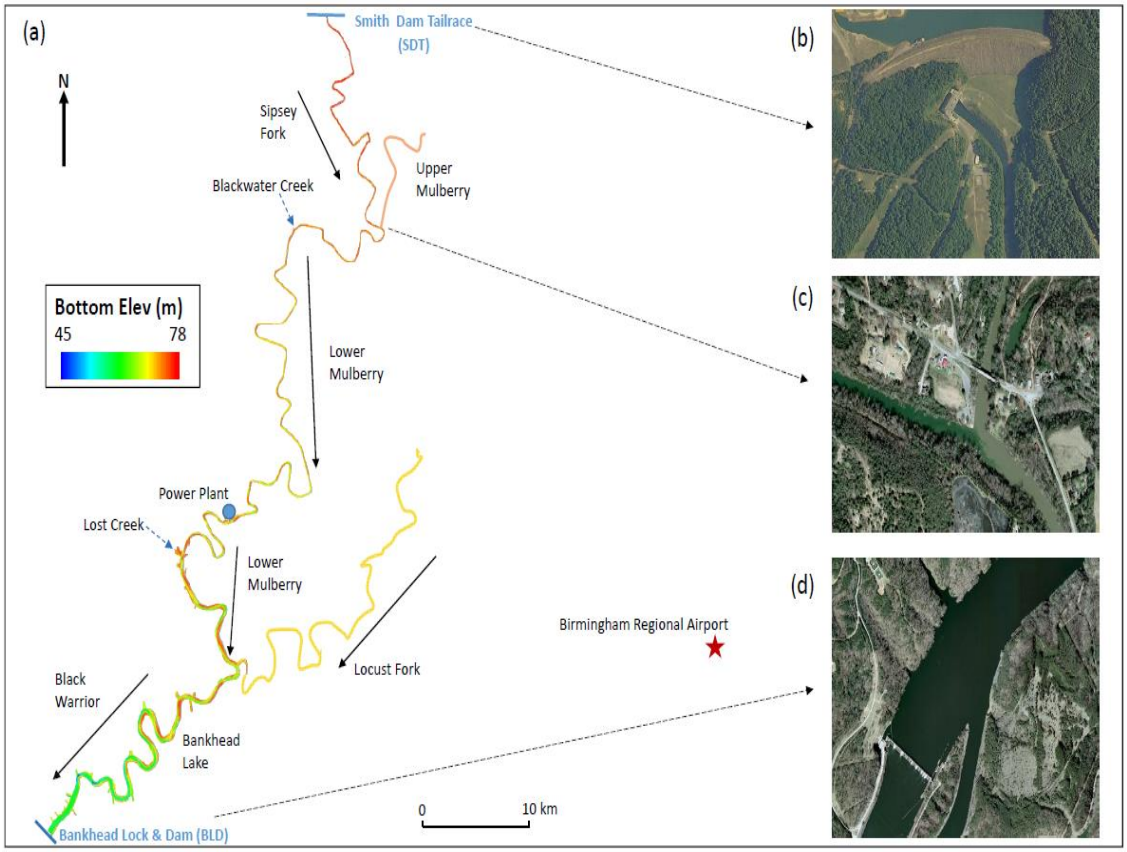

Fig. 1.2 (a) Color contours of the bottom elevation in the study area and the location of Birmingham weather station used for the study; Satellite images showing (b) Smith Dam tailrace (SDT), (c) Junction of Sipsey Fork and Upper Mulbery, (d) Bankhead Lock and Dam (BLD).

The bottom elevations in the upstream portion of BRRS (~64 km downstream from SDT) range from about 65.8 to 77.2 m above mean sea level (using NAVD 1988 datum). The average bottom slope is 0.014% but local slopes vary from -0.2% to 0.2% over each ~2 km distance. The bottom elevations at the Bankhead lake (Fig. 1.1d) range from about 59.48. to 63.99 m above mean sea level. The water releases from Smith Dam to BRRS is normally 2.83 m^3/s, but during late spring, summer, and early fall, large amount of intermittent water releases up to 280 m^3/s (typically about 140 m^3/s) is practiced to meet peak electric generating demand. The water surface elevation in BRRS depends on water releases from Lewis Smith Dam, flows from its tributaries (Upper Mulberry, Locust Fork, Lost Creek, and Blackwater Creek), and the water surface elevation in BLD influenced by outflow through hydro turbines, spillage through gates of BLD, and loss of water through the Bankhead navigation lock. During the normal water releases, water depths in Sipsey Fork range from 2.16 to 4.55 m, in the lower Mulberry Fork from 4.71 to 11.47 m, and in the Bankhead Lake from 12.12 to 17.73 m. The water surface elevation at Bankhead L&D is typically about 77.66 m (with relatively small variations) above mean sea level. More information about the study area is given in other chapters.

1.3 Research Objectives

The overall objectives of the study are to apply a three-dimensional numerical model developed for BRRS and to investigate/understand the unsteady flow dynamics focusing on density current movement and temperature distributions (heat transport) under varying reservoir releases and atmospheric conditions. Surface heat exchange and vertical heat distribution are affected by diurnally varying solar radiation and air temperature and by seasonal pattern or fluctuation of atmospheric conditions.

In this study, the density current movement is different from the classic density current. Bottom slopes in this river-reservoir system are much smaller than steep bottom slopes in other lakes or reservoirs, e.g., 3%–20% in Toolik Lake (Rueda and MacIntyre 2010). At the upstream boundary of BRRS, the intermittent large release with temperature of about 12 ^{o}C and flow rate of 140 m^3/s starts from 1:00 pm and typically lasts for a few hours (2, 4, 6 hrs, etc.). During the other period, there is a constant small release with temperature of about 8 ^{o}C in the summer and flow rate of 2.83 m^3/s. The momentum or push effect from the large release provides driving force for the movement or propagation of density currents at downstream locations along the river bottom in the river-reservoir system. Both daily repeated intermittent releases, solar heating or the surface heat exchange are different from other laboratory experimental studies and simple numerical experiments in which the density current only moves downstream under existing density stratification and due to inflow momentum from one constant release. The large release generates dynamic surface waves that propagate downstream. After the surface waves are attenuated, two-layer flow, water in the surface layers moving upstream and in the bottom layers moving downstream, could form due to the backwater

effect from BLD (downstream boundary). The interactions and dynamics of density currents, dynamic surface waves, and solar heating are complex and three dimensional. There is a power plant in the study area. The once-through cooling water system for the power plant is designed to withdraw cold water from the bottom layers at the river inlet to maintain high plant efficiency. The reservoir release is to maintain lower temperature at downstream locations after thermal discharge returns to the natural river. Hence, the 3D EFDC model is applied in the river-reservoir system to simulate flow dynamics and temperature distributions. The densimetric Froude number $Fr = u/\sqrt{g'h}$ is often used for many studies of simple and classic density currents (Fig. 1.1), where u is a characteristic flow velocity, h is a characteristic length, and g' is the reduced gravity acceleration or buoyant acceleration $= g(\rho_2 - \rho_1)/\rho_1$ (ρ_1 and ρ_2 are the densities of ambient water and gravity current). In this study, the densimetric Froude number was not computed for three dimensional flow because of variations of velocity, density, and depth in different computational cells.

The study is divided into four parts. In the first part of the study (Chen et al. 2015), distributions of simulated flow and temperatures and particle tracking at various locations were analyzed and revealed the complex interactions of density currents, dynamic surface waves, and solar heating. The second part focuses on understanding and analysis of formation and propagation of density currents under different short-duration (a few hours) large flow releases into the river-reservoir system. The complex density currents in the river-reservoir system form at different reaches, are destroyed at upstream locations due to the flow momentum of the releases, and form again due to solar heating.

In the third part of the study, EFDC dye model component was activated to simulate dye concentrations for each computation cell to understand density current movement. Though the dye is just a tracer which is not coupled with temperature simulation in the EFDC model, it still gives us some idea for the delay effect of density current. Dye distributions are useful to track how the density current moves. The fourth part of the study is to further understand the bottom temperature dynamics due to combined effects of variable meteorological condition and DRLRs. For various scenarios that are used for EFDC model runs, model input data (boundary conditions) were modified into constant representative values excluding upstream boundary conditions and climate conditions. The results of these four parts of the study are important with regard to water quality modeling and management, habitat assessment in rivers, and management of thermal discharges from a power plant.

1.4 Methods and Models Used in the Study

1.4.1 Hydrodynamic and Temperature Simulation Model

The study deals with a relatively narrow river-reservoir system, which could be modeled using a 2D longitudinal-vertical hydrodynamic and water quality model, such as CE-QUAL-W2 model (Cole and Wells 2010). To more accurately simulate complex flow , temperature and dye distributions in BRRS especially near the power plant, the 3D EFDC hydrodynamic model was applied for the project to understand the hydrodynamics of density currents formed by upstream reservoir releases. The EFDC model is a general purpose modeling package that can be configured to simulate1D, 2D, and 3D flow, transport, and biogeochemical processes in various surface water systems including

rivers, lakes, estuaries, reservoirs, wetlands, and coastal regions (Shen and Lin 2006; Caliskan and Elci 2009; Jeong et al. 2010; Wang et al. 2010; Kim and Park 2012; Devkota and Fang 2014). The EFDC model was originally developed at the Virginia Institute of Marine Science and the version of EFDC used for the study with pre- and post-processing tools was EFDC-DSI (Craig 2010) from the Dynamic Solutions-International, LLC (http://efdc-explorer.com/). EFDC solves three-dimensional turbulent-averaged equations of motions for a variable-density fluid. EFDC's hydrodynamics are based on the 3D hydrostatic equations formulated in curvilinear-orthogonal horizontal coordinates and a sigma vertical coordinate system. The Mellor-Yamada level 2.5 turbulence closure scheme (Mellor and Yamada 1982) is used to calculate turbulence parameters; vertical turbulent diffusion coefficients of momentum and mass. The horizontal eddy viscosity, A_H is calculated using the Smagorinsky subgrid scale scheme (Smagorinsky 1963), which can be written in the two-dimensional Cartesian coordinate as:

$$A_H = C\Delta x\Delta y\left[\left(\frac{\partial u}{\partial x}\right)^2+\left(\frac{\partial v}{\partial y}\right)^2+\frac{1}{2}\left(\frac{\partial u}{\partial y}+\frac{\partial v}{\partial x}\right)^2\right]^{\frac{1}{2}} \tag{1.1}$$

where C is horizontal mixing constant, Δx and Δy are model grid sizes in x and y directions, u and v are velocity components in x and y directions. The numerical scheme used in EFDC to solve the momentum equations uses a second-order accurate spatial finite difference on a staggered or C grid. The time integration is implemented using a second-order accurate three-time level, semi-implicit finite difference scheme with an internal-external mode splitting scheme to separate the internal shear or baroclinic mode

from external free surface gravity wave or barotropic mode. Details of governing equations and numerical schemes for EFDC hydrodynamic model are given by Hamrick (1992).

The continuity and momentum equations that are used in EFDC model (Hamrick 1992) are as follows:

$$\begin{aligned}&\partial_t(m_x m_y Hu)+\partial_x(m_y Huu)+\partial_y(m_x Hvu)+\partial_z(m_x m_y wu)-m_x m_y f_c Hv=\\&-m_y H\partial_x(p+gH+gz_b^*)-m_y(\partial_x h-z\partial_x H)\partial_z p+m_x m_y\partial_z(H^{-1}A_v\partial_z u)+Q_u\end{aligned} \tag{1.2}$$

$$\begin{aligned}&\partial_t(m_x m_y Hv)+\partial_x(m_y Huv)+\partial_y(m_x Hvv)+\partial_z(m_x m_y wv)-m_x m_y f_c Hu=\\&-m_y H\partial_y(p+gH+gz_b^*)-m_x(\partial_y h+z\partial_y H)\partial_z p+m_x m_y\partial_z(H^{-1}A_v\partial_z v)+Q_v\end{aligned} \tag{1.3}$$

$$\partial_z p=-gHb=-gH(\rho-\rho_0)\rho_0^{-1} \tag{1.4}$$

$$\partial_t(m_x m_y H)+\partial_x(m_y Hu)+\partial_y(m_x Hv)+\partial_z(m_x m_y w)=Q_H \tag{1.5}$$

$$m_x m_y f_c=m_x m_y f-u\partial_y m_x+v\partial_x m_y \tag{1.6}$$

where u and v are the horizontal velocities in the curvilinear-orthogonal horizontal coordinates (x, y); w is the vertical velocity in the stretched vertical coordinate z; p is the excess pressure above the reference density hydrostatic pressure divided by the reference density, ρ_0 (Eq. 1.3); z_s^* is the free surface elevation; z_b^* is the bottom or topography elevation; $H(=z_s^*-z_b^*)$ is the total water column depth in a grid; A_v is the horizontal eddy or turbulent viscosity; f_c is the Coriolis parameter; Q_u and Q_v represent additional forces or momentum sources and sinks, including horizontal turbulent momentum diffusion, vegetation resistance, and wave Reynolds stress due to high frequency gravity waves; Q_H is the source/sink term used to represent direct rainfall, evaporation, groundwater interaction, water withdrawals, and point and nonpoint source discharges;

and m_x and m_y are dimensionless scale factors for curvilinear horizontal coordinates. The sigma coordinate z is dimensionless, $z = 0$ at the bottom topography, and $z = 1$ at the free surface for all grids, but water depth H is a function of time and location and solved by the EFDC.

The generic transport equation in EFDC for a dissolved or suspended constituent C (Hamrick 1992a) is:

$$\begin{aligned}&\partial_t(m_x m_y HC) + \partial_x(m_y HuC) + \partial_y(m_x HvC) + \partial_z(m_x m_y wC) = \\ &m_x m_y \partial_z(H^{-1}\partial_z K_b C + \sigma C) + m_x m_y HR_C + Q_C\end{aligned} \tag{1.7}$$

where K_b is the vertical turbulent or eddy diffusivity; σ is the settling velocity, which is zero for a dissolved constituent or tracer modeled in this study; and R_C is the reactive sources and sinks. The horizontal turbulent diffusion and external sources and sinks associated with volumetric withdrawals and discharges are accounted for using Q_C.

The transport of dynamically active constituents such as salinity, temperature, and suspended sediment is coupled with the momentum equations through an equation of state and the hydrostatic approximation (Eq. 1.3), which is valid for the river-reservoir system.

The second moment turbulence closure model developed by Mellor and Yamada (1982) and modified by Galperin et al. (1988) and Blumberg et al. (1992) is used in the EFDC model to relate vertical turbulent viscosity and diffusivity to the turbulent intensity q, a turbulent length scale l, and a Richardson number R_q:

$$A_v = \phi_v q l = 0.4(1+8R_q)ql(1+36R_q)^{-1}(1+6R_q)^{-1} \tag{1.8}$$

$$K_b = \phi_b ql = 0.5ql(1+36R_q)^{-1} \tag{1.9}$$

$$R_q = -gH\partial_z bl^2 H^{-2} q^{-2} \tag{1.10}$$

where ϕ_v and ϕ_b account for reduced and enhanced vertical mixing or transport in stable and unstable vertically density-stratified environments.

The EFDC model for BRRS were designed to model or simulate temperature distributions along the Black Warrior River and along depth. Therefore, temperature model component in EFDC was activated to model thermal or heat budget for each computational cell. Fig. 1.3 shows the control volume of the river-reservoir system showing the overall heat budget. The heat input is from the upstream release water. It's the source of the lower water temperature which can make the downstream temperature lower. The measured upstream release temperatures varying with time directly link to the upstream computation cells. At the downstream boundary of study area, water (heat) flux leaves the control volume. The model has the surface heat exchange between the atmosphere and the water surface. The heat exchange with the sediment is also applied around the river bed.

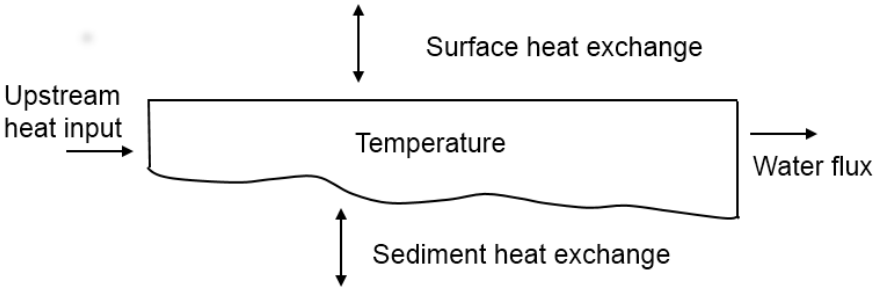

Fig. 1.3 Control volume for temperature in EFDC

While using EFDC Explorer we have four options for doing the surface-atmosphere heat exchange calculations. Among the four computation options, CE-QUAL-W2 equilibrium method is the most robust method; therefore, for the Gorgas model, we have used CE-QUAL-W2 method for water temperature modeling. The following paragraphs provide some basic information of the governing equations and heat exchange processes in a water body. The information provided here was based on the CE-QUAL-W2 manual (Cole and Wells 2004).

Surface heat exchange can be formulated as a term by-term process using the explicit adjacent cell transport computation as long as the integration time step is shorter than or equal to the frequency of the meteorological data. Surface heat exchange processes depending on water surface temperatures are computed using previous time step data and are therefore lagged from transport processes by the integration time step. Surface heat exchange is computed as:

$$H_n = H_s + H_a + H_e + H_c - (H_{sr} + H_{ar} + H_{br}) \quad (1.11)$$

where:

H_n = the net rate of heat exchange across the water surface, $W\ m^{-2}$

H_s = incident short wave solar radiation, $W\ m^{-2}$

H_a = incident long wave radiation, $W\ m^{-2}$

H_{sr} = reflected short wave solar radiation, $W\ m^{-2}$

H_{ar} = reflected long wave radiation, $W\ m^{-2}$

H_{br} = back radiation from the water surface, $W\ m^{-2}$

H_e = evaporative heat loss, $W\ m^{-2}$

H_c = heat conduction, $W\ m^{-2}$

The short wave solar radiation is either measured directly (read from input file aser.inp) or computed from sun angle relationships and cloud cover within CE-QUAL-W2 or EFDC program. The long wave atmospheric radiation is computed from air temperature and cloud cover or air vapor pressure using Brunts formula. Several terms in the right-hand of equation (1.11) terms are water surface temperature dependent.

Water surface back radiation (H_{br}) is computed as:

$$H_{br} = \varepsilon\sigma\ (T_s + 273.15\ )^4 \quad \text{(1.12)}$$

where:

E = emissivity of water, 0.97

σ = Stephan-Boltzmann constant, $5.67 \times 10^{-8}\ W\ m^{-2}\ °K^{-4}$

T_s = water surface temperature, $°C$

Like the remaining terms, it is computed for each surface layer cell on each iteration time step.

Evaporative heat loss is computed as:

$$H_e = f(W)\ (\ a_s - e_a\ ) \quad \text{(1.13)}$$

where:

$f(W)$ = evaporative wind speed function, $W\ m^{-2}\ mm\ Hg^{-1}$

e_s = saturation vapor pressure at the water surface, $mm\ Hg$

e_a = atmospheric vapor pressure, $mm\ Hg$

Evaporative heat loss depends on air temperature, dew point temperature or relative humidity, and wind speed. Saturation vapor pressure (e_s) is computed from the surface temperature for each surface cell on each iteration.

Surface heat conduction is computed as:

$$H_c = C_c f(W) (T_s - T_a) \quad (1.14)$$

where:

C_c = Bowen's coefficient, $0.47\ mm\ Hg\ °C^{-1}$

T_a = air temperature, $°C$

Short wave solar radiation penetrates the surface and decays exponentially with depth according to Bears law:

$$H_s(z) = (1- \beta)H_s e^{-\eta z} \quad (1.15)$$

where:

$H_s(z)$ = short wave radiation at depth z, $W\ m^{-2}$

β = fraction absorbed at the water surface

η = extinction coefficient, m^{-1}

H_s = short wave radiation reaching the water surface, $W\ m^{-2}$

Evaporation and convective heat losses has a user defined wind speed formula of the form

$$f(W)= a + b W^c \quad (1.16)$$

where:

$f(W)$ = wind speed function, $Wm^{-2}\ mm\ Hg^{-1}$

a = empirical coefficient, 9.2 default

b = empirical coefficient, 0.46 default

c = empirical coefficient of exponent, 2 default

W = wind speed measure at 2 m above the ground, $m\ s^{-1}$

Equilibrium temperature is used for heat exchange computation in CE-QUAL-W2. Because some of the terms in the term-by-term heat balance equation are surface temperature dependent and others are measurable or computable input variables, the most direct route to simplify computation is to define an equilibrium temperature, T_e, as the temperature at which the net rate of surface heat exchange is zero.

Linearization of the term-by-term heat balance along with the definition of equilibrium temperature allows expressing the net rate of surface heat exchange, H_n, as:

$$H_{aw} = -K_{aw}(T_w - T_e) \quad \ldots\ldots\ldots\ldots\ldots\ldots\ldots\ldots\ldots\ldots\ldots\ldots\ldots\ldots\ldots\ldots\ldots\ldots \quad (1.17)$$

where:

H_{aw} = rate of surface heat exchange, $W\,m^{-2}$

K_{aw} = coefficient of surface heat exchange, $W\,m^{-2}\,°C^{-1}$

T_w = water surface temperature, °C

T_e = equilibrium temperature, °C

Sediment heat exchange with overlying water is generally small compared to surface heat exchange and many previous modelers have neglected it. Investigations on several reservoirs have shown the process must be included to accurately reproduce hypolimnetic temperatures primarily because of the reduction in numerical diffusion that previously swamped the numerical solution. Basically, it's just heat conduction, and the formulation is similar to surface heat exchange:

$$H_{sw} = -K_{sw}(T_w - T_s) \quad \ldots\ldots\ldots\ldots\ldots\ldots\ldots\ldots\ldots\ldots\ldots\ldots\ldots\ldots\ldots\ldots\ldots\ldots \quad (1.18)$$

where H_{sw} is rate of sediment/water heat exchange, $W\,m^{-2}$; K_{sw} is coefficient of sediment/water heat exchange, $W\,m^{-2}\,°C^{-1}$; T_w is water temperature, $°C$; and T_s is

sediment temperature, °*C*. T_s was set at 13 °C for the initial bed temperature in the study during the summer.

Then applying the heat transport equation, the heat is simulated with the dispersion and convection velocity. So the heat flux associated with temperature can move longitudinally from one location to another. The heat can also transport in the vertical direction due to vertical turbulent or eddy diffusion. In this study, the flow momentum is an input; when it is large, it can mix water in the whole depth of the cross sections in the upstream portion of the study reach. That's related to the vertical turbulent and eddy diffusion. In some experimental studies and nature conditions, the flow momentum is relative weak and small, therefore, it may only affect a small region near the inflow.

The general transport equation in EFDC for temperature is:

$$\partial_t(m_x m_y \mathrm{HT}) + \mathrm{A(T)} = m_x m_y \partial_z(H^{-1} K_b \partial_z T + \sigma T) + m_x m_y H R_T + S_T \qquad (1.19)$$

where m_x and m_y are dimensionless scale factors for curvilinear horizontal coordinates, T is temperature, H is total water column depth, $A(T)$ is related to the horizontal dispersion and eqal to $\partial_x(m_y HuT) + \partial_y(m_x HvT) + \partial_z(m_x m_y wT)$, K_b is the vertical turbulent or eddy diffusivity for heat, and σ is a positive settling velocity (e.g., for sediments) that is not used for temperature simulation. Reactive sources and sinks are represented by R_T, but R_T is also not applied for temperature simulation. The term S_T includes the horizontal thermal turbulent diffusion and external sources and sinks.

1.4.2 Model Setup

The EFDC horizontal model grids developed for BRRS were based on NAVD 1988 horizontal datum and Universal Transverse Mercator (UTM) projection coordinate system. The horizontal grids were developed using the shoreline GIS shapefile of the Black Warrior River downloaded from AlabamaView (http://www.alabamaview.org/). The shoreline data were further validated using AutoCAD data and hydrographic data developed by the U.S. Army Corps of Engineers (USACE).

The EFDC model applied for the study area has a total of 6974 curvilinear orthogonal grids and 10 horizontal layers (determined through a sensitivity analysis) along the depth direction; therefore, there are a total of 69740 computational cells. The bathymetry was based on hydrographic data in an AutoCAD file for intake and discharge canals of the power plant; *x*, *y*, and *z* coordinates from USACE for Black Warrior River and the lower Mulberry Fork; and HEC-RAS geometry file for Sipsey Fork. The grid size ΔX in transverse direction along the river ranged from 9.5 m to 189.8 m and ΔY in longitudinal flow direction ranged from 10.0 m to 277.1 m. Average grid sizes ΔX and ΔY were 25.7 m and 100.9 m, respectively. The horizontal layer thicknesses (ΔZ) ranged from ~0.2 m to ~1.8 m. Sipsey Fork near the upstream boundary was represented by two to three grid cells along the cross section (Fig. 1.4a). The reservoir cross-sections near BLD are much wider than cross-sections at other river reaches of BRRS. Therefore, there are eight grid cells along the cross section near BLD to better represent the bathymetric details (Fig. 1.4b). The simulation domain includes grid cells to represent four tributaries flowing into BRRS (Blackwater Creek, the upper Mulberry Fork, Locust Fork, and Lost Creek) where streamflow measurements were available from the U.S. Geological Survey

(USGS) gauging stations. The model also designates specific cells for direct flow inputs from 15 relatively small streams where simulated hydrographs from a watershed model were available (Weems 2013). Fig. 1.4c shows model grids near the power plant. The model includes withdrawal and return flow boundaries (Hamrick and Mills 2000) to simulate withdrawals and discharges for power plant operations.

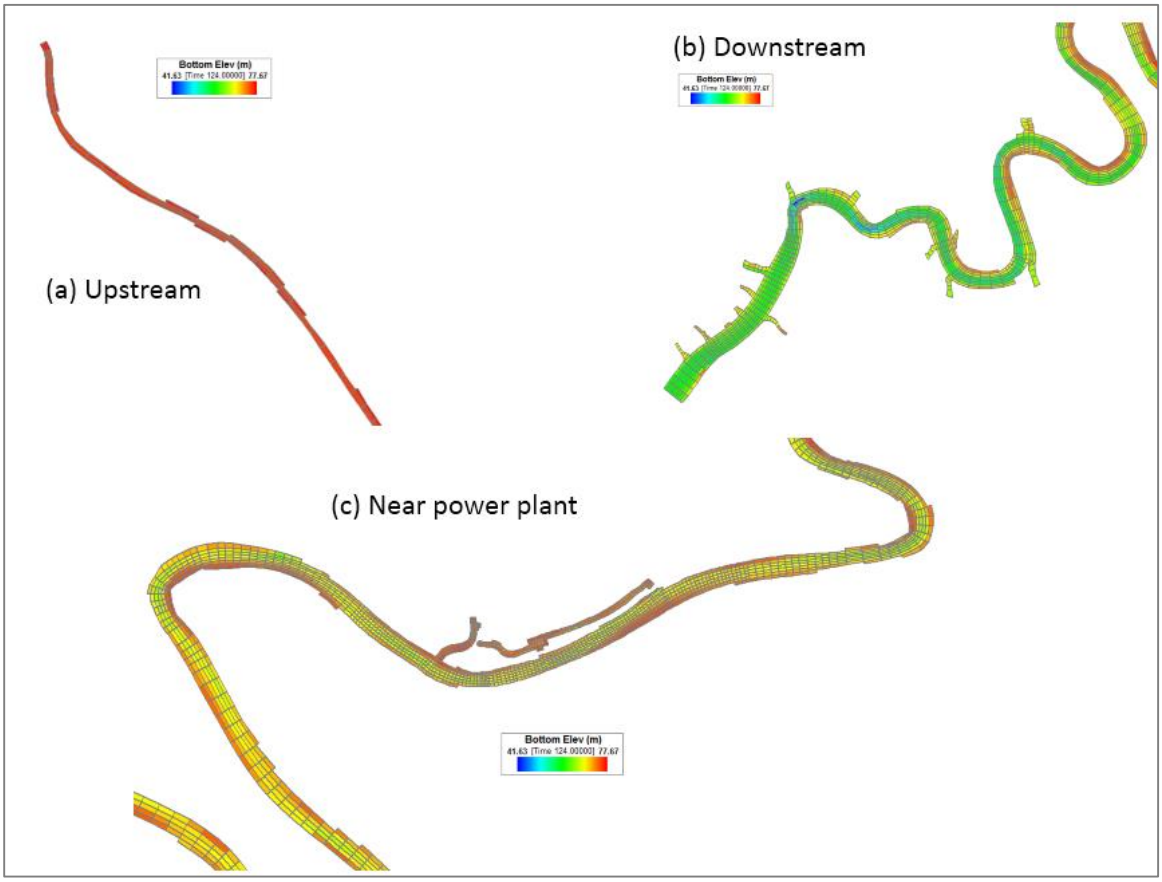

Fig. 1.4 Model grids near (a) the upstream boundary (SDT), (b) the downstream boundary (BLD) , and (c) the power plant.

Several model parameters were adjusted with calibration. In the EFDC model, the horizontal eddy viscosity was calculated by using the Smagorinsky formula

(Smagorinsky 1963). The horizontal mixing constant, C, has typical values between 0.10 and 0.20, and in the EFDC model, C = 0.1 was used. Vertical eddy viscosity is the parameter that is responsible for the vertical mixing. Measured surface and bottom water temperatures were highly stratified at all APC monitoring stations along the Black Warrior River, therefore, there was not much vertical mixing along depth. In the Gorgas model, we have used smaller values for vertical eddy viscosity ($1x10^{-6}$ m^2/s) and vertical molecular diffusivity ($1x10^{-9}$ m^2/s). The maximum kinematic eddy viscosity used was $1x10^{-6}$ m^2/s or $1x10^{-2}$ cm^2/s. Normally, horizontal eddy diffusivity is ten thousand to ten million times larger than the average vertical eddy diffusivity.

Attenuation coefficient (m^{-1}) for solar radiation is function of water itself, total suspended solids (TSS), and chlorophyll-a concentration. For the EFDC model study, the model does not model TSS and phytoplankton or chlorophyll-a concentration. Light attenuation (extinction) coefficient in the EFDC model was assumed 1.2 m^{-1}, which is equivalent to an assumed Secchi depth (Zs) about 1.5 m [attenuation coefficient ~ 1.84/Zs, (Hondzo and Stefan 1993)].

A fraction of solar radiation that is absorbed in the top layer of a water body varies from 0.2 to 0.45, and a typical value of 0.4 was used in the EFDC Model. Heat exchange between water and riverbed is typically not significant compared to solar radiation. In the EFDC model, a 2 m riverbed with a constant temperature of 16.3^{o}C was used, and the heat transfer coefficient between riverbed and water column was 0.05 $W/m^2/^{o}C$. In the EFDC model, the channel roughness coefficient was calibrated as 0.02.

The wind-sheltering coefficient calibrated for the EFDC model was 1.0, and atmospheric shading to solar radiation was 0.6.

In fluid mechanics, the Reynolds number (R_e) is a dimensionless quantity that is used to help predict similar flow patterns in different fluid flow situations. Fluid flow in natural rivers is generally turbulent flow (chaotic), and changes of river cross sections and surface roughness can result in very different flows. Reynolds number is defined as $R_e = V L / v$, where V is average velocity (m/s), L is a characteristic length (m), v is kinematic viscosity (m^2/s) and a function of water temperature. For open channel flow, either hydraulic depth or hydraulic radius is used for the characteristic length. The hydraulic depth is defined as the flow area divided by channel width at the water surface. The hydraulic radius is defined as the flow area divided by wetted perimeter.

Table 1.1 shows estimation of Reynolds number when there is small constant release (~2.83 m^3/s), and simulated velocities are relatively small at 5 different cross sections (MSF, UPJ, MJC, Cordova, and GOUS from upstream to downstream). Water depth is used as a rough estimation of hydraulic radius. The kinematic viscosity is set as 10^{-6} at 20 °C for all situations. R_e at the five cross sections are between 1.78E+04 and 2.03E+05 under the small constant release. Table 1.1 also shows estimations of Reynolds number when a large release (~140 m^3/s) just stopped. Simulated velocities at the five cross section showed large increase. The water depth also increased a lot, especially at the cross sections that are close to the SDT. At these five cross sections, R_e are between 5.47E+05 and 2.89E+06 after the large release just stopped. Therefore, the flow in BRRS is turbulent under different releases from SDT.

The Courant–Friedrichs–Lewy (CFL) condition is a necessary condition for convergence while explicitly solving certain partial differential equations (usually hyperbolic PDEs) numerically by the method of finite differences. It arises in the numerical analysis of explicit time integration schemes, when these are used for the numerical solution. As a consequence, the time step must be less than a certain time in many explicit time-marching computer simulations, otherwise the simulation will produce incorrect results. In the EFDC model, time integration uses a second-order accurate, three time level and finite difference scheme. Momentum and continuity equations are solved by internal-external model splitting procedure. For the external and internal model, semi-implicit and implicit schemes are applied, respectively. Hence, the EFDC model is not fully implicit. In the study, maximum time step is controlled by CFL condition based on the gravity wave phase speed. Due to the large variations of bottom elevation downstream of the power plant, the time step of computation cells in BRRS cannot be larger than 3.5 seconds for both small constant and large flow release. The ΔT for Courant–Friedrichs–Lewy (CFL) condition at 6 different cross sections from EFDC model under small constant release and when one large release just stopped are listed in Table 1.2. ΔT range from 0.67 to 1.51 seconds at six cross sections under different releases from SDT, which are smaller than the 3.5 seconds. For all the model runs of study, the time step is set as 2 seconds before the model runs and does not change during the simulation period.

Table 1.1 Estimation of Reynolds number under the small constant release and when one large release just stopped from the SDT.

Constant	MSF	UPJ	MJC	Cordova	GOUS
Velocity (m/s)	0.01	0.006	0.02	0.012	0.02
Temperature (°C)	20.9	22.1	21.7	18.7	24.7
Depth (m)	4.82	2.96	3.34	9.24	10.13
ν (m^2/s)	0.000001	0.000001	0.000001	0.000001	0.000001
Re	4.82E+04	1.78E+04	6.68E+04	1.11E+05	2.03E+05

Large Release	MSF	UPJ	MJC	Cordova	GOUS
Velocity (m/s)	0.477	0.343	0.16	0.072	0.11
Temperature (°C)	12.68	23.3	24.43	21.04	25.12
Depth (m)	6.05	3.33	3.42	9.33	10.16
ν (m^2/s)	0.000001	0.000001	0.000001	0.000001	0.000001
Re	2.89E+06	1.14E+06	5.47E+05	6.72E+05	1.12E+06

Table 1.2 ΔT at 6 different cross sections from EFDC model under small constant release and when one large release just stopped.

ΔT	**SDT**	**MSF**	**UPJ**	**MJC**	**Cordova**	**GOUS**
Small Constant release	1.10	0.93	1.6	1.35	0.90	0.88
Release just stopped	0.67	0.83	1.51	1.33	0.89	0.86

1.4.3 Temperature Boundary Conditions of Hydrodynamic Model

The research also involves to develop simple but accurate models for calculating hourly water temperatures in rivers. These temperature estimates are temperature boundary condition of the 3D EFDC hydrodynamic and temperature model for the river-reservoir system and are used for all numerical experiments presented in Chapters two to five.

In this research topic, direct linear and non-linear (logistic) regression models with time lags (4–5 hours or hr) were firstly used to calculate hourly water temperature

(Chen and Fang 2015b). For the second method, (Chen et al. 2016) uses modified sine and sinusoidal wave functions (MSSWF) to estimate hourly water temperatures in 8 rivers (Table 1.3). We investigated and applied seasonal variations in the daily maximum and minimum stream water temperatures based on observed daily maximum and minimum air temperatures. The sinusoidal wave function (SWF) model, originally used to calculate hourly air temperature, was then modified and applied to estimate hourly water temperature in rivers in Alabama. Estimated hourly water temperatures in streams can be used to calculate saturated dissolved oxygen concentrations over diurnal cycles and determine temperature-dependent chemical and biological reaction rates (Chapra 1997) for water quality control and management study. Water quality models, e.g., one-dimensional dynamic hydraulic and water quality simulation model EPD-RIV1 (Martin and Wool 2002), two-dimensional longitudinal/vertical water quality and hydrodynamic model CE-QUAL-W2 (Cole and Wells 2010), and three-dimensional Water Quality Analysis Simulation Program WASP (Wool et al. 2001), need to set appropriate temperature boundary conditions of streams flowing into the simulation domain, which may not have observed temperature data and can be estimated using models developed in this study.

Chen and Fang (2015b) developed two regression models (linear and logistic function) and the MSSWF model to determine the model accuracy when they were used to calculate hourly water temperature in a river from air temperatures. The regression models use hourly air temperature as inputs, while the WSSWF model uses daily maximum and minimum air temperatures and the day of year (DOY) as input.

Regression Models

Linear regression model is the simplest regression model shown as Equation (1.20), which was used in many previous studies for daily or weekly temperature regressions (Stefan and Preud'homme 1993; Erickson and Stefan 2000):

$$T_w(t) = a \cdot T_a(t) + b \tag{1.20}$$

where $T_w(t)$ is hourly water temperature; $T_a(t)$ is hourly air temperature with or without lag; a and b are regression coefficients. Water temperatures calculated from the linear model follow diurnal variations of hourly air temperatures. The coefficients a and b in Equation (1.20) are scale and translation parameters.

Table 1.3 Location, drainage area, distance to Birmingham International Airport (BHM), data period, mean, minimum and maximum hourly measured water temperatures of 8 river stations in Alabama, USA.

River Station	Lat., Long.	Drainage Area (km^2) & distance (km)	Starting Date [a]	Hourly Temperature (°C)		
				Mean	Min	Max
Kelly Creek near Vincent, AL	33°26'51", 86°23'13"	500 (30.8)	7/12/2008	17.01	0.30	30.60
Tallapoosa River near Mont. Water Works, AL	32°26'23", 86°11'44"	12,033 (132.9)	10/1/2007	18.38	5.30	31.70
Little Cahaba River below Leeds, AL	33°32'04", 86°33'45"	55 (12.2)	10/17/2008	17.20	4.50	27.30
Cahaba River near Hoover, AL	33°22'09", 86°47'03"	585 (23.0)	10/1/2007	17.85	1.20	32.80
Chattahoochee R.36 mi DS WFG Dam, AL/GA	31°37'17", 85°03'36"	19,321 (264.3)	5/28/2010	20.35	6.40	31.40
Cahaba River at Trussville, AL	33°37'20", 86°35'58"	50 (10.9)	10/23/2007	16.13	1.00	29.50
Fivemile Creek near Republic, AL	33°35'49", 86°52'05	133 (17.0)	10/4/2007	17.54	0.20	32.40
Village Creek at Avenue W at Ensley, AL	33°31'03", 86°52'45"	86 (18.2)	10/1/2007	18.26	2.00	33.80

Note: Lat.: latitude; Long.: longitude; Min.: minimum; Max.: maximum; AL/GA: at the Alabama (AL) and Georgia (GA) state line. The river stations are list according to the station ID numbers from the USGS. [a] The starting data for available hourly water temperature data, and the ending data is 1/23/2015 for all stations.

The logistic regression model has been used over the last few decades to develop air and water temperature relationships (Mohseni et al. 1998), and it is a four-parameter model defined using Equation (1.21):

$$T_w = \mu + \frac{\alpha - \mu}{1 + e^{\gamma(\beta - T_a)}} \tag{1.21}$$

where μ (°C) is a coefficient that estimates minimum water temperature, α (°C) is a coefficient that estimates maximum water temperature, γ (dimensionless) represents the steepest slope (inflection point) of the logistic T_w function when plotted against T_a, and β (°C) is air temperature at the inflection point.

Modified Sine and Sinusoidal Wave Functions (MSSWF) Model

The sine function was used in the last few decades to develop daily air and water temperature relationships with respect to day of year (DOY) (Kothandaraman and Evans 1972; Caissie et al. 2001; Benyahya et al. 2007; Lambrechts et al. 2011), Considering consistent seasonal variations/patterns of water and air temperatures, the sine function given as Equation (1.22) is used to calculate daily air and water temperatures *T(t)*:

$$T\,(t) = \overline{T} + T_{am} \sin(\omega t - \theta) \tag{1.22}$$

where $\overline{T}$ = annual mean temperature of air or water (°C), T_{am} = amplitude (°C) of the sine function, t = DOY (January 1 is t = 1 and December 31 is t = 365 for a non-leap year or 366 for a leap year), θ = phase shift (radians), ω = angular frequency of temperature variations (radians day^{-1}), which is fixed as $2\pi/365$ when it is assumed that temperature repeats its variation year by year. Sine functions are developed and used to estimate daily

maximum and minimum water temperatures in a river for the MSSWF model that are then used to estimate hourly water temperatures using SWF (Equations 1.23 and 1.24).

Reicosky et al. (1989) used SWF to predict hourly air temperatures from daily maximum and minimum air temperatures, and assumed that maximum air temperature is at 14:00 hr and minimum air temperature is at sunrise in each day. Considering the time lag of water temperatures from air temperatures (Stefan and Preud'homme 1993), times of maximum and minimum water temperatures should be set differently from times for maximum and minimum air temperatures. The average time of maximum water temperatures for the 8 rivers in Alabama is 16:18, which is same as statistical results of the time of daily maximum water temperature being between 16:00 and 17:00 in 122 stream-temperature data logger sites in the Great Lake basin, Ontario, Canada (Chu et al. 2009). The average time of minimum water temperatures is 08:05. The sunrise and sunset at BHM from October 1, 2007 to January 23, 2015 were calculated day by day; it was found that the mean sunrise and sunset for the 8 rivers are 05:43 and 17:54, respectively. Therefore, the modified SWF assumes the maximum river temperature is at 16:00 and the minimum river temperature is at the sunrise plus 2 hrs (Chen and Fang 2015b).

The modified SWF model for predicting hourly water temperatures are given in Equations (1.23) and (1.24) based on previous studies (De Wit 1978; Hoogenboom and Huck 1986). The intervening temperatures at time H hour (0:00 to 24:00 hr) are calculated from the following equations:

For $0 \leq H < (RISE + 2)$ and 16:00 hr $< H \leq$ 24:00 hr

$$T_W(H) = T_{WAVE} + AMP\ (\cos\ (\pi\ H'/(10 + RISE))) \quad (1.23)$$

For $(RISE + 2) \leq H \leq 16{:}00$ hr

$$T_W(H) = T_{WAVE} - AMP\ (\cos\ (\pi\ ((H - RISE - 2)/(16 - RISE - 2))) \quad (1.24)$$

where *RISE* is the time of sunrise in hours in each day and $T_W(H)$ is the water temperature at time H hour, $H' = H + 8$ if $H < (RISE + 2)$, $H' = H - 16$ if $H > 16{:}00$ hr, and T_{WAVE} and *AMP* are defined as $T_{WAVE} = (T_{WMIN} + T_{WMAX})/2$ as daily mean temperature and $AMP = (T_{WMAX} - T_{WMIN})/2$ as temperature amplitude, respectively. T_{WMAX} and T_{WMIN} are estimated daily maximum and minimum water temperatures from sine functions using daily maximum and minimum air temperatures as input.

The specific procedures and applications of above models are given in the Appendix B.

1.5 Organization of Dissertation

This dissertation is organized into 6 chapters. Chapters two to five are organized in one conference paper for World Environmental and Water Resources Congress and three journal papers format prepared for Hydrological Sciences Journal (HSJ), ASCE Journal of Hydrologic Engineering, and Water — Open Access Journal. Chapter two (Paper 1) has already been published in Hydrological Sciences Journal, and Chapter three (Paper 2) has already been published in Water — Open Access Journal. Chapter four (Paper 3) has been submitted to 2016 World Environmental and Water Resources Congress. Chapter five (Paper 4) has been submitted to Journal of Hydro-environment Researchand is under review by the time this dissertation was completed. Literature

review for the study is given in Chapters two to five for corresponding journal papers. The references for all four papers were combined, sorted, and listed at the end of the dissertation.

In the chapter two, the 3D EFDC model was applied and calibrated in a river-reservoir system from the Smith Dam tailrace (SDT) to the Bankhead Lock & Dam (BLD) in Alabama (AL), USA. The calibrated model was then used to investigate the unsteady flow dynamics focusing on density current movement and heat transport under varying reservoir releases and atmospheric heat exchange due to diurnally varying solar radiation and air temperature. The work of this chapter has been published in Hydrological Sciences Journal (HSJ) as Paper 1:

> Chen, G., Fang, X., and Devkota, J. (2015). "Understanding flow dynamics and density currents in a river-reservoir system under upstream reservoir releases." Hydrological Sciences Journal. DOI:10.1080/02626667.2015.1112902.

Chapter three deals with the calibrated EFDC model presented in paper 1 or Chapter two to focus on understanding and analysis of formation and propagation of density currents under different short-duration (a few hours) large flow releases into a confined river-reservoir system. The study is to perform a series of model scenario runs and conduct in-depth result analysis to further investigate flow dynamics and temperature distributions in order to understand and quantify formation and propagation of density currents caused by daily repeated upstream releases (DRLR) of different durations and solar heating. The work of this chapter has been published in Water — Open Access Journal as Paper 2:

Chen, G. and Fang, X. 2015a. Sensitivity Analysis of Flow and Temperature Distributions of Density Currents in a River-Reservoir System under Upstream Releases with Different Durations. Water, 7(11), 6244-6268.

In the Chapter four, EFDC dye model components were activated to simulate dye concentrations for each computation cell to understand density current movement. Dye distributions are useful and clear to track how the density current moves. This study has been accepted as the conference paper (paper 3) and oral presentation:

Chen, Gang, Fang, Xing (2016). "Simulations of Flow and Dye Distributions of Density Currents in a River-Reservoir System under Different Upstream Releases". World Environment and Water Resources Congress. 2016, ASCE/EWRI, West Palm Beach, FL.

Chapter five is to further understand the bottom-layer water temperature dynamics due to combined effects of meteorological condition and DRLR. For scenario analysis performed in this study, various input data (boundary conditions) were modified into constant representative values excluding upstream boundary conditions and climate conditions. Therefore, we can focus on studying effects of dynamic releases from the upstream reservoir and variable atmospheric conditions on density current formations and movement. The work of chapter five is a journal paper submitted for the publication as Paper 4:

Chen, Gang and Fang, Xing (2016). "Influences of meteorological conditions and daily repeated upstream release on temperature distributions in a river-reservoir system". Journal of Hydro-environment Research, submitted on February 19, 2016.

Chapter six summarizes the study performed as conclusions and provides limitations of the study and the future study in this area.

Appendix A discusses about the calibration parameters and calibration procedure used in the calibration of EFDC model in the river-reservoir system. The calibration parameters used in the EFDC models and the literature values are also listed.

Appendix B provides the results of estimating hourly water temperature in rivers from air temperature, which the theory is briefly discussed in Chapter 1.4.3. The detailed procedure of calculating hourly water temperature is explained. The work of this part has been published as two jorunal papers below:

Gang Chen and Xing Fang, 2015b. "Accuracy of hourly water temperatures in rivers calculated from air temperatures", Water, 7(3), 1068-1087 (Online Open Access)

Gang Chen, Xing Fang and Hui Fan, 2016. "Estimating Hourly Water Temperatures in Rivers using Modified Sine and Sinusoidal Wave Functions", ASCE Journal of Hydrologic Engineering, in press.

Chapter 2. Understanding Flow Dynamics and Density Currents in a River-reservoir System under Upstream Reservoir Releases

2.1 Abstract

A three-dimensional flow and temperature model was applied for a 124 km river-reservoir system from Smith Dam tailrace to Bankhead Lock & Dam, Alabama. The model was calibrated against measured water levels, temperatures, velocities, and flow rates from 4 May to 3 September 2011 under small constant release (2.83 m^3/s) and large intermittent releases (~140 m^3/s) from an upstream reservoir. Distributions of simulated flow and temperatures and particle tracking at various locations were analyzed which revealed the complex interactions of density currents, dynamic surface waves, and solar heating. Flows in the surface and bottom layers moved in both upstream and downstream directions. If there was small constant release only from Smith Dam, simulated bottom temperatures at Cordova were on average 4.8 ^oC higher than temperatures under actual releases. The momentum generated from large releases pushed bottom density currents advancing towards downstream, but the released water took several days to reach Cordova.

2.2 Introduction

River regulation as a means of water resources management is a common operating procedure all over the world. Reservoir release is becoming a prominent characteristic for regulated rivers to meet hydro-electric power demands (Petts et al.

1985). Increasing flow release leads to larger flow depths at downstream river, where rapid stage changes of more than 1 m are common. Stage changes have been detected more than 100 km downstream of the large dams after the wave attenuation (Petts 1984). Operational constraints considering water temperature in downstream river focused on a minimum flow requirement for water quality and temperature control (Carron and Rajaram 2001). The need of minimum flow is usually during the warm season of the year, especially during the summer to maintain lower water temperatures downstream (Wunderlich and Shiao 1984; Consultants 1986). Atmospheric conditions have a large effect on river temperature after the reservoir release. Due to the solar heating, typically water temperature in a shallow river is much warmer than release temperature of stored water in the reservoir.

Toffolon et al. (2010a) used a coupled hydro-thermodynamic deterministic model, and analytical solutions for river water temperature have been developed to get a better insight into the physical properties associated with the propagation of both hydrodynamic and thermal peaking waves in downstream receiving river. The hydro-wave and thermal wave dynamics are rather complex, propagation of the thermal wave is always slower than the hydrodynamic wave, and the two waves are slowly damped. The study by Toffolon et al. (2010a) does not consider the formation of density currents in the receiving river.

A significant number of river-reservoir systems all over the world have large diurnal variations in atmospheric heating rates and develop density currents in the downstream river/reservoir due to colder denser flow releases from an upstream

reservoir. A plunging density current occurs when the density of the water flowing into a reservoir or lake is greater than the density of the ambient water. In the riverine portion of a reservoir, the denser inflow mixes homogeneously with the reservoir or lake water first due to the flow momentum. When the inflow momentum diminishes, the inflowing water eventually plunges under the ambient water and flows along the bottom as a density current (Farrell and Stefan 1989). The intermittent denser flow releases from an upstream reservoir create very complex and unsteady density currents that are not well understood yet.

Many laboratory and numerical model studies focusing on density currents have been conducted in the last decades. Density currents have been studied in situ by various researchers (Serruya 1974; Smith 1975; Carmack et al. 1979; Fischer and Smith 1983; Alavian and Ostrowski Jr 1992; Chikita 1992; Dallimore et al. 2001). The density currents were also investigated in the laboratory (Akiyama and Stefan 1984; Hauenstein and Dracos 1984; Alavian 1986; Hallworth et al. 1996). Most studies in the past dealt with sloping channels having a rectangular cross section, and various simplifying assumptions were made to develop analytical models with laboratory data to understand density currents (Singh and Shah 1971; Savage and Brimberg 1975; Denton 1985; Kranenburg 1993; Fernandez and Imberger 2008b; Fernandez and Imberger 2008a).

A one-dimensional integral model was developed by Fang and Stefan (2000) for a discharge from a channel over a horizontal or a sloping bottom into a reservoir or a lake to determine dilution up to plunging for density current computations. Two-dimensional hydrodynamic models were developed to study density current by assuming that the

density current does not participate in the dynamics of heating and mixing but the entrainment takes place from the ambient reservoir into the downflow (Imberger and Patterson 1980; Buchak and Edinger 1984; Jokela and Patterson 1985). Gu (2009) used a validated two-dimensional (2D) simulation model CE-QUAL-W2 (Cole and Wells 2010) to quantify systematically the effects of inflow and ambient parameters on the behavior of a density-induced contaminant current in various flow regimes in a stratified reservoir through numerical experiments. Several studies about three-dimensional (3D) gravity currents were conducted recently using laboratory data and numerical models (Imran et al. 2007; Firoozabadi et al. 2009; Rueda and MacIntyre 2010; An and Julien 2014). Rueda and MacIntyre (2010) used a 3D free surface hydrodynamic model with fine grid resolution to simulate negatively buoyant density currents on steep bottoms with varying slopes in Toolik Lake, AK.

In the last several decades, 3D Environmental Fluid Dynamics Code (EFDC) (Hamrick 1992) has been widely used in modeling river, estuarine and coastal hydrodynamics and transport processes. In order to quantify numerical and modeled entrainment, Kulis and Hodges (2006) explored the grid resolution required in EFDC to capture gravity current motions in an idealized basin with and without a turbulence closure. The study basin was scaled and based on a shallow bay, Corpus Christi Bay in Texas, USA, which is affected by the underflow from Oso Bay. Liu and Garcia (2008) used modified 3D EFDC model to simulate the density current and bi-directional flows in the Chicago River system.

None of the studies considered dynamic releases from an upstream reservoir and heat exchange from the atmosphere in a river-reservoir system at the same time. The simple numerical or laboratory study cannot reveal the complex processes and interactions such as cooling, heating, and flow dynamics (mixing and density current movement). In this paper, the 3D EFDC model was applied and calibrated in a river-reservoir system from the Smith Dam tailrace (SDT, Fig. 1) to the Bankhead Lock & Dam (BLD) in Alabama (AL), USA. The calibrated model was then used to investigate the unsteady flow dynamics focusing on density current movement and heat transport under varying reservoir releases and atmospheric heat exchange due to diurnally varying solar radiation and air temperature.

2.3 Materials and Methods

2.3.1 Study Area

The study deals with flow and temperature simulations in a river-reservoir system (124.2 km) from SDT (upstream flow boundary) to BLD (downstream water level boundary) in Walker County, AL, USA (Fig. 2.1). The river reach includes Sipsey Fork (21.9 km), the lower Mulberry Fork (70.6 km), and a reservoir segment (31.7 km) of Bankhead Lake (Fig. 2.1), which is also called Black Warrior River. Sipsey Fork and the lower Mulberry Fork are the riverine portions of Bankhead Lake, therefore, the study area is referred here as the Bankhead river-reservoir system (BRRS). The Black Warrior River is formed about 40 km west of Birmingham by the confluence of the Mulberry Fork and the Locust Fork, which join as arms of Bankhead Lake, a narrow reservoir formed by BLD. The Black Warrior River is impounded by a series of locks and dams to

form a chain of reservoirs that not only provide a path for an inland waterway, but also yield hydroelectric power, drinking water, and industrial water.

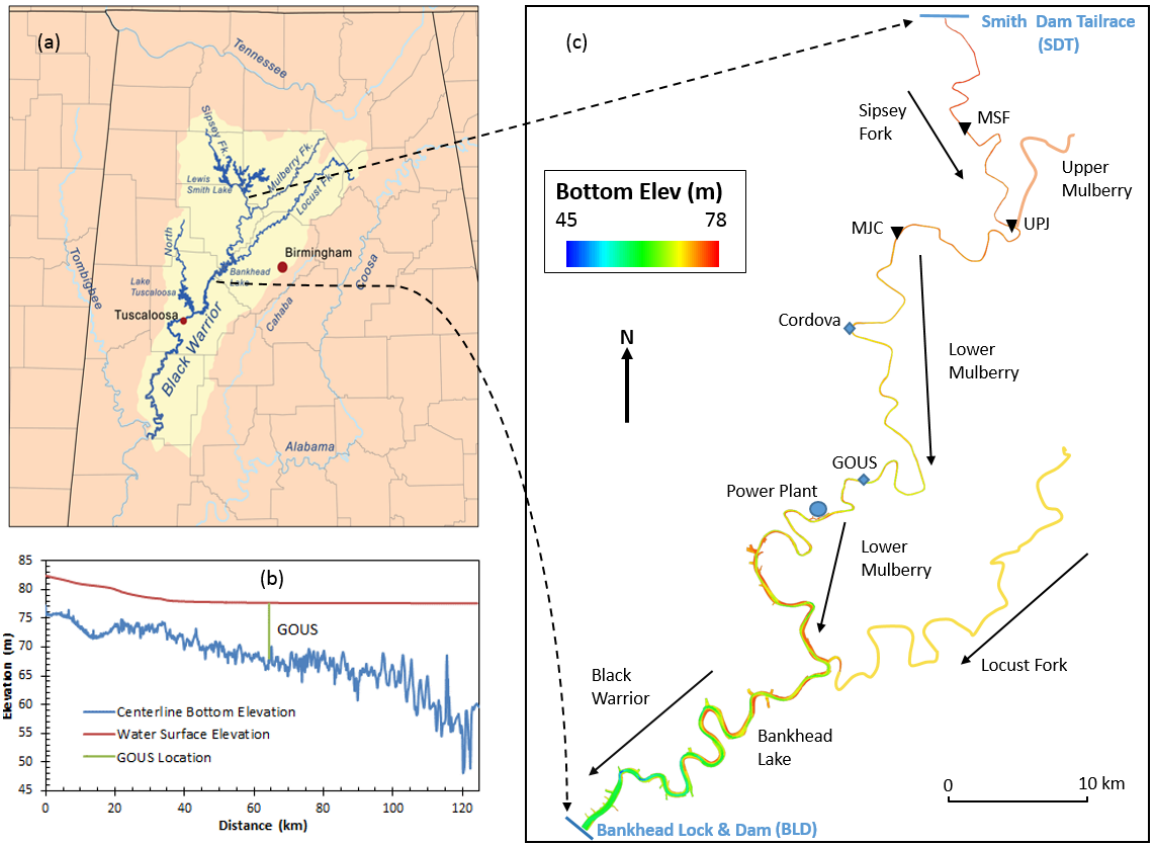

Fig. 2.1 (a) Geographic location of the study area and the location of Birmingham weather station used for the study, (b) Longitudinal bottom elevation along the centerline of BRRS and water surface elevation profile after a large release from Smith Dam Tailrace to Bankhead Lock & Dam, (c) Images with color contours of the bottom elevation showing Sipsey Fork, the lower Mulberry Fork, and Black Warrior River as the model simulation domain; two monitoring stations (Cordova and GOUS), model upstream and downstream boundary locations (Smith Dam tailrace and Bankhead L&D), three locations for reporting simulation results (MSF, UPJ, and MJC, Table 2.2).

The EFDC model was applied to simulate unsteady flow patterns and temperature distributions in BRRS including the intake canal and the discharge canal of a power plant (Fig. 2.1c) near Parrish, AL. The water surface elevation in BRRS depends on water releases from Lewis Smith Dam, flows from its tributaries (e.g., Locust Fork, Lost Creek and Blackwater Creek), and the water surface elevation in BLD influenced by outflow through hydro turbines, spillage through gates of BLD, and loss of water through the Bankhead navigation lock. The bottom elevations of the centerline of BRRS ranged from about 59.5 to 77.2 m above mean sea level (using NAVD 1988 datum, Fig. 2.1b). The average bottom slope is 0.00014 but there are local slope variations (ranging from -0.002 to 0.002 over each ~2 km distance) as shown in Fig. 2.1 (b) (having different scales in depth and distance). Bottom slopes in BRRS are much smaller than steep bottom slopes (0.03–0.2) in Toolik Lake (Rueda and MacIntyre 2010). A typical water surface profile after a large release from Smith Dam displayed in Fig. 2.1b depicts the response of water level increase in the upstream portion of BRRS only.

Table 2.1 Statistical summary of the intermittent flow releases from Smith Dam.

Statistical Parameters	Starting time of release (hour)	Duration of release (hour)	Average release flow rate (m^3/s)
Minimum	4.83	0.17	104.02
25st percentile	12.02	3.63	137.30
Median	13.02	4.42	138.76
75rd percentile	14.02	6.17	142.05
Maximum	20.25	116.17	273.54
Average	12.97	6.86	148.69
Standard deviation	2.42	14.38	33.92

The water releases from Smith Dam to BRRS are normally 2.83 m^3/s, but during later spring, summer and early fall, intermittent water releases of high discharges (Table 2.1) are practiced to meet peak electric generating demand. During the normal water releases, water depths in Sipsey Fork range from 2.16 to 4.55 m, in the lower Mulberry Fork from 4.71 to 11.47 m, and in the Black Warrior River (Bankhead Lake) from 12.12 to 17.73 m. The water surface elevation at BLD is about 77.66 m (Fig. 2.1b) above mean sea level.

The monitoring stations and cross sections for result analysis are shown in Fig. 2.1c and summarized in Table 2.2. The middle cross section of Sipsey Fork (MSF) is located at 11.1 km downstream from SDT. The cross section at a short distance (0.64 km) upstream of the junction of Sipsey Fork and the upper Mulberry Fork is called UPJ. The middle section between the junction and Cordova is called MJC. The monitoring station at 5.58 km upstream the power plant is called GOUS (Fig. 2.1c).

Table 2.2 Description and abbreviation of cross sectional locations used in the study (Fig. 1 (c)).

Abbreviation	Description
Cordova	USGS monitoring station at Cordova on the lower Mulberry River
GOUS	Monitoring station upstream the power plant
MSF	Middle cross section of Sipsey Fork
UPJ	Just upstream of the junction of Sipsey Fork and the upper Mulberry Fork
MJC	Middle cross section between the junction and Cordova
SDT	Smith Dam tailrace (upstream boundary of EFDC model)
BLD	Bankhead Lock & Dam (downstream boundary of EFDC model)

2.3.2 Hydrodynamic Simulation Model Used

The study deals with a relatively narrow river-reservoir system, which could be modeled using a 2D longitudinal-vertical hydrodynamic and water quality model, such as CE-QUAL-W2 model (Cole and Wells 2010). To more accurately simulate complex flow and temperature distributions in BRRS especially near the power plant, the 3D EFDC hydrodynamic model was applied for the project to understand the hydrodynamics of density currents formed by upstream reservoir releases. The EFDC model is a general purpose modeling package that can be configured to simulate1D, 2D, and 3D flow, transport, and biogeochemical processes in various surface water systems including rivers, lakes, estuaries, reservoirs, wetlands, and coastal regions (Shen and Lin 2006; Caliskan and Elci 2009; Jeong et al. 2010; Wang et al. 2010; Kim and Park 2012; Devkota and Fang 2014). The EFDC model was originally developed at the Virginia Institute of Marine Science and the version of EFDC used for the study with pre- and post-processing tools was EFDC-DSI (Craig 2010) from the Dynamic Solutions-International, LLC (http://efdc-explorer.com/). EFDC solves three-dimensional turbulent-averaged equations of motions for a variable-density fluid. EFDC's hydrodynamics are based on the 3D hydrostatic equations formulated in curvilinear-orthogonal horizontal coordinates and a sigma vertical coordinate system. The Mellor-Yamada level 2.5 turbulence closure scheme (Mellor and Yamada 1982) is used to calculate turbulence parameters; vertical turbulent diffusion coefficients of momentum and mass. The horizontal eddy viscosity, A_H is calculated using the Smagorinsky subgrid scale scheme (Smagorinsky 1963), which can be written in the two-dimensional Cartesian coordinate as:

$$A_H = C\Delta x\Delta y\left[\left(\frac{\partial u}{\partial x}\right)^2 + \left(\frac{\partial v}{\partial y}\right)^2 + \frac{1}{2}\left(\frac{\partial u}{\partial y} + \frac{\partial v}{\partial x}\right)^2\right]^{\frac{1}{2}} \quad (2.1)$$

where C is horizontal mixing constant, Δx and Δy are model grid sizes in x and y directions, u and v are velocity components in x and y directions. The numerical scheme used in EFDC to solve the momentum equations uses a second-order accurate spatial finite difference on a staggered or C grid. The time integration is implemented using a second-order accurate three-time level, semi-implicit finite difference scheme with an internal-external mode splitting scheme to separate the internal shear or baroclinic mode from external free surface gravity wave or barotropic mode. Details of governing equations and numerical schemes for EFDC hydrodynamic model are given by Hamrick (1992).

2.3.3 Model Setup

The EFDC horizontal model grids developed for BRRS were based on NAVD 1988 horizontal datum and Universal Transverse Mercator (UTM) projection coordinate system. The horizontal grids were developed using the shoreline GIS shapefile of the Black Warrior River downloaded from AlabamaView (http://www.alabamaview.org/). The shoreline data were further validated using AutoCAD data and hydrographic data developed by the U.S. Army Corps of Engineers (USACE).

The EFDC model applied for the study area has a total of 6974 curvilinear orthogonal grids and 10 horizontal layers (determined through a sensitivity analysis) along the depth direction; therefore, there are a total of 69740 computational cells. The bathymetry was based on hydrographic data in an AutoCAD file for intake and discharge

canals of the power plant; *x*, *y*, and *z* coordinates from USACE for Black Warrior River and the lower Mulberry Fork; and HEC-RAS geometry file for Sipsey Fork. The grid size ΔX in transverse direction along the river ranged from 9.5 m to 189.8 m and ΔY in longitudinal flow direction ranged from 10.0 m to 277.1 m. Average grid sizes ΔX and ΔY were 25.7 m and 100.9 m, respectively. The horizontal layer thicknesses (ΔZ) ranged from ~0.2 m to ~1.8 m. Sipsey Fork near the upstream boundary was represented by two to three grid cells along the cross section. The reservoir cross-sections near BLD are much wider than cross-sections at other river reaches of BRRS. Therefore, there are eight grid cells along the cross section near BLD to better represent the bathymetric details. The simulation domain includes grid cells to represent four tributaries flowing into BRRS (Blackwater Creek, the upper Mulberry Fork, Locust Fork, and Lost Creek) where streamflow measurements were available from the U.S. Geological Survey (USGS) gauging stations. The model also designates specific cells for direct flow inputs from 15 relatively small streams where simulated hydrographs from a watershed model were available (Weems 2013). The model includes withdrawal and return flow boundaries (Hamrick and Mills 2000) to simulate withdrawals and discharges for power plant operations.

2.3.4 Unsteady Boundary Conditions

The EFDC model applied for BRRS was run from Julian Day 104 to 304 in 2011 (i.e., April 14 to October 31) because of available input data. The majority of observed data available for the project at various monitoring stations (Table 2.2) were from Julian Day 124 to 246 in 2011 (i.e., May 4 to September 3, Fig. 2.2). The upstream boundary of

the EFDC model used one-minute time-series data (unsteady) of water releases (m^3/s) at SDT (Fig. 2.2a). There are two types of water releases from Smith Dam: (1) more or less constant continuous release (2.83 m^3/s) to support the downstream environment and ecosystem; (2) intermittent releases from hydro-turbine units of Smith Dam in order to meet peak electric generation demand (Fig. 2.1). During the simulation period, total volume of constant water release was 49.4×10^6 m^3 and intermittent releases were 588.6×10^6 m^3. Therefore, constant water release with lower temperature (8–9 ^oC) was about 7.7% of the total release from Smith Dam. The intermittent releases from Smith Dam had average discharge of about 140 m^3/s that lasted about 4 hours and started around 1:00 pm (Table 2.1). The study was performed to reveal how these intermittent releases create and affect density currents near the river bottom.

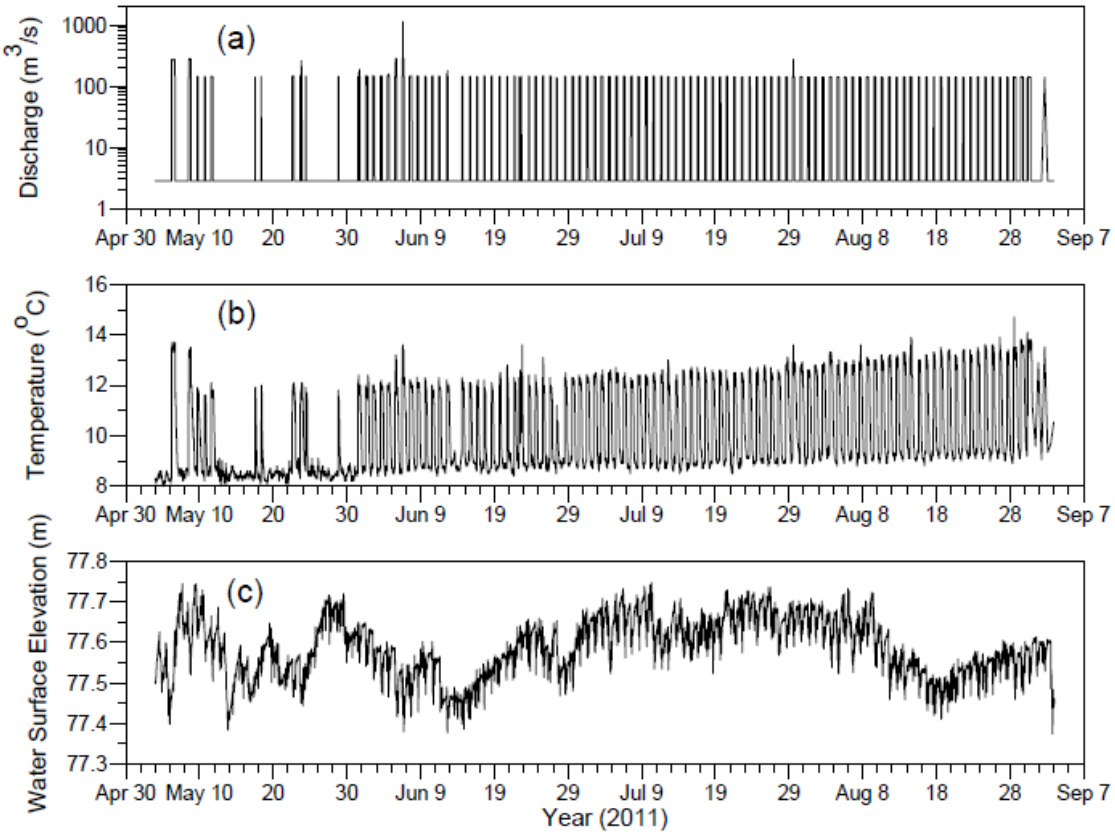

Fig. 2.2 Time-series plots of (a) upstream unsteady flow releases, (b) upstream temperature boundary conditions, and (c) downstream water surface elevation (m) in 2011.

Fig. 2.2b shows a time-series plot of measured water temperatures at SDT used as the upstream temperature boundary. Water temperatures at the tailrace from May 4 to September 3 increased from 8 to 9 ^{o}C during the constant release, and water temperatures during the intermittent large releases were 12–14^{o}C, which were 4–5 ^{o}C higher than temperatures during the constant release only from Smith Dam. This is because constant release occurred from a deep water depth and intermittent releases were from a shallower

depth of Smith Dam; and there was lower water temperature in the hypolimnion due to thermal stratification in the summer.

The downstream boundary of the EFDC model was 15-minute water surface elevation (WSE) measured at BLD (Fig. 2.2c). Observed WSEs ranged from 77.35 m to 77.75 m from May 4 to September 3, 2011 with an average elevation of 77.59 m (standard deviation of 0.07 m).

The atmospheric boundary condition was meteorological data from the Birmingham regional airport obtained from NOAA's Southeast Regional Climate Center (SERCC). The data include hourly air temperature, atmospheric pressure, wind speed, wind direction, rainfall, and cloud cover. Required solar radiation data were not available from SERCC but obtained from Cleveland, AL (the closest Auburn Mesonet station from the study area).

2.4 Model Calibration Results

The EFDC model applied for BRRS was calibrated from 4 May (Julian day 124) to 3 September 2011 (Julian day 246). The model was calibrated for water surface elevation (Fig. 2.3 and Table 2.3), water temperature (Fig. 2.4 and Table 2.4), velocity and discharge (Fig. 2.5) at two monitoring stations: Cordova and GOUS (Fig. 2.1). Two commonly used calibration parameters for flow, bottom roughness height and the dimensionless horizontal momentum coefficient in EFDC were calibrated to obtain the best match between observed and modeled water surface elevations. In this study, the bottom roughness height of 0.02 m was determined during the calibration. The

dimensionless horizontal momentum coefficient ("C" in Equation 1) was calibrated to be 0.0025 for the BRRS EFDC model.

Fig. 2.3 shows the time series plot of measured and simulated WSE at the USGS Cordova monitoring station from 4 May to 3 September, 2011. The agreement between observed and modeled WSEs at Cordova is very good with median difference of 0.032 m (Table 2.3). The average difference (Observed - Modeled) between observed and modeled WSEs at GOUS is -0.076 m (ME in Table 2.3, negative sign indicates that modeled is larger than observed).

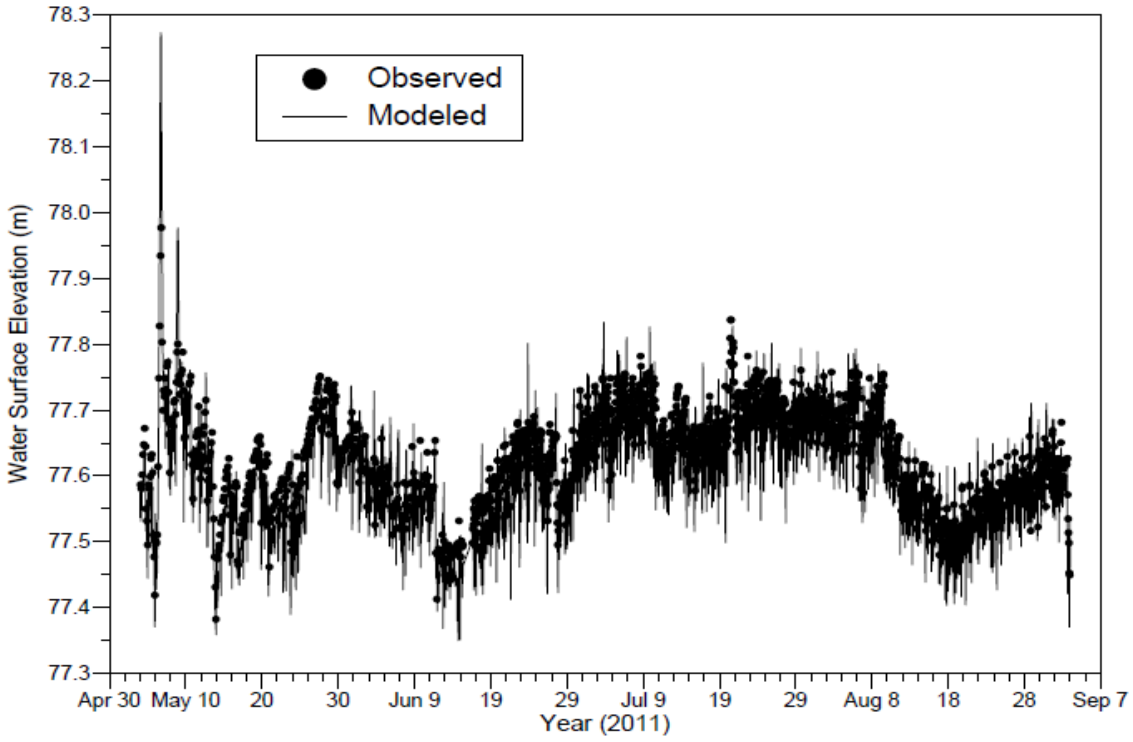

Fig. 2.3 Time-series plot of observed and modeled water surface elevations (m) at the monitoring station Cordova from 4 May to 3 September 2011.

Table 2.3 Statistics for model performance evaluation on water surface elevation (m) and water temperature (°C) simulations at the Cordova and GOUS monitoring stations.

Location	Observed Mean	Modeled Mean	ME	MAE	RMSE	RE (%)	RRE (%)
Water surface elevation (m)							
Cordova	77.633	77.605	-0.028	0.042	0.052	0.05	8.53
GOUS	77.670	77.587	-0.083	0.083	0.088	0.11	20.57
Water temperature (^{o}C)							
Cordova (Shallow)	20.19	20.29	0.10	1.41	1.87	6.97	13.33
GOUS (Deep)	19.94	19.38	-0.56	0.87	1.11	4.36	10.49

Note: ME is the mean error between observed and modeled, MAE is the mean absoluate error, RMSE is the root mean square error, RE is the relative error that is MAE divided by the observed mean, RRE is the relative RMSE error (Ji 2008) that is RMSE divided by the observed range (maximum – minimum).

Table 2.4 Calculated averages and ranges of flow rates and total volumes in the bottom and surface layers at MSF, Cordova and GOUS from June 1–5, 2011.

Locations	Average and range of flow rate (m^3/s)	Volumes towards downstream (m^3)	Volumes towards upstream (m^3)
MSF (Bottom [1])	2.95 (0.01–10.25)	938×10^3	1.9×10^3
Cordova (Bottom)	2.50 (0.01–8.64)	624×10^3	49.3×10^3
GOUS (Bottom)	1.95 (0.04–6.87)	485×10^3	56.7×10^3

Note: [1] for bottom layers, only positive flow rates, which mean the flow moving towards downstream (Bankhead L&D), were used to compute averages and ranges of flow rates.

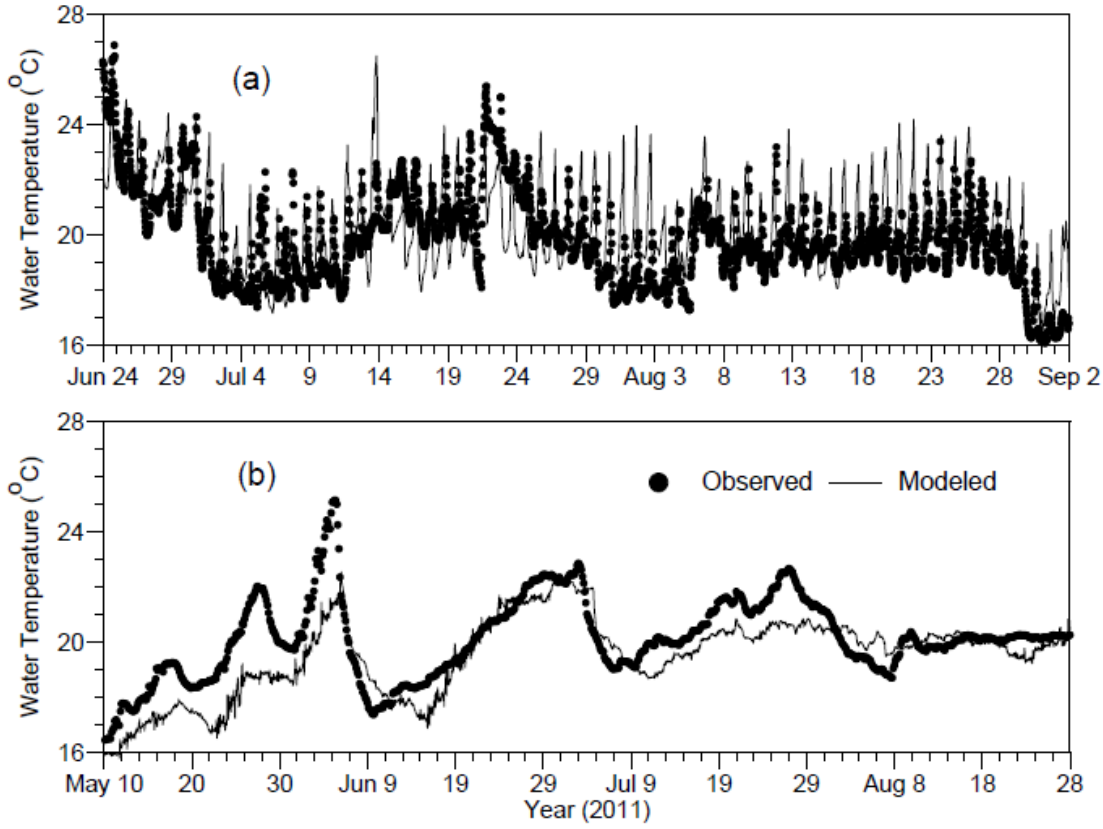

Fig. 2.4 Time-series plots of observed and modeled (a) surface water temperature (°C) at the Cordova monitoring station and (b) bottom temperature at GOUS (Fig. 2.1 and Table 2.2).

Observed temperatures at the USGS Cordova and GOUS monitoring stations were available from 10 May to 2 September for temperature calibration. Modeled surface temperatures at Cordova follow the trend of observed temperatures over time (Fig. 2.4a) reasonably well. Statistical summary of differences and absolute differences between observed and modeled temperatures at the two stations is given in Table 2.3. Fig 2.4b shows that modeled bottom temperatures at GOUS closely follow the pattern of

the variation of observed bottom temperatures. There are several periods of measured bottom temperature drops at GOUS: a drop from 22.0 to 19.8 °C between Julian Day 148 and 150 (28–30 May, 2011), a drop from 25.1 to 17.3 °C between Julian Day 156 and 161 (5–10 June, 2011), a drop from 22.8 to 19.7 °C between Julian Day 183 and 189 (2–8 July, 2011), etc. The EFDC model predicted the magnitude and duration of those temperature drops with reasonable accuracy. Average and absolute differences between observed and modeled bottom temperatures at GOUS are 0.56 and 0.87 °C (Table 2.3), respectively. It is essential and very important that the EFDC model can accurately predict the bottom temperatures at GOUS because they are directly related to how the model can accurately predict the density currents along the river bottom, which is the focus of the study and presented in the next section.

In June 2011, flow velocities at Cordova were measured from 22 June, 10:50 AM, to 23 June, 9:25 AM (approximately one day) using Acoustic Doppler Current Profiler (ADCP). The ADCP data were processed using a velocity mapping software VMS (Kim et al. 2009) to obtain cross sectional average velocities and discharge (Fig. 2.5), which were compared with modeled results at Cordova from the EFDC model. Negative velocity in Fig. 2.5a indicates the flow direction from downstream towards upstream. Visually, modeled mean velocities matched reasonably well with observed mean velocities (Fig. 2.5a). Modeled and measured discharges match reasonably well and exhibit the response of the large release from Smith Dam from 22 June, 5:00 PM, to 7:00 PM (lasted 2 hours with a flow rate of 143.13 m^3/s). It can be inferred that the discharge at Cordova started to increase roughly 2.5–3.0 hr after the large release at Smith Dam.

Observed peak discharge at Cordova was about 70 m^3/s (attenuated from 143 m^3/s) and the discharge wave (increasing and decreasing) moving towards downstream lasted about 9 hours at Cordova in response to the two-hour release at Smith Dam.

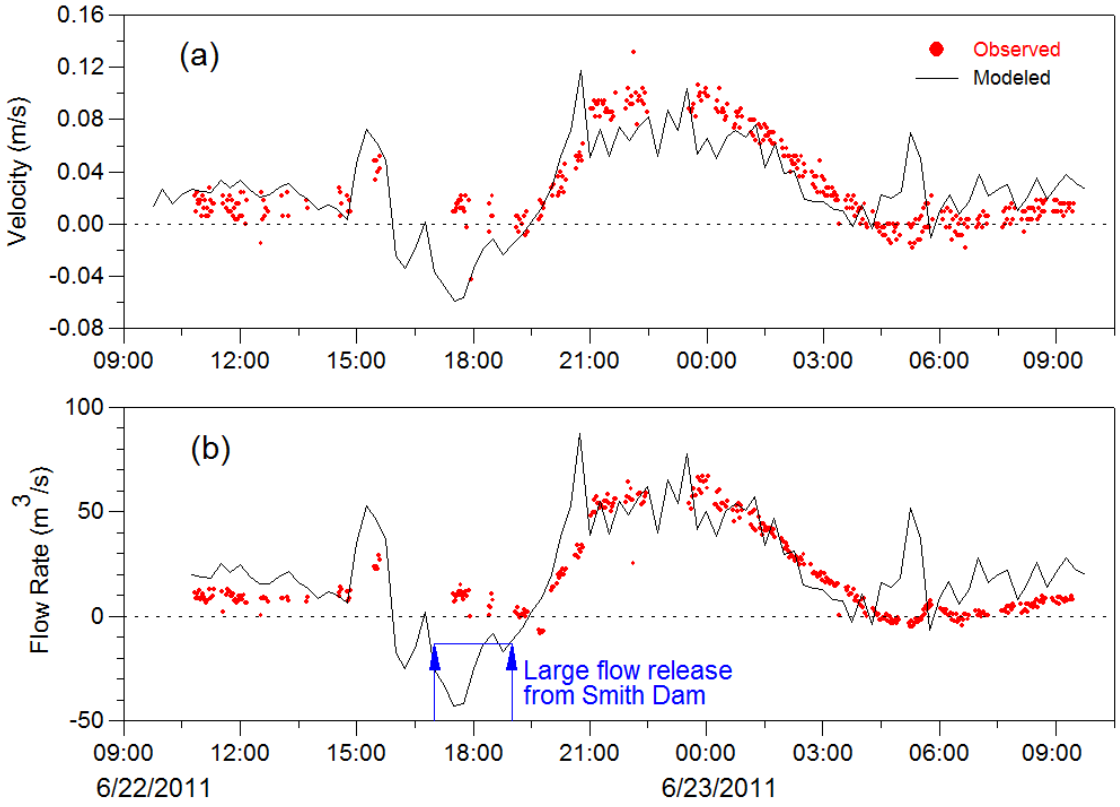

Fig. 2.5 Time-series plots of observed and modeled average velocity and total discharge at the cross section of Cordova.

2.5 Simulation Results of Flow Properties and Density Currents

2.5.1 Velocity and Flow Variations

An in-depth analysis of observed data and EFDC modeled results at various locations of BRRS were conducted to understand flow properties and dynamics (formation and propagation) of density currents under different flow releases from Smith Dam. Fig 2.6 shows time-series of (a) modeled cross sectional average velocity and water depth, (b) modeled flow rates in the surface (the 10th layer in EFDC model) and bottom (the 1st layer) layers at MSF (Table 2.2) from 31 May to 4 June, 2011, including the flow releases from Smith Dam. Simulated depth averaged velocity at MSF reached 0.48 m/s during each large release but had very small magnitudes (~ < 0.05 m/s) during the constant small release (2.83 m^3/s). Simulated water depth at MSF was about 4.7 m during small release and increased to 6.3–6.6 m after large releases (Fig. 2.6a). For each release, average velocity at MSF followed closely with the release pattern and reached more or less constant velocity shortly after the release started, but the water depth continuously increased and reached the maximum level shortly after the end of the release (Fig. 2.6a). Therefore, the flow rates at the surface and bottom layers also continuously increased and reached the maximum values shortly after the end of the release (Fig. 2.6b). The positive discharges meant the flow direction was from upstream (SDT) to downstream (BLD).

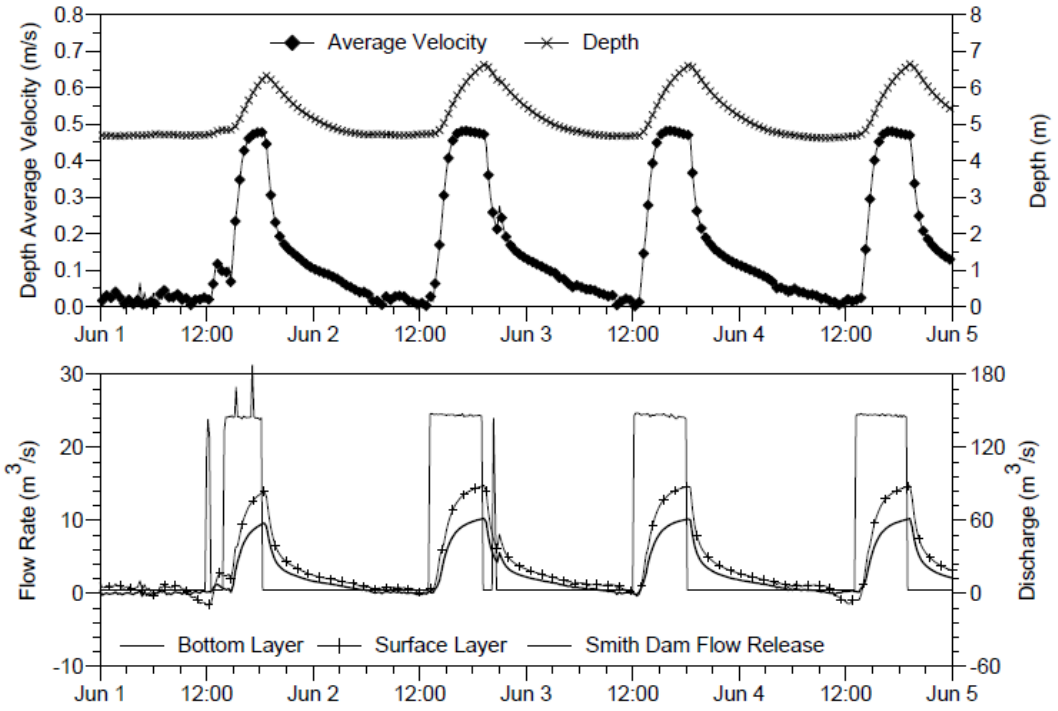

Fig. 2.6 Time-series of (a) modeled cross sectional average velocity and water depth, (b) modeled flow rates in the surface, and bottom layers at the middle of Sipsey Fork from May 31 to June 4, 2011 including the release from Smith Dam.

When there was a daily large flow release from Smith Dam at or after the noon, MSF responded with the increase of flow rate relatively quickly. For example, the release on 2 June started at 12:10 pm, the flow rate increase started at 1:00 pm (50 minutes later) and the maximum flow rates in the surface and bottom layers occurred at 6:25 pm when the release stopped at 6:00 pm (Fig. 2.6). Water depth, velocity, and flow rates gradually and steadily decreased with time after the release stopped, and the recession lasted more than 12 hours (e.g., lasted up to 6:00 am on 3 June for the release on 2 June). The flows in different layers at MSF were from upstream towards

downstream most of the time, but there were short periods (1–3 hours) with negative surface flows (Fig. 2.6b), i.e., from downstream towards upstream but bottom water still flows from upstream towards downstream.

Fig. 2.7 shows time-series of simulated water surface elevations (WSEs) and cross sectional average velocities (m/s) at the MSF, UPJ, MJC, Cordova, and GOUS (Fig. 2.1c and Table 2.2) after daily large releases from 3–9 June, 2011. The distance from UPJ and MJC is 11.1 km. The water surface levels at MSF and UPJ had direct responses (rise ~2 m at MSF and then fall) from each release of ~140 m^3/s, but water surface levels at MJC, Cordova and GOUS showed more complex interactions (fluctuations) between upstream releases and backwater effects from BLD. The releases on 6–7 June were much larger (~ 280 m^3/s) and resulted in ~0.5 m rise of WSE at MJC also. Both time series of WSEs and average velocity show that the response of each release lasted 4–6 hours was about 20–24 hours at MSF, UPJ, and MJC. Due to the backwater effect from BLD, average velocities at Cordova and GOUS had two rises and falls with certain fluctuations afterwards for those daily releases of ~140 m^3/s. On 7 and 8 June, average velocities at Cordova and GOUS also increased and then decreased with time when the flow releases was up to 287 m^3/s. Simulated flow rate at each individual layer (shown in Fig. 2.8) provides more information on flow dynamics at different locations.

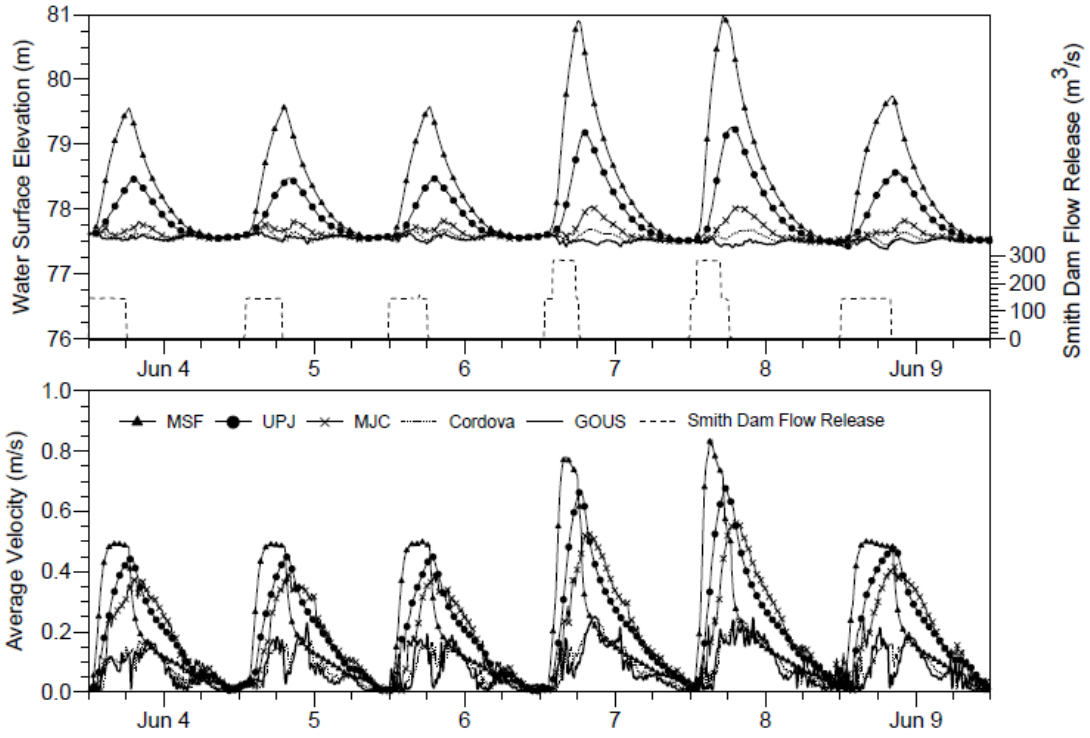

Fig. 2.7 Time-series of modeled cross sectional average velocities (m/s) at MSF, UPJ, MJC, Cordova, and GOUS (Table 2) after daily large releases from June 3–9.

Modeled flow rates in the bottom layer and surface layer at Cordova and GOUS monitoring stations (Fig. 2.8) exhibited much more variations than flow rates at MSF (Fig. 2.6), which were closely related to the release from Smith Dam. When there was a daily large flow release from Smith Dam, Cordova and GOUS responded with surface-layer flow rate changing from moving upstream (SDT) to moving downstream (BLD) roughly 2–3 hours after the release. There were no flow releases on 30 and 31 May (Fig. 2.8), the flow rates in the bottom layer at Cordova and GOUS were very small and moved either upstream or downstream (Fig. 2.8). After each flow release (especially on 2–4 June), the positive flow rates in the bottom layer indicate the obvious increases of flow

moving downstream. The cumulative effects of daily releases were clearly shown at Cordova: the bottom water flux after 1:00 pm on 4 June (after two daily releases) moved downstream all the time, and before that time the bottom water moved either upstream or downstream. These daily releases promoted and enhanced the movement of density currents moving from upstream towards downstream. The maximum flow rate moving downstream occurred few hours after the release stopped. This does not mean that released water from Smith Dam had reached Cordova and GOUS in a few hours after the release, but these flow rate increases occurred due to the momentum transfer or effect due the large releases from Smith Dam.

For the surface flows at Cordova and GOUS, the maximum flow rates moving upstream were almost the same magnitudes as the maximum flow rates moving downstream (14–16 m^3/s). The surface flow moving upstream was due to the backwater effect from the downstream boundary–BLD after the flood wave resulted from the large release reached the downstream boundary. Fig. 2.8 shows that the surface water moved in the same or opposite directions of the bottom water at Cordova and GOUS. For example, from 2:45 am to 4:30 pm on 4 June (the period near two arrows in Fig. 2.8a) surface water dominantly moved upstream but bottom water (density current) moved downstream at Cordova, which formed a two-layer flow. The total duration of all releases form 1 June to 5 June (4 days) was 22.7 hours (23.6% of the time) and resulted in 92%, 75%, and 75% of the time with the bottom flow (denser and cooler water) moving from upstream towards downstream at MSF (Fig. 2.6), Cordova, and GOUS, respectively.

Average and ranges of flow rates moving towards downstream at the bottom layer at MSF, Cordova, and GOUS are summarized in Table 2.4. When the flow rate was

multiplied by the time interval for the data shown in Fig. 2.8, volume of bottom water moving downstream and upstream were calculated at MSF, Cordova, and GOUS from 1 June to 5 June and reported in Table 2.4. Calculated results in the bottom layers indicate that density currents in MSF moved faster than the currents at Cordova and GOUS. Even though there were small amount of bottom flow moving towards upstream, the density currents at the river bottom did dominantly move towards downstream when there are daily large flow releases.

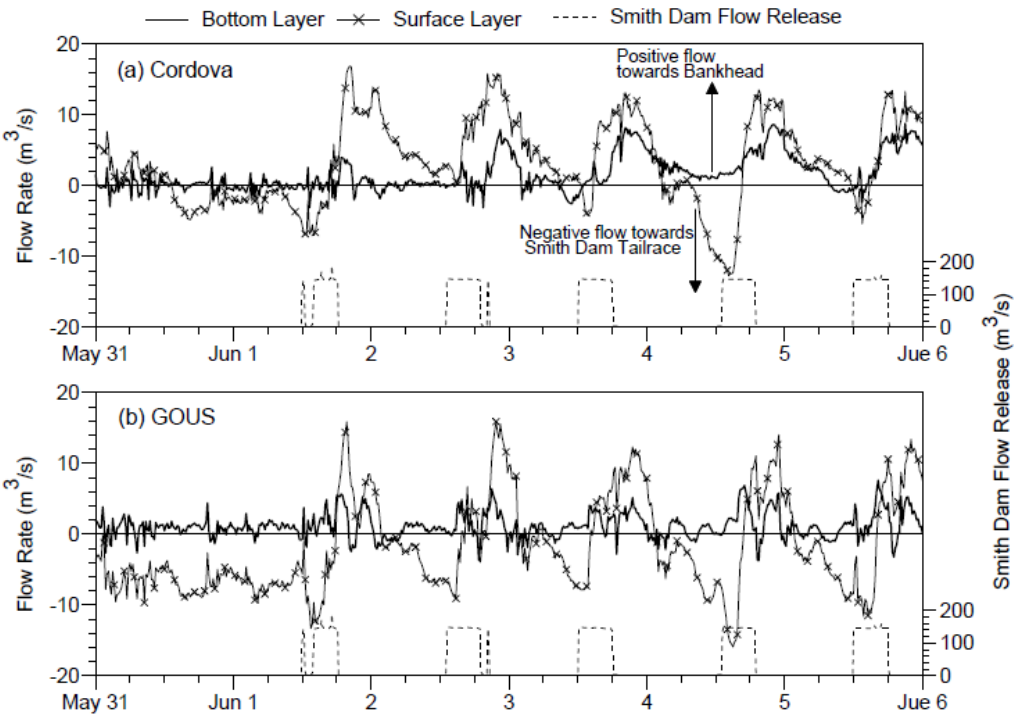

Fig. 2.8 Time-series of modeled flow rates (major y axis, -20–20 m^3/s) in the surface and bottom layers at the Cordova and GOUS monitoring stations including the release from Smith Dam (the secondary y axis with a different scale, 0–200 m^3/s).

Fig. 2.9 shows vertical velocity profiles at the centerlines of MSF, UPJ, MJC, Cordova and GOUS at 13:15 hr on 7 June (1 hr after the large release began), 22:15 hr on 7 June (4 hrs after the large release stopped) and 11:45 hr on 8 June (18 hrs after the large release stopped) in 2011. The release on 7 June lasted 6 hrs and had the maximum flow of 287 m^3/s at SDT (Fig. 2.7). When the large flow was released for 1 hr from Smith Dam, the flow momentum began to affect the velocities at MSF where all water moved downstream (positive velocity) with the maximum velocity 0.22 m/s at the surface. The velocities at UPJ, MJC and Cordova indicate that the flow momentum effect did not reach there yet and velocities were small and moved towards downstream or upstream (negative velocity). At the GOUS, the velocities were negative at the surface layer (-0.15 m/s) which means surface flow moved towards upstream due to the backwater effect from the downstream because of the large release on 6 June. The bottom velocities were positive because the density current or flow momentum effect might reach GOUS from the previous day release. When the large flow release stopped for 4 hrs, the flow momentum came close to GOUS when the surface and bottom velocities at GOUS began to increase. The velocities at all 5 different locations were all positive showing that the entire flow was moving downstream. The velocities increased to 0.4 m/s for the surface layer at MJC. When the large flow release stopped for 18 hrs, the velocities at MSF decreased to less than 0.06 m/s, but the velocities were all positive at MSF this may be due to the small constant flow release from the Smith Dam or no backwater effect yet. There were more complex flow dynamics at UPJ, MJC, Cordova, and GOUS. The small constant flow could not produce strong flow momentum effect on downstream locations but formed a density current along channel bottom due to lower release temperature,

which is indicated by positive velocities at the bottom layers at UPJ. Small negative surface velocities at UPJ might indicate backwater effect reached there.

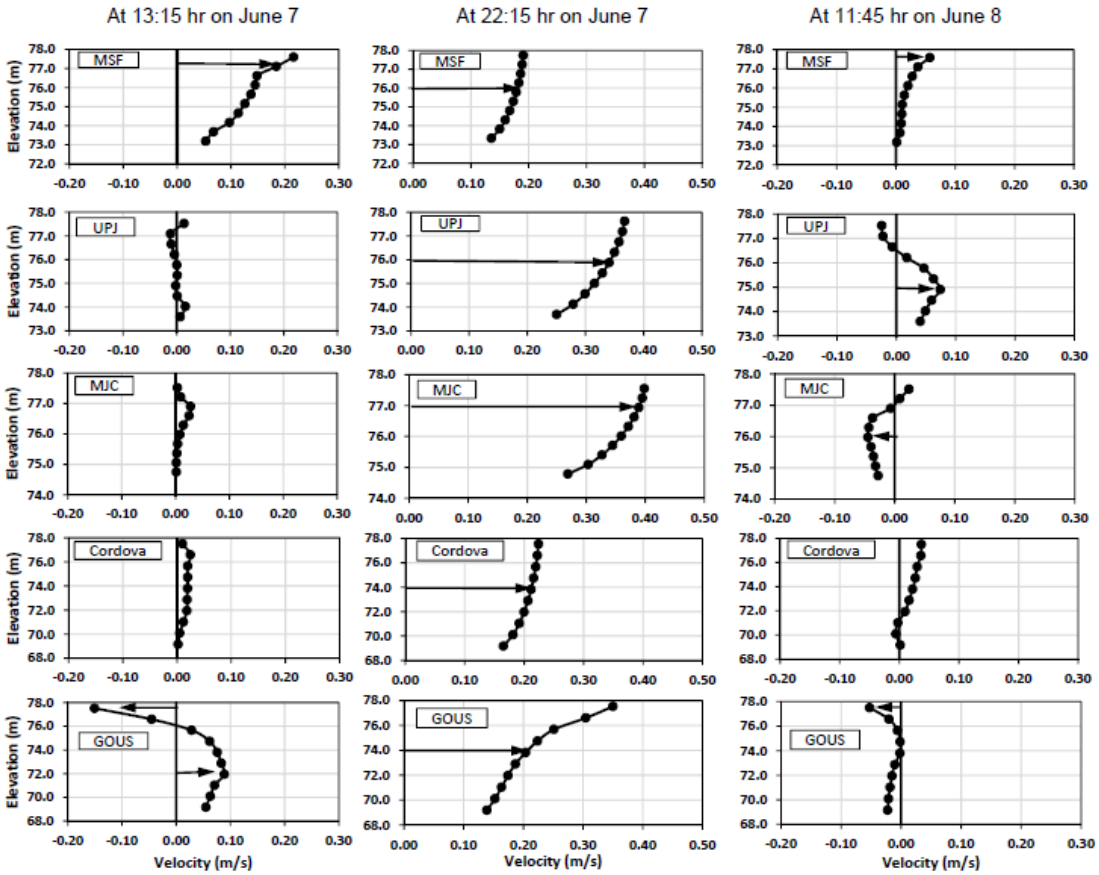

Fig. 2.9 Vertical velocity profiles at the centerlines (10 layers/cells along depth) of MSF, UPJ, MJC, Cordova and GOUS at 13:15 hr on June 7 (1 hr after the large release began), 22:15 hr on June 7 (4 hrs after the large release stopped) and 11:45 hr on June 8 (18 hrs after the large release stopped) in 2011. Zero velocity is indicated by a vertical line. Positive and negative velocities mean the flow moving downstream (from SDT to BLD) and upstream (from BLD to SDT), respectively.

2.5.2 Temperature Distributions at BRRS

The flow releases from Smith Dam resulted in not only complex flow variations in BRRS but also complex and interesting temperature dynamics and distributions. Fig. 2.10 shows temperature distributions along the channel centerline at BRRS from SDT to GOUS at three different times after a large release on 7 June, 2011: (a) 1 hour after the large release started (13:15 hr), (b) 4 hours after the large release stopped (22:15 hr), and (c) about 18 hours after the large release stopped. The duration of the large release on 7 June was 6 hours (Fig. 2.7, from 12:15 to 18:15 hr). The water surface elevation increased from < 78 m (a normal condition similar to that in Fig. 2.10c just before the next large release) to about 82 m at SDT at 13:15 (Fig. 2.10a). The flow momentum pushed colder water downstream about 9 km that is close to the MSF. There are temperature stratifications downstream the MSF due to solar heating and backwater effect (flow) from BLD (Fig. 2.10a). At 4 hours after the release stopped, the effect of flow momentum seemed to reach GOUS where is about 64 km downstream from SDT (Fig. 2.10b). The water surface elevation dropped to 79.25 m at SDT. It shows there was almost no thermal stratification from SDT to GOUS due to mixing effect of the flow momentum during the large release and no solar heating during the night. There were temperature gradients from SDT (~12 ^{o}C) to GOUS (~20 ^{o}C) as large flow momentum with colder water pushed warmer water in BRRS downstream. Fig. 2.10c at 11:45 hr on 8 June shows the temperature stratifications were developed almost everywhere after the large release stopped for 18 hours, which gives temperature distribution just less than 1 hour before the next large release on 8 June. The water surface elevations were almost same (77.63 m) from SDT to GOUS when there was no large release effect. The small

constant inflow (2.83 m^3/s) after the large release still pushed the cold water downstream, but the density current near SDT moved very slowly and did not have much effect on water movement further downstream. The cold-water current (blue color) near SDT just moved about 3 km over 18 hours of small flow release.

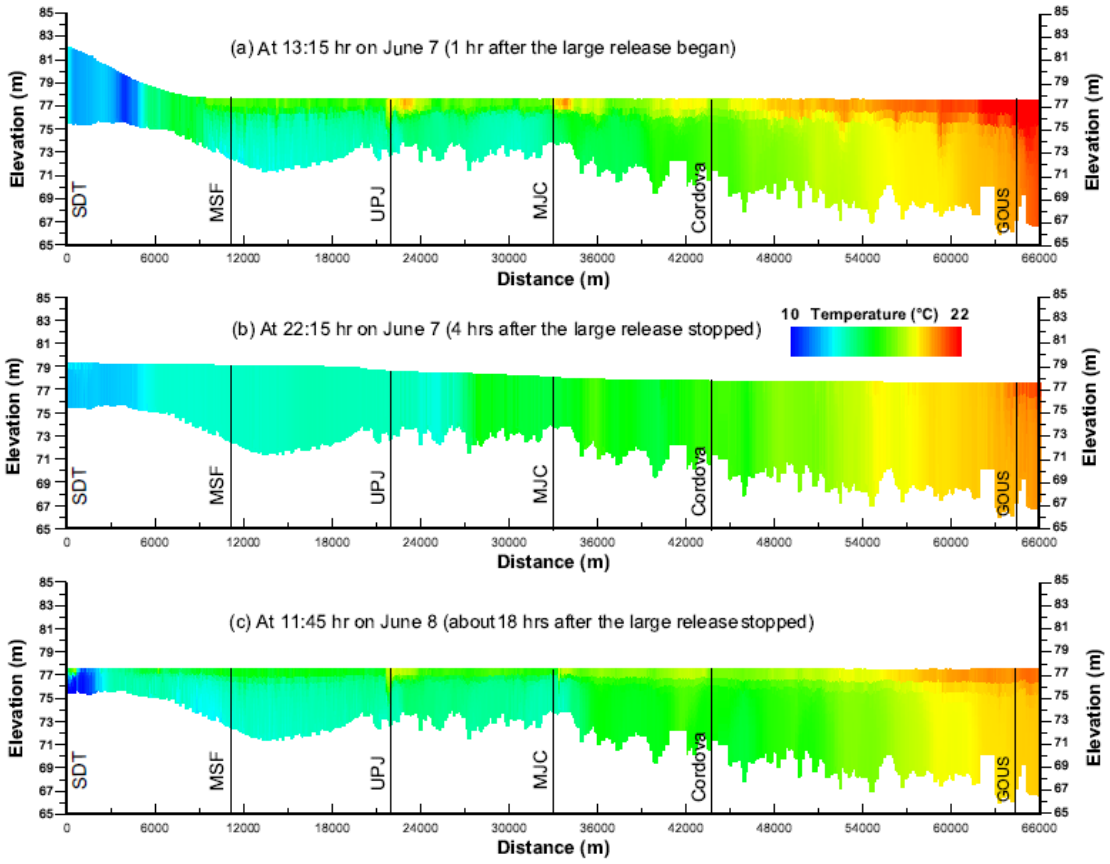

Fig. 2.10 Simulated temperature distributions (contours) along the channel centerline of BRRS from SDT to GOUS at three different times after a large release on June 7, 2011: (a) 1 hour after the large release started, (b) 4 hours after the large release stopped, and (c) about 18 hours after the large release stopped.

2.5.3 Temperature Variations at Sipsey Fork

Fig. 2.11 shows time-series of air temperature at the Birmingham airport and modeled surface and bottom temperatures (15-minute model output) at MSF from 31 May to 4 June, 2011, including flow releases (m^3/s) and temperatures (^oC) measured at SDT. When there were no large releases from Smith Dam on 30 and 31 May (Fig. 2.8), temperature stratification of 5.5 ^oC between surface and bottom layers was developed on 1 June (Fig. 2.11). There was a short release that lasted for 23 minutes starting from 12:00 pm on 1 June, but the release did not have significant impact on the thermal stratification at MSF (Fig. 2.11). The second release of 141.7 m^3/s on 1 June started from 2:00 pm and lasted for 4 hours and 20 minutes (4.33 hours). The flow momentum created by the second release significantly reduced the thermal stratification at MSF (temperature became more or less well mixed). The period of completely mixed condition (assuming surface and bottom temperature difference < 0.5 ^oC) started from 3:45 pm on 1 June to 7:00 am on 2 June (lasted 15 hours and 15 minutes). The well-mixed condition at SDT was developed immediately after the large release from Smith Dam, but the well-mixed condition at MSF was developed 1.75 hours after the release started. It would take about 6 hr to travel 10.9 km with 0.48 m/s velocity (Fig. 2.6) from SDT to MSF but actually the velocity decreased from 1.41 m/s at SDT to 0.48 m/s at MSF; therefore, it only took less than 2 hours to develop the well-mixed condition at MSF. Water temperatures at MSF decreased from 20.9 ^oC at 3:45 pm to 12.9 ^oC at 6:20 pm (end of the release) because the release had a water temperature of 12 ^oC, and then remained more or less constant temperature up to 7:00 am on 2 June because of lack of

solar heating during the night. Surface temperature at MSF started to increase after 7:00 am due to solar heating and convection/conduction with warm air temperature and reached a maximum temperature of 17.7 ^{o}C at 12:50 pm on 2 June when air temperature increased from 23.9 to 36.7 ^{o}C. Water temperature in the bottom layer at MSF stayed more or less constant with small decrease. The temperature stratification at MSF reached 5.4 ^{o}C before the next daily release on 2 June.

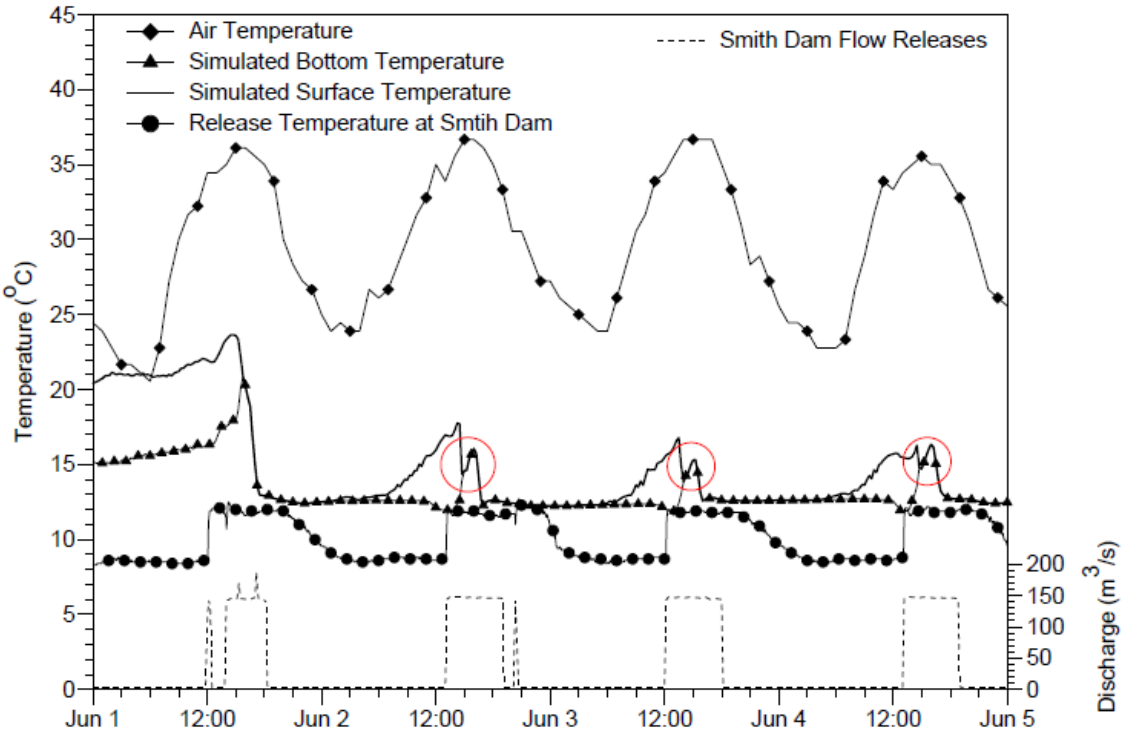

Fig. 2.11 Time-series of modeled surface and bottom temperatures at MSF from May 31 to June 4, 2011 including air temperature at Birmingham, release flow and temperature measured at SDT.

The similar process described above repeated for other large releases (Fig. 2.11). For example, for the release on 3 June, well-mixed temperature occurred at 2:45 pm, which corresponded to the flow increase at 1:00 pm (Fig. 2.11). Without large releases for more than 2 days before 1 June, surface temperature reached a maximum value of 23.6 ^{o}C, and with a large release each day after 1 June, the maximum surface temperatures at MSF only reached 16.2–17.7 ^{o}C. After a few hours of heating, maximum temperature differences at MSF reached 3–5 ^{o}C before the stratification was removed by the next release. Both surface and bottom water temperatures at MSF increased with time over 1–2 hours due to solar heating (circled by three red circles in Fig. 2.11) after the completely mixing occurred, and then decreased with time to about 12.5 ^{o}C.

Time series of modeled surface and bottom temperatures at MSF from 21 May to 10 June (Fig. 2.12a) show the comparison of temperature variations at MSF with and without daily large releases from Smith Dam. From 21 May to 31 May there were four irregular large releases from Smith Dam that resulted in strong stratification between surface and bottom layers during day and night at MSF. The maximum temperature difference between surface and bottom layers was up to 5.9 °C in 26–29 May, 2011. Bottom temperatures at MSF steadily increased from ~13.0 °C to ~18.0 °C for the periods of 21–23 May, 26–29 May (13.9 to 17.9 °C), and 31 May–1 June. Although small constant release had a lower temperature of ~8.5 °C (Fig. 2.12), the release of 2.83 m^3/s could not overcome the temperature increases in Sipsey Fork due to solar heating. Surface temperatures at MSF increased with time with a few degrees of diurnal variations and maximum surface temperature reached 23.8 °C. When a large flow release from Smith Dam occurred at 2:00 pm on 23 May (lasted for 6 hours), the large flow

momentum completely mixed released water with warmer water in Sipsey Fork and caused higher surface temperature to decrease and lower bottom temperature to increase (Figs. 2.11 and 2.12). Three releases on 23–25 May resulted in bottom temperatures at MSF about 12.5 °C (Fig. 2.12). There was a short release starting at 8:00 pm on 29 May and lasting for only one hour (Fig. 2.12). As a result of this 1-hr release, bottom temperatures at MSF dropped from 19.8 °C (after more or less completely mixing) to 13.5 °C over 24 hour period, but surface temperatures at MSF started to increase after 5 am on 30 May. From 23 May to 1 June, the maximum and average temperature differences between surface and bottom layers were 7.1 and 4.4 °C excluding well-mixed periods resulted from four irregular large releases. With daily regular releases from 1 June to 9 June (Fig. 2.12a), the maximum and average temperature differences between surface and bottom layers were 5.3 and 2.4 °C (excluding well-mixed periods). Fig. 2.12a clearly shows regular daily large releases did maintain relatively lower water temperatures at the bottom layers that promoted the density current formation at further downstream of Sipsey Fork, but solar heating resulted in water temperature increases at the surface layer before the next large release.

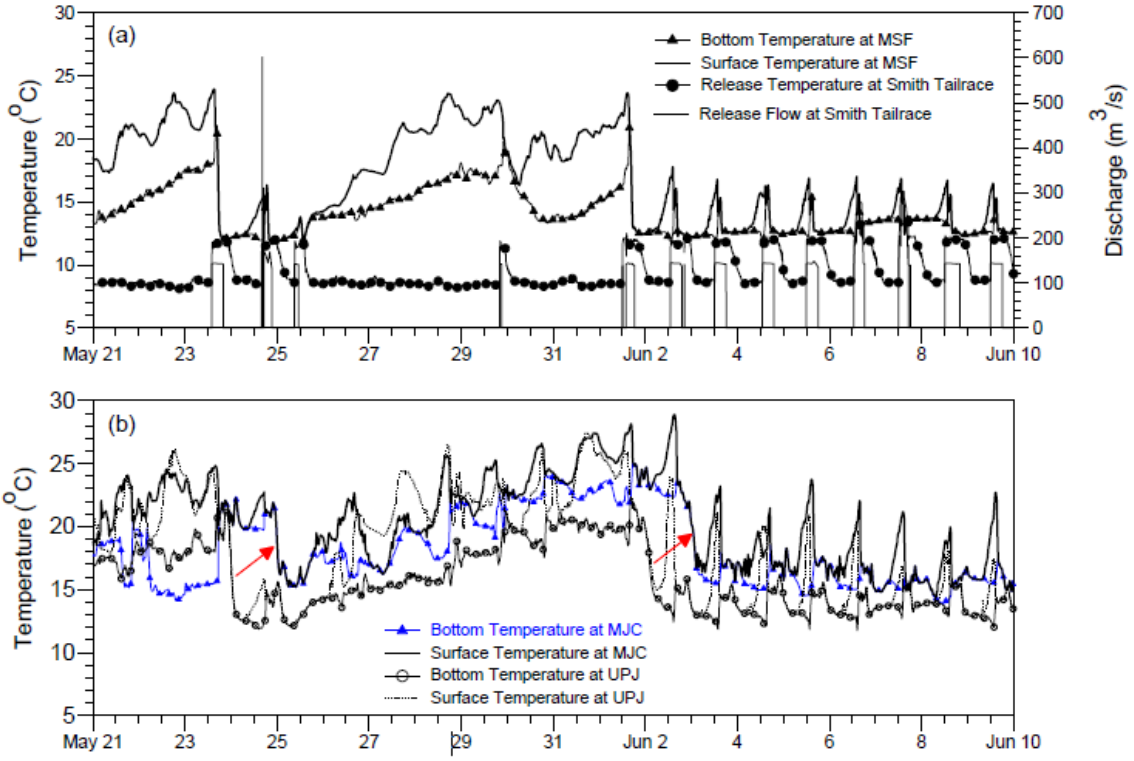

Fig. 2.12 Time-series of modeled surface and bottom temperatures at the middle of Sipsey Fork, upstream of the junction and downstream of the junction from May 22 to June 11, 2011 including release flow and temperature measured at Smith Tailrace.

2.5.4 Temperature Variations at UPJ and MJC

Fig. 2.12b shows simulated surface and bottom temperatures at UPJ and MJC (Fig. 2.1). Surface temperatures at UPJ and MJC had distinct diurnal variations (Fig. 2.12b). From 21 May to 1 June, the maximum and average temperature differences between surface and bottom layers at UPJ were 9.7 and 4.4 °C. During these 11 days, there were about 77% of the time with temperature differences greater than 0.5 °C and

23% of the time with well-mixed conditions resulted from four irregular large releases. With daily regular releases from 1 June to 9 June (Fig. 2.12b), the maximum and average temperature differences between surface and bottom layers at UPJ were 10.7 and 3.5 °C (excluding well-mixed periods), but during these 8 days, there were only 30% of the time with temperature differences greater than 0.5 °C and 70% of the time with well-mixed conditions at UPJ.

In an attempt to closely examine the impact of each large release from Smith Dam on surface and bottom temperatures at downstream locations, Fig. 2.12b shows interesting information of the movement of well-mixed flows after the releases (see Fig. 2.10b). The large release on 23 May resulted in the well mixed conditions with sharp temperature drop at MSF and UPJ just a few hours after the release, but the same condition at MJC occurred around the middle night of 25 May. This block or trunk of well-mixed water took more than 24 hours to travel from SDT to MJC (33 km distance). The same phenomenon occurred for the release on 1 June (indicated by two red arrows for these two situations).

The daily releases from Smith Dam on 2–10 June created the well-mixed conditions in MSF in a few hours and stratification occurred in the next day with higher temperatures due to the solar heating (Fig. 2.12a). These daily releases occurred about 1-2 hours after the noon, the well-mixed conditions then occurred in the same afternoon and during the night at UPJ, and thermal stratification occurred in the next day due to solar heating of surface waters (Fig. 2.12b). Bottom temperatures at MJC (blue line with triangles) are typically higher than bottom temperatures at other upstream locations (MSF

and UPJ shown in Fig. 2.12), which means solar heating can penetrate and reach the deeper waters near the river bottom (Fig. 2.12b).

2.5.5 Temperature Variations at Cordova

Fig. 2.13a shows time-series of modeled surface and bottom temperatures at the USGS Cordova monitoring station including release flow (m^3/s) from Smith Dam and other tributary flows from 11 April 11 to 28 October, 2011. It clearly shows how strong temperature stratification existed between surface and bottom temperatures at Cordova. It seems that temperature stratification was much larger when there was only small constant release from Smith Dam. During large rain fall events (15–31 April and 6–8 September), surface and bottom temperatures were completely mixed due to runoff and streamflow from tributaries and watersheds.

Fig. 2.13b was zoomed into a short period—from 21 May to 10 June, 2011 to further illustrate simulated temperature stratification at Cordova. Simulated temperature stratification between surface and bottom layers at Cordova was up to 11.4 °C with an average temperature difference of 1.53 °C and standard deviation of 1.94 °C under actual flow releases from Smith Dam. Twenty five percent (25%) of simulated surface and bottom temperatures at Cordova had temperature stratification less than 0.17 °C from 11 April to 28 October, 2011. The more or less completely mixed condition occurred around midnight of 3 June at Cordova (Fig. 2.13b, pink circle) that was about 1.5 days after the release from Smith Dam on 1 June. The density current created from the flow release on 1 June seems to have travelled about 36 hours before it reached Cordova. The

1-hour flow release occurred on 29 May did show its impact in Sipsey Fork (Fig. 2.12a), but it showed no impact on temperature stratification at Cordova (Fig. 2.13).

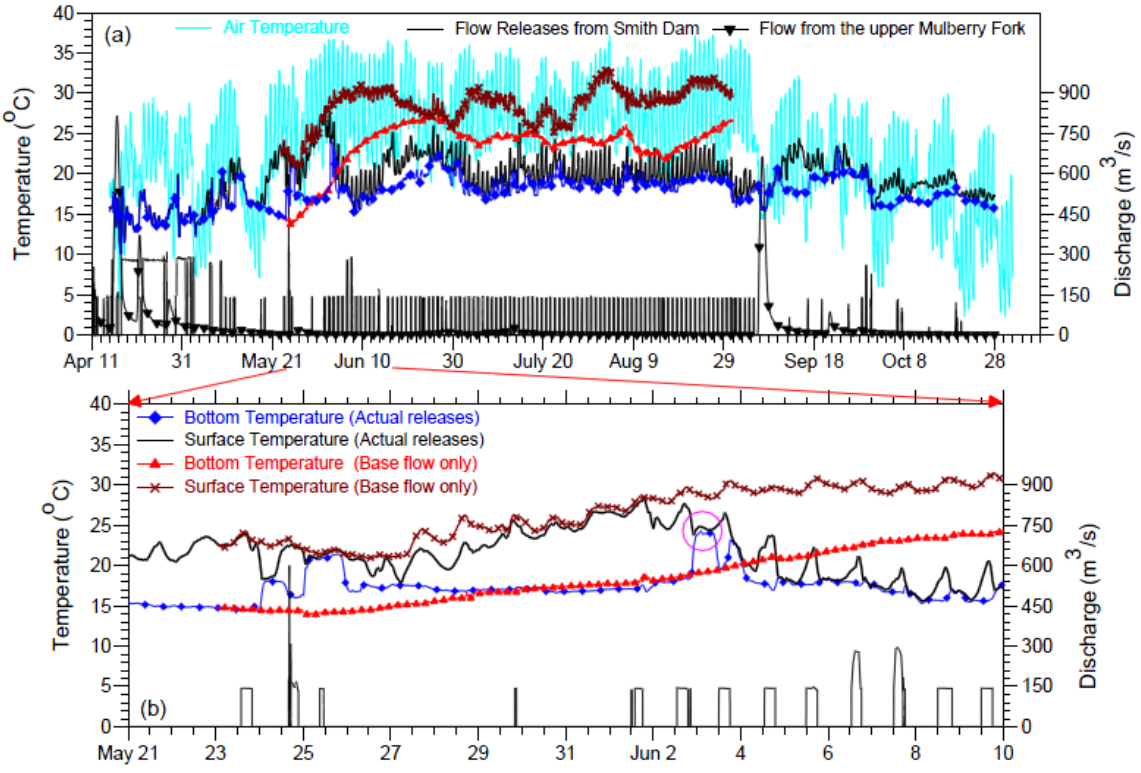

Fig. 2.13 (a) Time-series of air temperature, modeled surface and bottom temperatures at the USGS Cordova monitoring station under actual releases and base flow only, tributary inflow, release flow (m^3/s) from Smith Dam from April 11 to October 28, 2011. (b) Zoom in from May 21 to June 10, 2011 including modeled deep depth temperatures with base flow release (2.83 m^3/s) from Smith Dam.

Fig. 2.13b shows that diurnal variations of surface temperature at Cordova were smaller (about a few degrees). Some sudden surface temperature decreases and bottom temperature increases shown in Fig. 2.13b were due to sudden flow releases from Smith

Dam, as explained using Figs. 2.10– 2.11. These temperature decreases and increases at Cordova responded with two releases between 23–24 May in ~12 hours, but responded with the releases between 1–2 June in more than 24 hours. These different responses were not well understood yet; but they might be related to the strength of stratification at Cordova before each release.

Fig. 2.13 also compares modeled surface and bottom temperatures at Cordova in 2011 under actual releases (constant release plus intermittent large releases) and assumed small constant or base flow (2.83 m^3/s) release only from Smith Dam. The simulation for base flow only is from 23 May to 30 August, 2011. It clearly shows that simulated bottom temperatures could keep on increasing before 25 June and surface temperatures are higher and follow with air temperature when there were no intermittent large releases from Smith Dam. Simulated maximum bottom temperature is 27.2 ^oC under base flow scenario and 24.3 ^oC under actual releases, which occurred on 3 June (Fig. 2.13b) resulted from the large release on 1 June. Under the base flow scenario, simulated average difference of surface and bottom temperatures is 8.0 ^oC (50% differences are greater than 5.3 ^oC), but under actual releases, average difference is 2.0 ^oC (only 25% differences are greater than 3.0 ^oC), even though the maximum surface and bottom temperature differences for both cases are the same (11.4 ^oC). Large releases on 23–25 May and 1–2 June actually resulted in higher bottom temperatures at Cordova when cooler bottom waters were completely mixed with warmer surface waters. Daily large releases starting from 1 June resulted in surface temperature decreased from 2 June (surface wave moving faster downstream) and bottom temperature decreased from 4 June (density currents at the bottom moving slowly downstream).

Statistical parameters for differences of surface or bottom temperatures simulated under the base flow only and actual releases are summarized in Table 2.5 for five locations (MSF, UPJ, MJC, Cordova, and GOUS) for the simulation period from 23 May to 30 August, 2011. Bottom temperatures at Cordova and GOUS under the base flow only are on average 4.81 and 4.26 ^{o}C higher than bottom temperatures simulated under actual flow releases (base flow plus intermittent large releases). Under the base flow only scenario, simulated surface temperature at GOUS is up to 15.64 ^{o}C (Table 2.5) higher than surface temperatures under actual releases from Smith Dam in 2011. Therefore, intermittent large releases significantly reduced surface and bottom temperatures in BRRS in comparison to the base flow release.

Table 2.5 Statistics of differences of simulated temperatures (°C) at different locations from May 23 to August 30, 2011, between under the base flow only and using actual releases from Smith Dam.

Location	Maximum	Minimum	Average	Standard Deviation	25th percentile	Median	75th percentile
MSF (Bottom)	11.25	-3.58	7.05	1.68	6.26	7.16	8.05
MSF (Surface)	7.53	0.00	4.12	1.41	3.30	4.23	5.13
UPJ (Bottom)	12.71	-2.23	7.31	2.46	6.27	7.75	9.08
UPJ (Surface)	8.94	-0.04	3.52	1.37	2.55	3.48	4.41
MJC (Bottom)	13.13	-7.12	6.36	3.15	4.56	6.94	8.56
MJC (Surface)	9.65	-0.04	2.62	2.10	0.79	2.30	4.05
Cordova (Bottom)	9.78	-7.37	4.81	2.80	4.16	5.46	6.65
Cordova (Surface)	14.29	-0.34	7.95	3.31	5.75	8.72	10.47
GOUS (Bottom)	8.88	-2.44	4.26	2.33	3.69	4.75	5.64
GOUS (Surface)	15.64	4.62	10.52	1.94	9.58	10.72	11.70

2.5.6 Particle Tracking on Density Current Movement

In order to understand the propagation of density currents along the river bottom in BRRS, EFDC's particle tracking method (Craig 2011) was used to trace the movement of density currents. One thousand particles were released in the middle depth layer at two locations: SDT and MJC (Fig. 2.1), at the noon of 3 June (Julian Day 153.5) when a large release from Smith Dam started. Particle counts in a 5-minute interval were reported in all grids over the cross sections of MSF, UPJ, MJC, Cordova, and GOUS, which give number of particles in defined control volumes (e.g., the volume at MSF covers about 90 m of Sipsey Fork). The 1000 particles released at Smith Dam first travelled and arrived at MSF, and 347 particles were reported at MSF at 3:35 pm on 3 June. Because the 5-minute interval was used to report particle count, particles passed through MSF between 3:30 and 3:35 pm were unknown. Based on particle count distribution at MSF, average travel time for particles arriving at MSF was 3 hr 40 minutes. Based on surface and bottom temperature distributions at MSF shown in Fig. 2.11, well-mixed conditions at MSF first occurred at 2:00 pm (15-minute reporting interval). It seems that the momentum developed from the large release at noon on 3 June generated the movement and mixing of water at MSF before released water or particles actually reached MSF.

First, 90 particles reached UPJ at 10:35 pm, which gave the travel time for these particles traveling through Sipsey Fork from SDT to UPJ (21.8 km distance). Four hundreds forty seven particles reached MJC between 9:20–11:15 pm on 4 June, which meant it took about 33 hours for released water at SDT to travel BRR system and reach

MJC (32.3 km travelling distance). First 54 particles reached Cordova monitoring station between 9:15–9:45 pm on 5 June, hence it took more than 2 days (~57.5 hours) for these particles to travel through Sipsey Fork and the lower Mulberry Fork to Cordova (43.6 km distance). A few particles showed at GOUS at 12:05 am (just after midnight) on 7 June and more particles showed up at 6:00 pm on 7 June, which corresponds to more than 4 days for particles released on 3 June to reach GOUS.

For 1000 particles released from MJC at noon on 3 June, about 110 particles reached Cordova at 10:25–11:00 am on 4 June, and only 14 particles reached GOUS at 10:55–11:55 pm on 7 June. Above preliminary results using particle tracking show that particles or water released from Smith Dam could take significant time to reach Cordova and GOUS but the momentum developed by the large releases affected downstream locations relatively shortly after the releases. This is further explained using Fig. 2.7 that gives cross sectional average velocities at MSF, UPJ, MJC, Cordova and GOUS. After each daily large releases around noon from 4–9 June, typically within 2 hours after the releases velocities started to increase at all five locations, even Cordova and GOUS had the velocity increase within 3 hours after the releases. On 7 June, the large release at 3:00 pm was more than 280 m^3/s (Fig. 2.11a) and resulted in maximum velocities at MSF, UPJ, MJC, Cordova and GOUS of about 0.84 m/s. 0.67 m/s, 0.55 m/s, 0.24 m/s and 0.24 m/s, respectively. Time of peak velocity occurred earlier at upstream locations and later at further downstream locations, but the time of peak velocity at GOUS occurred about 7 hours after the release (not several days). Therefore, the momentum or push effect from the large release is the ultimate driving force for the density current movement at different locations along the river bottom in BRRS. Average velocities did

attenuate to small magnitudes within 24 hours at all cross sections (Fig. 2.7), which indicates daily regular releases are necessary to promote the movement or advancement of the density current towards downstream.

2.6 Summary and Conclusions

A three-dimensional hydrodynamic EFDC model was applied to simulate unsteady flow patterns and temperature distributions under various upstream releases and variable atmospheric forcing in BRRS. The calibrated EFDC model provided simulated water surface elevation, temperature, velocity and discharge at different layers (depths) for all grids in different cross sections (Fig. 2.1). Overall, the EFDC model was able to predict the temporal and spatial distributions of flow and temperature (Fig. 2.10) and revealed complex interactions and density currents due to dynamic upstream releases and solar heating from atmosphere. The major findings of the study are summarized as follows:

a) Simulated water depth, velocity, and flow rate in Sipsey Fork increased first, then gradually and steadily decreased with time after the release from Smith Dam, and the recession lasted more than 12 hours at MSF (Figs. 2.6–2.7). After a few hours of heating, maximum temperature differences at MSF reached 3–5 ^{o}C before the stratification was removed by the next release (Fig. 2.10). Simulation results clearly show that regular daily large releases did maintain relatively lower water temperatures at the bottom layers (Figs. 2.12–2.13) that promoted the density current formation at further downstream of Sipsey Fork. Strong temperature stratification existed between surface and bottom temperatures at Cordova (e.g., 26–31 May, Fig. 2.13) without daily releases

from Smith Dam. Simulated surface and bottom temperatures at Cordova kept on increasing first and then varied with air temperature trend when it was assumed that there were no intermittent large releases from Smith Dam.

b) The flow momentum created by the large release removed the thermal stratification at MSF. The well-mixed condition at MSF was developed at 1.75 hours after the release started. When there was a daily large flow release from Smith Dam, Cordova and GOUS responded with surface-layer flow rate changing from moving upstream (SDT) to moving downstream (BLD) roughly 2–3 hours after the release. The flow rates moving downstream in the bottom layer had obvious increases. These daily releases promoted and enhanced the movement of density current moving from upstream towards downstream.

c) Preliminary results using particle tracking show that particles or water released from Smith Dam could take several days to reach Cordova and GOUS, and the momentum developed by the releases did push the cooler water near the river bottom moving downstream. The momentum or push effect from the large release provides driving force for the density current movement along the river bottom in the BRR system.

Chapter 3. Sensitivity Analysis of Flow and Temperature Distributions of Density Currents in a River-Reservoir System under Upstream Releases with Different Durations

3.1 Abstract

A calibrated three-dimensional Environmental Fluid Dynamics Code model was applied to simulate unsteady flow patterns and temperature distributions in the Bankhead river-reservoir system in Alabama, USA. A series of sensitivity model runs were performed under daily repeated large releases (DRLRs) with different durations (2, 4, and 6 hrs) from Smith Dam Tailrace (SDT) when other model input variables were kept unchanged. The density currents in the river-reservoir system form at different reaches, are destroyed at upstream locations due to the flow momentum of the releases, and form again due to solar heating. DRLRs (140 m^3/s) with longer durations push the bottom cold water further downstream and maintain the bottom water temperature cooler. For the 6-hr DRLR, the momentum effect definitely reaches Cordova (~43.7 km from SDT). There are 48.4%, 69.0%, and 91.1% of time with positive bottom velocity (density currents moving downstream) with average velocity of 0.017, 0.042, and 0.053 m/s at Cordova for the 2-hr, 4-hr, and 6-hr DRLR, respectively. Results show that DRLRs lasting for at least 4 hrs can maintain lower water temperatures at Cordova. When the 4-hr and 6-hr DRLRs repeat more than 6 and 10 days, respectively, bottom temperatures at Cordova become lower than ones for the constant small release (2.83 m^3/s). These large releases

overwhelm the mixing effects due to inflow momentum and maintain temperature stratification at Cordova.

3.2 Introduction

A density difference can exist between two fluids because of a difference in temperature, salinity, or concentration of suspended sediment. A density current is kept in motion by the force of gravity acting on differences in density. Density currents in nature such as turbidity currents typically flow along the bottom of oceans or lakes or reservoirs. Many laboratory and numerical model studies of density currents have been conducted in the last several decades. Density currents have been studied in situ (Serruya 1974; Smith 1975; Carmack et al. 1979; Fischer and Smith 1983; Alavian and Ostrowski Jr 1992; Chikita 1992). Because it is quite challenging to study the density currents in the natural systems, the density currents are often investigated in the laboratory (Akiyama and Stefan 1984; Hauenstein and Dracos 1984; Alavian 1986). Most of the previous studies dealt with sloping channels and rectangular cross section. Various simplifying assumptions were made to develop analytical models with laboratory data to understand density currents (Singh and Shah 1971; Savage and Brimberg 1975; Denton 1985; Kranenburg 1993). Fang and Stefan (2000) developed an integral model for a discharge from a river channel over a horizontal or a sloping bottom into a reservoir or a lake to determine dilution up to plunging for density current computations. Using a series of laboratory experiments in a two-layered ambient stratification, Cortes and others (Cortés et al. 2014) developed a theory to predict the partition of the buoyancy flux into the interflow and underflow and how a gravity current splits in two upon reaching the sharp density step.

Two-dimensional hydrodynamic models were developed to study density current by assuming that the density current does not participate in the dynamics of heating and mixing but the entrainment takes place from the ambient reservoir into the downflow (Imberger and Patterson 1980; Buchak and Edinger 1984; Jokela and Patterson 1985). Gu (2009) used a validated two-dimensional (2D) simulation model CE-QUAL-W2 (Cole and Wells 2010) to quantify systematically the effects of inflow and ambient parameters on the behavior of a density-induced contaminant current in various flow regimes in a stratified reservoir through numerical experiments. The k-ε turbulence model has been applied to study density currents plunging into reservoirs (Farrell and Stefan 1986; Fukushima and Watanabe 1990). Bournet (1999) developed the modified k-ε model with buoyancy effects to describe the characteristics of density currents in terms of plunge point and entrainment in an inclined channel of constant width and then in a diverging channel. Soliman and others (Soliman et al. 2014) developed a 2D multi-phase numerical model for incompressible, immiscible, and variable density fluids based on Navier-Stokes equations. Shlychkov and Krylova (2014) proposed a numerical model for studying the dynamic mixing of sea and river waters in estuary areas, which is based on 2D longitudinal vertical stratified fluid mechanics equations and an equation of salt transport.

Several studies about three-dimensional (3D) gravity currents have been conducted recently using laboratory data and numerical models (Imran et al. 2007; Firoozabadi et al. 2009; An and Julien 2014). In the last several decades, 3D Environmental Fluid Dynamics Code (EFDC) (Hamrick 1992) has been widely used in modeling river, estuarine and coastal hydrodynamics and transport processes. Hamrick and Mills (2000) developed and used the EFDC model to simulate thermal transport and

water temperature distributions in Conowingo Pond that was influenced by thermal discharges from the Peach Bottom atomic power plant. In order to quantify numerical and modeled entrainment, Kulis and Hodges (2006) explored the grid resolution required in EFDC to capture gravity current motions in an idealized basin with and without a turbulence closure. Their study was based on the underflow from Oso Bay into Corpus Christi Bay in Texas, USA. Liu and Garcia (2008) used modified 3D EFDC model to simulate the density current and bi-directional flows in the Chicago River system. Xie et al. (2010) used a calibrated 3D EFDC model developed for Yangtze River estuary to study the migration behavior of the movement of fine silt particles in dumped silt. Lyubimova et al. (2014) used 3D numerical simulations and in situ measurements to study the upstream propagation of vertical stratification of water mineralization, which is observed only under small (200 m^3/s) or moderate (700 m^3/s) seasonal flow rates but absent when flow rates in the rivers is larger than 1400 m^3/s. Do An (2014) used the Flow-3D (Hirt and Nichols 1988) model to simulate the propagation dynamics of density currents under the same conditions as the laboratory experimental setup and focused on the intrusive density flows into a two-layer ambient fluid.

There are many studies about flow in natural systems such as flows from a river into a lake, a reservoir, an ocean, or an estuary. Fatih and Varcin (2012) developed a mathematical model solving nonlinear, unsteady continuity, momentum, energy, and k-ε turbulence equations and applied the model to successfully simulate the formation of density currents and plunging flow in Eğrekkaya Dam Reservoir. Wells and Nadarajah (2009) presented theory and laboratory experiments describing the intrusion depth of a density current into a linearly stratified water column. They concluded that, if the

buoyancy flux of a dense current was to double while the stratification in ambient water remained constant, then the intrusion depth would only increase 25%, whereas doubling the stratification would result in a 50% decrease of the intrusion depth. Soliman and others (Soliman et al. 2014) applied the 2D multi-phase numerical model to simulate the density current propagation and salinity intrusion into Ohashi River that connects Nakaumi and Shinji coastal lakes and concluded the further refinement of the model is needed for field study application. Biton and others (Biton et al. 2008) studied density current formation and flow dynamics in the northern Gulf of Eilat, Red Sea, and demonstrated the intrinsic nonlinearity of density currents, which is poorly represented in the general circulation model, affect properties of simulated density currents. Owens et al. (2012) provided hourly measurements to study stream plunging and used the hydrodynamic and transport model ELCOM (Estuary Lake and Coastal Ocean Model) (Hodges and Dallimore 2006) to simulate the plunging behavior of two tributaries in Onondaga Lake, New York. Cook and Richmond (2004) conducted a field monitoring study and used the Flow-3D (Hirt and Nichols 1988) model to simulate the complex 3D density currents at the Clearwater and Snake River confluence and discovered several predictable stratification patterns that would develop depending upon the discharge ratio and the thermal gradients between the two rivers. Jackson et al. (2008) studied density currents in the Chicago River mostly resulted from salinity differences between the North Branch and the main stem of the Chicago River, whereas temperature difference does not appreciably affect the creation of density currents.

In our previous study (Chen et al. 2015), preliminary simulation results using particle tracking show that particles or water released from Smith Dam could take several

days to reach Cordova and GOUS, the momentum developed by the releases did push the cooler water near the river bottom moving downstream. The momentum or push effect from the large release provides driving force for the density current movement along the river bottom in the river-reservoir system. In this study, we focus on understanding and analysis of formation and propagation of density currents under different short-duration (a few hours) large flow releases into a confined river-reservoir system. We studied constant small release (2.83 m^3/s), single large releases (140 m^3/s), and daily repeated large releases from an upstream reservoir. The primary objective of this study is to perform a series of model scenario runs and conduct in-depth result analysis to further investigate flow dynamics and temperature distributions in order to understand and quantify formation and propagation of density currents caused by daily repeated upstream releases of different durations and solar heating. The model simulations include solar heating during day and cooling during night through the water surface. Both daily repeated intermittent releases and solar heating are different from other laboratory experimental studies and simple numerical experiments in which the density current only moves downstream under existing density stratification and due to inflow momentum from one constant release. The results of this study are important with regard to water quality modeling and management, habitat assessment in rivers, and management of thermal discharges from a power plant. The once-through cooling water system for the power plant in the study area is designed to withdraw cold water from the bottom layers at the river inlet to maintain high plant efficiency.

3.3 Study Area

The study deals with model simulations of flow and temperature in a river-reservoir system (124.2 river km) starting from Smith Dam Tailrace (SDT) to Bankhead Lock& Dam (BLD, about 23.5 m height and 426.7 m long) in Alabama (AL), USA (Fig. 3.1). The river reach from upstream to downstream includes Sipsey Fork (21.9 km), the lower Mulberry Fork (70.6 km), and a reservoir segment (31.7 km) of Bankhead Lake. Sipsey Fork and the lower Mulberry Fork are the riverine portions of Bankhead Lake. The Black Warrior River is formed about 40 km west of Birmingham, AL, by the confluence of the Mulberry Fork and the Locust Fork, which join as arms of Bankhead Lake, a narrow reservoir formed by constructing BLD in 1963. The study area is referred here as the Bankhead river-reservoir system (BRRS).

The bottom elevations along the centerline of BRRS in the upstream portion of BRRS (Fig. 3.1b) ranged from about 65.8 to 77.2 m above mean sea level (using NAVD 1988 datum). The average bottom slope is 0.014% but there are local slope variations (ranging from -0.2% to 0.2% over each ~2 km distance). The water surface elevation in BRRS depends on water releases from Lewis Smith Dam, flows from its tributaries (Upper Mulberry, Locust Fork, Lost Creek, and Blackwater Creek), and the water surface elevation in BLD influenced by outflow through hydro turbines, spillage through gates of BLD, and loss of water through the Bankhead navigation lock. A typical water surface profile after a large release from Smith Dam displayed in Figure 1b depicts the response of water level increase in the upstream portion of BRRS from Smith Dam to the Gorgas upstream cross section (GOUS, Fig. 3.1c).

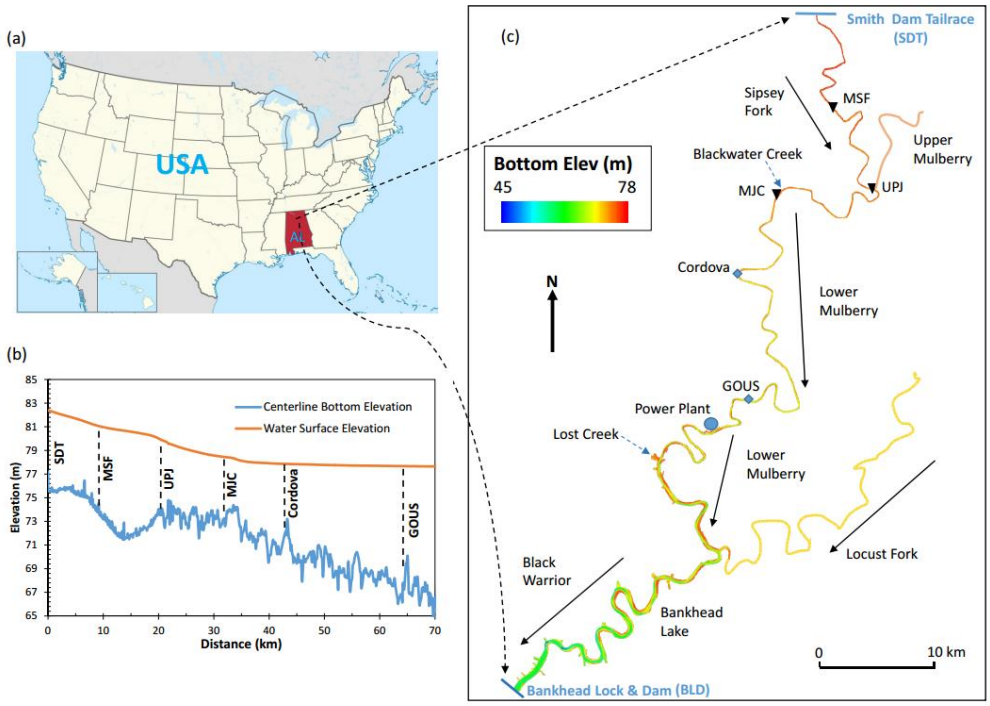

Fig. 3.1 (a) Geographic location of the study area–Bankhead river-reservoir system (BRRS), (b) Longitudinal bottom elevation along the centerline of BRRS and water surface elevation after a large release from the Smith Dam tailrace (SDT) to GOUS, and (c) Color contours of the bottom elevation showing Sipsey Fork, the lower Mulberry Fork, and Black Warrior River as the model simulation domain; two monitoring stations (Cordova and GOUS), model upstream and downstream boundary locations: Smith Dam tailrace (SDT) and Bankhead Lock & Dam (BLD), three cross sections for reporting simulation results (MSF, UPJ, and MJC).

The water releases from Smith Dam to BRRS is normally 2.83 m^3/s, but during late spring, summer, and early fall, large amount of intermittent water releases is practiced to meet peak electric generating demand. During the normal water releases,

water depths in Sipsey Fork range from 2.16 to 4.55 m, in the lower Mulberry Fork from 4.71 to 11.47 m, and in the Bankhead Lake from 12.12 to 17.73 m. The water surface elevation at Bankhead L&D is typically about 77.66 m (with relatively small variations) above mean sea level.

The monitoring stations and selected cross sections for result analysis are shown in Fig. 3.1c and summarized in Table 3.1 including abbreviation used thereafter and description. The middle cross section of Sipsey Fork (MSF) is located at 11.1 km downstream from SDT. The cross section at a short distance (0.64 km) upstream of the junction of Sipsey Fork and the upper Mulberry Fork is called UPJ. The middle cross section between the junction and Cordova is called MJC. The monitoring station at 5.58 km upstream the power plant is called GOUS (Fig. 3.1c).

Table 3.1 Abbreviation and description of cross sectional locations used in the study (Figure 3.1c).

Abbreviation	Description
BLD	Bankhead Lock & Dam (downstream boundary of EFDC model)
Cordova	USGS[1] monitoring station at Cordova on the lower Mulberry River
GOUS	Monitoring station upstream the power plant
MSF	Middle cross section of Sipsey Fork
MJC	Middle cross section between the junction and Cordova
SDT	Smith Dam tailrace (upstream boundary of EFDC model)
UPJ	Just upstream of the junction of Sipsey Fork and the upper Mulberry Fork

3.4 Model Application, Boundary Conditions, and Calibration Results

In this study, a three-dimensional (3D) Environmental Fluid Dynamics Code (EFDC) model (Hamrick 1992c) configured for BRRS (Chen et al. 2015) was applied to

simulate unsteady flow patterns and temperature distributions in BRRS including the intake canal and the discharge canal of a power plant (Fig. 3.1c) near Parrish, AL. This study mainly focuses on the EFDC simulations and result analysis from SDT to GOUS, upstream portion of BRRS under different large releases from Smith Dam. The EFDC model is a general purpose modeling package that can be configured to simulate 1D, 2D, and 3D flow, transport, and biogeochemical processes in various surface water systems including rivers, lakes, estuaries, reservoirs, wetlands, and coastal regions (Shen and Lin 2006; Caliskan and Elci 2009; Jeong et al. 2010; Wang et al. 2010; Kim and Park 2012; Devkota and Fang 2014). The Mellor-Yamada level 2.5 turbulence closure scheme (Mellor and Yamada 1982) is used in EFDC to calculate vertical turbulent diffusion coefficients of momentum and mass, which are linked to vertical turbulent intensity, turbulent length scale, and the Richardson number. Details of governing equations and numerical schemes for EFDC hydrodynamic model are given by Hamrick (Hamrick 1992c).

In addition to hydrodynamic model, EFDC temperature model component was activated to simulate unsteady water temperatures for each computation cell to understand density current movement. While using EFDC temperature model we have four options for calculating the surface heat exchange. The CE-QUAL-W2 equilibrium method is the most robust method among the four options; therefore, it was used in this study for water temperature modeling. The surface heat exchange includes incident and reflected short and long wave solar radiations, back radiation, evaporative heat loss, and heat conduction from the water surface. The depth distribution of the solar heating (short wave radiation) after penetrating the water surface is calculated by the Beer's law using

radiation or light attenuation coefficient as one of the model input parameters. Sediment heat exchange with overlying water is also included in the EFDC temperature model. The detailed information of the governing equations for the heat exchange processes in a water body is given in the CE-QUAL-W2 manual (Cole and Wells 2010). The EFDC hydrodynamic and temperature model applied to BRRS was previously calibrated and validated using extensive field data measured in 2010 and 2011 (Fang et al. 2013; Chen et al. 2015).

The upstream boundary of the EFDC model for BRRS is one-minute time-series data of water releases (m^3/s) at SDT. There are two types of water releases from Smith Dam: (1) more or less constant continuous release (2.83 m^3/s) to support the downstream environment and ecosystem; (2) intermittent releases from hydro-turbine units of Smith Dam in order to meet peak electric generation demand. Measured water temperatures used for upstream boundary condition at SDT from 8 September to 18 October, 2010, was almost constant (9.6 ^oC) during the constant release, and water temperatures during the intermittent large releases were 10–15 ^oC, which were 4–5 ^oC higher than temperatures during the constant release only from Smith Dam (Fig. 3.2a). This is because constant release occurred from a deep water depth and intermittent releases were from a shallower depth of Smith Dam; and there was lower water temperature in the hypolimnion due to thermal stratification in the summer.

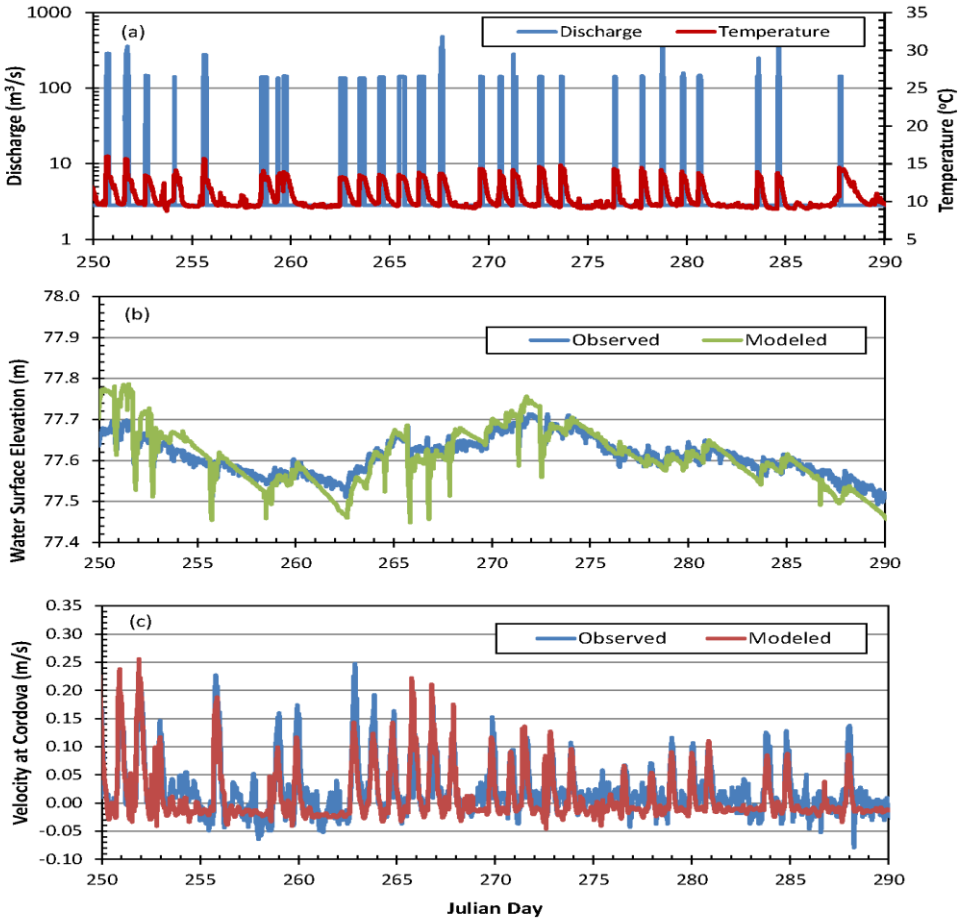

Fig. 3.2 (a) Time-series plot of discharge and water temperature at the Smith Dam tailrace, (b) Time-series plot of observed and modeled water surface elevation (m) at GOUS, and (c) Time-series plot of modeled (depth averaged) and observed velocity at the USGS Cordova gaging station from 8 September to 18 October (Julian day 250 to 290), 2010.

The EFDC model applied for BRRS was calibrated in the period of 2010 and 2011 year. In the previous study (Chen et al. 2015), the 3D hydrodynamic EFDC model was applied to simulate unsteady flow patterns and temperature distributions under

various upstream releases and variable atmospheric forcing in BRRS in 2011. The calibrated EFDC model provided simulated water surface elevation, temperature, velocity and discharge at different layers (depths) for all grids in different cross sections.

In addition to calibration results previously presented (Chen et al. 2015), Fig. 3.2b shows the time series plot of observed and modeled water surface elevation (WSE) at GOUS from 8 September to 18 October 2010. The agreement between observed and modeled WSEs at GOUS is very good with median difference of 0.008 m. The average difference between observed and modeled WSEs at GOUS is -0.020 m. Flow velocities at Cordova measured from 8 September to 18 October 2010 by USGS were compared with modeled results from the EFDC model. Negative velocity in Fig. 3.2c indicates the flow direction from downstream towards upstream due to backwater effect from BLD. Visually, modeled cross sectional mean velocities matched reasonably well with observed mean velocities. After each large release from Smith Dam, the velocity at Cordova started to increase from ~0 to ~0.12 m/s (depend on the release flow rate and duration) with a few hours of lag. Overall, the EFDC model was able to simulate the temporal and spatial distributions of flow and temperature in BRRS and reveal complex interactions and density currents due to dynamic upstream releases and solar heating from atmosphere (Chen et al. 2015).

3.5 Model Scenarios

In previous model simulations for BRRS (Fang et al. 2013; Chen et al. 2015), time series of observed upstream releases, observed or estimated discharges from rivers, observed water levels and temperatures were used for model boundary conditions. For

scenario analysis performed in this study, various input data (boundary conditions) were modified into constant representative values excluding upstream boundary conditions. Therefore, we can focus on studying effects of dynamic releases from the upstream reservoir only on density current formations and movement. The inflows from all tributaries and small streams (Fig. 3.1) were set at average inflows calculated from time series of inflows used for model calibration. Average inflows from the Upper Mulberry Fork, Lost Creek, Blackwater Creek and Locust Fork are 4.42, 5.54, 2.60, and 8.70 m^3/s for all scenario model runs. At BLD, water level was used as downstream boundary condition. Observed water surface elevations ranged from 77.35 m to 77.75 m from 4 May to 3 September 2011 with an average elevation of 77.60 m (standard deviation of 0.07 m). Therefore, water surface elevation at BLD was set at 77.60 m (constant) for the scenario runs. Based on the sensitive analysis, the constant water level at BLD would not affect overall flow dynamics in the upstream portion of BRRS (from SDT to GOUS). For the atmospheric boundary conditions, weather data in a relatively warm day of the year were used to perform scenario model runs: hourly climate data from Birmingham, AL (Chen et al. 2015), on Julian day 140 (20 May, 2011) were repeated day by day in each 24 hour period. Because diurnal effect (solar heating during day and cooling during night) is important, hourly climate variations were kept for model scenario runs but there is no warming and cooling trend over simulation period (up to 18 days). Hourly air temperatures on 20 May ranged from 19.4 to 31.1 ^oC, and solar radiation from 57 to 888 $watts/m^2$.

Flow releases from SDT varies during the summer based on power demand. Based on 2011 release data, average flows during the intermittent release periods ranged

from 104.0 to 273.5 m^3/s with average and median flows about 140 m^3/s (Chen et al. 2015). In 2011, 60.1% of the intermittent releases from SDT had a duration from 2 to 6 hours, and most of the releases started around 1:00 pm (Chen et al. 2015). The percentages of all 2011 releases with durations of about 2 hr (from 1.8 hr to 2.2 hr), 4 hr (3.8 hr to 4.2 hr), and 6 hr (5.8 hr to 6.2 hr) are 5.2%, 15.5% and 14.6%, respectively. Therefore, we used the intermittent daily large releases with these three durations (2, 4, and 6 hr) for the sensitivity analysis.

The model scenario runs are distinguished as two groups. The first group of model scenario runs are to study flow and temperature dynamics resulted from one large release (LR): Smith Dam has constant small release (CSR, i.e., 2.83 m^3/s) for 6 days, then one large release with different durations in the 7th day, and then CSR for another 6 days again. The model runs are restarted at the time of Julian day 142.53 (~1:00 pm on 22 May) using EFDC's restart file (Craig 2012), which was created from the calibration model run. The second group of scenario runs are similar to the actual releases that large flow release repeats day by day after Julian day 140 using EFDC's restart file (Craig 2012). The large releases from Smith Dam have a flow rate of 140 m^3/s, which is average discharge of the intermittent releases from Smith Dam based on data analysis (Chen et al. 2015), and last for 2, 4, and 6 hrs for different cases, respectively. In the following discussions, the first group of the scenario runs are called 2-, 4-, and 6-hr single large releases (SLRs), and the second group of the scenario runs are called 2-, 4-, and 6-hr daily repeated large releases (DRLRs).

The restart file created by the calibration model run starting from Julian Day 104 under actual flow releases in 2011 was used to set initial conditions for EFDC sensitivity

model runs in this study. The model spin up period is about 18 days. The initial conditions such as temperature stratification and water depth are representative environmental conditions in the BRRS in May. If we used initial conditions in June or other months, specific results presented here might be somewhat different, but the overall conclusions of the study are the same.

3.6 Results and Discussion

3.6.1 Velocity Distributions

The density current formation and propagation in the natural system is complex and dynamic. Fig. 3.3 shows simulated vertical velocity profiles at the centerlines of MSF, UPJ, MJC, Cordova, and GOUS when DRLRs at SDT last 2, 4, and 6 hrs each day and at three different time: 1 hr after the large release begins (left panels), 4 hrs (middle) and 18 hrs (right) after the large release stops. When the large flow is released for 1 hr from Smith Dam, the flow momentum begins to affect the velocities at MSF where water at all layers move downstream (positive velocity) with the maximum velocity of ~ 0.15 m/s at the surface for all three duration releases. The velocities at UPJ indicate that the flow momentum effect does not reach UPJ yet at 1 hr after the releases (Chen et al. 2015). Flow dynamics at UPJ, MJC, Cordova, and GOUS are more complex and may be resulted from the release in previous days, as indicated by and discussed later for velocity profiles at 18 hrs after the release. The density currents are clearly showed in the bottom layers moving to the downstream at UPJ and GOUS for all three-duration DRLRs, and at Cordova for 6-hr DRLR.

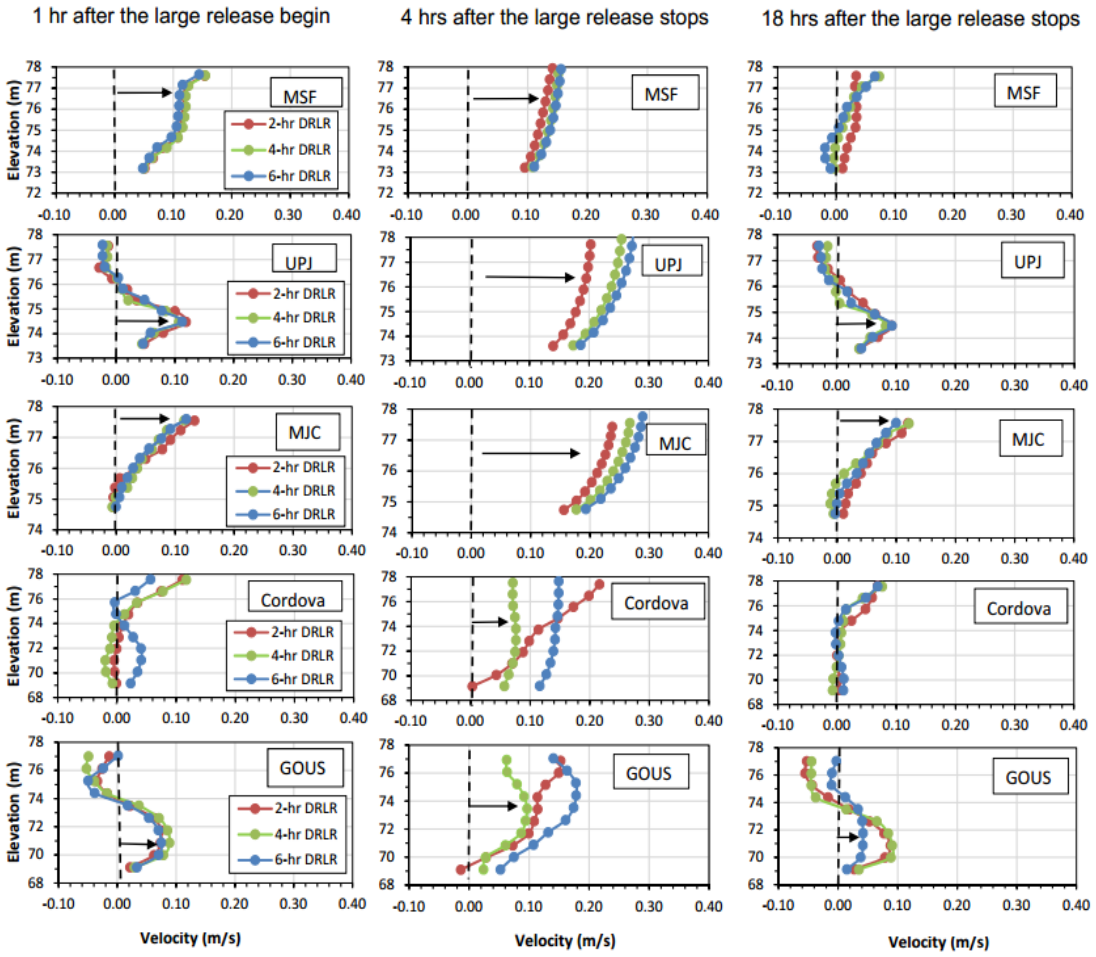

Fig. 3.3 Simulated vertical velocity profiles at the centerlines of MSF, UPJ, MJC, Cordova, and GOUS when DRLRs at SDT last 2, 4, and 6 hrs each day and at three different time: 1 hr after the large release begins (left panels), 4 hrs (middle) and 18 hrs (right) after the large release stops (right).

When the large flow release has stopped for 4 hrs, for the 2-hr DRLR, vertical velocity profiles at Cordova and GOUS have steep gradients with near zero velocity in the bottom layer. This indicates that the flow momentum for the 2-hr DRLR is not strong enough to move/push bottom water and density current at Cordova and GOUS. For 4-hr

and 6-hr DRLRs, the flow momentum reaches GOUS and is strong enough to affect whole velocity profiles because the surface and bottom velocities at GOUS begin to increase. The velocities at all 5 locations are all positive that indicates the flow all moving downstream. Therefore, the momentum effect resulted from the release creates adequate mixing to destroy or wipe out existing density currents at these locations, which are further discussed later using temperature distributions. Vertical velocity distributions at MSF, UPJ, and MJC clearly show that longer release durations from Smith Dam result in larger velocities in all depths. The simulated velocities in the surface layer at MJC for 2-hr, 4-hr, and 6-hr DRLRs are 0.24, 0.27, and 0.29 m/s, respectively.

When the large flow release has stopped for 18 hrs, i.e., just before large release starts in the next day, the velocities at MSF decrease to less than 0.07 m/s. At UPJ, MJC, Cordova, and GOUS, the velocity profiles are similar to the profiles at 1 hr after the large release (Fig. 3.3). The density current along the channel bottom at UPJ (indicated by positive velocities) can be due to low-discharge constant release with colder temperature. Small negative surface velocities at UPJ may indicate certain backwater effect from BLD (downstream obstruction). The river-reservoir system in the study is relatively narrow and meandering (Fig. 3.1), hence, it is not the wind that changes the flow direction. At MJC and Cordova, flows in the surface layers move downstream with small velocities. At GOUS, the velocities are negative in the surface layers and positive in the bottom layers. These complex flow dynamics are also explained using time-series plots (Fig. 3.4) and should be further studied using the particle tracking method (Harlow 1962; Ahlstrom et al. 1977; Abrahams et al. 1986; Guo-Qing et al. 2011) and other advanced analysis methods.

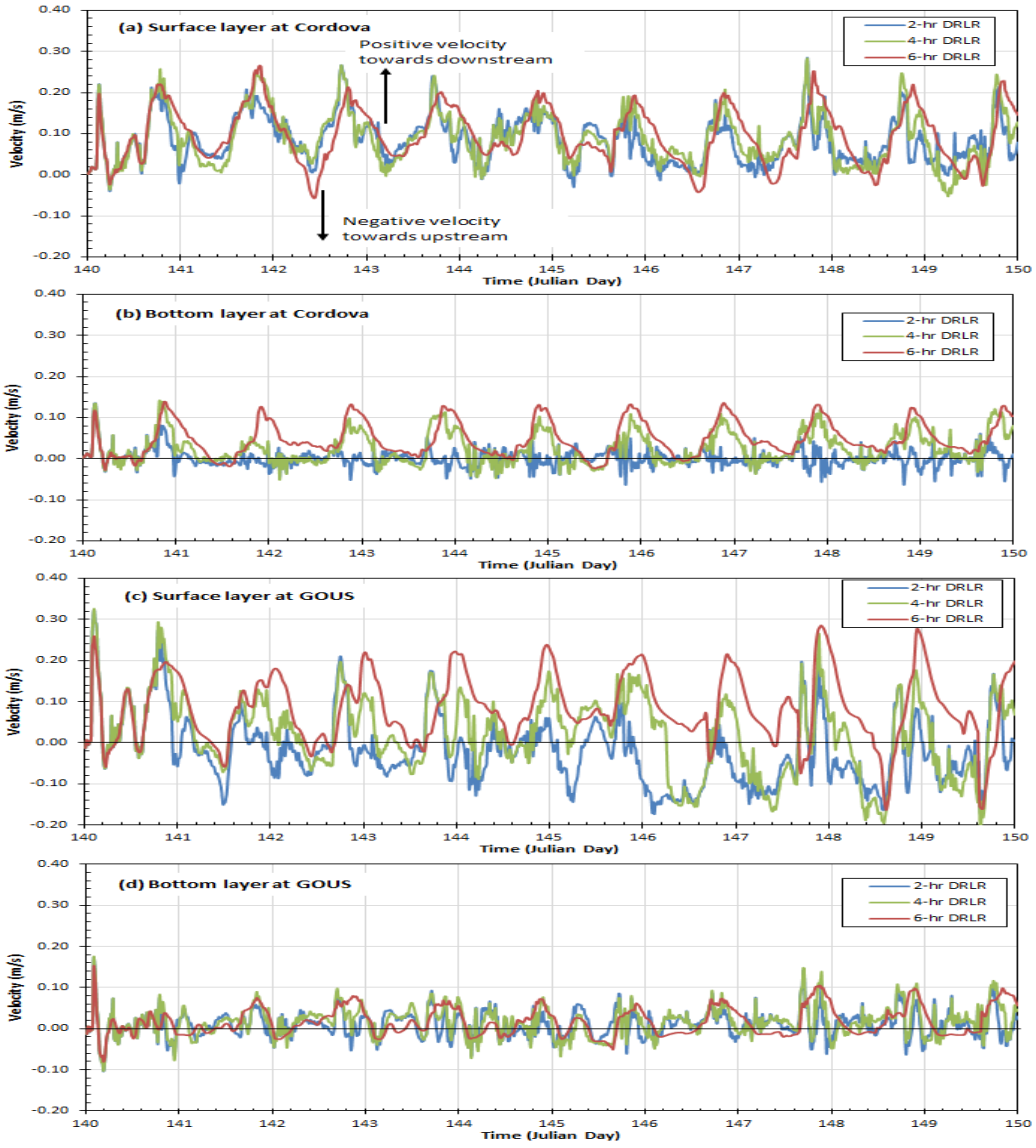

Fig. 3.4 Time series of simulated velocities in the surface and bottom layers at the centerlines of Cordova and GOUS when DRLRs at SDT last 2, 4, and 6 hrs each day.

Fig. 3.4 shows time-series plots of simulated velocities in the surface and bottom layers at the centerlines of Cordova and GOUS when DRLRs at SDT last 2, 4, and 6 hrs each day. In the surface layer at Cordova, the flow moves downstream most of times for the 2-hr, 4-hr and 6-hr DRLRs (Fig. 3.4a, 93.0–97.4% in Table 3.2). There are short

periods of time that have negative velocities, which may be due to the backwater effect from BLD. In Fig. 4b, velocities in the bottom layer at Cordova start to increase at ~4–6 hrs after each DRLR stops, have a maximum velocity greater than 0.1 m/s (maximum velocity is 0.139 m/s for the 6-hr DRLR, Table 3.2), and have positive magnitude (density currents move downstream) most of times for the 4-hr and 6-hr DRLRs. However, for the 2-hr DRLR, flow in the bottom layer at Cordova has small velocities (absolute average velocity of 0.015 ± 0.015 m/s) and moves either downstream or upstream. There are 48.4%, 69.0%, and 91.1% of time with positive bottom velocity with average value of 0.017, 0.042, and 0.053 m/s at Cordova for the 2-hr, 4-hr, and 6-hr DRLR, respectively (Table 3.2). Therefore, the moment effects creating by the 2-hr DRLR cannot have much impacts on bottom water at Cordova (Fig. 3.4b). The repeated releases with longer durations push the bottom colder water from SDT downstream to form density currents and make the bottom water temperature in downstream locations to be cooler.

At GOUS, the surface flow moving towards upstream is more obvious due to the backwater effect. For the 2-hr DRLR, the surface flow mainly move towards upstream (66.9% of time, Table 3.2). For the 4-hr DRLR, the surface flow (with average velocity of 0.085 m/s) moves towards downstream when the large momentum from SDT reach at GOUS; the surface flow (with average velocity of 0.069 m/s) also moves towards upstream when the backwater effect from BLD comes. The durations moving downstream and upstream at GOUS are 140.5 and 99.5 hrs during the 10 days of simulation (240 hrs) for the 4-hr DRLR (Table 3.2). For the 6-hr DRLR, the surface flow dominantly moves towards downstream (Fig. 3.4c). The durations moving downstream

and upstream are 203.5 (84.8%) and 36.5 hrs, respectively, during the 10-day simulation period for the 6-hr DRLR (Table 3.2). In the bottom layer at GOUS, it seems that the flow momentum still has relatively strong impacts at GOUS for 6-hr DRLRs (Fig. 3.4d), i.e., indication of the movement of density currents at GOUS.

Table 3.2 Statistical information of simulated velocities (m/s) at Cordova and GOUS.

Location	Release	Layer	Maximum	Average	Deviation	Percent Hrs[2]
Cordova	2-hr	Surface	0.283(-0.041) [1]	0.085(-0.010)	0.055(0.011)	97.4% (2.6%)
	DRLR	Bottom	0.135(-0.064)	0.017(-0.013)	0.018(0.012)	48.1% (51.9%)
	4-hr	Surface	0.282(-0.053)	0.093(-0.017)	0.060(0.015)	95.2% (4.8%)
	DRLR	Bottom	0.142(-0.052)	0.042(-0.012)	0.033(0.010)	69.0% (31.0%)
	6-hr	Surface	0.266(-0.057)	0.104(-0.021)	0.061(0.015)	93.0% (7.0%)
	DRLR	Bottom	0.139(-0.028)	0.053(-0.011)	0.038(0.007)	91.1% (8.9%)
GOUS	2-hr	Surface	0.325(-0.176)	0.072(-0.065)	0.066(0.043)	33.1% (66.9%)
	DRLR	Bottom	0.172(-0.104)	0.029(-0.021)	0.023(0.016)	62.2% (37.8%)
	4-hr	Surface	0.326(-0.212)	0.085(-0.069)	0.057(0.052)	58.5% (41.5%)
	DRLR	Bottom	0.174(-0.103)	0.034(-0.022)	0.027(0.017)	69.1% (30.9%)
	6-hr	Surface	0.285(-0.164)	0.106(-0.037)	0.068(0.041)	84.8% (15.2%)
	DRLR	Bottom	0.151(-0.081)	0.038(-0.015)	0.027(0.011)	60.9% (39.1%)

3.6.2 Temperature Distributions

3.6.2.1 Single Large Release

To understand how the density current moves under the CSR (2.83 m^3/s) and one large release, simulated temperature distributions are output for the 4-hr SLR simulation. Simulated water temperatures range from 10 °C (blue color) to 30 °C (red color) as shown by color contours. Fig. 3.5 shows simulated water temperature distributions from SDT (Distance = 0) to GOUS (~ 64 km) at the following 6 different time: model initial condition at Day 142.573, about 3 and 6 days having CSR at SDT, when the 4-hr SLR just stops in the 7th day, about 1 and 4 days after the large release. Temperature

stratification along the depth exists at the most locations from SDT to GOUS under the model initial condition (Day 142.573), which was simulated from the calibrated EFDC model and resulted from actual flow releases and solar heating before 142 (Chen et al. 2015). Due to solar heating, temperature increases and stratification changes at the most cross sections in 3 and 6 days having CSR only. Surface temperatures from MSF to GOUS are all greater than 25 °C at Julian Day 148.52 (6 days). With the CSR only, the cold water current (blue color) near SDT has moved downstream about 4 km in 6 days. With the 4-hr SLR, the cold water can move from Smith Dam to UPJ (~22 km) in a few hours. The simulated water temperatures increase further due to the solar heating if there is no large release in the next few days. The CSR (2.83 m^3/s) after the SLR still forms the cold water or density current and moves slowly downstream, but the density current near SDT without much momentum doesn't have much effect on downstream water movement. One day after SLR, density currents form in the bottom layers in different parts of BRRS from SDT to GOUS, and two examples of density currents are shown by dashed-dark-line polygons (Fig. 3.5). Density or temperature stratifications has developed due to solar heating when inflow momentum vanishes. Density currents are also discontinuous because some parts of BRRS have weak or no stratification after the release. Due to the interaction of the large release and solar heating with ambient water in BRRS, the density current formation and propagation before and after a SLR is complex and dynamic.

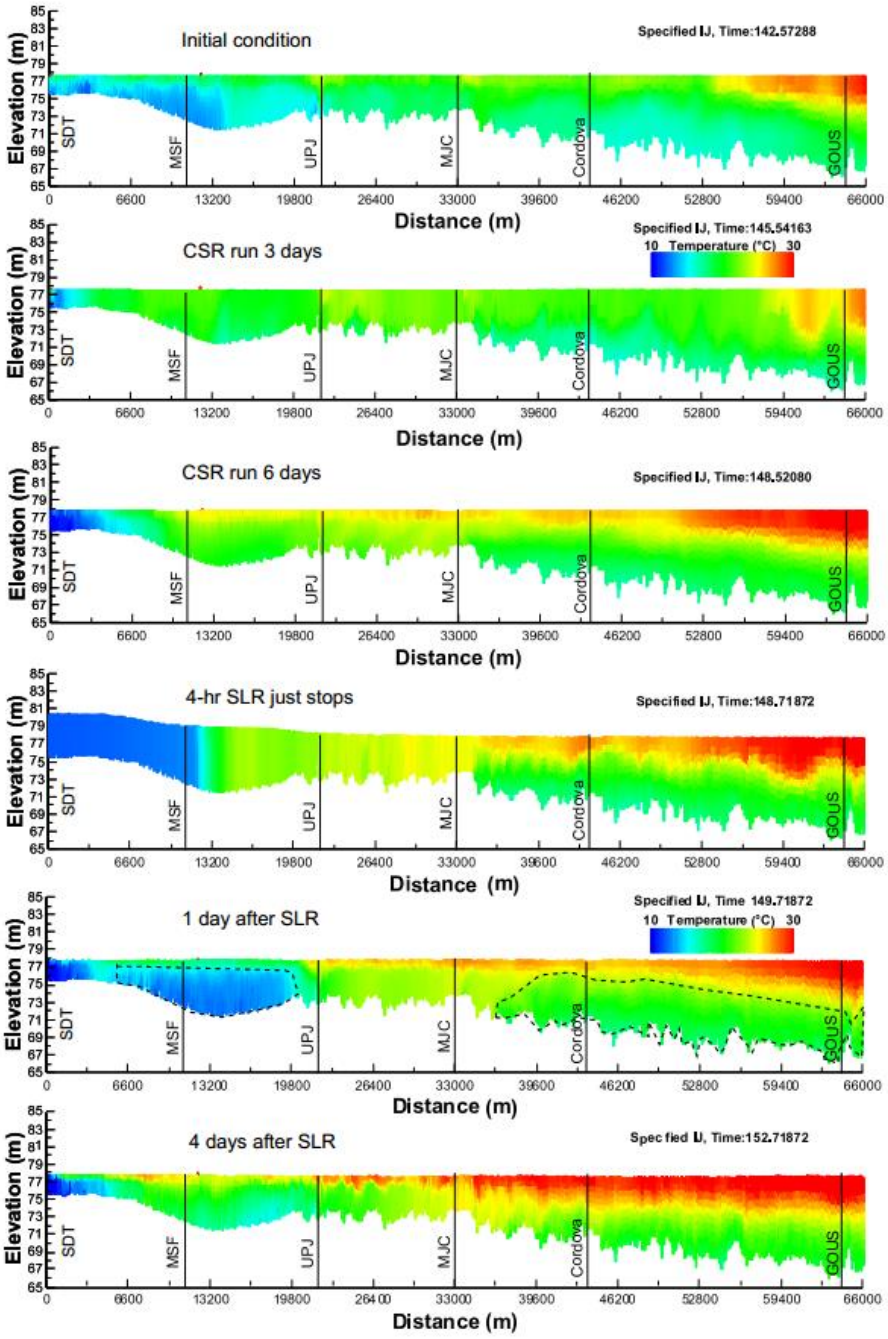

Fig. 3.5 Simulated water temperature distributions from SDT to GOUS at 6 different time for the 4-hr SLR simulation: at the beginning of the model run (initial condition), about 3 and 6 days with CSR, when the 4-hr SLR stops (in the 7th days), about 1 and 4 days after SLR.

Surface temperature warms up continuously in the surface layers due to solar heating in the 12 days of the simulation period (Fig. 3.5). At 4 days after the large release, water temperatures at most depths become higher. These temperature increases are due to solar heating. Surface temperature increases may also be related to backwater effect from the downstream boundary (BLD).

Fig. 3.6 shows time-series plots of simulated water temperatures in the surface and bottom layers at MSF and Cordova for four sensitivity runs: CSR only, 2-hr, 4-hr, and 6-hr SLR. For CSR, surface and bottom temperatures gradually increase with time due to the solar heating. The typical water depth at MSF is 4.9 m, smaller than the depth at Cordova (9.2 m). At MSF after 6 days, the bottom temperatures have smaller variations, while the surface temperatures still fluctuate with air temperature. At Cordova, the bottom temperature has smaller increase but the increase lasts more days. The SLR starts at 1:00 pm on Julian day 148. Due to momentum effect and mixing, both surface and bottom water temperatures at MSF have quickly dropped to ~12 °C shortly after the large release starts from SDT (Fig. 3.6a). Surface and bottom temperatures begin to increase at a few hours after the release, more or less continuously increase for about 5 days, and eventually reach to temperatures simulated under CSR. The 2-, 4- and 6-hr SLRs have similar impacts on water temperature at MSF. When the flow momentum from a SLR comes to Cordova, longer period SLR has more mixing and keeps the surface temperature lower (Fig. 3.6b). The 2-hr and 4-hr SLRs have little effect on the bottom temperature at Cordova. The flow momentum from the 6-hr SLR seems strong enough to mix or stir the bottom water, and its temperature has an increase and decrease for a few hours then gradually increases with time (Fig. 3.6b) due to solar heating. Fig. 3.6 shows

us that one SLR does not have long-term impact on downstream surface and bottom temperatures. Regular (daily repeated) large releases are required to maintain downstream temperature stratification, which will be discussed in the next section.

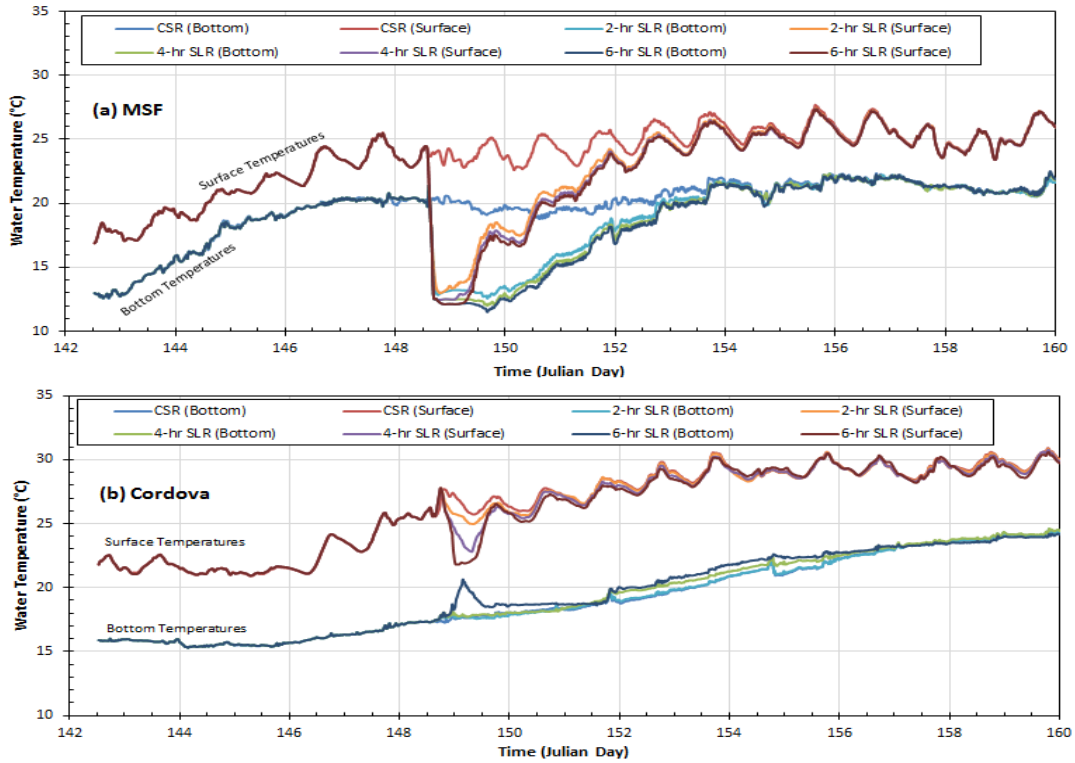

Fig. 3.6 Time series of simulated water temperatures in the surface and bottom layers at MSF and Cordova for four sensitivity runs: CSR only, 2-hr, 4-hr, and 6-hr SLRs.

3.6.2.2 Daily Repeated Large Releases

In comparison to a SLR, DRLRs are more close to the actual releases to BRRS during the summer, which might have daily variations in discharge and duration; and occasionally there is no large release for one or two days (Chen et al. 2015). Fig. 3.7

shows the simulated water temperature distributions for 2-hr, 4-hr and 6-hr DRLRs at three different time: (a) just before the large release on Day 142, (b) the large release just stops, and (c) when SDT's WSE decreases to the normal level. In comparison to 2-hr and 4-hr DRLRs, 6-hr DRLR can push cold water further downstream and surface temperatures are less affected by the solar heating. Fig. 3.7a shows that the bottom layer temperatures from SDT to GOUS after 2 days of 4-hr and 6-hr DRLRs are cooler than temperatures for 2-hr DRLRs because large releases started in Julian Day 140 and repeated every day. Without DRLR, water temperature in BRRS increases gradually due to the warmer air temperature and solar heating. After the large release stops (Fig. 3.7b), a relatively large longitudinal temperature gradient develops and is from ~10 °C at SDT to ~20 °C at GOUS when large flow momentum with colder water pushes relatively warmer water in BRRS downstream. Temperature stratification is very weak in the upstream part of BRRS due to the momentum mixing, for example, water from SDT to UPJ for 2-hr DRLR, to MJC for 4-hr DRLR, and to Cordova for 6-hr DRLR has almost no vertical stratification (Fig. 3.7b). This indicates the momentum effect for the 6-hr DRLR definitely reaches Cordova (~43.7 km from SDT). From Fig. 3.6c, it seems colder denser water moves from downstream MSF to UPJ due to remaining momentum of the 6-hr DRLR. When the flow momentum pushes water downstream, it also mixes pre-existing water in rivers. The density currents moving downstream gradually form in the next day due to the remaining momentum along the bottom layers and solar heating. Before the next large release, density currents forming at different parts of BRRS are similar to ones shown in Fig. 3.7a.

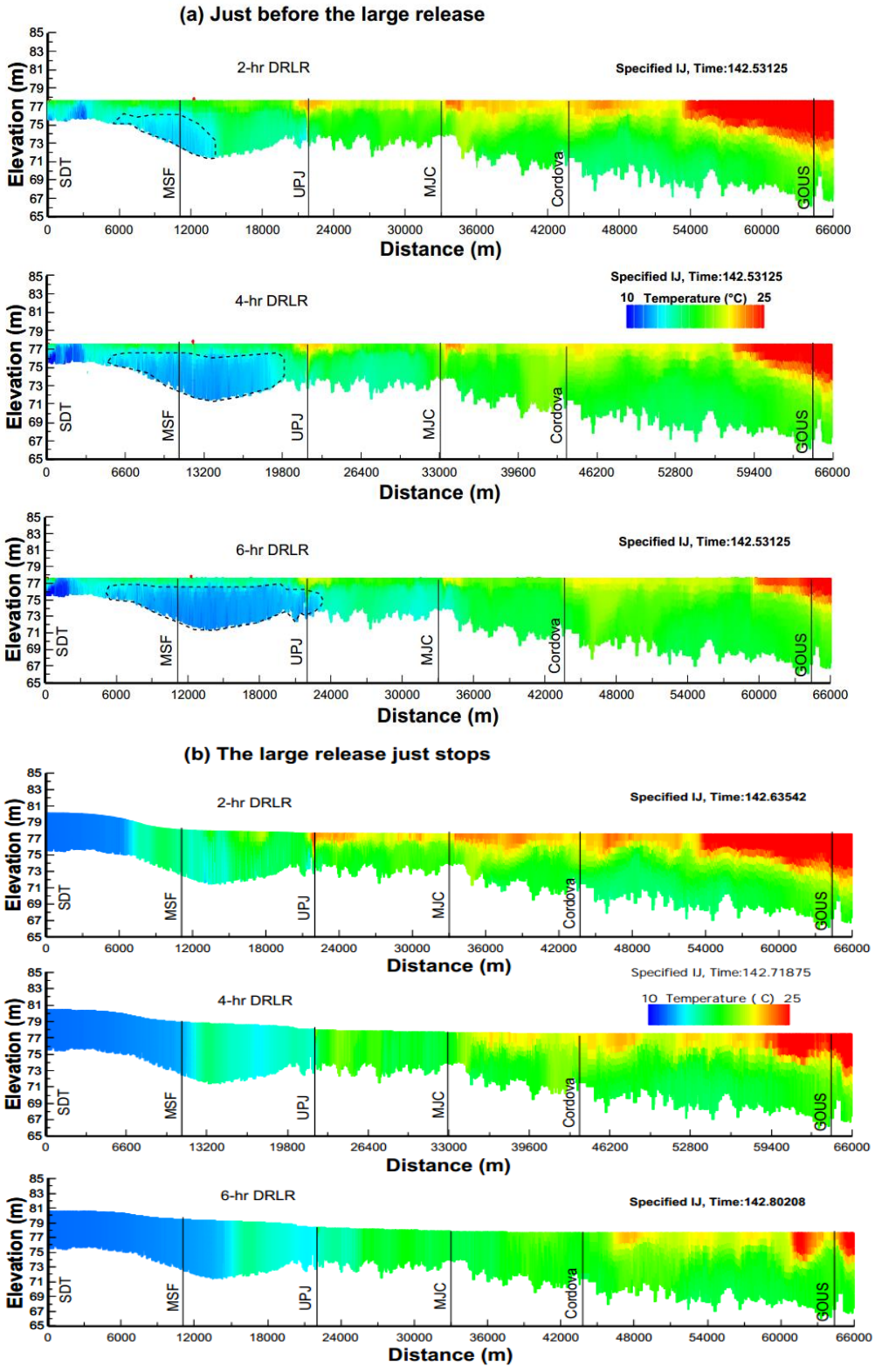

Figure 3.7 Continued on the next page.

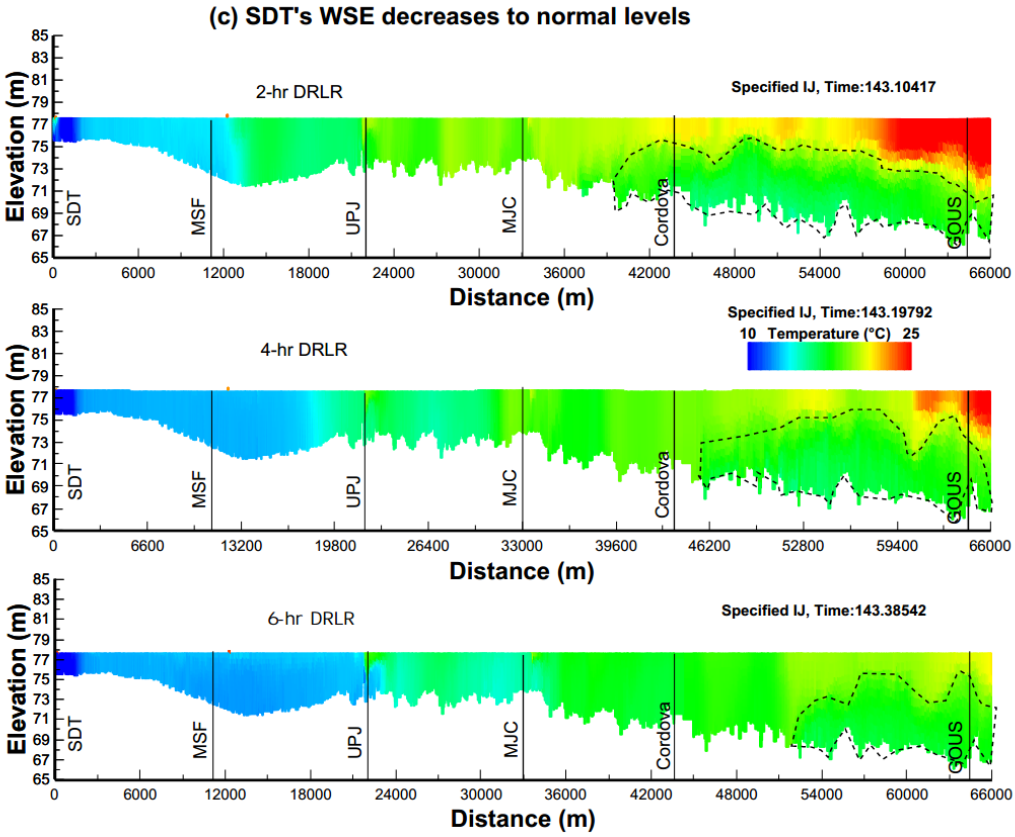

Fig. 3.7 Simulated water temperature distributions for 2-hr, 4-hr and 6-hr DRLRs at three different time: (a) just before the large release, (b) the large release just stops, and (c) when SDT's WSE decreases to normal levels.

Fig. 3.8 shows simulated water temperature distributions at 12:45 on Julian day 146 for 2-hr, 4-hr, and 6-hr DRLRs since the first DRLR started from Julian Day 140 (May 21), i.e., DRLRs lasted for 6 days. By comparing with Fig. 3.7a, which is only 2 days after May 21, the 4- and 6-hr DRLRs lasted for 6 days can make the downstream temperature cooler, especially at the reach from Cordova to GOUS. The momentum effect can also push the surface warmer water at GOUS downstream when 6-hr DRLRs repeated less than 6 days. The 4- and 6-hr DRLRs lasted for 6 days result in temperature

decreases from UPJ to GOUS from Julian day 142 and 143 (Fig. 3.7). However, the 2-hr DRLRs lasted for 6 days cannot override or compensate solar heating effect because water temperatures from UPJ to GOUS have increases from Julian day 142 (Fig. 3.7a) and 143 (Fig. 3.7c). DRLRs with longer durations push colder density currents (highlighted by dashed-dark-line polygons) further downstream from SDT.

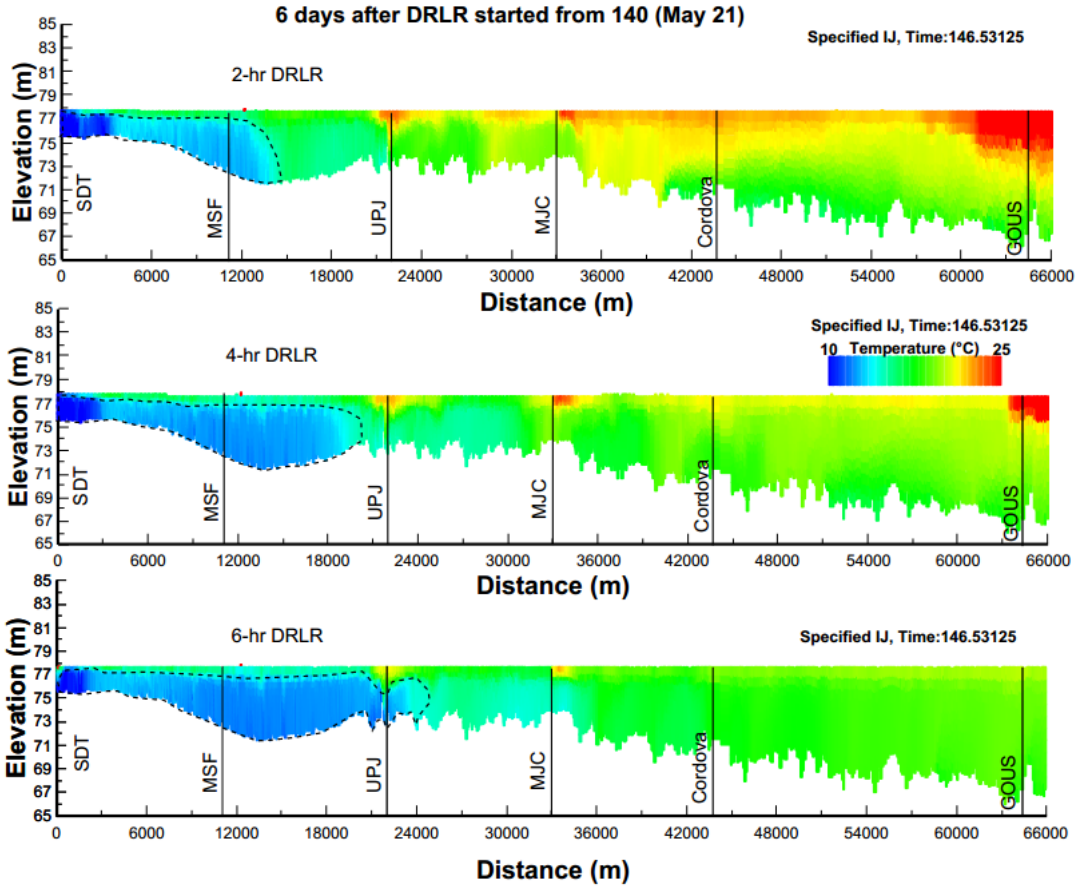

Fig. 3.8 Simulated water temperature distributions for 2-hr, 4-hr and 6-hr DRLRs lasted for 6 days from Julian Day 140 (May 21).

Results of sensitivity model runs for 2-hr, 4-hr, and 6-hr DRLRs are shown in Fig. 3.9 including results for CSR only for comparison. At MSF, which is close to the release location (SDT), surface and bottom water temperatures are well mixed during each DRLR (Fig. 3.9a). Simulated water temperatures maintain constant for a few hours during the night. When the sun rises in the next day, the surface water temperature increases gradually. For the longer repeated release, the water temperatures at MSF are a little bit cooler (Fig. 3.9a). Comparing with simulated temperatures for SLRs (Fig. 3.6), DRLRs can have lasting impacts on water temperatures in the surface (Fig. 3.9b) and bottom (Fig. 3.9c) layers at Cordova. Simulated surface temperatures at Cordova have certain daily variations due to solar heating and cooling (diurnal effects) but do not gradually increase with time instead of maintaining lower average temperatures during the simulation period.

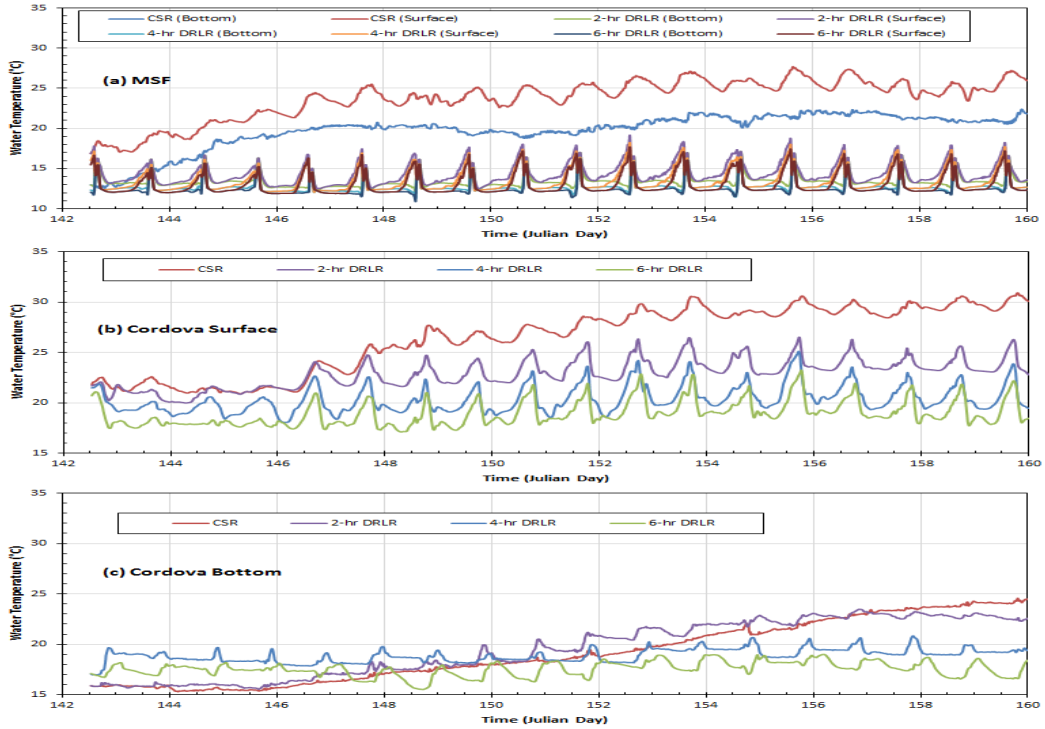

Fig. 3.9 Time series of simulated water temperatures in the surface and bottom layers at MSF and Cordova for CSR only, 2-, 4-, and 6-hr DRLRs.

Overall average bottom temperatures at Cordova are lower for longer duration of DRLRs: 19.63 ^{o}C for the 4-hr DRLR and 18.24 ^{o}C for the 6-hr DRLR. For bottom temperatures at Cordova, the 4-hr and 6-hr DRLRs can maintain lower water temperatures with small daily variations, but for the 2-hr DRLR temperatures still have the gradual increase with time. The bottom temperatures simulated with the 4-hr and 6-hr DRLRs are higher than temperatures under CSR for the first 6–8 days because cooler bottom water temperatures are mixed with warmer surface temperatures by the large flow momentum. Simulated bottom temperatures at Cordova under the 2-hr DRLR are larger than ones under CSR in the first 14 days, but become lower afterwards, which eventually exhibits the effect of DRLR.

3.6.2.3 Comparison between CSR and DRLR

For CSR only, surface and bottom temperatures at Cordova increase more than 8 ^{o}C over 17 simulation days due to solar heating (Fig. 3.9). The average differences between surface and bottom temperatures for CSR only are 3.99 °C, 7.26 °C, and 12.45 °C at MSF, Cordova, and GOUS (Table 3.3), respectively. The strength of the vertical temperature stratification increases from upstream to downstream, which is primarily due to the increase of the water depth. For DRLRs, the average differences between surface and bottom temperatures are much smaller (e.g., < 1 ^{o}C at MSF) due to the large flow momentum to mix water (Table 3.3). For three DRLRs, the average temperature differences at Cordova are larger than ones at MSF (Table 3.3). The temperature differences between surface and bottom layers at GOUS (Table 3.3) indicate that DRLR with longer duration such as 6-hr results in stronger mixing at downstream and can still have strong impact on temperature dynamics and stratification at GOUS (~64 km from SDT).

Table 3.3 Statistical summary of simulated differences (°C) between surface and bottom temperatures at MSF, Cordova, and GOUS for CSR only, 2-hr, 4-hr, and 6-hr DRLRs.

Location	Release Type	Difference (Surface - Bottom) (°C)			
		Maximum	Minimum	Average	Deviation
MSF	CSR	6.60	1.71	3.99	1.08
	2-hr DRLR	6.60	-0.02	0.94	1.32
	4-hr DRLR	6.35	-0.01	0.76	1.32
	6-hr DRLR	5.72	-0.01	0.65	1.26
Cordova	CSR	10.44	4.96	7.26	1.43
	2-hr DRLR	7.51	-0.01	3.35	2.02
	4-hr DRLR	6.07	-0.01	1.47	1.37
	6-hr DRLR	5.61	-0.01	1.38	1.51
GOUS	CSR	14.62	9.20	12.45	0.97
	2-hr DRLR	13.63	6.66	11.33	1.35
	4-hr DRLR	12.24	1.88	8.53	2.40
	6-hr DRLR	10.79	0.58	4.71	2.69

For time-series plots in Fig. 3.9, the average differences of surface temperatures simulated under the 6-hr DRLR and CSR only are -10.63 °C at MSF and -7.53 °C at Cordova (Table 3.4). The average differences of bottom temperature simulated under the 6-hr DRLR and CSR only are -7.49, 1.64, and -1.10 °C at MSF, Cordova, and GOUS, respectively (Table 3.4). The average difference of bottom temperatures at Cordova between 2-hr DRLR and CSR is positive (0.38 °C) but negative (-0.30 or -16.4 °C) between 4-hr or 6-hr DRLR and CSR only (Table 3.4).

Time series of simulated water temperatures in the surface and bottom layers at GOUS have similar patterns as ones at Cordova under different releases, so they are not plotted in Fig. 3.9. After 17 days of daily repeated releases (Julian day 142 to 160), bottom temperatures at GOUS simulated with 2-, 4-, and 6-hr DRLR are 1.64, 2.06, and 3.35 °C lower than one from CSR only. Results in Fig. 3.9 and Table 3.3 and Table 3.4

clearly show that DRLRs lasting for at least 4 hrs maintain lower water temperatures at Cordova and GOUS. When the 4-hr and 6-hr DRLRs repeat more than 6 and 10 days, respectively, bottom temperatures at Cordova become lower than ones for CSR. These releases overwhelm the mixing effects due to flow momentum and maintain downstream temperature stratification.

Table 3.4 Statistical summary of differences (°C) of simulated temperatures between 2-hr, 4-hr, 6-hr DRLRs and CSR only for surface and bottom layers at MSF, Cordova, and GOUS.

Location	Temp Difference	Maximum	Minimum	Average	Deviation
MSF (Surface)	2-hr DRLR - CSR	0.23	-13.72	-9.35	2.49
	4-hr DRLR - CSR	-0.41	-14.65	-10.25	2.56
	6-hr DRLR - CSR	-0.92	-14.67	-10.63	2.53
Cordova (Surface)	2-hr DRLR - CSR	0.36	-7.35	-3.53	2.24
	4-hr DRLR - CSR	-0.33	-10.82	-6.10	2.84
	6-hr DRLR - CSR	-1.01	-12.63	-7.53	2.76
GOUS (Surface)	2-hr DRLR - CSR	0.67	-3.90	-1.49	0.70
	4-hr DRLR - CSR	-0.55	-9.43	-4.29	1.65
	6-hr DRLR - CSR	-1.56	-12.91	-8.84	2.20
MSF (Bottom)	2-hr DRLR - CSR	3.53	-9.23	-6.30	2.39
	4-hr DRLR - CSR	3.00	-9.95	-7.01	2.35
	6-hr DRLR - CSR	2.75	-10.23	-7.29	2.34
Cordova (Bottom)	2-hr DRLR - CSR	2.19	-2.08	0.38	0.81
	4-hr DRLR - CSR	3.98	-5.11	-0.30	2.63
	6-hr DRLR - CSR	2.72	-7.98	-1.64	2.86
GOUS (Bottom)	2-hr DRLR - CSR	1.20	-2.88	-0.38	0.70
	4-hr DRLR - CSR	1.06	-2.95	-0.38	0.90
	6-hr DRLR - CSR	0.54	-4.48	-1.10	1.17

3.7 Summary and Conclusions

The 3D EFDC model configured for BRRS was applied to simulate unsteady flow patterns and temperature distributions under large releases with different durations from SDT (upstream boundary). This study mainly focuses on result analyses of the EFDC simulations from SDT to GOUS, upstream portion of BRRS. A series of model scenario or sensitivity runs were performed to understand and quantify the formation and propagation of density currents caused by upstream releases and solar heating when all other input variables were kept unchanged. The summaries of key findings from the study are as follows:

(a) The density current formation and propagation in the natural system under intermittent large releases is complex and dynamic. The density currents in BRRS form at different reaches, are destroyed at upstream locations due to the flow momentum of the releases, and form again due to solar heating. Both the duration of large releases and solar heating affect and control the formation and spread of density currents when the release flow rate is unchanged (140 m^3/s).

(b) There are 48.4%, 69.0%, and 91.1% of time with positive bottom velocity (density currents moving downstream) with average positive velocity of 0.017, 0.042, and 0.053 m/s at Cordova for the 2-hr, 4-hr, and 6-hr DRLR, respectively (Table 3.2). The repeated releases with longer durations push the bottom colder water from SDT downstream and make the bottom water temperature in downstream locations to be cooler. For the 6-hr DRLR, the momentum effect definitely reaches Cordova (~43.7 km from SDT).

(c) With the CSR only, the cold water current (blue color) near SDT has moved downstream about 4 km in 6 days. With the 4-hr SLR, the cold water density current can move from Smith Dam to UPJ (21 km) in a few hours (Fig. 3.5). However, time-series plots of simulated surface and bottom temperatures at MSF and Cordova show that one SLR does not have long-term impact on downstream surface and bottom temperatures (Fig. 3.6). Regular (daily repeated) large releases are required to push density currents moving downstream and maintain temperature stratification in downstream locations (Fig. 3.9).

(d) Overall average surface and bottom temperatures are lower for longer duration of DRLR. The average difference between surface and bottom temperatures for 6-hr DRLR is 1.38 ^{o}C, while for 2-hr DRLR is 3.35 ^{o}C at Cordova (Table 3.3). Results in Fig. 3.9 and Table 3.3 and 3.4 clearly show that DRLRs lasting for at least 4 hrs maintain lower water temperatures at Cordova. When the 4-hr and 6-hr DRLRs repeat more than 6 and 10 days, respectively, bottom temperatures at Cordova become lower than ones for CSR only. These releases overwhlem the mixing effects due to inflow momentum and maintain downstream temperature stratification.

Chapter 4. Simulation of Flow and Dye Distributions of Density Currents in a River-Reservoir System under Different Upstream Releases

4.1 Abstract

A three-dimensional Environmental Fluid Dynamics Code model was calibrated and applied to simulate unsteady flow patterns, dye distributions and concentration in the Bankhead river-reservoir system in Alabama, USA. A series of sensitivity model runs were performed under different large releases (140 m^3/s) from Smith Dam Tailrace (SDT) when other input variables were kept unchanged. The cold-water current from SDT moves to MSF (~11 km) during the 4-hr single large release (SLR) and advances to ~18 km in 1 day after the release stops. In the following 4 days with constant small release only (after SLR stops), the dye moves downstream very slowly, less than 4 km. Daily repeated large releases (DRLRs) with longer durations push the dye to move further downstream. In the period without the large release, the dye spreads and mixes with the surrounding water due to turbulent diffusion and dispersion (due to backwater effect). When the next large release comes, the dye released at SDT is pushed downstream again. For the 4-hr DRLR, the dye moves to UPJ (~22 km from SDT), MJC (~33 km from SDT), Cordova (~43.7 km from SDT) and GOUS (~64.3 km from SDT) at 12 hrs, 34 hrs, 60 hrs, and 145 hrs after the dye release from SDT. For the 4-hr DRLR, the momentum effect has some impacts at Cordova but does not reach GOUS. For the 6-hr DRLR, the momentum effect

definitely reaches Cordova and the dye pattern repeats daily, and also has certain impact at GOUS.

4.2 Introduction

Regulating river flows is a common operating procedure as a means of water resources management all over the world. Reservoir release becomes a prominent characteristic for regulated rivers to meet hydro-electric power demands (Petts et al. 1985). Large flow release leads to larger flow depths at downstream river locations, where rapid water-level changes more than 1 m are common. These water-level changes have been detected more than 100 km downstream of the large dams after the wave attenuation (Petts 1984). Operational constraints considering water temperature in downstream river focused on a minimum flow requirement for water quality and temperature control (Carron and Rajaram 2001). The minimum flow is necessary during the warm months of the year, especially during the summer to maintain lower water temperatures downstream (Wunderlich and Shiao 1984; Consultants 1986). Atmospheric conditions (e.g., air temperature and solar radiation) have a large effect on river temperature after the reservoir release. Due to the solar radiation, typically water temperature in a shallow river is much warmer than release temperature of stored water in the reservoir.

Many laboratory and numerical model studies focused on density currents have been conducted in the last several decades. Density currents have been studied in situ by various researchers (Carmack et al. 1979; Alavian and Ostrowski Jr 1992; Dallimore et al. 2001). The density currents are also investigated in the laboratory (Akiyama and Stefan 1984; Hallworth et al. 1996). Most studies in the past dealt with sloping channels having rectangular cross section, and various simplifying assumptions were made to

develop analytical models with laboratory data to understand density currents (Denton 1985; Fernandez and Imberger 2008a). In the last several decades, 3D Environmental Fluid Dynamics Code (EFDC) (Hamrick 1992) has been widely used in modeling river, estuarine and coastal hydrodynamics and transport processes. Hamrick and Mills (2000) developed and used the EFDC model to simulate thermal transport and water temperature distributions in Conowingo Pond that was influenced by thermal discharges from the Peach Bottom atomic power plant. In order to quantify numerical and modeled entrainment. Liu and Garcia (2008) used modified 3D EFDC model to simulate the density current and bi-directional flows in the Chicago River system.

In this study, the dye model component in the EFDC model was activated to simulate dye concentration and distribution for each computation cell. We focused on understanding and analysis of flow dynamics generated from different types of the short-duration (a few hours) large flow releases into a confined river-reservoir system and formation and propagation of density currents. We studied constant small release (2.83 m^3/s), single large releases (140 m^3/s), and daily repeated large releases from an upstream reservoir. The results are important with regard to water quality modeling and management, habitat assessment, and management of thermal discharges in the river-reservoir system.

4.3 Study Area

The study deals with model simulations of flow and dye in a river-reservoir system (124.2 river km) starting from Smith Dam Tailrace (SDT) to Bankhead Lock& Dam (BLD) in Alabama (AL), USA (Fig. 4.1). It includes a part of the Black Warrior

River that is formed about 40 km west of Birmingham, AL, by the confluence of the Mulberry Fork and the Locust Fork, which join as arms of Bankhead Lake, a narrow reservoir formed by constructing BLD in 1963.

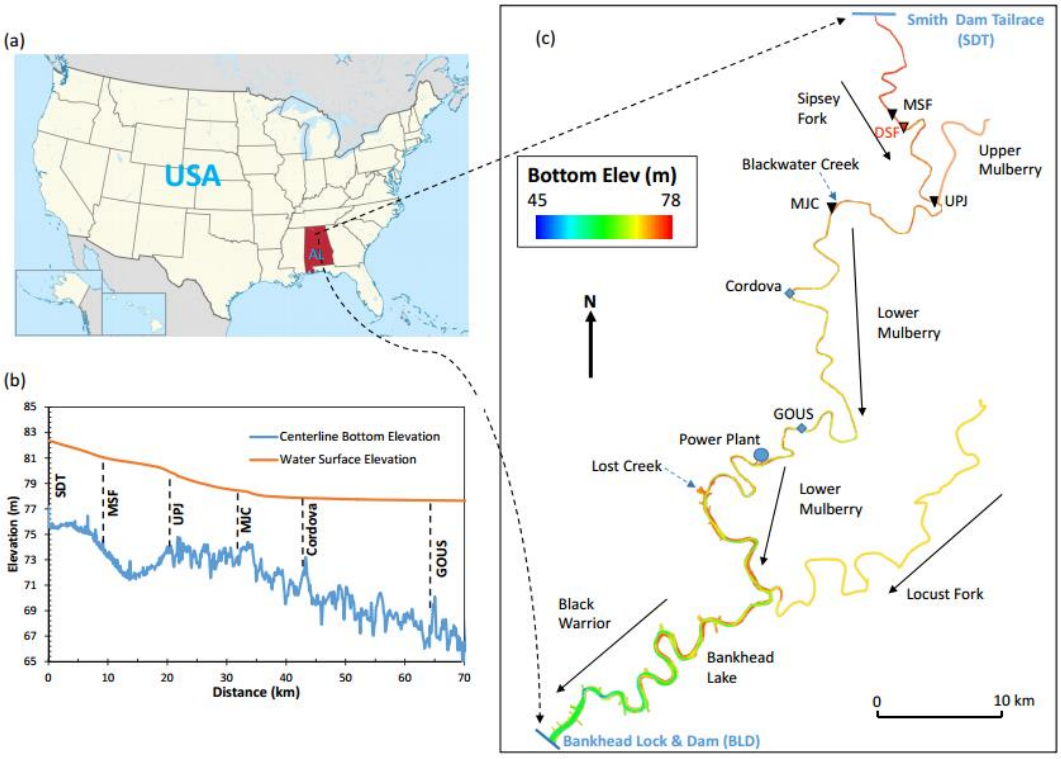

Fig. 4.1 (a) Geographic location of the study area–Bankhead river-reservoir system (BRRS), (b) Longitudinal bottom elevation along the centerline of BRRS and water surface elevation after a large release from the Smith Dam tailrace (SDT) to GOUS, and (c) Color contours of the bottom elevation showing Sipsey Fork, the lower Mulberry Fork, and Black Warrior River as the model simulation domain; two monitoring stations (Cordova and GOUS), model upstream and downstream boundary locations: Smith Dam tailrace (SDT) and Bankhead Lock&Dam (BLD), three cross sections for reporting

simulation results (MSF, UPJ, and MJC), two cross sections for dye release: SDT and the deepest part of Sipsey Fork (DSF).

The study river reach from upstream to downstream includes Sipsey Fork (21.9 km), the lower Mulberry Fork (70.6 km), and a reservoir segment (31.7 km) of Bankhead Lake. Sipsey Fork and the lower Mulberry Fork are the riverine portions of Bankhead Lake. The study area is referred here as the Bankhead river-reservoir system (BRRS).

The bottom elevations along the centerline of BRRS in the upstream portion of BRRS (Fig. 4.1b) ranged from about 65.8 to 77.2 m above mean sea level (using NAVD 1988 datum). The average bottom slope is 0.014% but there are local slope variations (ranging from -0.2% to 0.2% over each ~2 km distance). The water surface elevation in BRRS depends on water releases from Lewis Smith Dam, flows from its tributaries (Upper Mulberry, Locust Fork, Lost Creek, and Blackwater Creek), and the water surface elevation in BLD influenced by outflow through hydro turbines, spillage through gates of BLD, and loss of water through the Bankhead navigation lock. A typical water surface profile after a large release from Smith Dam displayed in Figure 1b depicts the response of water level increase in the upstream portion of BRRS from Smith Dam to the Gorgas upstream cross section (GOUS, Fig. 4.1c).

The monitoring stations and selected cross sections for result analysis are shown in Fig. 4.1c. The middle cross section of Sipsey Fork (MSF) is located at 11.1 km downstream from SDT. The cross section having the deepest local depth in Sipsey Fork for dye release is called DSF. The cross section at a short distance (0.64 km) upstream of the junction of Sipsey Fork and the upper Mulberry Fork is called UPJ. The middle cross

section between the junction and Cordova is called MJC. The monitoring station at 5.58 km upstream the power plant is called GOUS (Fig. 4.1c).

4.4 Model Application, Boundary Conditions, and Calibration Results

The EFDC model is a general purpose modeling package that can be configured to simulate one-, two- and three-dimensional flow, transport, and biogeochemical processes in various surface water systems including rivers, lakes, estuaries, reservoirs, wetlands, and coastal regions (Caliskan and Elci 2009; Devkota and Fang 2014). Details of governing equations and numerical schemes for EFDC hydrodynamic model are given by Hamrick (Hamrick 1992c). The EFDC model applied to BRRS in this study was previously calibrated and validated using extensive field data measured in 2010 and 2011 (Fang et al. 2013; Chen et al. 2015).

The upstream boundary of the EFDC model for BRRS is one-minute time-series data of water releases (m^3/s) at SDT. There are two types of water releases from Smith Dam: (1) more or less constant continuous release (2.83 m^3/s) to support the downstream environment and ecosystem; (2) intermittent releases from hydro-turbine units of Smith Dam in order to meet peak electric generation demand. Measured water temperatures used for upstream boundary condition at SDT from 8 September to 18 October, 2010, was almost constant (9.6 ^oC) during the constant release, and water temperatures during the intermittent large releases were 10–15 ^oC, which were 4–5 ^oC higher than temperatures during the constant release only from Smith Dam. This is because constant release occurred from a deep water depth and intermittent releases were from a shallower

depth of Smith Dam; and there was lower water temperature in the hypolimnion due to thermal stratification in the summer.

In a previous study (Chen et al. 2015), the three-dimensional hydrodynamic EFDC model was applied to simulate unsteady flow patterns and temperature distributions under various upstream releases and variable atmospheric forcing in BRRS in 2011. The calibrated EFDC model provided simulated water surface elevation, temperature, velocity and discharge at different layers (depths) for all grids in different cross sections. Overall, the EFDC model was able to simulate the temporal and spatial distributions of flow and temperature in BRRS and reveal complex interactions and density currents due to dynamic upstream releases and solar heating from atmosphere (Chen et al. 2015). Results on flow dynamics and temperature distributions at different river cross sections are summarized and presented elsewhere (Chen et al. 2015; Chen and Fang 2015a).

4.5 Dye Distributions and Concentration

For scenario analysis performed in this study, various input data (boundary conditions) were modified into constant representative values excluding upstream boundary conditions. Therefore, we can focus on studying effects of dynamic releases from the upstream reservoir only on density current formations and movement using dye. The inflows from all tributaries and small streams (Fig. 4.1) were set at average inflows calculated from time series of inflows used for model calibration. Average inflows from the Upper Mulberry Fork, Lost Creek, Blackwater Creek and Locust Fork are 4.42, 5.54, 2.60, and 8.70 m^3/s for all scenario model runs. At BLD, water level was used as

downstream boundary condition. Observed water surface elevations ranged from 77.35 m to 77.75 m from 4 May to 3 September 2011 with an average elevation of 77.60 m (standard deviation of 0.07 m). Therefore, water surface elevation at BLD was set at 77.60 m (constant) for the scenario runs. Based on the sensitive analysis, the constant water level at BLD would not affect overall flow dynamics in the upstream portion of BRRS (from SDT to GOUS). For the atmospheric boundary conditions, weather data in a relatively warm day of the year were used to perform scenario model runs: hourly climate data from Birmingham, AL (Chen et al. 2015).

EFDC dye model components were activated to simulate dye concentrations for each computation cell to understand density current movement. The dye was released at SDT or the deepest local depth in Sipsey Fork (DSF, Fig. 4.1c) for model scenario runs. The model scenario runs are distinguished as two groups. The first group of model scenario runs are to study dye dynamics resulted from one large release (LR): Smith Dam has constant small release (CSR, i.e., 2.83 m^3/s) for 6 days, then one 4-hr large release in the 7th day, and then SCR for another 6 days again. The model runs are restarted at the time of Julian day 142.53 (~1:00 pm on 22 May) using EFDC's restart file (Craig 2012), which was created under the calibration model run. The duration of dye release is same as one 4-hr large flow release at Smith Dam. The second group of scenario runs are similar to the actual releases that large flow and dye release repeats day by day: the model run is started at Julian day 140 using EFDC's restart file (Craig 2012) and all the cases have the same large release repeated day by day after the day 140. After 2 days of model warm up period, the dye release is started from the Julian day 142.54 (1:00 pm each day) for 6 hrs each day. The large releases from Smith Dam have a flow rate of 140 m^3/s, which is

average discharge of the intermittent releases from Smith Dam based on data analysis (Chen et al. 2015), and last for 2, 4, and 6 hrs for different cases, respectively. We set the dye release for 6 hrs for all model runs in each day by using the longest release duration. The dye release is set as 1 mg/l at two locations: SDT and DSF which is located between MSF and UPJ shown in Figure 1c. In the following discussions, the first group of the scenario runs are called 2-, 4-, and 6-hr single large releases (SLR), and the second group of the scenario runs are called 2-, 4-, and 6-hr daily repeated large releases (DRLRs).

4.5.1 Single Large Releases (SLRs)

Dye distributions are useful and clear to track how the density current moves. Fig 4.2 shows simulated dye distributions under a 4-hr SLR and then CSR at four different time (panels from top to bottom): the 4-hr SLR just stops, 1, 2, and 4 days after the release stops (CSR only) when the dye is released from (a) SDT (left panels) and (b) DSF (right panels). The dye released is set at 1 unit (red color), and the blue color is for zero dye concentration in Fig. 4.2a. The cold-water current from SDT moves to MSF (~11000 m) during the 4-hr SLR and advances to ~18000 m for 1 day after the release stops. In the following 4 days with CSR only (after SLR stops), the dye moves towards downstream very slowly, less than 4000 m (Fig. 4.2a). In Fig. 4.2b, the dye introduced at DSF responds the release quickly to spread over the whole depth (all 10 layers) over about 6000 m of the river distance due to momentum transfer or push effect of the large release from SDT when the dye is released only five bottom layers at DSF because the released water has not reached at DSF yet at that time (Fig. 4.2a). About 2 days after the release

stops, the dye from DSF is not affected by the CSR but slowly spreads and moves downstream.

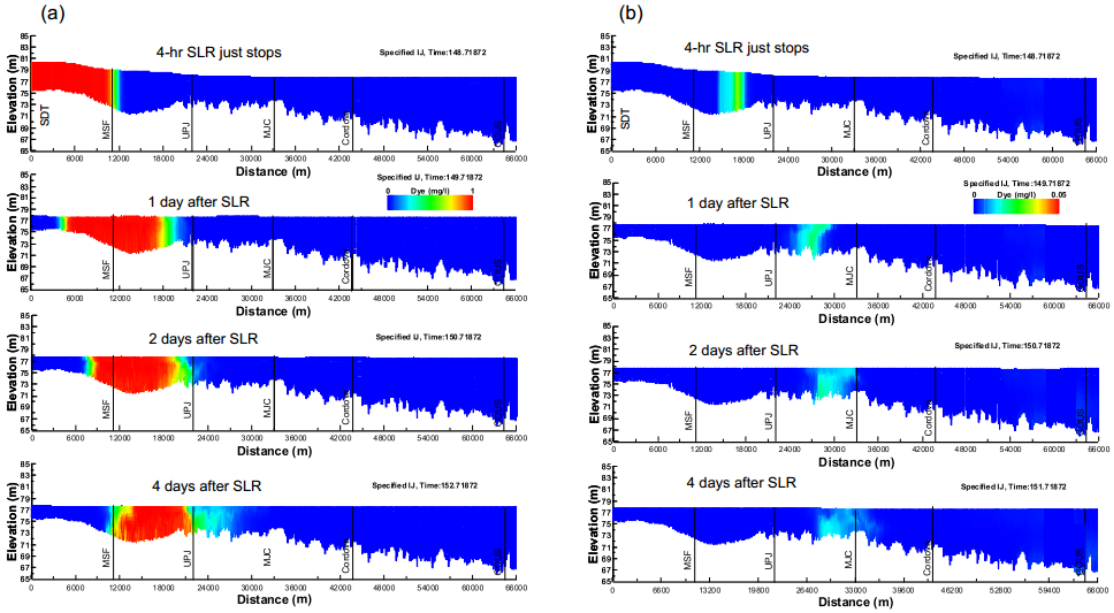

Fig. 4.2 Simulated dye distributions under a 4-hr SLR at four different time (panels from top to bottom): the 4-hr release just stops, 1, 2, and 4 days after the release stops (CSR only) when the dye is released from (a) SDT (left panels) and (b) DSF (right panels).

Fig. 4.3 shows time series plots of simulated average dye concentration and total water volume in the domain from SDT to MSF, MSF to UPJ when the dye is released from SDT during and after the 4-hr SLR period. The 4 dash lines in Figs. 4.3 and 4.4 indicate 4 different time corresponding to Fig. 4.2, i.e., the 4-hr SLR just stops, 1, 2, and 4 days after the release stops. In the domain from SDT to MSF, the dye concentration sharply increases from 0 to 1 mg/l during the 4-hr SLR (Fig. 4.3a). After the release stops, the dye concentration in the SDT to MSF gradually decrease because the flow momentum inertia pushes released colder water passing MSF and moving to UPJ (Fig.

4.2a). When it is Julian day 153 (about 4 days after the release), there is no dye (i.e., colder released water) upstream MSF. The total volume reaches to the maximum when the 4-hr SLR just stops and increases from 0.9 to 2.0 million m^3. In the domain from MSF to UPJ (Fig. 4.3b), the dye concentration begins to increase when the large release stops, which means the dye takes about 4 hrs moving from SDT to MSF, as also indicated and seen by Fig. 4.2a. Being different from the upstream domain (SDT to MSF), it takes about 3 days for the dye concentration to reach the maximum value of 0.94 mg/l. The total volume of water changes from 1.9 (before the release) to 2.5 million m^3 shortly (~1 hr) after the release stops. At 11–12 hrs after the release stops, the total volume of water in both domains reduces to the amount before the release and has small variations afterwards. This means the surface wave created by the large release attenuates in 11–12 hrs.

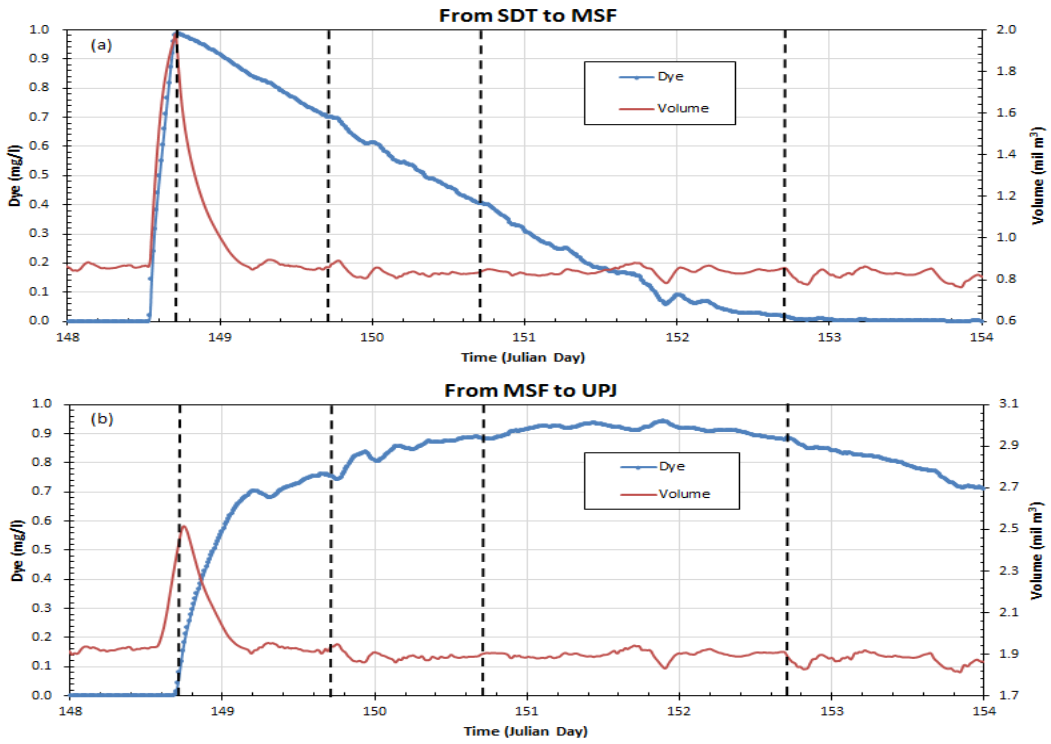

Fig. 4.3 Simulated dye concentration and water volume in the domain from SDT to MSF, MSF to UPJ when the dye is released from SDT during and after a 4-hr SLR.

Fig. 4.4 shows time series plots of simulated dye concentration and total volume of water in the domain from MSF to UPJ and from UPJ to MJC when the dye is released from DSF (a separate model run) during and after the 4-hr SLR. The released dye concentration at DSF is also 1 mg/l. In the EFDC model, the dye can only be introduced by an inflow. The dye is released at SDT through the large release (Fig. 4.3), but a hypothetical inflow with negligible flow rate (so that it does not have any impacts to overall flow dynamics in BRRS) is introduced at DSF (bottom five layers) for the dye release; therefore, the magnitude of dye concentration is very small in Fig. 4.4. In the domain from MSF to UPJ, the dye concentration begins to increase quickly after SLR starts (Fig. 4.4). This further indicates the momentum transfer or push effect reaches and

impacts DSF before the released water arrives (Fig. 4.2b). In the domain from UPJ to MJC, the dye concentration begins to increase after the large release stops for 2 hrs. It also shows that momentum transfer or push effect reaches to UPJ before the release water arrives (Fig. 4.2). Higher dye concentration lasts about 3–4 hrs from SMF to UPJ but about two days from UPJ to MJC. From UPJ to MJC, total volume of water increases from 2.75 to 2.95 million m^3, which indicates the surface wave attenuates with distance quickly. The volume increase is 0.2 million m^3 from UPJ to MJC due to the large release, but several ~0.1 million m^3 variations occur in later days, which indicates possible complex interactions of surface waves due to the backwater effects.

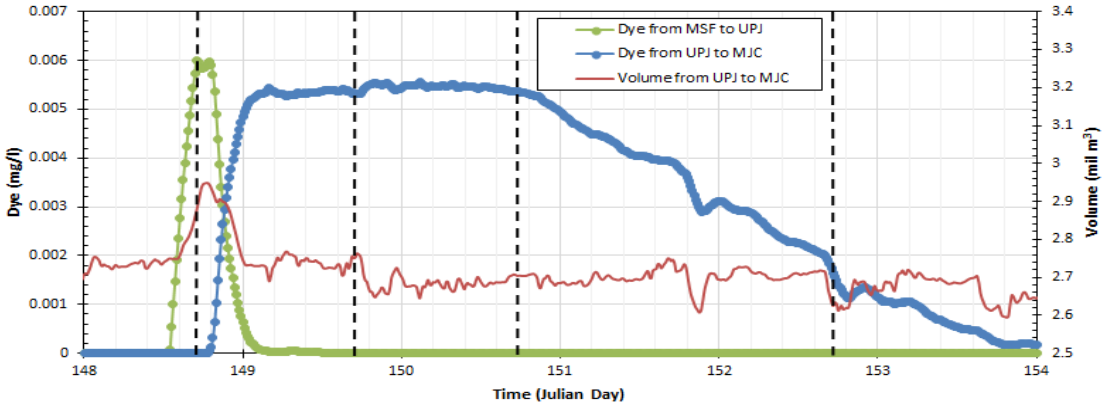

Fig. 4.4 Simulated average dye concentrations in the domain from MSF to UPJ and from UPJ to MJC and water volume from UPJ to MJC when the dye is released from DSF during and after the 4-hr SLR.

Fig. 4.5 shows time series plots of simulated average dye concentrations at three cross sections: MSF, UPJ, and MJC when the dye is released from SDT for 6 hrs under the 2-hr, 4-hr, and 6-hr SLR scenarios. All SLRs occur at 1:00 pm on Julian day 148 (28 May). At the MSF cross section, the dye concentration starts to increase almost

immediately after the release has started for all three duration releases. This is because MSF is close to SDT (the dye release location) and the momentum effect. The dye concentration at MSF takes slightly longer time to its maximum value for the 2-hr SLR in comparison to the 4- and 6-hr SLRs. At MSF, the maximum dye concentrations are all ~1 mg/l for 3 duration SLRs. At UPJ and MJC, the dye concentration of the 6-hr release starts to increase first, then the increase starts for the 4-hr release, and the last increase is for the 2-hr release. At UPJ, for the 6-hr SLR, the dye concentration increases to 0.90 mg/l in ~8 hrs, then it decreases to 0.56 mg/l, after that it begins to increase to 0.93 mg/l again. This situation may due to the backwater effect from downstream. But the maximum dye concentration gradually decreases when the flow momentum pushes the dye downstream. The 2-hr and 4-hr SLR dye concentration at UPJ have the same pattern as the 6-hr SLR has. The maximum dye concentration at UPJ for shorter duration large releases is smaller than ones for the longer duration releases.

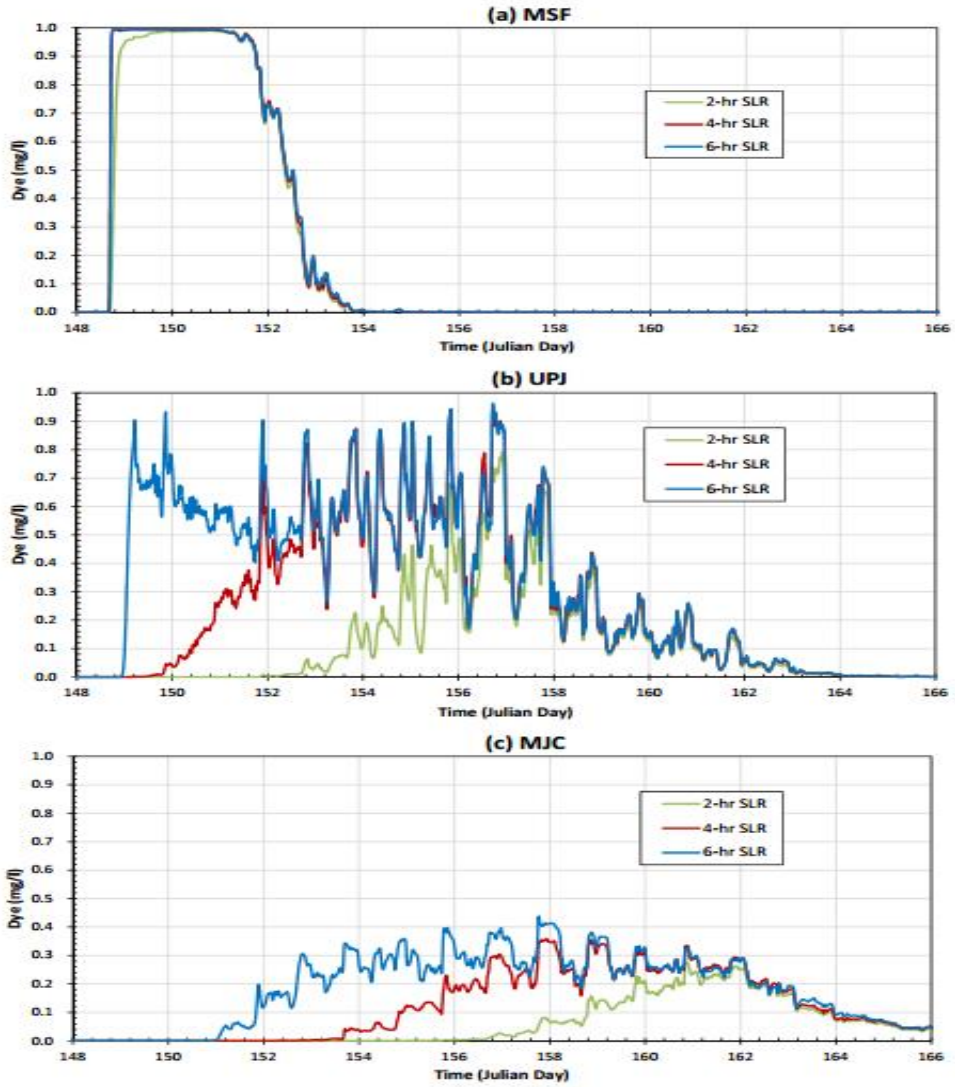

Fig. 4.5 Simulated average dye concentrations at three cross sections: MSF, UPJ, and MJC when the dye was released from SDT for the 2-hr, 4-hr, and 6-hr SLR scenarios.

At MJC, the maximum dye concentration reduces to less than 0.4 mg/l for all three different duration releases. After the large release stops for ~3, ~7, ~13 days, the dye concentration at MSF, UPJ and MJC decreases in the same pattern for all three different duration releases, respectively. Figs. 4.2–4.5 all show the density current

movement for SLRs, which are different from DRLRs; but help us to understand better dynamics and mechanism of flow and density current at different locations.

4.5.2 Daily Repeated Large Releases (DRLRs)

The second group scenario runs with DRLRs are close to the actual release patterns. Fig. 4.6 shows simulated dye distributions at (a) 1 day (top panels), (b) 2 days (middle), and (c) 4 days (bottom) when DRLRs at SDT last 2, 4, and 6 hrs each day, and the dye is released for 6 hrs at SDT each day. The dye is advanced day by day when the large release is repeated each day. It's obvious that longer-duration flow release (6-hr) pushes the dye to move further downstream. The dye front moves to UPJ (about 21 km) in 1 day after the 6-hr DRLR starts. In the period without the large release, the dye spreads and mixes with the surrounding water due to turbulent diffusion and dispersion (due to backwater effect). When the next large release comes, the dye released at SDT is pushed downstream again. Fig. 4.6 clearly shows dye concentration and dye movement due complex interaction of moment push and diffusion after several large releases. At 2 days after the dye release on Day 142, the dye front from 6-hr releases moves to 36 km (passes MJC). With DRLR for 5 days, density current with cold water moves downstream all the way to GOUS (projections from Fig. 5.6c).

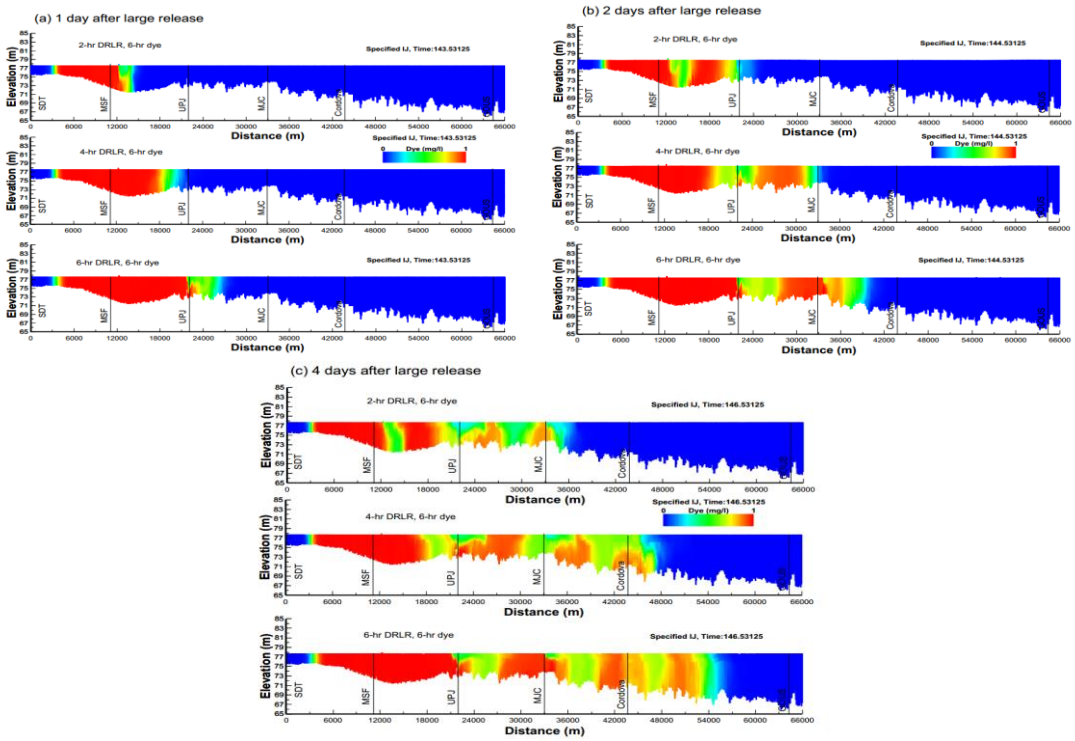

Fig. 4.6 Simulated dye distributions at (a) 1 day (top panels), (b) 2 day (middle), and (c) 4 day (bottom) when the DRLRs at Smith Dam tailrace last 2, 4, and 6 hrs each day, and the dye release for 6 hrs at Smith Dam each day.

Fig. 4.7 shows time-series plots of simulated dye concentrations in the cross sections MSF, UPJ, MJC, Cordova and GOUS when the 6-hr dye is released from SDT for (a) 2-hr, (b), 4-hr, and (c) 6-hr DRLRs. The dye front moves to MSF at almost same time for 2-hr, 4-hr, and 6-hr DRLRs. For the locations downstream of MSF, it clearly shows that dye of the longer-duration flow release moves downstream quicker. Taking the 4-hr DRLR as an example, the dye moves to UPJ, MJC, Cordova and GOUS at Julian day 143.0313, 143.9583, 145.0313, and 148.5833, respectively, which means 12 hrs, 34 hrs, 60 hrs, and 145 hrs after the dye release from SDT (Fig. 4.7b). At MSF, the dye

concentration increases to ~1 mg/l immediately, it keeps ~22 hrs (up to day143.6563), the dye concentration drops to 0.4 mg/l (day 143.6875), then due to the next day large release, the dye concentration increases to 1 mg/l (day 143.7396) again. The same situation repeats at the MSF in the following days.

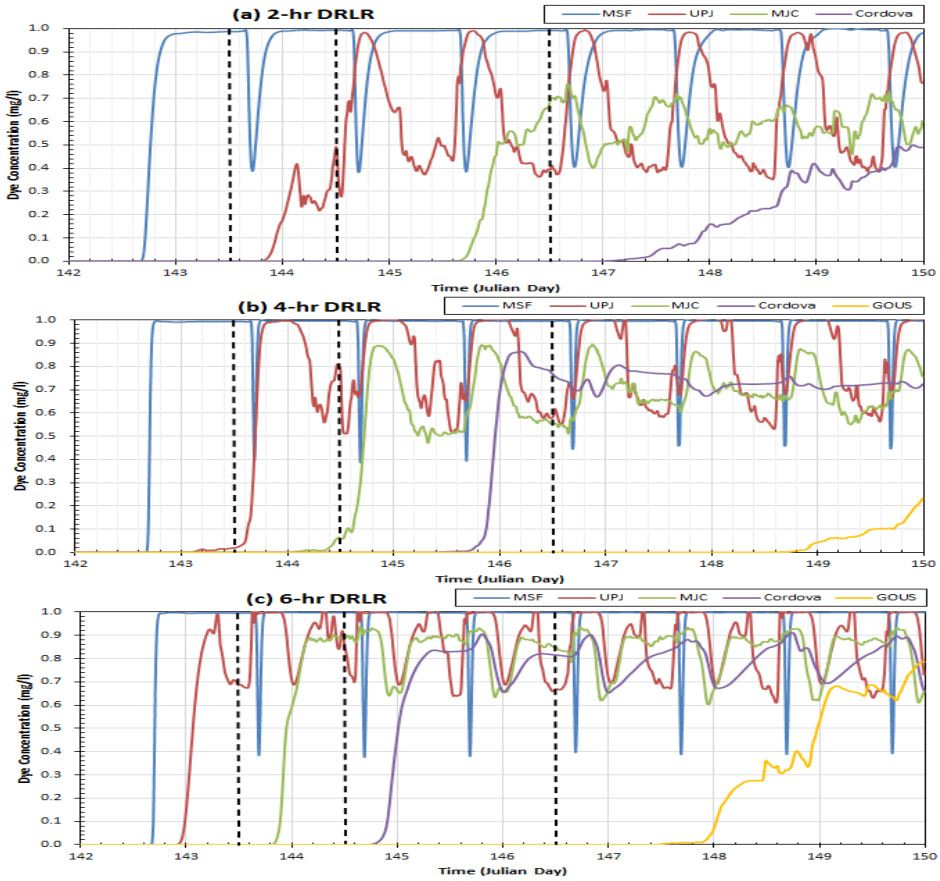

Fig. 4.7 Simulated dye concentrations in the cross sections MSF, UPJ, MJC, Cordova, and GOUS when the 6-hr dye is released from SDT for (a) 2-hr, (b), 4-hr, and (c) 6-hr DRLR.

At UPJ and MJC, the overall pattern is similar to the pattern at MSF, but the dye concentration fluctuates with time (increased and decreased) when the large flow momentum effect vanishes and before the next daily large release starts again. This may be due to the backwater effect from downstream. For the 2-hr DRLR, it seems the momentum effect does not reach Cordova because dye at Cordova does not have sudden increase instead of gradual increase (Fig. 4.7a). For the 4-hr DRLR, the momentum effect has some impacts at Cordova but does not reach GOUS (Fig. 4.7b). For the 6-hr DRLR, the momentum effect definitely reaches Cordova and the dye pattern repeats daily, and also has certain impact at GOUS (Fig. 4.7a).

4.6 Conclusion

The cold-water current from SDT moves to MSF (~11 km) during the 4-hr SLR and advances to ~18 km in 1 day after the release stops. In the following 4 days after SLR stops but there is CSR only, the dye moves downstream very slowly, less than 4 km (Fig. 4.2a). At 11–12 hrs after the 4-hr SLR stops, the total volume of water in both domains of SDT to MSF and MSF to UPJ reduces to the amount before the release and has small variations afterwards. This means the surface wave created by the large release attenuates in 11–12 hrs (Fig. 4.3). The dye is advanced day by day when the large release is repeated each day, i.e., DRLR. The longer-duration DRLR (e.g., 6-hr) pushes the dye to move further downstream. The dye front moves to UPJ (about 21 km) in 1 day after the 6-hr large release (Fig. 4.6). In the period without the large release, the dye spreads and mixes with the surrounding water due to turbulent diffusion and dispersion (due to backwater effect). When the next large release comes, the dye released at SDT is pushed

downstream again. For the 4-hr DRLR, the momentum effect has some impacts at Cordova but does not reach GOUS. For the 6-hr DRLR, the momentum effect definitely reaches Cordova and the dye pattern repeats daily (Fig. 4.7).

Chapter 5. Influences of Meteorological Conditions and Daily Repeated Upstream Release on Temperature Distributions in a River-reservoir System

5.1 Abstract

A calibrated three-dimensional Environmental Fluid Dynamics Code model was applied to simulate temperature distributions under various hypothetical weather conditions and daily repeated large releases (DRLRs) from the upstream boundary in a river-reservoir system in Alabama. Both the duration of large releases and weather conditions affect and control the formation and spread of density currents and then affect the bottom-layer temperatures. The repeated releases with longer durations push the colder bottom water towards downstream and make the bottom-layer water temperature in downstream locations cooler. The daily drop rate of bottom-layer water temperature under 6-hr DRLRs are 0.3, 0.5 and 0.4 °C/day for 2, 4, 6 days of 2 °C/day air temperature drop. Average bottom temperature at the river intake under 4-hr DRLRs is 2.3 ^{o}C lower than one under 2-hr DRLRs and only 1.1 ^{o}C higher than one under 6-hr DRLRs in the whole simulation period. The daily drop rate and dropping duration of bottom temperature are almost same for 2-, 4- and 6-hr DRLRs due to the same drop and rise pattern for weather conditions. The maximum differences between the constant weather scenario and the 11-day drop and rise weather scenario range from 3.1 to 4.2 °C under different releases. The lower bottom-layer water temperatures at GOUS and the river

intake are primarily due to the lower air temperatures and solar radiations during the 11 days and less affected by the release pattern. To identify more efficient release operations should be further studied.

5.2 Introduction

Water temperature is one of the significant and important water quality characteristics of surface waters (Kothandaraman and Evans 1972). Water temperature affects all biological and chemical reactions and the density of water that influences the transport of water and pollutants in aquatic systems (Thomann and Mueller 1987). Natural processes or human activities such as industrial production, deforestation, and climate change would affect water temperatures (Caissie 2006). Many climate and environmental parameters can also possibly affect water temperature in streams/rivers, for example, solar radiation, relative humidity, wind speed, water depth, groundwater inflow, artificial heat inputs, and thermal conductivity of the sediments (Pilgrim et al. 1998; Johnson et al. 2009). Weather condition is not the only physical parameter influencing water temperature but a very important parameter. Harmeson and Schnepper (1965) and the Texas Water Development Board (1970) indicated graphically that water temperatures in rivers follow closely the pattern of variations in daily mean air temperatures.

The alteration of flow in the river can also be responsible for changes in river water temperature (Morse 1972; Sinokrot and Gulliver 2000). River regulation as a means of water resources management is a common operating procedure all over the world. To meet hydro-electric power demands, upstream reservoir release is becoming a

prominent characteristic for regulated rivers (Petts et al. 1985). The requirement of minimum flow is usually during the warm season of a year, especially during the summer to maintain lower water temperatures downstream (Wunderlich and Shiao 1984; Consultants 1986). Increasing flow release leads to larger flow depths at downstream river, and it is common the release results in rapid stage changes such as more than 1 m (Fang et al. 2013; Chen et al. 2015). Stage changes have been detected more than 100 km downstream of the large dams after the wave attenuation (Petts 1984). Besides the momentum effect from the upstream large release, atmospheric conditions will continue have a large effect on river temperature after the reservoir release. Due to the solar heating, typically water temperature in a shallow river is much warmer than release temperature of stored water in the reservoir, which makes the variations of river temperature more complex.

There are a significant number of the river-reservoir systems that have large diurnal variations in atmospheric heating rates and develop density currents in the downstream river/reservoir due to colder denser flow releases from an upstream reservoir (Fang et al. 2013; Chen et al. 2015). A plunging density current occurs when the density of the water flowing into a reservoir or lake is greater than the density of the ambient water. Due to the flow momentum, the denser inflow mixes homogeneously with the reservoir or lake water first. When the inflow momentum diminishes, the inflow eventually plunges under the ambient water and flows along the river bottom as a density current (Farrell and Stefan 1989). The intermittent denser flow releases from an upstream reservoir create very complex and unsteady density currents, which are also

affected by the meteorological conditions, but climatic affects on density cureents have not been systematically quantified yet.

Many laboratory and numerical model studies focused on density currents have been conducted in the last several decades. Density currents have been studied in situ by various researchers (Serruya 1974; Carmack et al. 1979; Fischer and Smith 1983; Chikita 1992; Dallimore et al. 2001). The density currents are often investigated in the laboratory due to challenges and difficulties of the study in the natural systems (Akiyama and Stefan 1984; Hauenstein and Dracos 1984; Alavian 1986). To understand density currents, various simplifying assumptions were made to develop analytical models with laboratory data (Savage and Brimberg 1975; Denton 1985; Kranenburg 1993). Most of the previous studies dealt with sloping channels and rectangular cross section. Fang and Stefan (2000) developed an integral model for a discharge from a river channel over a horizontal or a sloping bottom into a reservoir or a lake to determine dilution up to plunging for density current computations.

Recently, there are many studies about density current in natural systems such as flows from a river into a lake, a reservoir, an ocean, or an estuary. Fatih and Varcin (2012) developed a mathematical model solving nonlinear, unsteady continuity, momentum, energy, and k-ε turbulence equations and applied the model to successfully simulate the formation of density currents and plunging flow in Eğrekkaya Dam Reservoir. Soliman et al. (2014) applied the two-dimensional (2D) multi-phase numerical model to simulate the density current propagation and salinity intrusion into Ohashi River that connects Nakaumi and Shinji coastal lakes and concluded the further refinement of the model is needed for field study application. Biton et al. (2008) studied density

current formation and flow dynamics in the northern Gulf of Eilat, Red Sea, and demonstrated the intrinsic nonlinearity of density currents, which is poorly represented in the general circulation model, affect properties of simulated density currents. Cook and Richmond (2004) conducted a field monitoring study and used the Flow-3D (Hirt and Nichols 1988) model to simulate the complex 3D density currents at the Clearwater and Snake River confluence and discovered several predictable stratification patterns that would develop depending upon the discharge ratio and the thermal gradients between the two rivers. Toffolon et al. (2010b) developed a coupled hydro-thermodynamic deterministic model and analytical solutions for river water temperature to get a better insight into the physical properties associated with the propagation of both hydrodynamic and thermal peaking waves in a downstream receiving river.

In a previous study (Chen et al. 2015), a three-dimensional (3D) Environmental Fluid Dynamics Code (EFDC) model (Hamrick 1992b) was configured and calibrated for a river-reservoir system (Fig. 1) in Alabama, USA, to simulate unsteady flow patterns and temperature distributions. The boundary conditions used for the model calibration were observed data in 2010 (Fang et al. 2013) and 2011 (Chen et al. 2015). The calibrated EFDC model provided simulated unsteady water surface elevation, temperature, velocity and discharge at different layers (depths) in different cross sections. Distributions of simulated flow and temperatures and particle tracking at various locations were analyzed and revealed the complex interactions of density currents, dynamic surface waves, and solar heating. In the following study (Chen and Fang 2015a), boundary conditions except the upstream release were kept as constant for the model scenario runs of two types of upstream release: one single large release (SLR) and daily

repeated large release (DRLR). A series of model scenario runs were conducted to understand and quantify formation and propagation of density currents which are caused by DRLRs of different durations and solar heating. The complex density currents in the river-reservoir system form at different reaches, are destroyed at upstream locations due to the flow momentum of the releases, and form again due to solar heating. Results show that DRLR can maintain lower water temperatures at downstream locations. In this study, we focus on combined or integrated effects of variable weather conditions and DRLRs on the downstream water temperatures. We examine simulated temperature distributions under different types of weather scenarios to evaluate site-specific correlation with weather conditions. The results of this study are important with regard to water quality modeling and management, habitat assessment in rivers, and management of thermal discharges from a power plant. The once-through cooling water system for the power plant in the study area is designed to withdraw cold water from the bottom layers at the river intake to maintain higher plant efficiency.

5.3 Material and Methods

5.3.1 Study Area

The study covers a river-reservoir segment (124.2 river km, Fig. 5.1) stretching from Smith Dam Tailrace (SDT) to Bankhead Lock & Dam (BLD, the height of 23.5 m and the width of 426.7 m) in Alabama (AL), USA. The river reach from upstream to downstream includes Sipsey Fork (21.9 km), the lower Mulberry Fork (70.6 km), and a reservoir segment (31.7 km) of Bankhead Lake. Sipsey Fork, the upper and the lower Mulberry Fork are the riverine portions of Bankhead Lake (Fig. 5.1). The Black Warrior

River is formed about 40 km west of Birmingham, AL, by the confluence of the Mulberry Fork and the Locust Fork, which are two arms of Bankhead Lake, a narrow reservoir formed by constructing BLD in 1963. The study area is referred here as the Bankhead river-reservoir system (BRRS). There is a power plant located at the bank of the upstream portion of the Bankhead Lake. The power plant withdraws cooler water from the Black Warrior River to manage the thermal discharges. The location of withdrawing water from the bottom layers in the Black Warrior River is called the river intake (Fig. 5.1). The monitoring station 5.58 km upstream of the power plant is called GOUS (Fig. 5.1), which is 64 km downstream from SDT. The deepest water depth at GOUS is about 10.0 m.

Bottom elevations of BRRS are shown as color contours in Fig. 5.1. The bottom elevations along the centerline of BRRS rang from about 59.5 to 77.2 m above mean sea level (using the 1998 North American Vertical Datum). The average bottom slope is 0.014% but there are local slope variations (ranging from −0.2% to 0.2% over each ~2 km distance). The water surface elevation in BRRS varies and depends on water releases from Lewis Smith Dam, flows from its tributaries (Upper Mulberry, Locust Fork, Lost Creek and Blackwater Creek), and the water surface elevation in BLD, which is influenced by outflow through hydro turbines, spillage through gates of BLD, and loss of water through the Bankhead navigation lock. The water release from Smith Dam to BRRS is normally 2.83 m^3/s, but during late spring, summer, and early fall a large amount of water is released over a few hours to meet peak electric generating demand. During normal water releases, water depths in Sipsey Fork range from 2.16 to 4.55 m, in the lower Mulberry Fork from 4.71 to 11.47 m, and in the Bankhead Lake from 12.12 to 17.73 m. Observed

water surface elevations at BLD in 2011 ranged from 77.43 to 77.74 m with an average elevation of 77.60 (standard deviation of 0.06 m) above mean sea level. Therefore, water surface elevation at the downstream boundary (BLD) is almost steady and has only small changes over time.

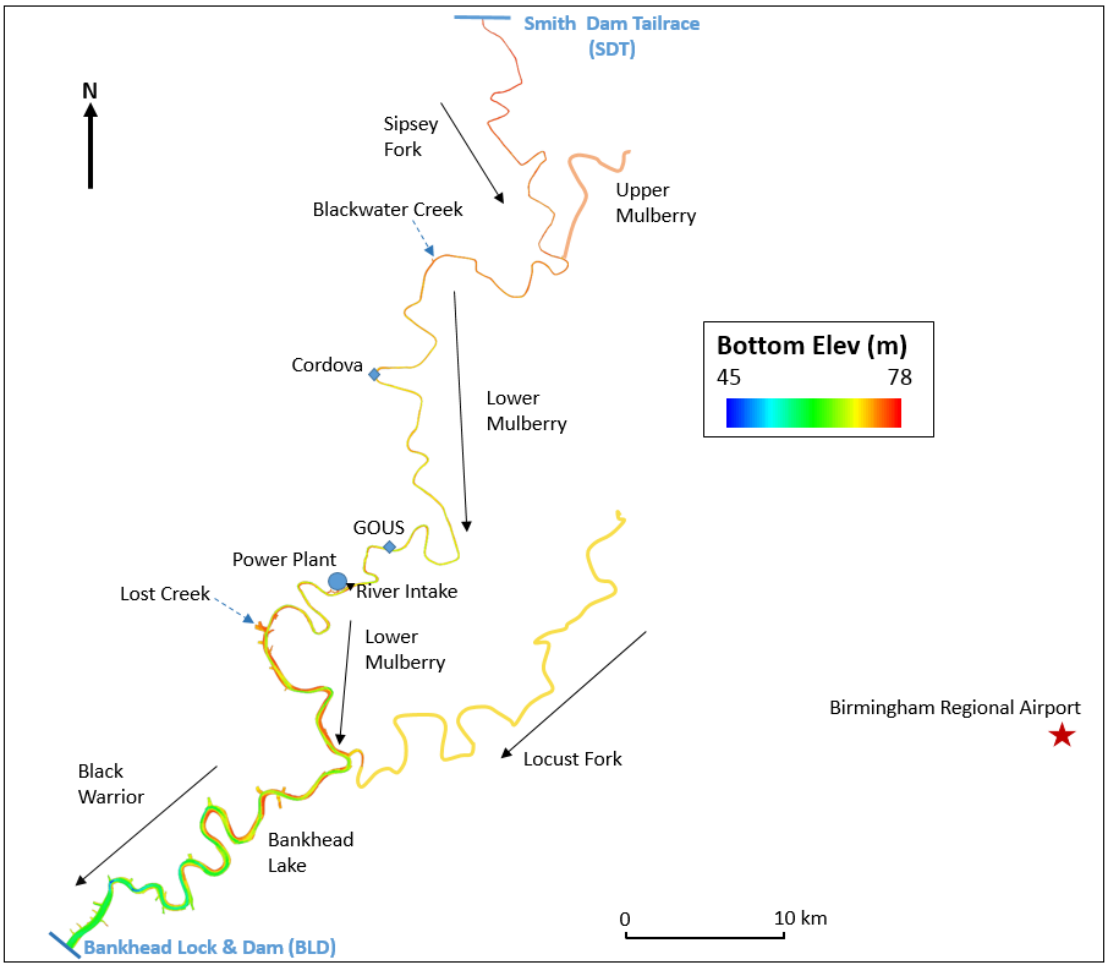

Fig. 5.1. Color contours of the bottom elevation showing Sipsey Fork, the lower Mulberry Fork, and Black Warrior River as the model simulation domain; two monitoring stations (Cordova and GOUS); model upstream and downstream boundary locations: Smith Dam tailrace (SDT) and Bankhead Lock & Dam (BLD), and weather station at Birmingham regional airport.

5.3.2 Numerical Simulation Model

The EFDC model is a general-purpose modeling package that can be configured to simulate one-, two- and three-dimensional flow, transport, and biogeochemical processes in various surface water systems including rivers, lakes, estuaries, reservoirs, wetlands, and coastal regions (Shen and Lin 2006; Jeong et al. 2010; Kim and Park 2012; Devkota and Fang 2014). The EFDC model was originally developed at the Virginia Institute of Marine Science and the version of EFDC used for the study with pre- and post-processing tools was EFDC-DSI (Craig 2010) from the Dynamic Solutions-International, LLC (http://efdc-explorer.com/). The Mellor-Yamada level 2.5 turbulence closure scheme (Mellor and Yamada 1982) is used in EFDC to calculate vertical turbulent diffusion coefficients of momentum and mass, which are linked to vertical turbulent intensity, turbulent length scale, and the Richardson number (Hamrick 1992b). Details of governing equations and numerical schemes for EFDC hydrodynamic model including temperature simulation are given by Hamrick (Hamrick 1992b).

In addition to the hydrodynamic model, the EFDC temperature model component was activated in this study to simulate unsteady water temperatures for each computation cell to understand density current movement in the river-reservoir system. In the EFDC temperature model, it is important to accurately model the heat exchange between the water surface and the atmosphere. The surface heat exchange includes incident and reflected short and long wave solar radiations, back radiation, evaporative heat loss, and heat conduction from the water surface. EFDC has four options available for calculating

the surface heat exchange (Hamrick 1992b). The CE-QUAL-W2 equilibrium temperature method is the most robust method among the four options; therefore, it was used in this study for water temperature modeling. The depth distribution of the solar heating (short-wave radiation) after penetrating the water surface is calculated by Beer's law using a radiation or light attenuation coefficient as one of the model input parameters. Sediment heat exchange with overlying water is also included in the EFDC temperature model. Detailed information on the governing equations for the heat exchange processes in a water body is given in the CE-QUAL-W2 manual (Cole and Buchak 1995).

The 3D EFDC model configured for BRRS (Chen et al. 2015) has a total of 6974 curvilinear orthogonal grids and 10 horizontal layers (determined through a sensitivity analysis) along the depth direction; therefore, there are a total of 69 740 computational cells. The grid size DX in transverse direction along the river ranged from 9.5 m to 189.8 m and DY in longitudinal flow direction ranged from 10.0 m to 277.1 m. Average grid sizes DX and DY are 25.7 m and 100.9 m, respectively. This study mainly focuses on the EFDC simulations and result analysis at GOUS in the middle of BRRS and the river intake, under different meteorological conditions and large releases from SDT.

5.3.3 Boundary conditions and calibration results

For the model calibration (Fang et al. 2013; Chen et al. 2015), the upstream boundary of the EFDC model for BRRS is one-minute time-series data of measured water releases (m^3/s) and temperature (^oC) at SDT. There are two types of water releases from Smith Dam: (1) More or less constant continuous release (2.83 m^3/s) to support the downstream environment and ecosystem; (2) Intermittent large releases (~140 m^3/s) from

hydro-turbine units of Smith Dam in order to meet peak electric generation demand (Fig. 5.2a). From the Julian Day 124 to 164 in 2011, there were some days without intermittent release or with very large releases (>>140 m^3/s). Afterwards, there were large releases every day (occasionally release discharges were much large). Therefore, the release pattern from SDT was irregular from May 4 to September 3 (Julian Day 124 to 246), 2011. Measured water temperatures used for the upstream boundary condition at SDT were more or less constant (9.6 °C) during the constant release periods. Water temperatures during the intermittent large releases were 10–15 °C, about 4–5 °C higher than temperatures during the constant release (Fig. 5.2a). This is because constant small release (CSR) occurred from a deep water depth and intermittent releases were from a shallower depth of Smith Dam. There are lower water temperatures in the hypolimnion of Smith reservoir due to thermal stratification in the summer.

The atmospheric boundary condition was meteorological data from the Birmingham regional airport (star on Fig. 5.1) obtained from NOAA's Southeast Regional Climate Center (SERCC). The data include hourly air temperature, atmospheric pressure, wind speed, wind direction, rainfall, and cloud cover. Required solar radiation data were not available from SERCC but obtained from Cleveland, AL (the closest Auburn Mesonet station from the study area). The time series of air temperature and solar radiation for atmospheric boundary condition are showed from 4 May to 3 September 2011 (Fig. 5.2b).

In the first study (Chen et al. 2015), a three-dimensional hydrodynamic and temperature EFDC model was calibrated with 2010 and 2011 observed data to simulate unsteady flow patterns and temperature distributions in BRRS under observed irregular

upstream releases and varying meteorological conditions recorded in Birmingham (Fig. 5.2). The calibrated EFDC model provided simulated water surface elevation (WSE) in different cross sections and temperature, velocity and discharge in 10 layers (depths) for all grids. The agreement between observed and modeled WSEs at Cordova is very good with median difference of 0.032 m. Modeled surface temperatures at Cordova follow the trend of observed temperatures over time reasonably well. Average difference and average absolute difference between observed and modeled bottom temperatures at GOUS (Fig. 5.3) are -0.56 and 0.87 °C, respectively. Modeled cross-sectional mean velocities and discharges matched reasonably well with data at Cordova, which were derived from two-day field observations using acoustic Doppler current profiler. Modeled and measured discharges exhibit the response of the large release from Smith Dam. Overall, the EFDC model was able to simulate the temporal and spatial distributions of flow and temperature.

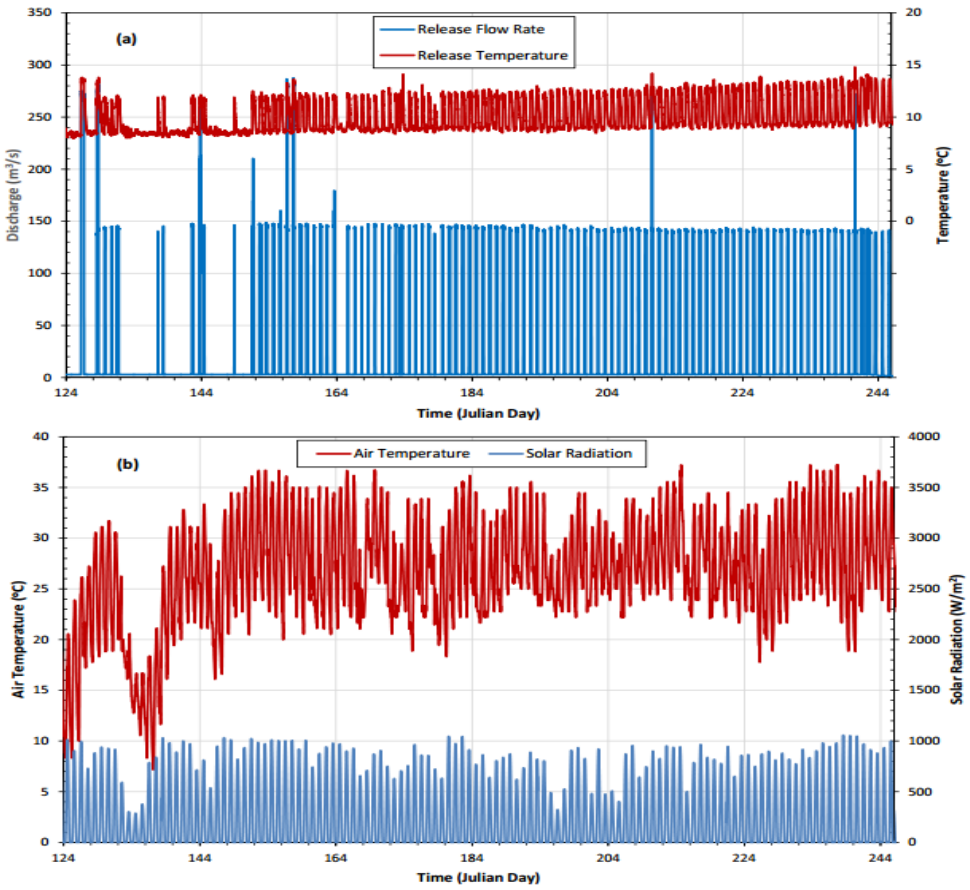

Fig. 5.2 Time-series plots of (a) discharge (m^3/s) and temperature (^oC) of upstream release from the Smith Dam tailrace (SDT), and (b) air temperature (^oC) and solar radiation (W/m^2)in Birmingham airport from May 4 to September 3 (Julian Day 124 to 246), 2011.

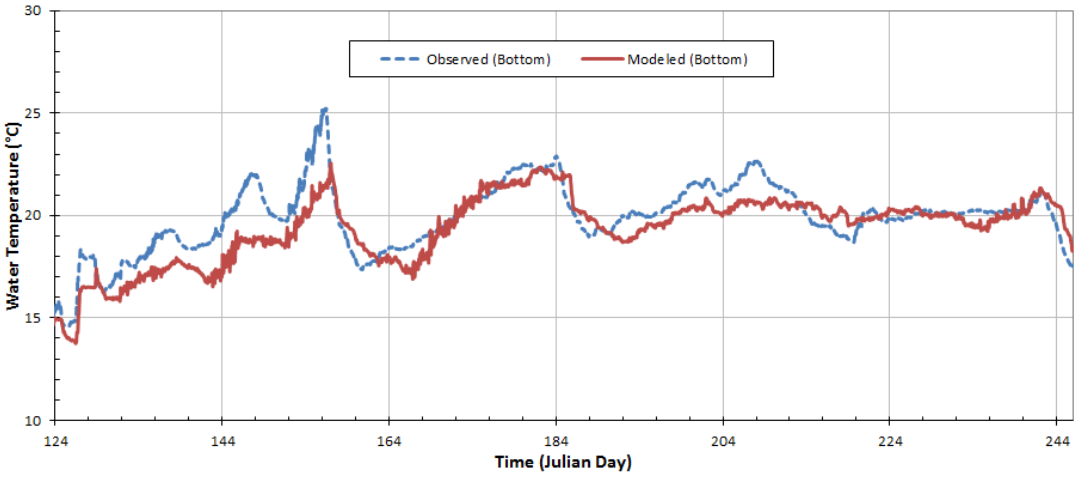

Fig. 5.3. Time-series plot of modeled and observed temperatures in the bottom layers at the Gorgas upstream (GOUS) monitoring station from May 5 to September 4 (Julian Day 124 to 246), 2011.

5.3.4 Previous Model Application Results

After each flow release from SDT, the positive flow rates simulated in the bottom layer indicate the obvious increases of flow moving downstream (Chen et al. 2015). These daily releases promoted and enhanced the movement of density currents moving from upstream towards downstream. The maximum flow rate moving downstream occurred few hours after the release stopped. This does not mean that released water from Smith Dam had reached Cordova and GOUS in a few hours after the release, but these flow rate increases occurred due to the momentum transfer or effect due to the large releases from Smith Dam. There was almost no thermal stratification from SDT to GOUS due to mixing effect of the flow momentum during the large release and no solar heating during the night. However, the temperature stratifications were developed almost

everywhere after the large release stopped for 18 hours due to solar heating in the next morning (Chen et al. 2015).

The boundary conditions in the first study (Chen et al. 2015) were observed data in 2011 (Fig. 2). For example, there were some irregular releases, cooling and warming periods from Julian Day 128 to 144. There was a large drop in air temperature (31.7 to 7.2 ^{o}C) and solar radiation (925 to 263 W/m^2) on Julian Days 130–136, but both observed and simulated bottom temperatures at GOUS (Fig. 3) in the same period did not exhibit much drop. Due to combined effects of different influencing factors, the real causes for these bottom temperature drops and increases were not clearly identified yet in the first study.

In order to understand the cause effect of upstream release on downstream bottom temperature in BRRS, all boundary conditions except the upstream release were fixed as constant in the second study (Chen and Fang 2015a). Hourly varying climate variables under hypothetical constant weather condition were used as atmospheric boundary and based on data from a relatively warmer day in 2011. Fig. 5.4 shows air temperature time-series used for EFDC modeling, which have no cooling or warming trend (called constant weather in this study) but have hourly variations in each day. The model scenario runs were for two types of upstream releases (SLR and DRLR) with different durations (2, 4, and 6 hours). The density currents in BRRS form at different reaches, are destroyed at upstream locations due to the flow momentum of the releases, and form again due to solar heating. Both the duration of large releases and solar heating affect and control the formation and spread of density currents when the release flow rate is unchanged (140 m^3/s). However, time-series plots of simulated surface and bottom temperatures at

Cordova and other locations show that one SLR does not have long-term impact on downstream surface and bottom temperatures. Regular (daily repeated) large releases are required to push density currents moving downstream and maintain temperature stratification in downstream locations. Overall average surface and bottom temperatures are lower for longer duration of DRLR.

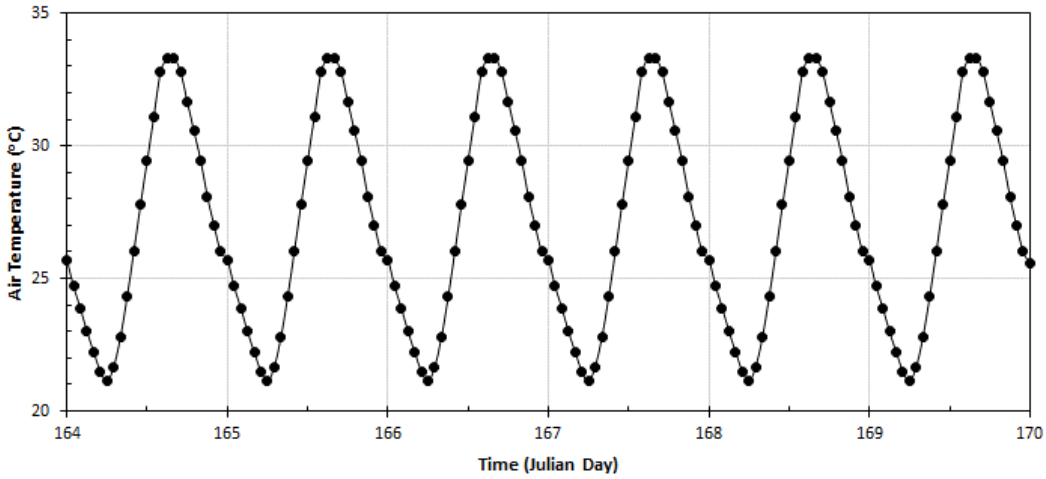

Fig. 5.4. Six-day (Julian Day 164–169) example time-series of hourly varying air temperatures under hypothetical constant weather condition (data from a relatively warmer day in 2011).

5.3.5 Durations of DRLR

In the first study, we analyzed 2010 and 2011 intermittent releases from SDT, and the statistical summary of the releases from SDT shows that both average and median releases were about 140 m^3/s and the releases typically started around 1:00 pm (Chen et al. 2015). The release of 140 m^3/s and the release starting of 1:00 pm was used for the

second study and will used for this study also. Before a series of new model scenario runs were conducted, additional data analysis was performed to determine what possible durations of DRLRs from SDT could be. Table 5.1 shows calculated release durations of DRLRs from 2010 to 2014 if the release discharge at SDT is set at 140 m^3/s. The available release data are about 184 days: mostly from Julian Day 120 (May 1) to 303 (October 31) in each year from 2010 to 2014. Total volume of water released from SDT varied from 359.6 $\times 10^6$ m^3 to 763.6 $\times 10^6$ m^3 in the last 5 years. With fixed release of 140 m^3/s in each day, calculated daily release duration ranges from 3.48 to 7.91 hours. Daily release durations were also calculated using observed release data from Julian Day 151 (May 31) to 273 (September 30) in each year (total 123 days). It was found that longer durations of large releases were typically required from the early summer to the later fall: calculated daily release durations range from 3.98 to 8.86 hours. The most release duration are from 4 to 6 hours. The percentages of all 2011 releases with durations of about 4 hours (3.8 to 4.2 hours) and 6 hours (5.8 to 6.2 hours) are 15.5% and 14.6%, respectively. Therefore, the durations of 4-hr and 6-hr for DRLRs will be used for most model scenario runs in this study. A few scenario runs will have the durations of 2-hr and 8-hr to generate comparative results, and the 8-hr DRLRs are highly possible in a relative warmer year, e.g., 2013 (Table 5.1)

Table 5.1 Calculated daily upstream release durations (if the release is fixed as 140 m^3/s) based on 2010 to 2014 release data.

Year	Data period	Days	Recorded Total Release Volume ($m^{3)}$	Calculated Duration for DRLR (hr)
2010	151 to 333	183	359,557,358	3.48 (4.72) [1]
2011	120 to 303	184	370,758,545	3.59 (3.98)
2012	121 to 304	184	443,569,903	4.39 (5.08)
2013	120 to 303	184	763,621,151	7.91 (8.83)
2014	120 to 303	184	631,369,260	6.45 (6.04)

Note: [1] – Number insider brackets is calculated duration for DRLR based on recorded total release volume from Julian Day 151 (May 31) to 273 (September 30) in each year (total 123 days).

5.3.6 Climate Scenarios

For the atmospheric boundary conditions, in addition to observed weather in 2011 (Fig. 5.2b), three types of meteorological scenarios were used in this study in order to identify specific weather impacts on density current movements: (1) constant weather (Fig. 5.4), (2) hypothetical cooling and constant weather (Fig. 5.5), and (3) hypothetical cooling and warming weather (Fig. 5.6). Constant weather was used in the second study and for a part of scenario model runs in this study and had diurnal variations in climate variables, which result in the solar heating during the day and cooling during the night. The daily maximum and minimum air temperatures are 33.3 and 21.1 °C (Fig. 5.4) (no change over the simulation periods for the constant weather), respectively, which was derived from a relatively warmer day in 2011 (Fig. 5.2). The daily maximum and minimum air temperatures in Birmingham range from 15.6 to 36.9 ^oC and 7.8 to 27.2 ^oC from Julian day 124 to 244 in 2011 (Fig. 5.2), respectively. The hourly air temperature

were calculated from the daily maximum and minimum temperature applying the sinusoidal wave function model (Reicosky et al. 1989; Chen and Fang 2015b).

How do surface and bottom water temperatures at the downstream locations of BRRS drop or increase with the changes of weather conditions such as cooling and warming trend over a few days? Changes of daily maximum and minimum air temperatures between each day and its previous day were calculated for Fig. 5.2 (Julian Day 124 to 244) and range from -7.8 to 6.1 ^{o}C and -4.6 to 7.2 ^{o}C, respectively. The seventy-five percent changes of daily maximum and minimum air temperatures are less than 1.5 and 1.3 ^{o}C, respectively. Therefore, three hypothetical weather scenarios were used for the model scenario or sensitivity analysis in BRRS, and they are for air temperature drops in 2, 4, and 6 days starting from Julian Day 164, and cooler constant weather conditions afterwards (Fig. 5.5). During the dropping period, both daily maximum and minimum air temperatures drop 2 °C each day. The daily maximum and minimum air temperatures before Julian Day 164 and after the temperature dropping period were assumed to not change with time (constant weather). It was assumed that solar radiation also drops about 80.9 W/m^2 per day (based on the data analysis) when air temperature drops for 2 ^{o}C per day. For the 4-day drop or 8 ^{o}C drop, the daily maximum and minimum air temperatures drop from 33.3 and 21.1 °C to 25.3 and 13.1 °C, respectively.

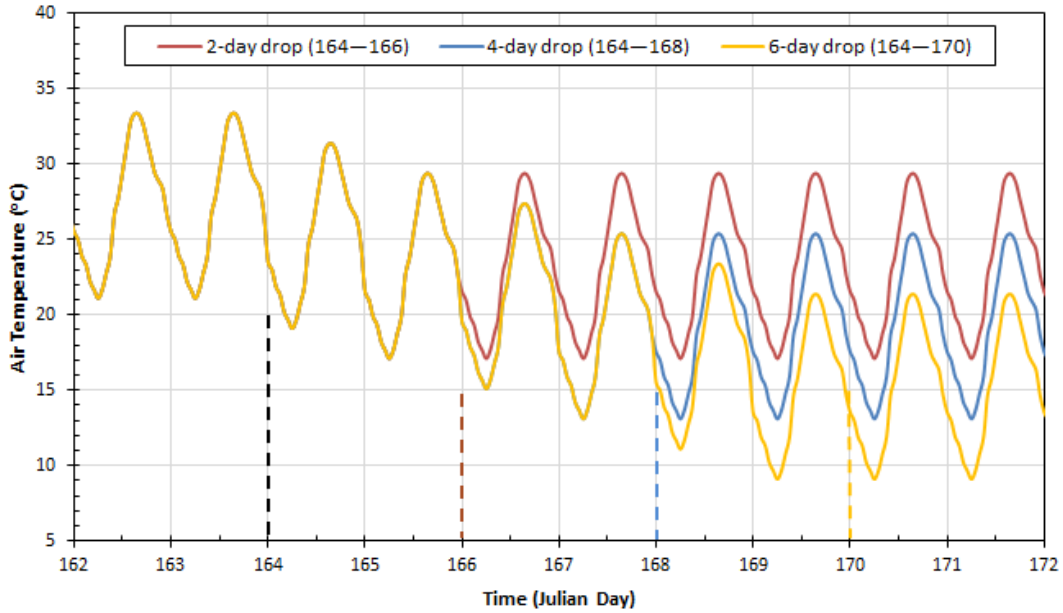

Fig. 5.5. Three hypothetical weather scenarios for air temperature drops in 2, 4, and 6 days starting from Julian Day 164, and cooler constant weather conditions afterwards.

During the summer when the intermittent release is the common practice, air temperature may have a drop but may not stay cooler for a very long period after the drop, instead it may start to warm up during the next few days, for example, variations of air temperature from Julian day 130 to 141 in 2011 (Fig. 5.2b): decreasing from 31.3 to 15.6 ^{o}C then increasing to 32.2 ^{o}C. To mimic typical weather variations, a new hypothetical weather scenario was proposed and developed: air temperature has a 6-day drop (Julian Day 164–169) and then a 6-day rise (Julian Day 169–174) of air temperature and solar radiation between Julian Day 163 to 175, and the constant weather was used before and after the drop and rise period (Fig. 5.6). This is an 11-day drop and rise period (Julian 164–174) in comparison with the warmer constant weather scenario (Fig. 5.4).

During the drop and rise period, the air temperature has a drop or rise of 2 °C each day. Therefore, these 11 days have a total of 72 °C-day lower air temperature than one under the constant weather scenario. The solar radiation has the same drop or rise pattern (trend) as the air temperature does, and it is assumed to be 10% change of the solar radiation under the constant weather condition each day (i.e., 809 W/m^2/day).

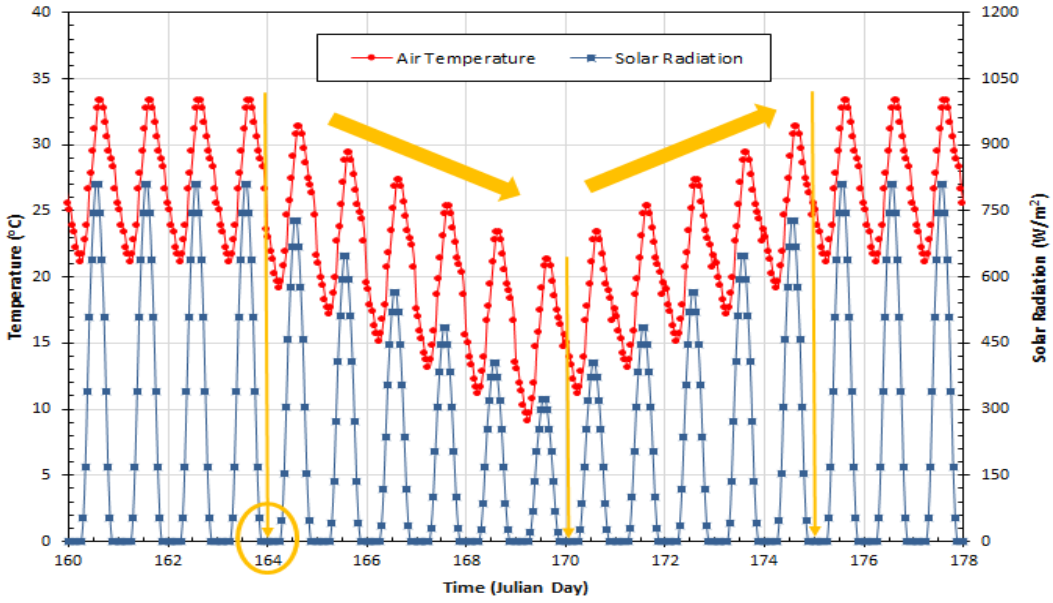

Fig. 5.6. Weather scenario showing 6-day drop and then 6-day rise of air temperature and solar radiation from Julian Day 164 to 174. The constant weather was used before and after the drop and rise period.

5.4 Results and Discussion

This paper presents the third study to further understand the bottom temperature dynamics due to combined effects of meteorological condition and DRLR. For scenario analysis performed in this study, various input data (boundary conditions) were modified into constant representative values excluding upstream boundary conditions and climate conditions. Therefore, we can focus on studying effects of dynamic releases from the upstream reservoir and variable atmospheric conditions on density current formations and movement. The inflows from all tributaries and small streams (Fig. 5.1) were set at average inflows calculated from time series of inflows used for model calibration (2010–2011). Average inflows from the Upper Mulberry Fork, Lost Creek, Blackwater Creek and Locust Fork are 4.42, 5.54, 2.60, and 8.70 m^3/s for all scenario model runs. At BLD, water level was used as downstream boundary condition. Observed water surface elevations ranged from 77.35 m to 77.75 m from 4 May to 3 September 2011 with an average elevation of 77.60 m (standard deviation of 0.07 m). Therefore, water surface elevation at BLD was set at 77.60 m (constant) for the scenario runs. Based on the sensitive analysis, the constant water level at BLD would not affect much on density-current flow dynamics in the upstream portion of BRRS (from SDT to GOUS).

5.4.1 Simulation dulations under the Constant Weather Scenario

First, three scenario runs with 2-hr, 4-hr and 6-hr DRLRs at SDT under constant weather conditions were conducted. The restart file on Julian Day 124, created by the calibration model run under actual flow releases and weather conditions in 2011, was used to set initial conditions for all model scenario runs in this study. Time series of

simulated surface and bottom water temperature at GOUS show the effect of initial conditions lasts for about 2 and 3 days (Fig. 5.7) for 2-hr, 4-hr and 6-hr DRLRs, respectively, under constant weather conditions. After 2–3 days, surface and bottom temperatures begin to increase in response to constant warmer weather. Simulated surface temperatures come to equilibrium about 40, 20 and 15 days for 2-, 4- and 6-hr DRLRs, respectively, but have diurnal variations due to the hourly variations of weather variables (e.g., Fig. 5.4). Diurnal variations of surface temperatures are about 1.7, 4.4 and 2.1 ^{o}C for 2-, 4- and 6-hr DRLRs, respectively, and are due to 12.2 ^{o}C air temperature diurnal variations (Fig. 5.4) and complex flow dynamics at GOUS resulted from upstream flow momentum after the large releases and backwater effects from Bankhead. Both field observations and model results show that there are two-layer flows at GOUS over certain time period after the release: surface-layer flowing backward to upstream and bottom-layer flowing downstream (Chen et al 2015). The equilibrium or daily mean surface temperature for 6-hr DRLR is much lower than the one for the 4-hr DRLR; and the difference is about 6 °C. The bottom temperatures at GOUS gradually increase and take about 36 days to arrive equilibrium for 2-, 4- and 6-hr DRLRs. The bottom temperature at GOUS under 2-hr DRLR is about 1 °C and 2 °C higher than the temperature under 4-hr DRLR and 6-hr DRLR, respectively. Simulation results show that two more hours of the release from 4-hr DRLR have larger impact on surface water temperature and relatively smaller impact on bottom temperature because more water from the releases move to the downstream in the form of surface waves, and also have less vertical temperature stratification because of stronger and longer momentum mixing effects. Under the constant weather conditions and constant durations (e.g., 4- or 6-hr) of

DRLR, water temperatures at different depths reach their stable equilibrium conditions: diurnal variations in the surface layer and little or no variations in the bottom layer (Fig. 5.7). When the water temperature reach equilibrium, the difference of daily average temperature between surface and bottom layers for 2-hr, 4-hr and 6-hr DRLR are 10.8, 7.6, and 1.7 °C, respectively. After Julian Day 164 in 2011 (Fig. 5.2), the actual daily releases from the SDT are similar to constant daily repeated large releases (Fig. 5.2a). Observed and simulated bottom temperatures at GOUS under 2011 weather show some drops and increases (Fig. 5.3); however, there are no drops and increases under the constant weather conditions under all 2-, 4- and 6-hr DRLRs. Therefore, these drops and increases are most likely due to the variations of weather parameters–weather effect, which will be approved in the next section.

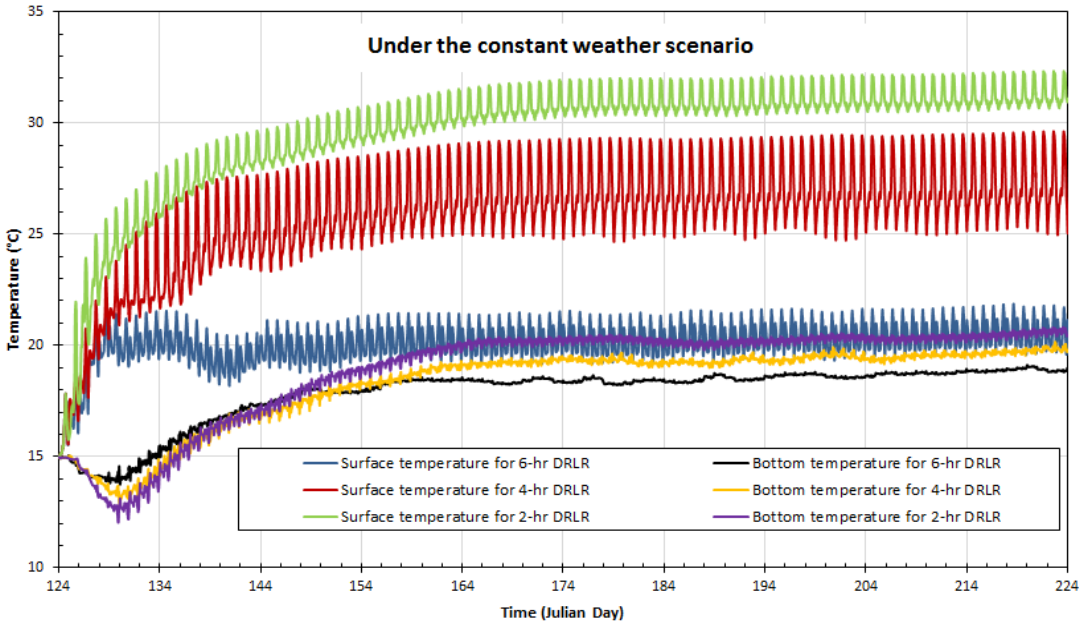

Fig. 5.7. Time series of simulated surface and bottom water temperature at GOUS for 2-hr, 4-hr and 6-hr DRLRs under constant weather conditions.

5.4.1.1 Varying the Release Pattern in 11 Days

Before we study combined effects on simulated bottom temperature at GOUS due to varying the air temperature pattern and the release pattern from SDT, we first study the effect due to varying the release pattern alone during the 12 days (Julian days 164–175). These 12 days are used later to have air temperature and solar radiation changes. Fig. 8a shows time series of simulated bottom-layer water temperatures at GOUS when 140 m^3/s DRLRs from SDT last for 2, 4, 6, and 8 hours in comparison to the results when there is no daily large release in those 12 days under the constant weather scenario. There are 4-hr DRLRs before Julian Day 164 and after 175. When there are 4-hr DRLRs during the whole simulation period, daily bottom temperature at GOUS only has very small increase from 18.3 to 19.6 ^oC from Julian Day 155 to 200. When there is the no large release from Julian Day 164 to 174, the bottom temperature at GOUS decreases about 1.6 °C due to the delay effect of 4-hr DRLRs before Julian Day 164. After the Julian Day 174, the bottom temperature at GOUS increases to 21.4 °C. The similar situation happens for 2-hr DRLR from Julian Day 164 to 174: the maximum drop of the bottom temperature at GOUS is 17.8 ^oC and the maximum temperature reaches 20.3 ^oC. Simulated bottom temperatures for the no large release and 2-hr DRLRs reach almost the same temperature with 4-hr DRLR on Julian Day 187 that is 12 days after the release pattern change has ended on Julian Day 175. For the 6- and 8-hr DRLRs from Julian Day 164 to 174, the bottom temperature increases about 4 and 5 days due to the mixing effect of the large flow momentum reaching GOUS. After the small temperature increase, the bottom temperature starts to decrease and maintain cooler temperature more than 35 days.

Before Julian Day 175, the minimum daily mean bottom temperatures for the 6- and 8-hr DRLRs are 18.0 and 17.2 ^{o}C, respectively. After the 6- and 8-hr DRLRs stops on Julian Day 175, the second minimum daily mean bottom temperatures for are 17.0 and 16.0 ^{o}C occurring on Julian Day 184, respectively. The second minimum temperature is due to combined effects of the 6- or 8-hr DRLR in 12 days and the 4-hr DRLR afterwards.

Fig 5.8b shows time series of simulated bottom-layer water temperatures at the river intake when 140 m^3/s DRLRs from SDT last for 2, 4, 6, and 8 hours or when there is no daily large release during those 12 days under the constant weather scenario. The river intake to a power plant is 5.58 km downstream the GOUS. Typical water depths at the river intake is about 11.15 meter at the deepest computational grid. The release with longer duration will make the bottom temperature at the river intake cooler. When there is the no large release from Julian Day 164 to 174, the bottom temperature at the river intake will gradually increases to a daily average maximum of 24.4 ^{o}C on Julian Day 175; while for the 8-hr DRLRs, the bottom temperature decreases to a daily-average minimum of 13.7 ^{o}C. For DRLRs with different durations or no release over 12 days, the impact periods on the intake's temperature are almost same for 24 days from Julian Day 165 to 188.

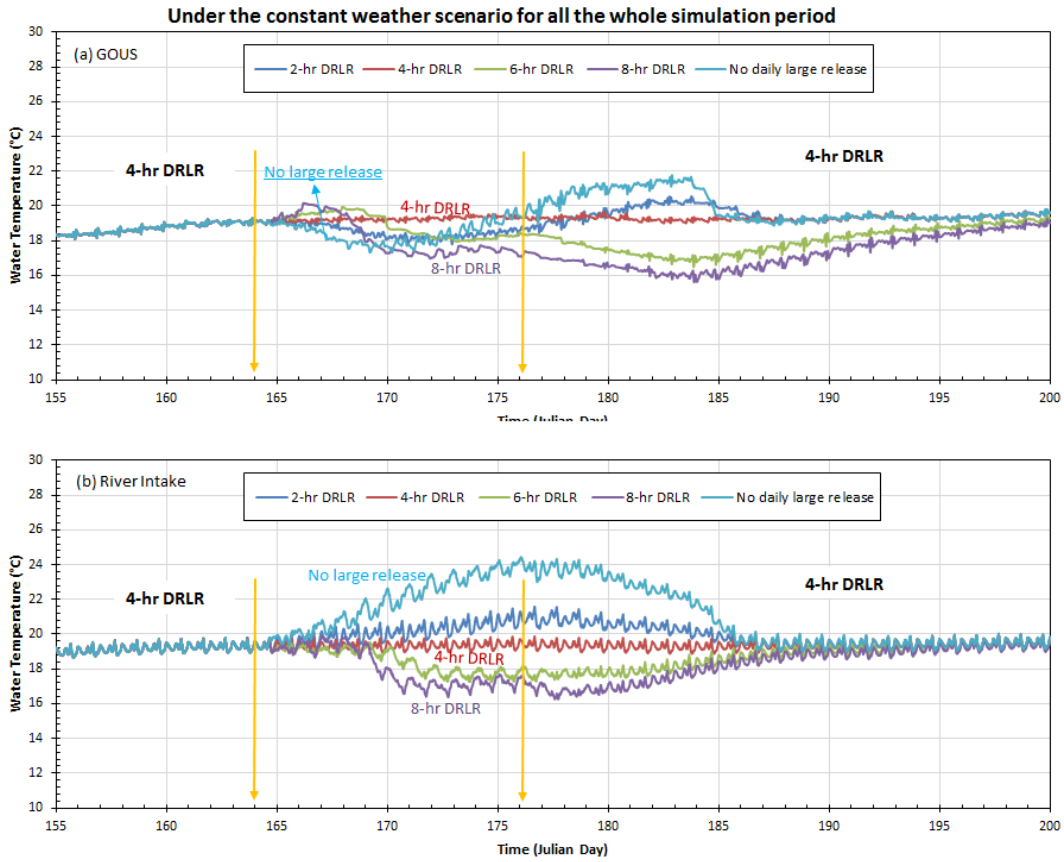

Fig. 5.8. Time series of simulated bottom-layer water temperatures at (a) GOUS and (b) the river intake when the DRLR release lasts for 2-hr, 4-hr, 6-hr, and 8-hr and when there is no daily large release from Julian Day 164 to 174. There are 4-hr DRLRs before Julian Day 164 and after 175. It is the constant weather scenario over the whole simulation period.

5.4.2 Simulation under Actual Weather Conditions

Comparing the results in Fig. 5.3 and Fig. 5.7 show that variations of the weather conditions (e.g., warming and cooling trends of air temperature and solar radiation) could be essential to the water temperature distribution and density current movement at the

downstream locations of BRRS. To approve the above point of view, Fig. 5.9 shows time series of simulated surface and bottom water temperature at GOUS for 4-hr and 6-hr DRLRs under 2011 weather conditions (Fig. 5.2). Simulated water temperature variations under 2011 weather are quite different from Fig. 7 under the constant weather for both 4- and 6-hr DRLRs. From Julian Day 124 to 164, simulated bottom and surface temperatures increase and decrease according to the weather conditions. For example, air temperature in 2011 began to drop from Julian Day 131, and after the 6 days drop, air temperature started to increase for about 5 days (Fig. 5.2b). Simulated surface temperature at GOUS responded quickly with the air temperature changes. Simulated surface temperature for both 4-hr and 6-hr DRLR show the same pattern as the air temperature. For the bottom temperature, there were about 6 days delay because simulated temperature at GOUS began to drop around Julian Day 137. However, predicted bottom temperature at GOUS gradually increase from Julian day 124 to 164 before it comes to equilibrium under the constant weather conditions (Fig. 5.7). After the Julian Day 174, bottom water temperatures at GOUS did not show sharp drops or increases during the short periods (Fig. 5.9) because the air temperature did not have a large variation (Fig. 5.2). The bottom and surface water temperatures still have the diurnal variations (larger for the surface temperatures).

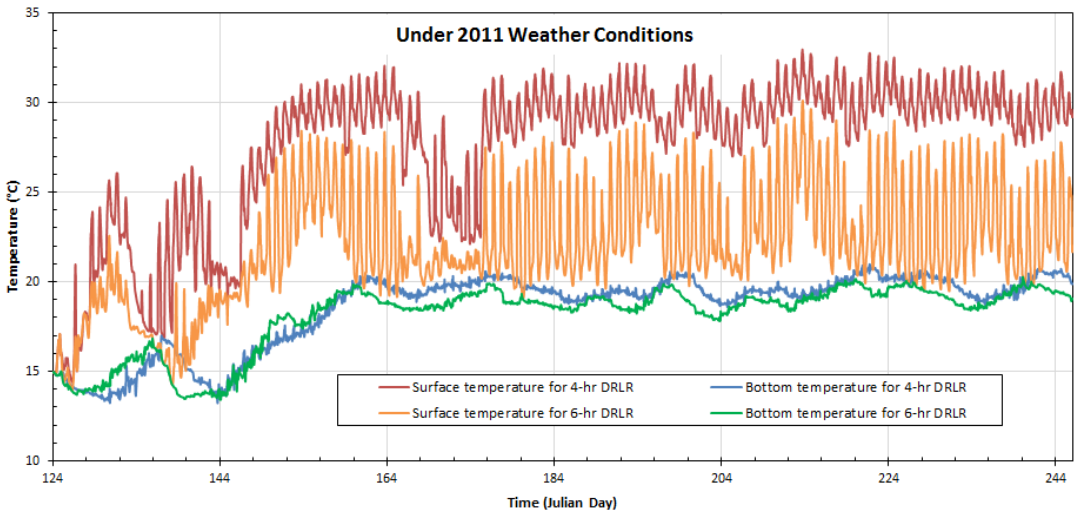

Fig. 5.9. Time series of simulated surface and bottom water temperatures at GOUS for 4-hr and 6-hr DRLRs under 2011 weather conditions (Fig. 5.2).

5.4.3 Simulations under Air Temperature Drop Scenarios

Fig. 5.10 shows time series of simulated bottom-layer water temperatures at GOUS for the constant weather and the 2-, 4- and 6-day air temperature drop scenarios (starting from Julian Day 164) under 4- and 6-hr DRLR from Julian Day 162 to 184. First of all, the drop of air temperature (2 ^{o}C/day) results in the drop of the bottom-layer water temperature at GOUS, but it has a delay of the drop for about 3 to 6 days for 2-, 4- and 6-day drops under 4-hr and 6-hr DRLRs (Table 5.2). Table 2 lists the bottom-temperature drop period including the beginning and end days (Julian Day) of the period for each scenario run. The beginning day is when simulated daily mean bottom temperature under the air temperature drop scenario is 0.1 ^{o}C less than one under the constant weather during the whole simulation period. The delay occurs when the beginning day is later than 164 (air temperature drop starts). The end day is when daily mean bottom

temperature under the air temperature drop scenario begins to increase. The delay of dropping bottom temperature is because GOUS is 64 km downstream from DRLRs at SDT and the depth at GOUS is about 10 m. The shorter delays for 4- and 6-hr DRLRs are because these DRLRs create relatively stronger mixing and larger momentum to push density current moving downstream. For the 2-, 4-, and 6-day drops of air temperature, the bottom temperature dropping periods are 5, 6, and 11 days, respectively, and are about the same under 4-hr and 6-hr DRLRs. These dropping periods are about 1.5–2.5 times longer than the air temperature drop period.

Simulated bottom temperatures under 6-hr DRLR decrease from 18.1 ^{o}C to 17.1±0.1, 15.3±0.1, and 13.6±0.2 °C for 2-, 4-, 6-day drops of air temperature, respectively. Above quasi-steady temperatures and standard deviations were calculated after the dropping periods when simulated bottom temperatures become more or less constant with small diurnal variations (Fig. 5.10). The average daily dropping rates of bottom temperature for 2-, 4- and 6-day drops under 6-hr DRLR are 0.3, 0.5 and 0.4 °C/day during 5, 6, and 11 days, respectively, under the air temperature drop rate 2 °C/day (Table 5.2). The daily dropping rates of bottom temperature at the first 5 or 6 days (before Julian Day 172) is larger than the temperature drop rate afterwards when air temperature has stopped for 2 or more days.

The differences of simulated bottom temperatures at GOUS between the constant weather and dropping temperature scenarios were calculated in the last day of the bottom temperature dropping periods, and the daily mean differences under the 2-, 4-, 6-day drops of air temperature are 1.5 °C, 3.3 °C, and 5.1 °C for 6-hr DRLRs, respectively, which are reported as the maximum difference in Table 5.2. These maximum differences

are almost linear proportional to the dropping days or degrees of air temperature. The total decreases and daily drop rates of simulated bottom temperature under 4-hr DRLR for 2-, 4-, and 6-day drops of air temperature are almost the same as ones under 6-hr DRLR (Table 5.2). The average daily drop rate for the 6-day drop of air temperature under 6-hr DRLR is 0.4 °C/day, which is slightly smaller than the average drop rate under the 4-hr DRLR (0.5 °C/day). It may due to the momentum effect that 6-hr DRLR creates more mixing on the downstream surface and bottom temperatures. Even though the average daily drop rates vary among different DRLR durations, the longer dropping period for air temperature still makes the larger total decrease in the bottom-layer water temperature: about 5.0, 2.8, and 1.2 ^{o}C total decrease (Table 5.2) for 6, 4, and 2 days of air temperature drop.

Table 5.2 Predicted bottom-layer water temperature drop, difference, daily drop rate at GOUS resulted from the air temperature drops (2 ^{o}C/day) in 2, 4 and 6 days under 4-hr and 6-hr DRLRs.

Air temp. drop period	Bottom temperature drop period	Simulated bottom temperature drop characteristics				
		From (°C)	To (°C)	Total decrease (°C)	Daily drop rate (°C/day)	Maximum Difference (^{o}C) [2]
2 days	5 days: 168–172 (170 to 174) [1]	18.1 (19.1) [1]	16.8 (18.0)	1.3 (1.1)	0.3 (0.2)	1.5 (1.3)
4 days	6 days: 167–172 (169 to 174)	18.1 (19.0)	15.2 (16.3)	2.9 (2.7)	0.5 (0.5)	3.3 (3.2)
6 days	11 days: 167–177 (169 to 179)	18.1 (18.7)	13.2 (13.6)	4.9 (5.1)	0.4 (0.5)	5.1 (5.4)

Note: [1] – the first number is for under 6-hr DRLRs and the number inside brackets is for under 4-hr DRLRs; [2] – daily mean difference of simulated bottom temperatures at GOUS between the constant weather and dropping temperature scenarios in the last day of the bottom temperature dropping periods.

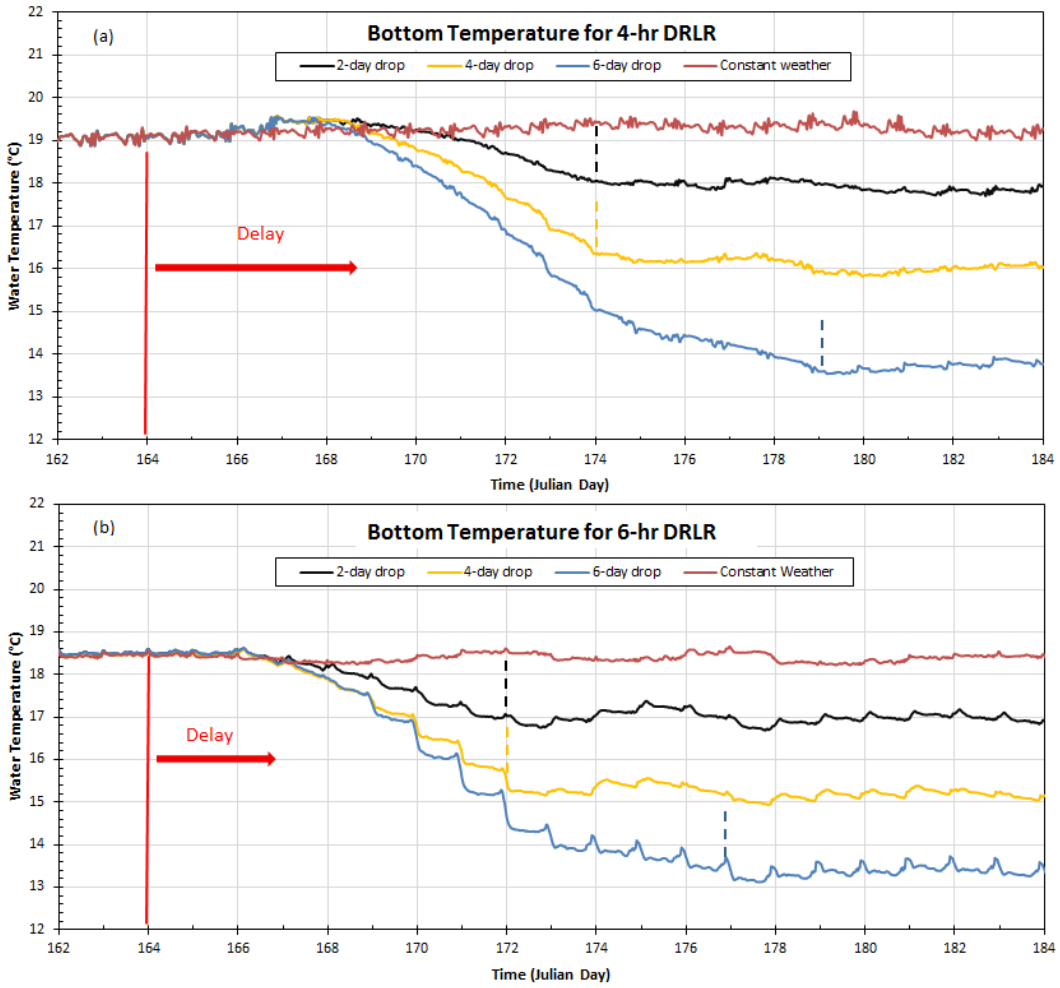

Fig. 5.10. Time series of simulated bottom water temperatures at GOUS for constant weather and 2, 4, 6 days air temperature drop scenarios (starting from Julian Day 164 drop 2 ^{o}C / day) under 4- and 6-hr DRLR from 162 to 184.

To further understand the air temperature dropping impact, three new scenarios with 1 °C air temperature drop per day for 2, 4 and 6 days starting from Julian Day 164 were also investigated under 6-hr DRLR from Julian Day 162 to 184. The effect from air temperature drops on bottom temperature at GOUS has a delay for about 5 days after

Julian Day 164 for 2-, 4- and 6-day drops under 6-hr DRLRs. This 5-day delay is longer than the 3- or 4-day delay under 2 ^{o}C air temperature drop because it takes longer time for bottom water temperature starting to drop under 1 ^{o}C air temperature drop when it compares with one under the constant weather. The bottom temperature dropping periods are about 4, 4, and 9 days, respectively, and they are 1–2 days shorter than the dropping period for 6-hr DRLR with air temperature drop rate of 2 °C/day. The average daily dropping rates of bottom temperature at GOUS are 0.2, 0.3 and 0.2 °C/day per °C within 4, 4, and 9 days when air temperature drops at 1 °C/day under 6-hr DRLR, respectively (Table 5.3). Above dropping rates of the bottom-layer water temperature are smaller than ones (Table 5.2) resulted from air temperature drop at 2 °C/day under 6-hr DRLR. Due to shorter dropping period and smaller dropping rate, the maximum difference of simulated bottom temperatures at GOUS between the constant weather and dropping temperature scenarios of 1 ^{o}C/day are much smaller than ones for 2 ^{o}C/day drop scenarios. Therefore, the average daily dropping rates of bottom temperature at GOUS are primarily related to the air temperature dropping rate and period.

Table 5.3 Predicted bottom-layer water temperature drop, difference, daily drop rate at GOUS resulted from the air temperature drops (1 ^{o}C/day) in 2, 4 and 6 days under 6-hr DRLRs.

Air temp. drop period	Bottom temperature drop period	Simulated bottom temperature drop characteristics				
		From (°C)	To (°C)	Total decrease (°C)	Daily drop rate (°C/day)	Maximum Difference (^{o}C) [1]
2 days	4 days: 169–172	18.3	17.7	0.6	0.2	0.6
4 days	4 days: 169–172	18.0	16.9	1.1	0.3	1.5
6 days	9 days: 169–177	18.0	15.9	2.1	0.2	2.4

[1] – It is defined same as one in Table 5.2.

5.4.4 Simulations under Air Temperature Drop and Rise Scenario

5.4.4.1 Results under Three Weather Scenarios

Fig. 5.11 shows time series of simulated surface- and bottom-layer water temperatures for 6-hr DRLR under three weather scenarios: the constant weather, the 6-day drop only, and the 11-day drop and rise. The drop of air temperature starts on Julian Day 164. Under the constant weather, daily mean bottom and surface temperatures are almost constant for 6-hr DRLR from Julian Day 155 to 200. For the 6-day drop only, the surface temperature begins to drop quickly when the air temperature begins to drop from Julian Day 164. However, the bottom temperature shows a 3-day delay (Table 5.2, Figs 5.10 and 5.11). After air temperature drops 3 days, the surface and bottom temperatures are well mixed most of times and continuously drop for 11 days as discussed before. Under the 6-day drop and 6-day rise scenario, the surface and bottom temperatures follow the same pattern of the 6-day drop only scenario at the beginning. When the air temperature starts to increase on Julian Day 170, the surface and bottom temperatures begin to increase with a 2-day delay. The surface temperature at GOUS rises quickly from 14.8 °C to 20 °C (constant daily-mean surface temperature under the constant weather condition) in 8 days. However, the bottom temperature takes much longer time to increase to the stable temperature simulated under the constant weather condition. Because of air temperature dropping and rising in 11 days, the bottom temperature can maintain cooler temperature about 24 (Julian Day 167 to 190) days. Overall, water temperature at GOUS (64 km downstream of DRLRs) increases or drops corresponding

to the air temperature change, but it can maintain the cooler condition for a longer period, especially for bottom layers.

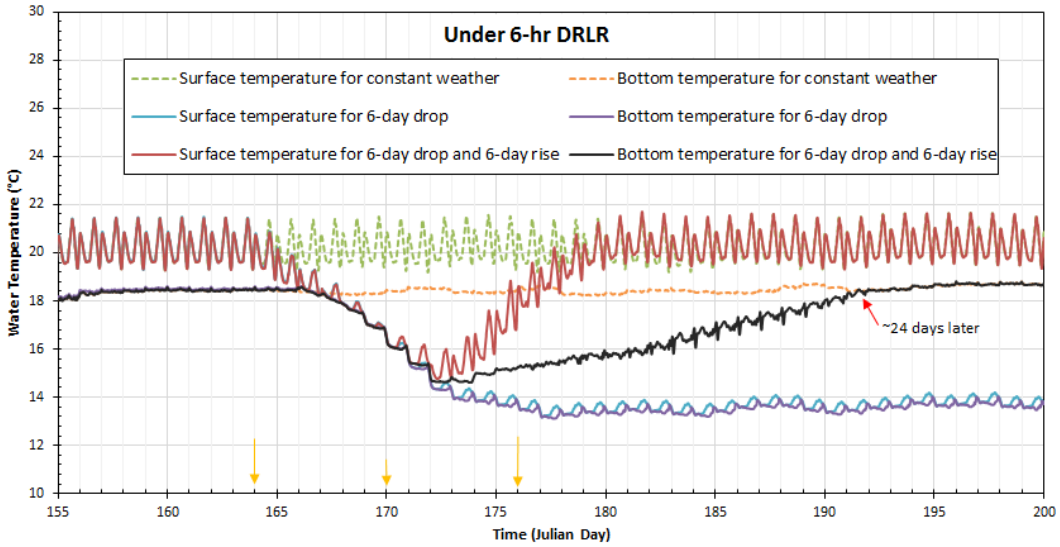

Fig. 5.11. Time series of simulated surface and bottom water temperatures for 6-hr DRLR under three weather scenarios: constant weather, 6-day drop only, and the 11-day drop and rise. The drop of air temperature starts on Julian Day 164.

5.4.4.2 Results under Three DRLR Durations

Fig. 5.12 shows time series of simulated bottom-layer water temperatures at GOUS and the river intake for the 2-hr, 4-hr, and 6-hr DRLRs over the whole simulation period (Julian Day 124–224) with the 11-day drop and rise weather scenario from Julian Day 164 to 174. There are the constant weather conditions before and after the weather change scenario period. Under the constant weather and 2-, 4- and 6-hr DRLRs, simulated daily mean bottom temperatures on Julian Day 164 at GOUS are 19.9, 19.1, and 18.4 °C, respectively. The weather change scenario with constant 2 °C /day air temperature drop and rise in 11 days (Fig. 5.6) results in bottom-layer water temperature

drops and rises over 24–58 days in GOUS and the river intake (Table 5.4). The beginning and end days of the lower temperature duration in Tables 4 and 5 are when simulated temperature under the drop and rise scenario is 0.1 ^{o}C lower than one under the constant weather scenario, i.e., the same way to determine the beginning day of the bottom temperature dropping period in Tables 5.2 and 5.3. During the 11-day drop and rise weather scenario, the bottom temperature under 6-hr DRLRs starts to drop firstly with 3 days delay, following with the drop under 4-hr and 2-hr DRLRs (5 and 7 days of delay). These differences in delaying the bottom-layer water temperature drop are due to stronger momentum and pushing effects of longer duration of the DRLRs. The overall drop rates for bottom-layer temperature are almost same (3.7–3.9 ^{o}C total decrease from Julian Day 164 to the lowest temperature day) for 2-hr, 4-hr and 6-hr DRLRs because the same drop rate of air temperature was used. The lowest daily mean bottom temperatures are 16.2, 15.2, and 14.7 °C for the 2-, 4-, and 6-hr DRLRs before the bottom temperature gradually increases to the temperature under the constant weather scenario. The 11-day drop and rise weather scenario results in 52, 38, and 24 days (4.7–2.2 longer drop and rise period) of lower bottom-layer water temperature at GOUS under the 2-, 4-, and 6-hr DRLRs (Table 5.4). Simulated temperature dynamics is complex at GOUS: under the same initial conditions and weather conditions, temperatures under 6-hr DRLRs are higher than ones under 2- and 4-hr DRLRs for the first 24 and 26 days, respectively, but lower for remaining days.

Under 2-hr DRLRs, the bottom-layer water temperature at the rive intake (Fig. 5.12b) on Julian Day 164 is about 2 ^{o}C higher than one at GOUS because the river intake is near the power plant and 2-hr DRLR has relatively weaker momentum or push effect.

Whereas, due to stronger momentum effect, the bottom temperature on 164 at the rive intake under 6-hr DRLRs is 0.5 ºC lower than one at GOUS. The water depth at the river intake is typically about 11.2 m and the temperature stratification exists between the surface and the bottom layers as GOUS does (Fig. 5.11). The lowest bottom-layer water temperature during dropping and rising period under 2-hr, 4-hr, and 6-hr DRLRs are 18.8, 15.4, and 14.1 °C with the cooler duration 58 (165–222), 37 (166–202), and 26 (165–190) days, respectively (Table 5.4). The lower temperature duration is shorter for 4- and 6-hr DRLRs, but the total temperature decrease is larger (3.8–3.9 ºC comparing with 3.2 ºC under 2-hr DRLRs). The average temperatures at the river intake under 2-hr, 4-hr, and 6-hr DRLRs are 21.4, 18.2, and 16.5 °C during the lower temperature durations and 20.6, 18.3, and 17.2 °C during the whole simulation period, respectively. The 4-hr DRLRs lower the bottom temperatures at the river intake from ones under 2-hr DRLRs more than 6-hr DRLRs do from ones under 4-hr DRLRs.

Table 5.4 Characteristics of simulated bottom-layer water temperatures (ºC) at GOUS and the river intake under three durations of DRLRs and the 11-day weather change scenario.

Location	GOUS			The river intake		
Parameters	Temp [1] at JD 164	Lowest temp (day [2])	Lower temp duration	Temp at JD 164	Lowest temp (day)	Lower temp duration
2-hr DRLR	19.9	16.2 (179)	52 (171–222)	22.0	18.8 (177)	58 (165–222)
4-hr DRLR	19.1	15.2 (179)	38 (169–206)	19.3	15.4 (175)	37 (166–202)
6-hr DRLR	18.4	14.7 (172)	24 (167–190)	17.9	14.1 (173)	26 (165–190)

Note: [1] – "temp" given is the daily mean temperature calculated from 15-minute simulated water temperatures in a day, [2] – day is Julian Day (JD) in a year.

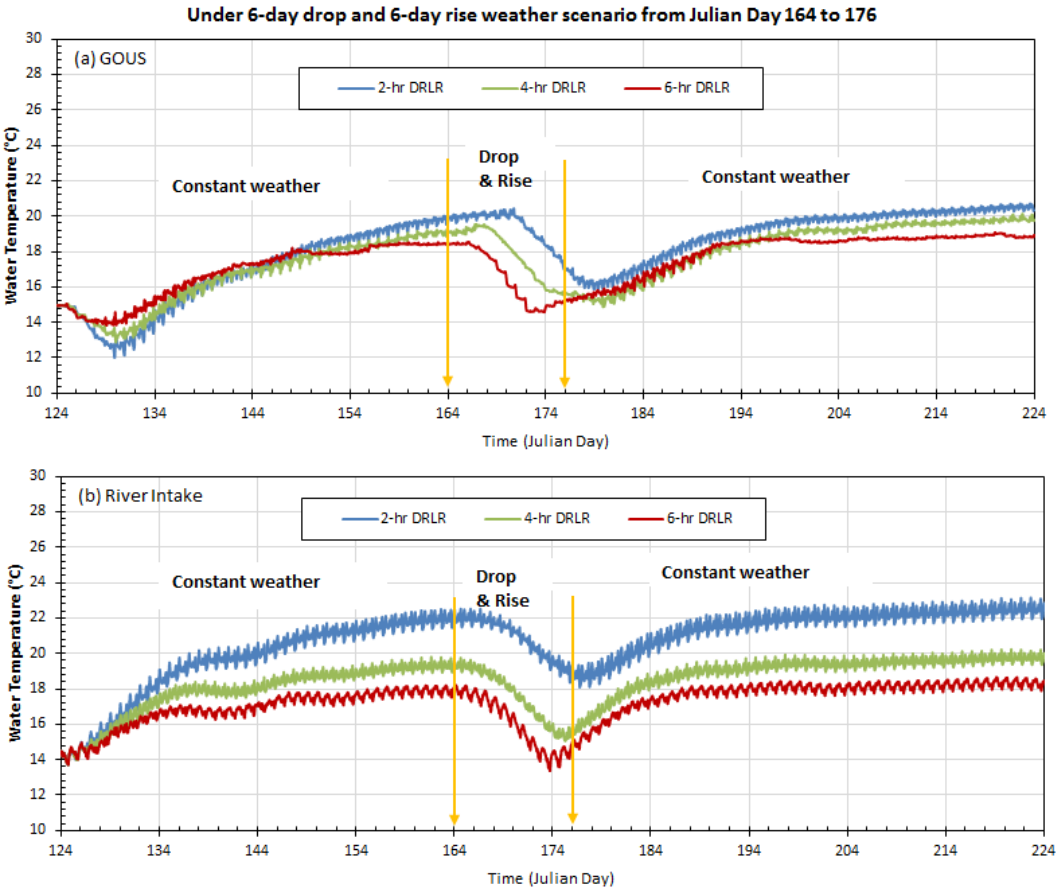

Fig. 5.12. Time series of simulated bottom temperatures at (a) GOUS, and (b) river intake with the 11-day drop and rise weather scenario from Julian Day 164 to 174 for the 2-hr, 4-hr, and 6-hr DRLRs over the whole simulation period (Julian Day 124–224). There are the constant weather conditions before and after the weather scenario period.

5.4.4.3 Results with Duration Changes during the Drop and Rise Period

Railsback (1997) concluded that significant saving can be realized using release patterns adapted to changing atmospheric conditions. If more water is released during the

cooler weather condition, could downstream temperatures be lower? Fig. 5.13 shows time series of simulated bottom-layer water temperatures at GOUS and the river intake under the 6-day drop and 6-day rise weather scenario when DRLRs at SDT over the 12 days last for 2, 4, 6, and 8 hours in comparison to the results when there is no daily large release. The bottom-layer water temperatures at GOUS and the river intake on Julian Day 164 (just before air temperature drop starts) are 19.1 and 19.3 ºC, respectively. There are 4-hr DRLRs and the constant weather before and after the 11-day (Julian days 164–174) air temperature drop and rise period. The bottom-layer temperature at GOUS just decreases 2.1 ºC and then reaches the highest temperature of 19.6 ºC on Julian Day 184 when there is no daily large release during the 11-day drop and rise period. This is most likely due to the delay effect of 4-hr DRLRs before Julian Day 164. There are 15 days with cooler temperatures at GOUS under no-large release scenario during the 11-day drop and rise period when it compares with the constant weather scenario (Fig. 5.8).

For the 2-hr and 4-hr DRLRs during the drop and rise period, the bottom-layer temperature at GOUS begins to drop after 7 and 5 days of delay (Table 5.5) when it compares temperature time-series under the constant weather. After the Julian Day 180, the bottom-layer temperature starts to increase but still maintains the cooler conditions due to the cooler water continuously and slowly flowing along the bottom layers as density current. The durations with cooler temperatures are 35 and 38 days for 2- and 4-hr DRLRs during the 12-day drop and rise period.

For the 6-hr and 8-hr DRLRs during the drop and rise period, the large flow momentum reaches GOUS in about one day. The bottom temperature in the next 2 or 3 days is higher than the temperature under 4-hr DRLRs due to the mixing with the warmer

surface temperature. Then the bottom temperature drops quickly for 6 days and increases for 6 days corresponding to the air temperature changes. The lowest daily mean bottom temperatures are 14.4 on Julian Day 173 (June 22) and 13.8 on Julian Day 172 (June 21) for 6- and 8-hr DRLRs during the 12-day drop and rise period, respectively. After Julian Day 178, the bottom water maintains more or less constant cooler temperature for about 2 days. The daily mean temperature on Julian Day 179 is almost the same (~ 15.3 ^{o}C) for the 4-, 6-, and 8-hr DRLRs during the drop and rise period. After Julian day 180, the bottom temperature gradually increases due to the constant warmer weather condition. The daily mean temperatures at GOUS on Julian Day 200 (July 19) for 2-hr, 4-hr, 6-hr, 8-hr DRLRs and no daily large release during the 11-day drop and rise weather scenarios are 19.3, 19.2, 19.0, 19.0, and 19.7 °C, respectively. The lowest bottom-layer water temperature at GOUS during the 11-day drop and rise period under 2-hr, 4-hr, 6-hr, and 8-hr DRLRs are 16.3, 15.2, 14.5, and 13.8 °C with the cooler duration 35 (171 - 205), 38 (169 - 206), 43 (167 - 209) days, and 37 (166 - 202) days, respectively (Table 5.5). The large releases with longer durations (e.g., 6 or 8 hours) can relatively quickly push cooler release water to GOUS; with the air temperature drop in the first 6 days, simulated bottom temperatures at GOUS for 6- and 8-hr DRLRs are lower than ones under 4-hr DRLRs but cooler temperatures only primarily occur during the air-temperature drop and rise period.

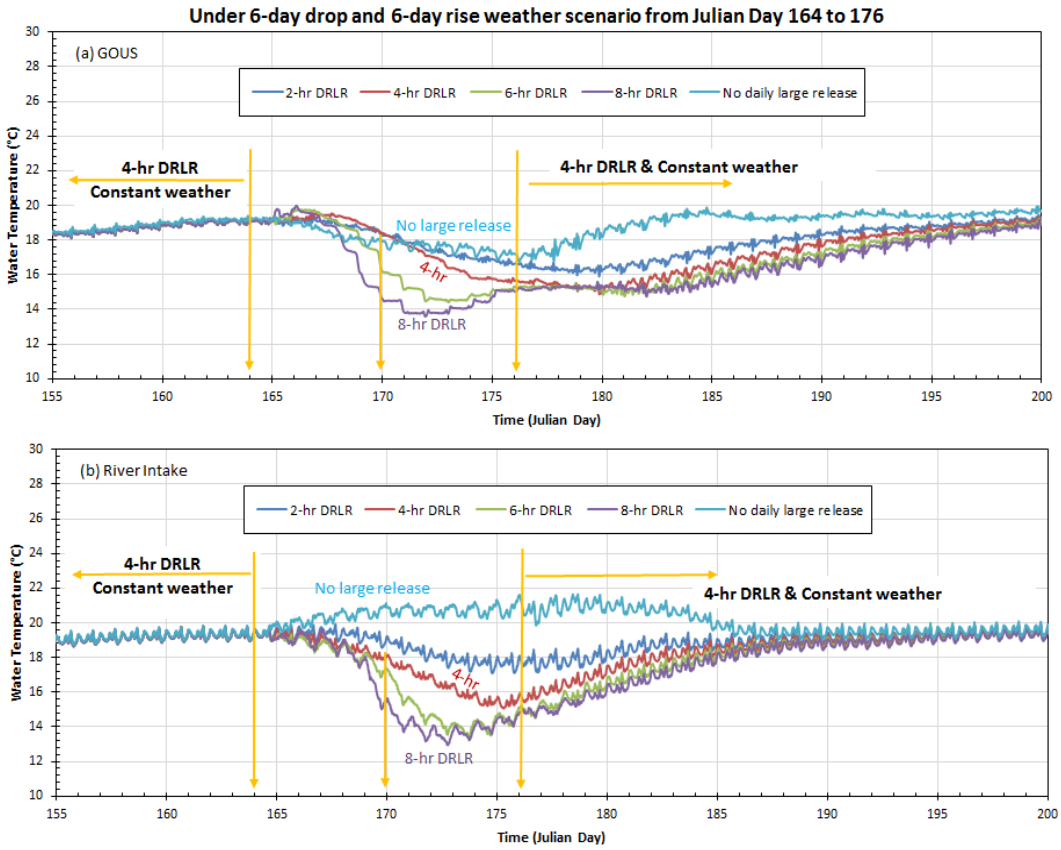

Fig. 5.13. Time series of simulated bottom temperatures at (a) GOUS and (b) the river intake when the DRLR release lasts for 2-hr, 4-hr, 6-hr, and 8-hr and when there is no daily large release from Julian Day 164 to 174 under 11-day drop and rise weather scenarios. There are 4-hr DRLRs and the constant weather before and after the air temperature drop and rise period.

Table 5.5 Delay time for GOUS and river intake, lowest simulated daily mean bottom-layer temperature during the drop and rise period, and cooler duration between the constant weather scenario and the 11-day drop and weather scenario.

Location	GOUS			The river intake		
Parameters	Delay days	Lowest temp (day)	Lower temp duration	Delay days	Lowest temp (day)	Lower temp duration
CSR [1]	6	17.1 (176)	15 (170–184)	3	N/A	19 (167–185)
2-hr DRLR	7	16.3 (178)	35 (171–205)	2	17.7 (174)	37 (166–202)
4-hr DRLR	5	15.2 (179)	38 (169–206)	2	15.4 (175)	37 (166–202)
6-hr DRLR	3	14.5 (173)	43 (167–209)	2	13.9 (173)	29 (166–194)
8-hr DRLR	2	13.8 (171)	37 (166–202)	2	13.5 (172)	26 (166–191)

Note: [1] – CSR stands for "constant small release" which is the same as "No large release" on Figure 13.

5.4.4.4 Differences under the Constant Weather and the Drop and Rise Scenarios

To identify the effect due to the 11-day drop and rise weather scenario alone, Fig. 5.14 shows time-series of differences of daily mean simulated bottom-layer temperatures between the constant weather scenario and the 11-day drop and rise scenario. Figs. 5.14a and 14b are derived from the data in Fig. 5.7 and Fig. 5.12 under three duration DRLRs over the whole simulation period (Julian Day 124–224). Figs. 5.14c and 5.14d are derived from the data in Fig. 5.8 and Fig. 5.13 under four duration DRLRs or no large release over 11 days (Julian Day 164–174) when there are weather changes. The positive differences indicate that the 11-day drop and rise weather scenario makes the bottom-layer water temperature at GOUS and the river intake further cooler. The daily mean differences at GOUS and the river intake show the similar pattern that relates to air

temperature and solar radiation drop and rise in Fig. 5.6. Characteristics of the differences (°C) of daily mean simulated bottom-layer water temperatures at GOUS and the river intake are summarized in Table 6 for Figs. 5.14a and 5.14b and Table 5.7 for Figs. 14c and 14d.

The maximum differences range from 3.1 to 4.2 °C (Tables 5.6 and 5.7) in comparions to 12 °C air temperature drop in 6 days (164–169). Mean differences with standard deviations were cacluted over the lower temperature periods (Tables 5.4 and 5.5) and range from 1.1 to 1.9 °C (1.1–1.4 °C standard deviation). To further understand the temperature difference distributions in Fig. 5.14, three parameters (Tables 5.6 and 5.7) are calculated: (1) average travel time (Chapra 1997), lower temperature integrations in °C-day (2) over the lower temperature duration and (3) over the 11 days (164–174). The average travel time at the river intake over the lower temperature duration under 2-hr, 4-hr, and 6-hr DRLRs (Fig. 5.14b) are 181.3, 177.1 and 175.0, which gives the controid of the lower temperature distribution. Except one case (8-hr DRLR, at the river intake, Table 5.7), average travel time occurs after Julian Day 174 or when the weather change has already stoped. To quantify the overall impact due to the cooler weather during the 11-day drop and rise period, all positive daily differences in the lower temperature duration were added together. For example, the total lower water temperatures at the river intake are 52.5, 44.1 and 37.2 °C-day under 2-hr, 4-hr, and 6-hr DRLRs from 124 to 224, i.e., 73.0%, 61.5%, and 51.4% of 72 °C-day lower air temperatures (Fig. 5.6), the driving force to lower the bottom-layer water temperature. The lower water temperature integration at the river intake over the 11 days (164–174) under 2-hr, 4-hr, and 6-hr DRLRs are 15.3, 20.8 and 22.1 days, which are directly related

to 72 ^{o}C-day lower air temperature (Table 5.6). Positive differences after Julian Day 174 are relaed to the movement of the density current in the bottom layers from upstream to downstream and taking time to warm up water in the bottom layer where the water depth is about 11 m. For the longer duration DRLRs, the maximum difference and average travel time appear earlier due to effect of the larger flow momentum.

For the 6-hr and 8-hr DRLRs during the drop and rise period (Fig. 5.14c and 5.14d), the cooling effect appears earlier when the maximum differences occur on Julian Day 171 or 172. For the 2- and 4-hr DRLRs and no daily large release during the 11-day drop and rise period, the maximum differences occur after Julian Day 176 due to the smaller flow momentum effect. The average traveling time for the lower temperature distributions at GOUS is later than ones at the river intake (Tables 5.6 and 5.7), and this may indicate the movement of the density current slows down from GOUS and the river intake. Fig. 5.14 and Tables 5.6 and 5.7 show that lower bottom-layer water temperatures at GOUS and the river intake are primarily due to the lower air temperatures and solar radiations during the 11 days and less affected by the release pattern. The 4-hr DRLRs over the whole simulation period seems be the most efficient release from SDT.

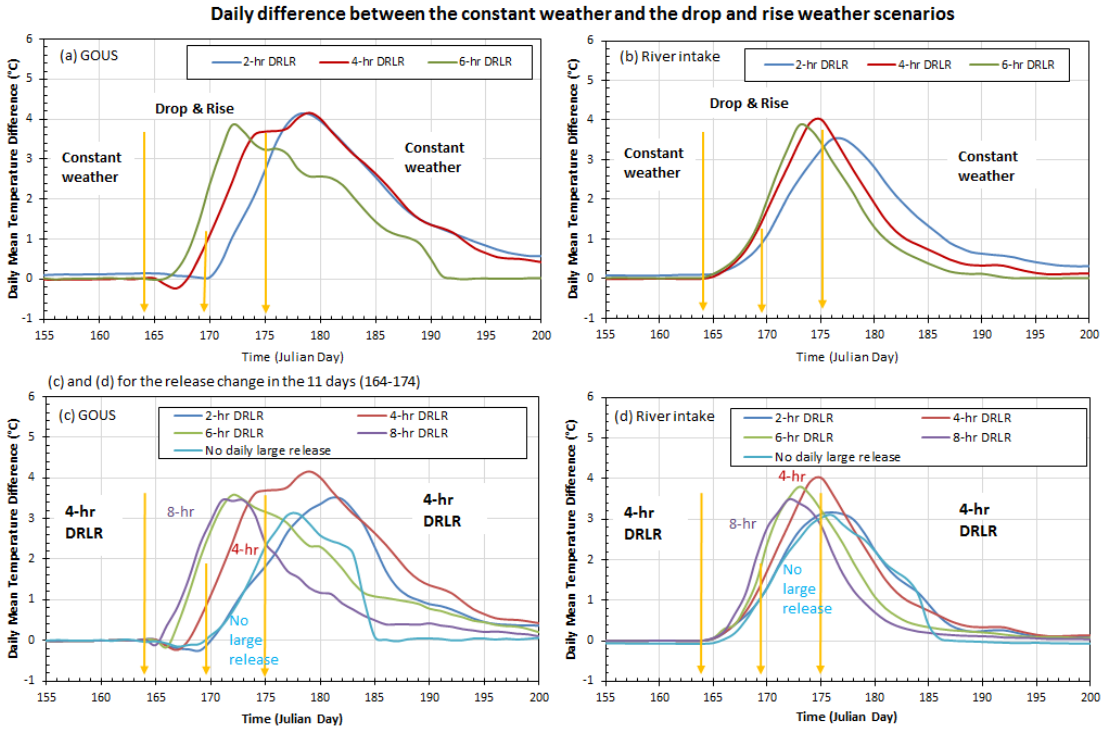

Fig. 5.14. Difference of daily mean simulated bottom-layer temperatures between the constant weather scenario and the 11-day drop and rise weather scenario at (a) GOUS and (b) the river intake for three DRLR over the whole simulation; and (c) GOUS and (d) the river intake under the 2-hr, 4-hr, 6-hr, and 8-hr DRLRs and when there is no daily large release in 11 days (Julian Day 164 to 174).

Table 5.6 Characteristics of differences (°C) of daily mean simulated bottom-layer water temperatures (°C) at GOUS and the river intake (Fig. 5.14 a and b) under three durations of DRLRs over the whole simulation period.

Location	GOUS			The river intake		
Parameters	Maxi. Diff. [1]	Mean Diff. (day) [2]	Lower temp integration [3]	Maxi. Diff.	Mean Diff (day)	Lower temp integration
2-hr DRLR	4.1	1.2±1.3 (184.4)	65.0 (8.1)	3.5	0.9±1.1 (181.3)	55.2 (15.3)
4-hr DRLR	4.2	1.8±1.4 (181.4)	69.4 (16.2)	4.0	1.2±1.3 (177.1)	44.1 (20.8)
6-hr DRLR	3.9	2.1±1.1 (177.3)	51.2 (22.1)	3.9	1.4±1.3 (175.0)	37.2 (22.1)

Note: [1] – maximum difference, [2] – mean difference with standard deviation, and the average traveling time or the centroid of the distribution in days is given inside brackets, and [3] – total lower temperature is °C-day after the integration, the first number is the integration over the whole lower temperature duration (Table 5.4), and the number inside brackets is the integration over the 11 days (164–174) with the air temperature drop and rise.

Table 5.7 Characteristics of differences (°C) of daily mean simulated bottom-layer water temperatures (°C) at GOUS and the river intake (Fig. 14 c and d) under CSR and four durations of DRLRs during the 11-day drop and rise period.

Location	GOUS			The river intake		
Parameters	Maxi. Diff. [1]	Mean Diff. (day) [2]	Lower temp integration [3]	Maxi. Diff.	Mean Diff (day)	Lower temp integration
CSR	3.1	1.9±1.0 (178.2)	28.8 (6.4)	3.1	1.9±0.9 (176.4)	35.3 (15.3)
2-hr DRLR	3.5	1.4±1.1 (182.6)	47.6 (5.7)	3.2	1.2±1.1 (177.6)	40.5 (16.4)
4-hr DRLR	4.2	1.8±1.4 (181.4)	69.4 (16.2)	4.0	1.2±1.3 (177.1)	44.1 (20.8)
6-hr DRLR	3.6	1.3±1.1 (178.8)	53.7 (23.0)	3.8	1.3±1.3 (175.1)	36.7 (22.6)
8-hr DRLR	3.4	1.1±1.1 (176.1)	40.1 (23.9)	3.5	1.2±1.2 (173.9)	32.1 (23.0)

Note: [1], [2], and [3] are defined in Table 5.7.

Results in Figs. 12–14 and Tables 4–7 are related to the 11-day 2 ^{o}C/day drop and rise weather scenario (Fig. 5.5). In future study, other drop and rise weather scenarios, e.g., 1, 2, 3, and 4 ^{o}C/day drop and rise in 3, 5, 7, and 9 days, should be inverstigated to understand impacts of various weather changes on bottom-layer water temperatures in BRRS.

5.5 Conclusion

In this paper we applied a previously calibrated 3D EFDC model for a river-reservoir system to simulate temperature distributions under various hypothetical weather conditions and daily repeated large releases or DRLRs from upstream boundary. A series of model scenario runs were performed to further understand the bottom-layer water temperature changes at downstream locations of BRRS (e.g., GOUS and the river intake) corresponding to hypothetical meteorological changes under different release scenarios. All hypothetical weather and release scenarios were based on the data analysis of local weather conditions and actual release patterns. The summaries of key findings from the study are as follows:

(a) Both the duration of large releases and weather conditions affect the formation and spread of density currents and then temperature distribution in BRRS. Under the constant weather conditions for 2-hr, 4-hr and 6-hr DRLR, the water temperatures at different depths and locations will achieve equilibrium values with diurnal fluctuations. The repeated releases with longer durations push the colder bottom water from SDT downstream and make the bottom water temperature in downstream locations cooler (Fig. 5.7). Simulated surface temperatures at GOUS under 6-hr DRLRs is about 6 ^{o}C lower

than ones under 4-hr DRLRs due to surface wave propagation of cooler released water. Simulated bottom temperatures at GOUS under 6-hr DRLRs is only about 1 °C and 2 ^{o}C lower than ones under 4-hr and 2-hr DRLRs.

(b) Variations of weather conditions (e.g., drops of air temperature and solar radiation) directly control variations of bottom-layer water temperature in BRRS. The daily drop rate of bottom temperature is related to the air temperature drop rate and period. The average daily dropping rates of bottom temperature for 2-, 4- and 6-day drops under 6-hr DRLR are 0.3, 0.5 and 0.4 °C/day during 5, 6, and 11 days, respectively, under the air temperature drop rate 2 °C/day (Table 5.2). Bottom-layer water temperature can maintain the cooler condition for a longer period than the surface temperature does. During the air temperature drop and rise in 11 days, the bottom water at GOUS can maintain cooler temperature about 24 days (Fig. 5.11).

(c) During the 11-day drop and rise weather scenario, the bottom temperature at GOUS for 6-hr DRLR over the whole simulation period starts to drop firstly with 2 days delay, following with the drop under 4-hr and 2-hr DRLRs (5 and 7 days of delay, Fig. 5.12a). The daily drop rate and the lower temperature duration are almost same for 2-hr, 4-hr and 6-hr DRLRs due to the same drop and rise pattern of air temperature and solar radiation. Average bottom temperature at the river intake under 4-hr DRLRs is 2.3 ^{o}C lower than one under 2-hr DRLRs and only 1.1 ^{o}C higher than one under 6-hr DRLRs in the whole simulation period (Fig. 5.12b).

(d) The maximum difference between the constant weather scenario and the 11-day drop and rise weather scenario range from 3.1 and 4.2 °C at different releases (Tables 5.6 and 5.7). The large releases with longer durations (e.g., 6 or 8 hours) can relatively

quickly push cooler release water to GOUS and the river intake; with the air temperature drop in the first 6 days, simulated bottom temperatures at GOUS for 6- and 8-hr DRLRs are lower than ones under 2- and 4-hr DRLRs but cooler temperatures only primarily occur during the air-temperature drop and rise period (Fig. 5.13). It seems the most efficient release under the cold front is not the longest release from SDT but under the 4-hr DRLR during the 6-day drop and 6-day rise period. Fig. 5.14 and Tables 5.6 and 5.7 show that lower bottom-layer water temperatures at GOUS and the river intake are primarily due to the lower air temperatures and solar radiations during the 11 days and less affected by the release pattern.

The 4-hr DRLRs over the whole simulation period seems be the most efficient release from SDT based on the scenarios modeled using EFDC in this study. For all scenario runs tested, the release flow rate from SDT is fixed as 140 m^3/s with different durations because. Under the actual release, there are some releases up to about 280 m^3/s in 2011 (Fig. 5.2a). In a future study, new scenarios with 280 m^3/s and different durations will be tested to identify more efficient release operations to compliance with temperature constraints downstream.

Chapter 6. Conclusions and Recommendations

6.1 Summary and Conclusions

This research work is related to the project "Watershed modeling, water balance analysis, three-dimensional flow and thermal discharge modeling for the William C. Gorgas plant". The objective of the overall study is to develop three-dimensional hydrodynamic and water quality models to simulate flow, temperature, dye in a river-reservoir segment (124.2 river km) stretching from Smith Dam Tailrace (SDT) to Bankhead Lock & Dam (BLD) in Alabama (AL), USA. River regulation as a means of water resources management is a common operating procedure to meet hydro-electric power demands. The requirement of minimum flow is usually during the warm season of a year, especially during the summer to maintain lower water temperatures in downstream river. These numerical models allow us to study the spatial and temporal distributions of flow, temperature, and dye in the whole area. The results of this study are important with regard to water quality modeling and management, habitat assessment in rivers, and management of thermal discharges from a power plant.

For the first phase of the study, a three-dimensional hydrodynamic EFDC model was applied to simulate unsteady flow patterns and temperature distributions under observed variable upstream releases and variable atmospheric forcing in BRRS. The calibrated EFDC model provided simulated water surface elevation, temperature, velocity

and discharge at different layers (depths) for all grids in different cross sections (Fig. 2.1). Overall, the EFDC model was able to predict the temporal and spatial distributions of flow and temperature (Fig. 2.10) and revealed complex interactions and density currents due to dynamic upstream releases and solar heating from atmosphere. The major findings of the study are summarized as follows:

a) Simulated water depth, velocity, and flow rate in Sipsey Fork increased first, then gradually and steadily decreased with time after the release from Smith Dam stopped, and the recession lasted more than 12 hours at MSF (Figs. 2.6–2.7). After a few hours of heating, maximum temperature differences at MSF reached 3–5 ^{o}C before the stratification was removed by the next release (Fig. 2.10). Simulation results clearly show that regular daily large releases did maintain relatively lower water temperatures at the bottom layers (Figs. 2.12–2.13) that promoted the density current formation at further downstream of Sipsey Fork. Strong temperature stratification existed between surface and bottom temperatures at Cordova (e.g., 26–31 May, Fig. 2.13) without daily releases from Smith Dam. Simulated surface and bottom temperatures at Cordova kept on increasing first and then varied with air temperature trend when it was assumed that there were no intermittent large releases from Smith Dam.

b) The flow momentum created by the large release removed the thermal stratification at MSF. The well-mixed condition at MSF was developed at 1.75 hours after the release started. When there was a daily large flow release from Smith Dam, Cordova and GOUS responded with surface-layer flow rate changing from moving upstream (SDT) to moving downstream (BLD) roughly 2–3 hours after the release. The flow rates moving downstream in the bottom layer had obvious increases. These daily

releases promoted and enhanced the movement of density current moving from upstream towards downstream.

c) Preliminary results using particle tracking show that particles or water released from Smith Dam could take several days to reach Cordova and GOUS, and the momentum developed by the releases did push the cooler water near the river bottom moving downstream. The momentum or push effect from the large release provides driving force for the density current movement along the river bottom in the BRR system.

For the second phase of the study, the 3D EFDC model configured for BRRS was applied to simulate unsteady flow patterns and temperature distributions under large releases with different durations from SDT (upstream boundary). This study mainly focuses on result analyses of the EFDC simulations from SDT to GOUS, upstream portion of BRRS. A series of model scenario or sensitivity runs were performed to understand and quantify the formation and propagation of density currents caused by upstream releases and solar heating when all other input variables were kept unchanged. The summaries of key findings from the study are as follows:

(a) The density current formation and propagation in the natural system under intermittent large releases is complex and dynamic. The density currents in BRRS form at different reaches, are destroyed at upstream locations due to the flow momentum of the releases, and form again due to solar heating. Both the duration of large releases and solar heating affect and control the formation and spread of density currents when the release flow rate is unchanged (140 m^3/s).

(b) There are 48.4%, 69.0%, and 91.1% of time with positive bottom velocity (density currents moving downstream) with average positive velocity of 0.017, 0.042,

and 0.053 m/s at Cordova for the 2-hr, 4-hr, and 6-hr DRLR, respectively (Table 3.2). The repeated releases with longer durations push the bottom colder water from SDT downstream and make the bottom water temperature in downstream locations to be cooler. For the 6-hr DRLR, the momentum effect definitely reaches Cordova (~43.7 km from SDT).

c) With the CSR only, the cold water current near SDT has moved downstream about 4 km in 6 days. With the 4-hr SLR, the cold water density current can move from Smith Dam to UPJ (21 km) in a few hours (Fig. 3.5). However, time-series plots of simulated surface and bottom temperatures at MSF and Cordova show that one SLR does not have long-term impact on downstream surface and bottom temperatures (Fig. 3.6). Regular (daily repeated) large releases are required to push density currents moving downstream and maintain temperature stratification in downstream locations (Fig. 3.9).

(d) Overall average surface and bottom temperatures are lower for longer duration of DRLR. The average difference between surface and bottom temperatures for 6-hr DRLR is 1.38 ^{o}C, while for 2-hr DRLR is 3.35 ^{o}C at Cordova (Table 3.3). Results in Fig. 3.9 and Tables 3.3 and 3.4 clearly show that DRLRs lasting for at least 4 hrs maintain lower water temperatures at Cordova. When the 4-hr and 6-hr DRLRs repeat more than 6 and 10 days, respectively, bottom temperatures at Cordova become lower than ones for CSR only. These releases overwhlem the mixing effects due to inflow momentum and maintain downstream temperature stratification.

For the third phase of the study, EFDC dye model components were activated to simulate dye concentrations for each computation cell to understand density current movement. Dye distributions are useful and clear to track how the density current moves.

The cold-water current from SDT moves to MSF (~11 km) during the 4-hr SLR and advances to ~18 km in 1 day after the release stops. In the following 4 days after SLR stops but there is CSR only, the dye moves downstream very slowly, less than 4 km (Fig. 4.2a). At 11–12 hrs after the 4-hr SLR stops, the total volume of water in both domains of SDT to MSF and MSF to UPJ reduces to the amount before the release and has small variations afterwards. This means the surface wave created by the large release attenuates in 11–12 hrs (Fig. 4.3). The dye is advanced day by day when the large release is repeated each day, i.e., DRLR. The longer-duration DRLR (e.g., 6-hr) pushes the dye to move further downstream. The dye front moves to UPJ (about 21 km) in 1 day after the 6-hr large release (Fig. 4.6). In the period without the large release, the dye spreads and mixes with the surrounding water due to turbulent diffusion and dispersion (due to backwater effect). When the next large release comes, the dye released at SDT is pushed downstream again. For the 4-hr DRLR, the momentum effect has some impacts at Cordova but does not reach GOUS. For the 6-hr DRLR, the momentum effect definitely reaches Cordova and the dye pattern repeats daily (Fig. 4.7).

For the fourth phase of the study, a previously calibrated 3D EFDC model for a river-reservoir system was applied to simulate temperature distributions under various hypothetical weather conditions and daily repeated large releases or DRLRs from upstream boundary. A series of model scenario runs were performed to further understand the bottom-layer water temperature changes at downstream locations of BRRS (e.g., GOUS and the river intake) corresponding to hypothetical meteorological changes under different release scenarios. All hypothetical weather and release scenarios

were based on the data analysis of local weather conditions and actual release patterns. The summaries of key findings from the study are as follows:

(a) Both the duration of large releases and weather conditions affect the formation and spread of density currents and then temperature distribution in BRRS. Under the constant weather conditions for 2-hr, 4-hr and 6-hr DRLR, the water temperatures at different depths and locations will achieve equilibrium values with diurnal fluctuations. The repeated releases with longer durations push the colder bottom water from SDT downstream and make the bottom water temperature in downstream locations cooler (Fig. 5.7). Simulated surface temperatures at GOUS under 6-hr DRLRs is about 6 ^{o}C lower than ones under 4-hr DRLRs due to surface wave propagation of cooler released water. Simulated bottom temperatures at GOUS under 6-hr DRLRs is only about 1 °C and 2 ^{o}C lower than ones under 4-hr and 2-hr DRLRs.

(b) Variations of weather conditions (e.g., drops of air temperature and solar radiation) directly control variations of bottom-layer water temperature in BRRS. The daily drop rate of bottom temperature is related to the air temperature drop rate and period. The average daily dropping rates of bottom temperature for 2-, 4- and 6-day drops under 6-hr DRLR are 0.3, 0.5 and 0.4 °C/day during 5, 6, and 11 days, respectively, under the air temperature drop rate 2 °C/day (Table 5.2). Bottom-layer water temperature can maintain the cooler condition for a longer period than the surface temperature does. During the air temperature drop and rise in 11 days, the bottom water at GOUS can maintain cooler temperature about 24 days (Fig. 5.11).

(c) During the 11-day drop and rise weather scenario, the bottom temperature at GOUS for 6-hr DRLR over the whole simulation period starts to drop firstly with 2 days

delay, following with the drop under 4-hr and 2-hr DRLRs (5 and 7 days of delay, Fig. 5.12a). The daily drop rate and the lower temperature duration are almost same for 2-hr, 4-hr and 6-hr DRLRs due to the same drop and rise pattern of air temperature and solar radiation. Average bottom temperature at the river intake under 4-hr DRLRs is 2.3 ^{o}C lower than one under 2-hr DRLRs and only 1.1 ^{o}C higher than one under 6-hr DRLRs in the whole simulation period (Fig. 5.12b).

(d) The maximum difference between the constant weather scenario and the 11-day drop and rise weather scenario range from 3.1 and 4.2 °C at different releases (Tables 5.6 and 5.7). The large releases with longer durations (e.g., 6 or 8 hours) can relatively quickly push cooler release water to GOUS and the river intake; with the air temperature drop in the first 6 days, simulated bottom temperatures at GOUS for 6- and 8-hr DRLRs are lower than ones under 2- and 4-hr DRLRs but cooler temperatures only primarily occur during the air-temperature drop and rise period (Fig. 5.13). It seems the most efficient release under the cold front is not the longest release from SDT but under the 4-hr DRLR during the 6-day drop and 6-day rise period. Fig. 14 and Tables 6 and 7 show that lower bottom-layer water temperatures at GOUS and the river intake are primarily due to the lower air temperatures and solar radiations during the 11 days and less affected by the release pattern.

The 4-hr DRLRs over the whole simulation period seems be the most efficient release from SDT based on the scenarios modeled using EFDC in this study. For all scenario runs tested, the release flow rate from SDT is fixed as 140 m^3/s with different durations because. Under the actual release, there are some releases up to about 280 m^3/s in 2011 (Fig. 5.2a). In a future study, new scenarios with 280 m^3/s and different durations

will be tested to identify more efficient release operations to compliance with temperature constraints downstream.

6.2 Discussion

The dynamics of the density currents developed in BRRS is different from classic ones investigated in other previous studies. Actually, traditional gravity/density currents just occur in various locations of BRRS in a short period between two daily large releases. In this study, the most releases from Smith Dam are 140 m^3/s and last 2, 4 or 6 hours. First, bottom slopes in this river-reservoir system are much smaller than steep bottom slopes, e.g., 3%–20% in Toolik Lake (Rueda and MacIntyre 2010). Large upstream release with about 12 ^oC under 140 m^3/s starts from 1:00 pm and typically lasts for a few hours. During the release period (e.g., 4 hours), the large flow momentum with colder water pushes and mixes with warmer water downstream. There is no thermal stratification due to the mixing effect in upstream portion of BRRS. It's similar to plug flow, but the velocity decreases from upstream towards downstream. It also has a relatively large longitudinal temperature gradient when large flow momentum with colder water pushes relatively warmer water downstream. Fig 3.7 shows the simulated water temperature distributions for 2-hr, 4-hr and 6-hr DRLRs when the large release just stops. For the 2-hr DRLR, the momentum effect roughly reaches to UPJ, but the density currents exist at further downstream. Same as the 4-hr and 6-hr DRLRs, the momentum effect reaches to MJC and Cordova, respectively. Temperature stratification is very weak in the upstream part of study area due to the momentum mixing.

After the release stops, the upstream release is a small constant release with a flow rate of 2.83 m^3/s (100 ft^3/s) and a lower temperature of about 8 ^oC (during the summer months). The small constant release forms the density current as the traditional gravity current does, but it moves slowly downstream along the river bottom due to the small slope and small inflow momentum. However, the density current forms near Smith Dam and doesn't have much effect on downstream water movement because of slow propagation. For the further downstream, after the large release stops, there are still momentum or inertia effect that can make the mixed-water move downstream. The density currents at further downstream also gradually move/advance towards the river inlet due to the remaining momentum. Water temperature in BRRS is not affected much during the night by air temperature. After the sunrise in the next day, surface temperature begins to increase first due to the surface heat exchange and the short-wave solar heating. It creates vertical temperature stratification and forms density current in the bottom layer; the density current moves slowly along the bottom (Fig. 3.7). There is only few hours left for traditional gravity current movement (Fig 1.1) before the next day large release starting at 1:00 pm. During those few hours, the gravity current moves based on the slope and gravity. The density currents form at different parts of the river-reservoir system. Then, when the next day large release comes, the colder water with large momentum mxies and pushes the warmer water downstream again. The density currents at upstream reaches are destroyed due to the large flow momentum from the release, but at the same time it pushes the density current at further downstream moving forward.

Due to these large momentum effect from upstream release, it's possible to withdrawal cold water from the bottom layers at the river inlet to maintain higher power-

plant efficiency. The power plant also needs reservoir releases to maintain lower downstream temperature after thermal discharge returns to the river. The typical water depth at river intake is around 11.1 m. Fig. 6.1 shows simulated surface and bottom temperatures in 5 days (180 is June 29) at the river intake under the actual release and weather conditions. Due to the solar heating, the highest surface temperature appears in the late afternoon which is around 5:30 pm. The bottom temperature maintains cold with small fluctuations under the actual daily large release from Smith Dam in these 5 days.

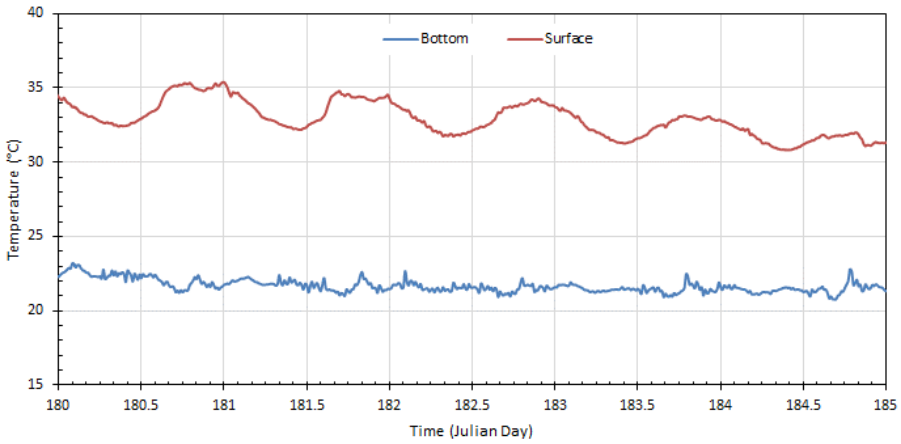

Fig. 6.1 Time-series plot of modeled bottom and surface temperature at river intake under actual release and weather conditions from Julian Day 180 to 184, 2011

When the large amount (140 m^3/s) of cold water releases from upstream at 1:00 pm, how long will the cold water reach to the river intake? The water movement can be distinguished into two parts. One is the surface wave propagating downstream that reaches to the river intake in roughly 2 or 3 hours. Another one is cold water movement near the channel bottom. The density current movement is much slower. When the large flow release at 1:00 pm, the density current doesn't move to the river intake at the same day. The daily repeated large release is needed because it's kind of cumulative effect. The

large release can push the cold water and advance downstream each day. With enough time, the density current makes the water temperature near river intake cold.

Though the dye is just a tracer which is not coupled with temperature simulation in the EFDC model, it still gives us some idea for the delay effect of density current. Fig. 4.7 shows time-series plots of simulated dye concentrations in the cross sections MSF, UPJ, MJC, Cordova and GOUS when the 6-hr dye is released from SDT for (a) 2-hr, (b), 4-hr, and (c) 6-hr DRLRs. The dye front moves to MSF at almost same time for 2-hr, 4-hr, and 6-hr DRLRs. For the locations downstream of MSF, it clearly shows that dye of the longer-duration flow release moves downstream quicker. Taking the 4-hr DRLR as an example, the dye moves to UPJ, MJC, Cordova and GOUS at Julian day 143.03, 143.96, 145.03, and 148.58, respectively, which means roughly 12 hrs, 34 hrs, 60 hrs, and 145 hrs after the dye release from SDT (Fig. 4.7b). For the 2-hr DRLR, it seems the momentum effect does not reach Cordova because dye at Cordova does not have sudden increase instead of gradual increase (Fig. 4.7a). For the 4-hr DRLR, the momentum effect has some impacts at Cordova but does not reach GOUS (Fig. 4.7b). For the 6-hr DRLR, the momentum effect definitely reaches Cordova and the dye pattern repeats daily, and also has certain impact at GOUS after 5 days (Fig. 4.7c).

Hence, the single large release (SLR) is not effective to maintain the colder water near the river intake. Fig. 3.6 shows time-series plots of simulated water temperatures in the surface and bottom layers at MSF and Cordova for four sensitivity runs: CSR only, 2-hr, 4-hr, and 6-hr SLR. For CSR, surface and bottom temperatures gradually increase with time due to the solar heating. The typical water depth at MSF is 4.9 m, smaller than the depth at Cordova (9.2 m). The SLR starts at 1:00 pm on Julian day 148. Due to

momentum effect and mixing, both surface and bottom water temperatures at MSF have quickly dropped to ~12 °C shortly after the large release starts from Smith Dam (Fig. 3.6a). Surface and bottom temperatures begin to increase at a few hours after the release, more or less continuously increase for about 5 days, and eventually reach to temperatures simulated under CSR. The 2-, 4- and 6-hr SLRs have similar impacts on water temperature at MSF. When the flow momentum from a SLR comes to Cordova, longer period SLR has more mixing and keeps the surface temperature lower (Fig. 3.6b). With ~2.5 hours delay, the momentum effect under 6-hr SLR reach to surface layer at Cordova. The 2-hr and 4-hr SLRs have little effect on the bottom temperature at Cordova. The flow momentum from the 6-hr SLR seems strong enough to mix or stir the bottom water, and its temperature has an increase and decrease for a few hours then gradually increases with time (Fig. 3.6b) due to solar heating. Under 6-hr SLR, it takes about 7 hours for the momentum effect reach to bottom layer at Cordova. Overall, Fig. 3.7 shows us that one SLR does not have long-term impact on downstream surface and bottom temperatures. Daily repeated large releases are required to push density currents moving downstream.

6.3 Limitations of the Study

The EFDC model considered in this study is not a completely three dimensional model. In the *z*-direction (along the depth), the water depth is divided into number of horizontal layers and momentum equations (*x* and *y* directions) are solved at each layer. A vertical sigma coordinate and a horizontal orthogonal-curvilinear coordinate are used in the EFDC model. However, it has been well known that sigma-coordinate

transformation also induces numerical errors in the horizontal pressure gradient force in the case of stratified flow over steep topography (Liu and Huang 2008). The EFDC model was adequate for the analysis performed in the study because bathymetries in the BRRS has relative smooth changes on bottom elevations, i.e. without steep topography. All the models developed were calibrated and validated with the observed data before performing any scenario analysis.

In all the EFDC model runs, ground water and surface water interaction was not considered. The reason for not including ground water in model simulation was that there is not significant interaction of ground water with surface water.

The EFDC model for BRRS needs well-defined boundary conditions at major tributaries also. Current EFDC model includes 10 grids for Upper Mulberry Fork (Fig. 2.1) and 22 grids for Locust Fork. The geometry data of the HEC-RAS model which provided by APC can be used to add more computational grids in order to better represent these two major tributaries. Additional HEC-RAS model runs can further quantify what inflow hydrographs we should use for the tributaries. There are several options to apply tributary inflow hydrographs for the EFDC model. Observed streamflow hydrographs at the USGS gaging stations can be used directly with and without applying the area ratio if the hydrographs have negligible attenuation. A hydrologic river routing (e.g., the Muskingum method) can be implemented to route observed USGS hydrographs when hydrograph routing (peak attenuation and time lag) is important. Tributary outflow hydrographs can be simulated from a watershed model such as WARMF. We have tested some of these options but were not able to quantify which option is more accurate.

There are 2 to 8 computational grids in the Gorgas EFDC model to represent the main channel of Black Warrior River. The FEDC grid used for 2011 simulation is accurate enough to simulate water surface elevations in the period without large rainfall events but created certain errors during large rainfall events. Therefore, additional girds should be added on both sides of the main channel to represent flood plain or overbank areas. Two new EFDC grids with overbank areas were developed for the Gorgas model but did not improve the model accuracy during the flood events. Black Warrior River does not have traditional wide-open flood plains but have relatively narrow overbank areas with high-density vegetation (trees and bushes). The overbank areas are dry under normal water level conditions but wet during large flood events. The EFDC model does have the capability to simulate drying and wetting process. Further studies including additional grids for overbank areas are necessary.

6.4 Future Study

In-depth dye studies such as isotherm flux analysis could be useful to understand the backwater effect from the downstream in the system. Isotherm flux analysis at any cross-section would allow us to understand what discharge and temperature are flowing downstream and what discharge and temperature are flowing upstream. We can also estimate the average temperature of water flowing towards upstream due to the backwater effect. Similar analysis has been performed by researchers to find out the salt flux in the rivers and estuaries. Sensitivity experiments with various flow release duration schemes would allow us to understand and make decision on management from the upstream release (SDT) in the natural system.

To find specific relationship between release temperature at Smith Dam and bottom temperature at downstream, several new sensitivity experiments will be used to find the relationship between them. A possible equation relating release temperature, release flow, release duration, bottom temperature at different locations and time lag (time difference between the flow release from and the time of resulting density currents reaching) will be very helpful to manage flow releases from Smith Dam.

For all the scenarios in the second, third and fourth phases of the study, water level at the Bankhead L&D was used as downstream boundary condition. Observed water surface elevations ranged from 77.35 m to 77.75 m from 4 May to 3 September 2011 with an average elevation of 77.60 m (standard deviation of 0.07 m). Therefore, water surface elevation at BLD was set at 77.60 m (constant) for the scenario runs. Based on the sensitive analysis, the constant water level at BLD would not affect much on density-current flow dynamics in the upstream portion of BRRS (from SDT to GOUS). These constant representative values will be revisited to check the impact for inflow and outflow in different cross sections by using isotherm flux analysis.

In the fourth phase of the study, the 4-hr DRLRs over the whole simulation period seems be the most efficient release from SDT based on the scenarios modeled using EFDC in this study. For all scenario runs tested, the release flow rate from SDT is fixed as 140 m^3/s with different durations because. Under the actual release, there are some releases up to about 280 m^3/s in 2011 (Fig. 5.2a). In a future study, new scenarios with 280 m^3/s and different durations will be tested to identify more efficient release operations to compliance with temperature constraints downstream.

Appendix A: Calibration Parameters in EFDC model

For any numerical model to be able to predict dependent unknown variables accurately, the model should be calibrated using reliable observed data. EFDC model is not a self-calibrated model. The modeler needs to adjust the model parameters based on the study area and hydrologic and hydrodynamic conditions. There are several parameters one may adjust to get the good calibration results. However, before tweaking any calibration parameters, it is very important and essential to represent the study area with appropriate model grid, bathymetry resolution, and boundary conditions. The tuning of model parameters in the calibration process is a recursive process. The values of the model parameters are generally obtained through direct measurement, estimation from other measured data, literature values, and model calibration. Based on literature review the parameters can be selected from a feasible range and adjusted to minimize differences between model results and measured data. For EFDC hydrodynamic models, the parameter determining the bottom friction, such as bottom roughness is often the first model parameter most often adjusted in the model calibration (Ji 2008). The turbulent parameters of Mellor-Yamada model (Mellor and Yamada 1982) are usually not adjusted in the model calibration process, unless there are well-justified reasons. The parameters that are usually adjusted in EFDC hydrodynamic models are as follows:

a. Parameter determining bottom friction, such as bottom roughness height.
b. Horizontal momentum diffusion coefficient

Bottom roughness height, is the one adjusted first and most in EFDC hydrodynamic calibration. According to literature the bottom roughness of the bed is frequently set to 0.02 m with a typical range between 0.01 and 0.1 m. In EFDC model, one needs to specify the empirical parameter C, when using Smagorinsky formula to compute the horizontal momentum diffusion coefficient. The typical values for the empirical parameter C range from 0.1 to 0.2.

A.1 Calibration Parameters and their Range

The calibration parameters used in the EFDC model for BRRS are shown in table A.1.

Table A.1 Calibration parameters used in EFDC model for BRRS and the calibration range for calibration parameters

Calibration Parameters	EFDC	Calibration Range
Smagorinsky Coefficient (empirical parameter c)	0.2	0.1 – 0.2
Roughness height	0.02 m	0.01 m – 0.1 m
Vertically Eddy viscosity	0.00001 m^2/s	$1.0E^{-7}$ – $1.0E^{-3}$ m^2/s
Horizontal Eddy Viscosity	2 m^2/s	Usually 10^2 – 10^7 greater than vertical eddy viscosity

Before adjusting any parameters of EFDC models for the study areas in BRRS, many iterative runs were performed initially to make sure the grid and the bathymetry used are representative for the study area. Grid cells and bathymetry were revised number of times because the topography of the study area is quite complex. After the higher degree of accuracy was attained in the grid cells and bathymetry, boundary conditions for

flow and temperature (used in rivers inflows) and water surface elevation (used to represent the downstream boundary) were analyzed and used to set the model run. Finally, the calibration parameters mentioned in the table A.1 were adjusted to have the best possible matches between the observed data and modeled water surface elevation, temperature, and velocity.

Appendix B: Estimating hourly water temperatures in rivers from air temperatures

B.1 Introduction

Water temperature is probably one of the most significant and widely measured parameters among the water quality characteristics of surface waters (Kothandaraman and Evans 1972). Most of the physical properties of water such as density and saturation concentration of dissolved oxygen are functions of temperature. Natural processes or human activities such as industrial production, deforestation and climate change would affect the water temperatures (Caissie 2006). Climate change has been identified as an important source of temperature disturbance on a large to global scale (Sinokrot et al. 1995). To predict/estimate river temperature, air temperature is not the only physical parameter influencing water temperature. Other parameters of influence are solar radiation, relative humidity, wind speed, water depth, groundwater inflow, artificial heat inputs, and thermal conductivity of the sediments (Pilgrim et al. 1998).

There are many models for predicting/estimating water temperature, and these models are classified into three groups: Regression, stochastic and deterministic models (Raphael 1962; Brown 1969; Cluis 1972). Linear regression models have been used to estimate water temperature using only air temperature for mostly weekly and monthly data as the input parameter (Johnson 1971). Studies have shown that as the time scale increases (daily, weekly, monthly, and annually), the model will be more accurate and reliable in

estimating water temperatures (Caissie et al. 2004). The logistic regression model has been recently and widely used to estimate river water temperature (Harvey et al. 2011). Morrill et al. (2005) evaluated the general temperature relationships (both linear and nonlinear) in 43 river and stream sites in 13 countries and indicated that the air/water temperature relationship is better fitted with non-linear regression. A stochastic modeling technique often involves separating the water temperature time series into two components, namely the long-term annual component (annual cycle) and the short-term component (Caissie et al. 1998). The stochastic model is not often used because it is relatively complex compared with regression models. Deterministic models employ an energy budget approach to predict river water temperature (Morin and Couillard 1990; Sinokrot and Stefan 1993). In addition, Cho and Lee (2011) present a newly developed model of the relationship between daily air and water temperature that was constructed on the basis of harmonic analysis.

The purpose of the study is to develop a simple but accurate model for calculating hourly water temperatures in rivers for water quality modeling in aquatic systems. In this study, direct linear and non-linear (logistic) regression models with time lags (4–5 hours or hr) were firstly used to calculate hourly water temperature. The second method used modified sine and sinusoidal wave functions (MSSWF) to estimate hourly water temperatures in 8 rivers (Table B.1). We investigated and applied seasonal variations in the daily maximum and minimum stream water temperatures based on observed daily maximum and minimum air temperatures. The sinusoidal wave function (SWF) model, originally used to calculate hourly air temperature, was then modified and applied to estimate hourly water temperature in rivers in Alabama. Estimated hourly water

temperatures in streams can be used to calculate saturated dissolved oxygen concentrations over diurnal cycles and determine temperature-dependent chemical and biological reaction rates (Chapra 1997) for water quality control and management study. Water quality models, e.g., one-dimensional dynamic hydraulic and water quality simulation model EPD-RIV1 (Martin and Wool 2002), two-dimensional longitudinal/vertical water quality and hydrodynamic model CE-QUAL-W2 (Cole and Wells 2010), and three-dimensional Water Quality Analysis Simulation Program WASP (Wool et al. 2001), need to set appropriate temperature boundary conditions of streams flowing into the simulation domain, which may not have observed temperature data and can be estimated using models developed in this study.

B.2 Materials and Methods

In this study, two regression models (linear and logistic function) and the MSSWF model were investigated to determine the model accuracy when they were used to calculate hourly water temperature in a river from air temperatures. The regression models use hourly air temperature as inputs, while the WSSWF model uses daily maximum and minimum air temperatures and the day of year (DOY) as input.

B.2.1 Regression Models

Linear regression model is the simplest regression model shown as Equation (B.1), which was used in many previous studies for daily or weekly temperature regressions (Stefan and Preud'homme 1993; Erickson and Stefan 2000):

$$T_w(t) = a \cdot T_a(t) + b \quad \text{(B.1)}$$

where $T_w(t)$ is hourly water temperature; $T_a(t)$ is hourly air temperature with or without lag; a and b are regression coefficients. Water temperatures calculated from the linear model follow diurnal variations of hourly air temperatures. The coefficients a and b in Equation (B.1) are scale and translation parameters.

Table B.1. Location, drainage area, distance to Birmingham International Airport (BHM), data period, mean, minimum and maximum hourly measured water temperatures of 8 river stations in Alabama, USA.

River Station	Lat., Long.	Drainage Area (km^2) & distance (km)	Starting Date [a]	Hourly Temperature (°C)		
				Mean	Min	Max
Kelly Creek near Vincent, AL	33°26'51", 86°23'13"	500 (30.8)	7/12/2008	17.01	0.30	30.60
Tallapoosa River near Mont. Water Works, AL	32°26'23", 86°11'44"	12,033 (132.9)	10/1/2007	18.38	5.30	31.70
Little Cahaba River below Leeds, AL	33°32'04", 86°33'45"	55 (12.2)	10/17/2008	17.20	4.50	27.30
Cahaba River near Hoover, AL	33°22'09", 86°47'03"	585 (23.0)	10/1/2007	17.85	1.20	32.80
Chattahoochee R.36 mi DS WFG Dam, AL/GA	31°37'17", 85°03'36"	19,321 (264.3)	5/28/2010	20.35	6.40	31.40
Cahaba River at Trussville, AL	33°37'20", 86°35'58"	50 (10.9)	10/23/2007	16.13	1.00	29.50
Fivemile Creek near Republic, AL	33°35'49", 86°52'05	133 (17.0)	10/4/2007	17.54	0.20	32.40
Village Creek at Avenue W at Ensley, AL	33°31'03", 86°52'45"	86 (18.2)	10/1/2007	18.26	2.00	33.80

Note: Lat.: latitude; Long.: longitude; Min.: minimum; Max.: maximum; AL/GA: at the Alabama (AL) and Georgia (GA) state line. The river stations are list according to the station ID numbers from the USGS. [a] The starting data for available hourly water temperature data, and the ending data is 1/23/2015 for all stations.

The logistic regression model has been used over the last few decades to develop air and water temperature relationships (Mohseni et al. 1998), and it is a four-parameter model defined using Equation (B.2):

$$T_w = \mu + \frac{\alpha - \mu}{1 + e^{\gamma(\beta - T_a)}} \tag{B.2}$$

where μ (°C) is a coefficient that estimates minimum water temperature, α (°C) is a coefficient that estimates maximum water temperature, γ (dimensionless) represents the

steepest slope (inflection point) of the logistic T_w function when plotted against T_a, and β (°C) is air temperature at the inflection point.

B.2.2 Modified Sine and Sinusoidal Wave Functions (MSSWF) Model

The sine function was used in the last few decades to develop daily air and water temperature relationships with respect to day of year (DOY) (Kothandaraman and Evans 1972; Caissie et al. 2001; Benyahya et al. 2007; Lambrechts et al. 2011), Considering consistent seasonal variations/patterns of water and air temperatures, the sine function given as Eq. (B.3) is used to calculate daily air and water temperatures *T(t)*:

$$T\,(t) = \overline{T} + T_{am}\sin(\omega t - \theta) \tag{B.3}$$

where $\overline{T}$ = annual mean temperature of air or water (°C), T_{am} = amplitude (°C) of the sine function, t = DOY (January 1 is t = 1 and December 31 is t = 365 for a non-leap year or 366 for a leap year), θ = phase shift (radians), ω = angular frequency of temperature variations (radians day^{-1}), which is fixed as $2\pi/365$ when it is assumed that temperature repeats its variation year by year. Sine functions are developed and used to estimate daily maximum and minimum water temperatures in a river for the MSSWF model that are then used to estimate hourly water temperatures using SWF (Equations B.4 and 5).

Reicosky et al. (1989) used SWF to predict hourly air temperatures from daily maximum and minimum air temperatures, and assumed that maximum air temperature is at 14:00 hr and minimum air temperature is at sunrise in each day. Considering the time lag of water temperatures from air temperatures (Stefan and Preud'homme 1993), times of maximum and minimum water temperatures should be set differently from times for maximum and minimum air temperatures. The average time of maximum water

temperatures for the 8 rivers in Alabama is 16:18, which is same as statistical results of the time of daily maximum water temperature being between 16:00 and 17:00 in 122 stream-temperature data logger sites in the Great Lake basin, Ontario, Canada (Chu et al. 2009). The average time of minimum water temperatures is 08:05. The sunrise and sunset at BHM from October 1, 2007 to January 23, 2015 were calculated day by day; it was found that the mean sunrise and sunset for the 8 rivers are 05:43 and 17:54, respectively. Therefore, the modified SWF assumes the maximum river temperature is at 16:00 and the minimum river temperature is at the sunrise plus 2 hr (Chen and Fang 2015b).

The modified SWF model for predicting hourly water temperatures are given in Equations (B.4) and (B.5) based on previous studies (De Wit 1978; Hoogenboom and Huck 1986). The intervening temperatures at time H hour (0:00 to 24:00 hr) are calculated from the following equations:

For $0 \leq H <$ ($RISE$ + 2) and 16:00 hr $< H \leq$ 24:00 hr

$$T_W(H) = T_{WAVE} + AMP\ (\cos\ (\pi\ H'/(10 + RISE))) \tag{B.4}$$

For ($RISE$ + 2) $\leq H \leq$ 16:00 hr

$$T_W(H) = T_{WAVE} - AMP\ (\cos\ (\pi\ ((H - RISE - 2)/(16 - RISE - 2))) \tag{B.5}$$

where $RISE$ is the time of sunrise in hours in each day and $T_W(H)$ is the water temperature at time H hour, $H' = H + 8$ if $H <$ ($RISE$ + 2), $H' = H - 16$ if $H >$ 16:00 hr, and T_{WAVE} and AMP are defined as $T_{WAVE} = (T_{WMIN} + T_{WMAX})/2$ as daily mean temperature and $AMP = (T_{WMAX} - T_{WMIN})/2$ as temperature amplitude, respectively. T_{WMAX} and T_{WMIN} are estimated

daily maximum and minimum water temperatures from sine functions using daily maximum and minimum air temperatures as input.

B.3 Model Error Parameters

To compare and determine model accuracy against observed hourly water temperatures, three model error parameters were used. The mean absolute error (*MAE*) and the root mean square error (*RMSE*) are defined as:

$$MAE = \frac{1}{n}\sum_{i=1}^{n} | T_{sim_i} - T_{obs_i} | \tag{B.6}$$

$$RMSE = \sqrt{\frac{\sum_{i=1}^{n}(T_{sim_i} - T_{obs_i})^2}{n}} \tag{B.7}$$

where T_{sim_i} is simulated or estimated hourly water temperature at *i* hour, T_{obs_i} is observed hourly water temperature at the same time, and *n* is the number of pairs of hourly estimated and observed water temperatures at a stream monitoring station.

To find the goodness of fit of the different model, the Nash-Sutcliffe efficiency (*NSE*) (Nash and Sutcliffe 1970) was also used and defined in Eq. (B.8).

$$NSE = 1 - \frac{\sum_{i=1}^{n}\left(T_{sim_i} - T_{obs_i}\right)^2}{\sum_{i=1}^{n}\left(\bar{T}_{obs} - T_{obs_i}\right)^2} \tag{B.8}$$

where $\bar{T}_{obs}$ is mean value of the observed water temperatures. *NSE* has a maximum value of unity and no minimum. An *NSE* equal to 1 represents a perfect model efficiency. *NSE* = 0 indicates that the model predictions are only as accurate as $\bar{T}_{obs}$, whereas *NSE* < 0 indicates that $\bar{T}_{obs}$ is a better predictor than the model.

B.3 Calculated Hourly Water Temperature from Hourly Water-Air Regression

Fig. B.1 shows a time-series plot of hourly water temperature of the Little Cahaba River below Leeds, Alabama; and hourly air temperature at Birmingham International Airport (BHM, airport code) from August 24 to 31, 2013. The distance between two monitoring stations are 12.2 km. Fig. B.1 shows typical water temperature response to air temperature during the day and night. Water temperature variations have a lagged response behind air temperature fluctuations. For the Little Cahaba River below Leeds, the lag was about 4 hr. Therefore, lag time was used in the regression models (linear and logistic) to investigate the model accuracy.

Figs. B.2a and 2b show graphic examples of linear and logistic regression models between hourly water temperatures in Kelly Creek near Vincent from July 28, 2008 to January 23, 2015 and Little Cahaba River below Leeds from October 17, 2008 to January 23, 2015 (abbreviated as Little Cahaba in Tables and Figures hereafter) and hourly air temperatures at BHM. For these two rivers, a 4 hr lag was incorporated for these regressions. For eight streams, the linear regression models with time lags (4–5 h) are consistently but only slightly better than the regression model without time lag. The *NSE* improves by 0.04 at Kelly Creek and 0.05 at Little Cahaba. The average improvement of *RMSE* for linear regression with time lag is about 0.3 °C. Stefan and Preud'homme (1993) had similar results of using lag times for regression models between daily water and air temperatures. They used a time lag, ranging from four hours to seven days depending on the depth of the stream and determined that introducing a lag time had an effect only for major rivers and improved the predictions by 0.5 °C or less.

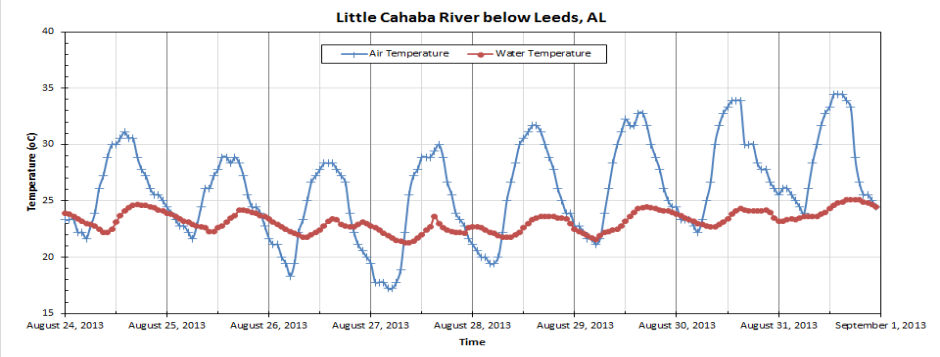

Fig. B.1. Time-series of observed hourly water temperature of Little Cahaba River below Leeds, AL and hourly air temperature at Birmingham International Airport from August 24 to 31, 2013.

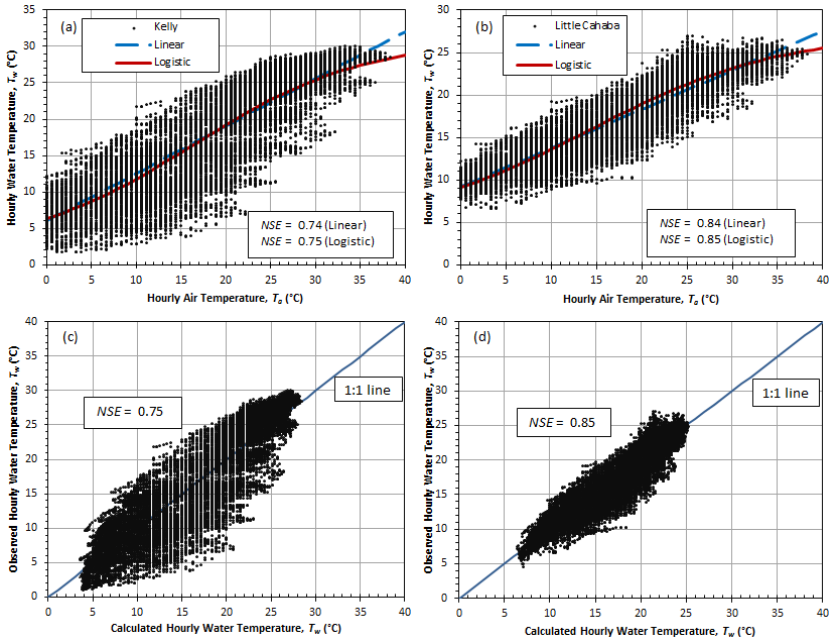

Fig. B.2. Hourly water−air temperature regressions of linear and logistic models for (**a**) Kelly Creek near Vincent from July 28, 2008 to January 23, 2015 and (**b**) Little Cahaba River below Leeds from October 17, 2008 to January 23, 2015. Scatterplot for estimated hourly water temperatures from hourly logistic regression *versus* observed hourly water temperatures at (**c**) Kelly Creek near Vincent and (**d**) Little Cahaba River below Leeds.

The physical interpretation of the water-air temperature relationship (Mohseni and Stefan 1999) shows that linear extrapolations to high and low air temperatures are not justified. Fig. B.2 shows that logistic regression lines are closer to the data but depart from linear regression as air temperature exceeds 30 °C and falls below 5 °C in Kelly Creek near Vincent and Little Cahaba River below Leeds. The logistic regression models fitted better to hourly data than the linear model did for high and low temperatures (Fig. B.2).

Table B.2. Statistical error parameters for linear and logistic regression models between hourly water temperatures and hourly air temperatures in eight rivers.

Rivers	***MAE* (°C)**	***RMSE* (°C)**	***NSE***
Kelly	2.90 (2.84)	3.57 (3.51)	0.74 (0.75)
Tallapoosa	2.82 (2.77)	3.42 (3.38)	0.69 (0.70)
Little Cahaba	1.55 (1.51)	1.92 (1.88)	0.84 (0.85)
Cahaba_Hoover	2.96 (2.92)	3.63 (3.58)	0.76 (0.76)
Chattahoochee	2.13 (2.08)	2.82 (2.77)	0.78 (0.79)
Cahaba_Trussville	2.67 (2.66)	3.01 (2.96)	0.76 (0.77)
Fivemile	2.80 (2.74)	3.37 (3.31)	0.80 (0.80)
Village	1.38 (1.36)	1.74 (1.70)	0.84 (0.85)
Average	**2.40 (2.36)**	**2.94 (2.89)**	**0.78 (0.78)**
Standard Deviation	**0.63 (0.63)**	**0.74 (0.73)**	**0.05 (0.05)**

Note: the numbers inside the brackets are corresponding error parameters for using logistic regression model.

Figs. B.2c and 2d show scatterplot for estimated hourly water temperatures from logistic regression models *versus* observed hourly water temperature in Kelly Creek near Vincent and Little Cahaba River below Leeds. *NSE* values are 0.75 and 0.85, respectively. Using time lag, the logistic models for hourly water−air temperature

regressions have slightly smaller *MAE* and *RMSE* and slightly larger *NSE*, compared with linear regression models (Table B.2). The *NSE* for individual rivers improved only 0.01 from the linear model with time lag. Average *MAE* and *RMSE* decreased up to 0.04 and 0.05 °C, respectively. Therefore, the logistic models for eight rivers are only slightly better than the linear model, but regression parameters for logistic regression models have more meaningful interpretations. For eight rivers in Alabama, *NSE* values for logistic model range from 0.70 to 0.85 with an average *NSE* of 0.78 (Table B.1). Further improvement of estimation from hourly air temperature to hourly water temperature is necessary.

B.4 Calculated Hourly Water Temperature from MSSWF Model

The second method using MSSWF was also implemented for estimating hourly water temperatures in rivers. For the MSSWF method, sine functions [Eq. (B.3)] were developed by minimizing errors between modeled and observed daily maximum and minimum air temperatures (T_{Amax} and T_{Amin}) at the weather stations and daily maximum and minimum water temperatures (T_{Wmax} and T_{Wmin}) in rivers. These sine functions give the same estimates of daily maximum or minimum temperatures on the same day in different years because the same DOY is used as input parameter.

In order to reflect climate variations in different years and to improve the model accuracy of the sine function models, the differences between observed temperature and estimated temperature from the fitted sine function were calculated (e.g., *observed_*T_{Amax} – *estimated_*T_{Amax}), and the deviation for daily maximum or minimum water temperature is correlated with the deviation for corresponding air temperature. Therefore, water

temperature variations are connected to climate variations that reflected through air temperature deviations from fitted sine functions. Abbreviated symbols $Diff\_T_{Wmax}$, $Diff\_T_{Wmin}$, $Diff\_T_{Amax}$, and $Diff\_T_{Amin}$ are above defined deviations for daily maximum water temperature, daily minimum water temperature, daily maximum air temperature, and daily minimum air temperature, respectively. In this study, these water temperature deviations from the sine functions ($Diff\_T_{Wmax}$ and $Diff\_T_{Wmin}$) were linearly correlated with air temperature deviations from the sine functions ($Diff\_T_{Amax}$ and $Diff\_T_{Amin}$) at the weather station. Therefore, modified or corrected sine functions were actually used to estimate daily maximum and minimum water temperature in rivers, and then modified SWF was used to estimate hourly water temperatures.

In summary, the MSSWF method uses the following five steps to estimate hourly water temperatures in a river when observed daily maximum and minimum air temperatures in a nearby weather station are available as input:

1. Estimate daily maximum and minimum water temperatures and air temperatures from fitted sine functions using DOY as input;
2. Calculate $Diff\_T_{Amax}$ and $Diff\_T_{Amin}$ from observed and estimated daily maximum and minimum air temperatures;
3. Calculate differences of daily maximum and minimum water temperatures ($Diff\_T_{Wmax}$ and $Diff\_T_{Wmin}$) from $Diff\_T_{Amax}$ and $Diff\_T_{Amin}$ using fitted linear regression equations;
4. Correct estimated daily maximum and minimum water temperatures from fitted sine functions by adding $Diff\_T_{Wmax}$ and $Diff\_T_{Wmin}$, respectively;

5. Calculate hourly water temperatures in each day using modified SWF presented by Equations (B.4) and (B.5).

The first four steps are used to produce more accurate estimates of daily maximum and minimum water temperatures in a river. In order to apply the MSSWF model, one has to develop six equations in addition to applying Equations (B.4) and (B.5). First, observed data are used to develop sine functions for daily maximum and minimum water and air temperatures versus DOY, which are four equations in the form of Equation (B.3). Two linear regression equations between $Diff\_T_{Wmax}$ and $Diff\_T_{Amax}$ and between $Diff\_T_{Wmin}$ and $Diff\_T_{Amin}$ are then developed.

Excellent agreement was found between observed and estimated hourly water temperatures using the MSSWF model developed for all eight rivers (Table B.3). The average *NSE* value for MSSWF models developed for individual rivers is 0.94 and all the *NSE* exceeds 0.91. Tallapoosa and Chattahoochee rivers are relatively far away from BHM; their distances from BHM are 132.9 and 264.3 km, respectively. The *NSE* values of individual MSSWF models for these two rivers are 0.91 and 0.95, respectively. The performance of the MSSWF models developed for individual rivers is not sensitive to the distance from the weather station when the distance is less than ~ 300 km (Table B.3). The MSSWF model includes not only season or annual trend (using sine function) and hourly variations (using SWF) of water temperatures but also reflects daily fluctuations of T_{Wmax} and T_{Wmin} by using the linear regressions with deviations of daily T_{Amax} and T_{Amin} fluctuations (from fitted sine functions) due to climate variations.

Table B.3. Statistical error parameters for individual MSSWF models in 8 rivers.

Rivers	Individual MSSWF Model		
	***MAE* (°C)**	***RMSE* (°C)**	***NSE***
Kelly	1.55	1.92	0.92
Tallapoosa	1.44	1.84	0.91
Little Cahaba	0.88	1.13	0.95
Cahaba_Hoover	1.34	1.69	0.95
Chattahoochee	1.18	1.48	0.95
Cahaba_Trussville	1.06	1.37	0.95
Fivemile	1.23	1.57	0.95
Village	1.00	1.27	0.96
Average	**1.21**	**1.53**	**0.94**
Standard Deviation	**0.23**	**0.28**	**0.02**

B.5 Conclusion

In this study, direct linear and non-linear (logistic) regression models with time lags (4–5 hr) were firstly developed and evaluated to calculate hourly water temperature. Overall model accuracy of direct regression models is not very high even though it is acceptable (average *NSE* 0.78). The second method using modified sine and sinusoidal wave functions (MSSWF) was then proposed and evaluated for estimating hourly water temperatures in rivers. The sinusoidal wave function (SWF), originally used to calculate hourly air temperature, was modified and applied to 8 rivers in Alabama when daily maximum and minimum water temperatures were estimated using fitted sine functions.

The MSSWF model includes not only season or annual trend and hourly variations of water temperatures but also reflects daily fluctuations of T_{Wmax} and T_{Wmin} by using the linear regressions with deviations of daily T_{Amax} and T_{Amin} fluctuations due to climate variations. The MSSWF model involves the five steps and develops six related equations.

The results show significant improvement by using the MSSWF model instead of direct regression methods. Excellent agreement was found between observed and estimated hourly water temperatures using MSSWF models developed for each of the 8 rivers in Alabama. The average *NSE* value for MSSWF models developed for individual rivers is 0.94 and all the *NSE* exceeds 0.91. The average *RMSE* is 1.53 °C with standard deviation 0.28 °C. The performance of the MSSWF models developed for individual rivers is not sensitive to the distance from the weather station when the distance is less than ~ 300 km (Tables B.3).

References

Abrahams, A. D., Parsons, A. J., and Luk, S. H. (1986). "Field measurement of the velocity of overland flow using dye tracing." *Earth surface processes and landforms*, 11(6), 653-657.

Ahlstrom, S., Foote, H., Arnett, R., Cole, C., and Serne, R. (1977). "Multicomponent mass transport model: theory and numerical implementation (discrete-parcel-random-walk version)." Battelle Pacific Northwest Labs., Richland, Wash.(USA).

Akiyama, J., and Stefan, H. G. (1984). "Plunging flow into a reservoir - Theory." *Journal of Hydraulic Engineering ASCE*, 110(4), 484-499.

Alavian, V. (1986). "Behavior of density currents on an incline." *Journal of hydraulic engineering*, 112(1), 27-42.

Alavian, V., and Ostrowski Jr, P. (1992). "Use of density current to modify thermal structure of TVA reservoirs." *Journal of Hydraulic Engineering*, 118(5), 688-706.

An, S., and Julien, P. Y. (2014). "Three-dimensional modeling of turbid density currents in Imha reservoir, South Korea." *Journal of Hydraulic Engineering*, 140(5).

Benyahya, L., St-Hilaire, A., Quarda, T. B., Bobée, B., and Ahmadi-Nedushan, B. (2007). "Modeling of water temperatures based on stochastic approaches: case study of the Deschutes River." *Journal of Environmental Engineering and Science*, 6(4), 437-448.

Biton, E., Silverman, J., and Gildor, H. (2008). "Observations and modeling of a pulsating density current." *Geophysical Research Letters*, 35(14).

Blumberg, A., Galperin, B., and O'Connor, D. (1992). "Modeling vertical structure of open-channel flows." *Journal of Hydraulic Engineering*, 118(8), 1119-1134, doi:doi:10.1061/(ASCE)0733-9429(1992)118:8(1119).

Bournet, P., Dartus, D., Tassin, B., and Vincon-Leite, B. (1999). "Numerical investigation of plunging density current." *Journal of Hydraulic Engineering*, 125(6), 584-594.

Brown, G. W. (1969). "Predicting temperatures of small streams." *Water resources research*, 5(1), 68-75.

Buchak, E., and Edinger, J. (1984). "Simulation of a density underflow into Wellington Reservoir using longitudinal-vertical numerical hydrodynamics." Document.

Caissie, D., El-Jabi, N., and St-Hilaire, A. (1998). "Stochastic modelling of water temperatures in a small stream using air to water relations." *Canadian Journal of Civil Engineering*, 25(2), 250-260.

Caissie, D., El-Jabi, N., and Satish, M. G. (2001). "Modelling of maximum daily water temperatures in a small stream using air temperatures." *Journal of Hydrology*, 251(1), 14-28.

Caissie, D., St-Hilaire, A., and El-Jabi, N. (2004). "Prediction of water temperatures using regression and stochastic models." *57th Canadian Water Resources Association Annual Congress., Montreal*, v.6.

Caissie, D. (2006). "The thermal regime of rivers: a review." *Freshwater Biology*, 51(8), 1389-1406.

Caliskan, A., and Elci, S. (2009). "Effects of selective withdrawal on hydrodynamics of a stratified reservoir." *Water resources management*, 23(7), 1257-1273.

Carmack, E. C., Gray, C. B., Pharo, C. H., and Daley, R. J. (1979). "Importance of lake-river interaction on seasonal patterns in the general circulation of Kamloops Lake, British Columbia." *Limnology and Oceanography*, 24(4), 634-44.

Carron, J. C., and Rajaram, H. (2001). "Impact of variable reservoir releases on management of downstream water temperatures." *Water Resources Research*, 37(6), 1733-1743.

Chapra, S. C. (1997). *Surface water-quality modeling*, McGraw-Hill series in water resources and environmental engineering, McGraw-Hill, New York, 844 p.

Chen, G., Fang, X., and Devkota, J. (2015). "Understanding flow dynamics and density currents in a river-reservoir system under upstream reservoir releases." *Hydrological Sciences Journal*.

Chen, G., and Fang, X. (2015a). "Sensitivity analysis of flow and temperature distributions of density currents in a river-reservoir system under upstream releases with different durations." *Water*, 7(11), 6244-6268.

Chen, G., and Fang, X. (2015b). "Accuracy of hourly water temperatures in rivers calculated from air temperatures." *Water*, 7(3), 1068-1087.

Chen, G., Fang, X., and Fan, H. (2016). "Estimating Hourly Water Temperatures in Rivers using Modified Sine and Sinusoidal Wave Functions." *ASCE Journal of Hydrologic Engineering*.

Chikita, K. (1992). "The role of sediment-laden underflows in lake sedimentation: glacier-fed Peyto Lake, Canada." *Journal of the Faculty of Science, Hokkaido University. Series 7, Geophysics*, 9(2), 211-224.

Cho, H.-Y., and Lee, K.-H. (2011). "Development of an air–water temperature relationship model to predict climate-induced future water temperature in estuaries." *Journal of Environmental Engineering*, 138(5), 570-577.

Chu, C., Jones, N. E., Piggott, A. R., and Buttle, J. M. (2009). "Evaluation of a simple method to classify the thermal characteristics of streams using a nomogram of daily maximum air and water temperatures." *North American Journal of Fisheries Management*, 29(6), 1605-1619.

Cluis, D. A. (1972). "Relationship between stream water temperature and ambient air temperature." *Nordic Hydrology*, 3(2), 65-71.

Cole, T. M., and Buchak, E. M. (1995). "CE-QUAL-W2: A two-dimensional, laterally averaged, hydrodynamic and water quality model, version 2.0. user manual." DTIC Document.

Cole, T. M., and Wells, S. A. (2010). "CE-QUAL-W2: A Two-Dimensional, Laerally Averaged, Hydrodynamic and Water Quality Model, Version 3.6 User Manual."

Consultants, W.-C. (1986). "Stanislaus project instream temperature study." *Pacific Gas and Electric Company, San Ramon, California*.

Cook, C. B., and Richmond, M. C. (2004). "Monitoring and simulating 3-D density currents at the confluence of the Snake and Clearwater rivers." *Critical Transitions In Water And Environmental Resources Management*, June 27-July 1, 2004, Salt Lake City, UT, G. Sehlke, D. F. Hayes, and D. K. Stevens, eds., ASCE, 1-9.

Cortés, A., Rueda, F., and Wells, M. (2014). "Experimental observations of the splitting of a gravity current at a density step in a stratified water body." *Journal of Geophysical Research: Oceans*, 119(2), 1038-1053.

Craig, P. M. (2010). "User's Manual for EFDC_Explorer: A Pre/Post Processor for the Environmental Fluid Dynamics Code." Dynamic Solutions, LLC, Knoxville, TN.

Craig, P. M. (2011). "User's Manual for EFDC_Explorer 6: A Pre/Post processor for the Environmental Fluid Dynamics Code." Dynamic Solutions, LLC, Knoxville, TN.

Craig, P. M. (2012). "User's Manual for EFDC_Explorer 7: A Pre/Post Processor for the Environmental Fluid Dynamics Code." Dynamic Solutions-International, LLC, Edmonds, Washington, USA.

Dallimore, C. J., Imberger, J., and Ishikawa, T. (2001). "Entrainment and turbulence in saline underflow in Lake Ogawara." *Journal of Hydraulic Engineering*, 127(11), 937-948.

De Wit, C. T. (1978). "Simulation of assimilation, respiration and transpiration of crops."

Denton, R. (1985). "Density current inflows to run of the river reservoirs." *21st IAHR World Congress, 13-18 August 1985, Melbourne, Australia*.

Devkota, J., and Fang, X. (2014). "Numerical simulation of flow dynamics in a tidal river under various upstream hydrologic conditions." *Hydrological Sciences Journal*, doi:DOI: 10.1080/02626667.2014.947989.

Do An, S. (2014). "Three-Dimensional Numerical Simulation of Intrusive Density Currents." *Journal of Environmental Science International*, 23(7), 1223-1232.

Erickson, T. R., and Stefan, H. G. (2000). "Linear air/water temperature correlations for streams during open water periods." *Journal of Hydrologic Engineering*, 5(3), 317-321.

Fang, X., and Stefan, H. G. (2000). "Dependence of dilution of a plunging discharge over a sloping bottom on inflow conditions and bottom friction." *Journal of Hydraulic Research*, 38(1), 15-25.

Fang, X., Weems, T. B., Devkota, J., and Chen, G. (2013). "Watershed modeling, water balance analysis, three-dimensional flow and thermal discharge modeling for the William C. Gorgas Plant." Department of Civil Engineering, Auburn AL 36849.

Farrell, G. J., and Stefan, H. G. (1986). "Buoyancy Induced Plunging Flow Into Reservoirs and Costal Regions."

Farrell, G. J., and Stefan, H. G. (1989). "Two-layer analysis of a plunging density-current in a diverging horizontal channel." *Journal of Hydraulic Research*, 27(1), 35-47.

Fatih, Ü., and Varcin, H. (2012). "Investigation of plunging depth and density currents in Eğrekkaya dam reservoir." *Teknik Dergi*, 23(1), 5725-5750.

Fernandez, R. L., and Imberger, J. (2008a). "Time-varying underflow into a continuous stratification with bottom slope." *Journal of Hydraulic Engineering*, 134(9), 1191-1198.

Fernandez, R. L., and Imberger, J. (2008b). "Relative buoyancy dominates thermal-like flow interaction along an incline." *Journal of Hydraulic Engineering*, 134(5), 636-643.

Firoozabadi, B., Afshin, H., and Aram, E. (2009). "Three-dimensional modeling of density current in a straight channel." *Journal of Hydraulic Engineering*, 135(5), 393-402.

Fischer, H. B., and Smith, R. D. (1983). "Observations of transport to surface waters from a plunging inflow to Lake Mead [Nevada]." *Limnology and Oceanography*.

Fukushima, Y., and Watanabe, M. (1990). "Numerical simulation of density underflow by the k− ε turbulence model." *J. Hydrosci. Hydr. Eng*, 8, 31-40.

Galperin, J., Kantha, L. H., Hassid, S., and Rosati, A. (1988). "A quasi-equilibrium turbulent energy model for geophysical flows." *Journal of the Atmospheric Sciences*, 45(1), 55-62.

Gu, R. R. (2009). "Impact of Inflow and Ambient Conditions on Density-Induced Current in a Stratified Reservoir." *Modern Physics Letters B*, 23(03), 429-432.

Guo-Qing, H., Yuan-Jie, D., Hui, W., Xian-Kui, Q., and Yan-Hua, W. (2011). "Laboratory testing of magnetic tracers for soil erosion measurement." *Pedosphere*, 21(3), 328-338.

Hallworth, M. A., Huppert, H. E., Phillips, J. C., and Sparks, R. S. J. (1996). "Entrainment into two-dimensional and axisymmetric turbulent gravity currents." *Journal of Fluid Mechanics*, 308(1), 289-311.

Hamrick, J. M. (1992a). "A three-dimensional environmental fluid dynamics computer code: Theoretical and computational aspects." Special Report 317, Virginia Institute of Marine Science, College of William and Mary, Gloucester Point, VA.

Hamrick, J. M. (1992b). "A three-dimensional environmental fluid dynamics computer code: Theoretical and computational aspects." Speical Report 317, The College of William and Mary, Virginia Institute of Marine Science, Gloucester Point, VA, 63.

Hamrick, J. M. (1992c). "A three-dimensional Environmental fluid dynamics code: Theoritical and computational aspects." Special Report No. 317 in Applied Marine Science and Ocean Engineering, Virginia Institute of Marine Science, Gloucester Point.

Hamrick, J. M., and Mills, W. B. (2000). "Analysis of water temperatures in Conowingo Pond as influenced by the Peach Bottom atomic power plant thermal discharge." *Environmental Science & Policy*, 3(Supplement 1), 197-209.

Harlow, F. H. (1962). "The particle-in-cell method for numerical solution of problems in fluid dynamics." Los Alamos Scientific Lab., N. Mex.

Harmeson, R. H., and Schnepper, V. M. (1965). "Temperatures of surface waters in Illinois." Illinois State Water Survey Report of Investigation 49, Champaign, IL, 45.

Harvey, R., Lye, L., Khan, A., and Paterson, R. (2011). "The Influence of air temperature on water temperature and the concentration of dissolved oxygen in Newfoundland Rivers." *Canadian Water Resources Journal*, 36(2), 171-192.

Hauenstein, W., and Dracos, T. (1984). "Investigation of plunging density currents generated by inflows in lakes." *Journal of Hydraulic Research*, 22(3), 157-179.

Hirt, C., and Nichols, B. (1988). "Flow-3D User's Manual." *Flow Science Inc*.

Hodges, B., and Dallimore, C. (2006). "Estuary, lake and coastal ocean model: ELCOM." *Science Manual. Centre of Water Research. University of Western Australia*.

Hondzo, M., and Stefan, H. G. (1993). "Lake water temperature simulation-model." *Journal of Hydraulic Engineering ASCE*, 119(11), 1251-1273.

Hoogenboom, G., and Huck, M. G. (1986). "Rootsimu v4. 0: a dynamic simulation of root growth, water uptake, and biomass partitioning in a soil-plant-atmosphere continuum: update and documentation." *Agronomy and soils departmental series-Auburn University, Alabama Agricultural Experiment Station (USA)*.

Imberger, J., and Patterson, J. (1980). "Dynamic Reservoir Simulation Model-DYRESM: 5." *Transport Models for Inland and Coastal Waters, Academic Press New York. 1981. Proceedings of a Symposium on Predictive Ability, Berkeley, California, August 18-20, 1980. p 310-361, 12 fig, 36 ref.*

Imran, J., Islam, M. A., Huang, H., Kassem, A., Dickerson, J., Pirmez, C., and Parker, G. (2007). "Helical flow couplets in submarine gravity underflows." *Geology*, 35(7), 659-662.

Jackson, P. R., García, C. M., Oberg, K. A., Johnson, K. K., and García, M. H. (2008). "Density currents in the Chicago River: Characterization, effects on water quality, and potential sources." *Science of the Total Environment*, 401(1), 130-143.

Jeong, S., Yeon, K., Hur, Y., and Oh, K. (2010). "Salinity intrusion characteristics analysis using EFDC model in the downstream of Geum River." *Journal of Environmental Sciences*, 22(6), 934-939.

Ji, Z.-G. (2008). *Hydrodynamics and water quality: modeling rivers, lakes, and estuaries*, John Wiley and Sons, Inc., New Jersey, 676.

Johnson, A. C., Acreman, M. C., Dunbar, M. J., Feist, S. W., Giacomello, A. M., Gozlan, R. E., Hinsley, S. A., Ibbotson, A. T., Jarvie, H. P., and Jones, J. I. (2009). "The British river of the future: how climate change and human activity might affect two contrasting river ecosystems in England." *Science of the Total Environment*, 407(17), 4787-4798.

Johnson, F. (1971). "Stream temperatures in an alpine area." *Journal of Hydrology*, 14(3), 322-336.

Jokela, J., and Patterson, J. (1985). "Quasi-two-dimensional modelling of reservoir inflow." *Preprinted proceedings: 21st Congress, International Association for Hydraulic Research, Melbourne, 19-23 August 1985. Volume 2. Theme B(Part 1): Fundamentals and computation of 2-D and 3-D flows.*, 317-322.

Kim, C.-K., and Park, K. (2012). "A modeling study of water and salt exchange for a micro-tidal, stratified northern Gulf of Mexico estuary." *Journal of Marine Systems*, 96–97(0), 103-115, doi:10.1016/j.jmarsys.2012.02.008.

Kim, D., Muste, M., Mueller, D., and Winkler, M. (2009). "VMS ADCP velocity mapping software." Coastal & Hydraulics Laboratory, Engineer Research and Development Center, US Army Corps of Engineers, Vicksburg, MS 39180.

Kothandaraman, V., and Evans, R. L. (1972). *Use of air-water relationships for predicting water temperature*, Illinois State Water Survey.

Kranenburg, C. (1993). "Gravity current fronts advancing into horizontal ambient flow." *Journal of Hydraulic Engineering*, 119(3), 369-379.

Kulis, P., and Hodges, B. R. (2006). "Modeling gravity currents in shallow bays using a sigma coordinate model."

Lambrechts, L., Paaijmans, K. P., Fansiri, T., Carrington, L. B., Kramer, L. D., Thomas, M. B., and Scott, T. W. (2011). "Impact of daily temperature fluctuations on dengue virus transmission by Aedes aegypti." *Proceedings of the National Academy of Sciences*, 108(18), 7460-7465.

Liu, X., and Garcia, M. H. (2008). "Numerical simulation of density current in Chicago river using Environmental Fluid Dynamics Code (EFDC)." *Ahupua'a Proceedings of the World Environmental and Water Resources Congress*, W. B. Roger and W. Raymond, eds., ASCE, v.316, 229.

Liu, X., and Huang, W. (2008). "An Effective Algorithm to Reduce Horizontal Pressure Gradient Errors in σ-Coordinate in EFDC Hydrodynamic Model." *Journal of Coastal Research*, 193-204, doi:10.2112/1551-5036-52.sp1.193.

Lyubimova, T., Lepikhin, A., Konovalov, V., Parshakova, Y., and Tiunov, A. (2014). "Formation of the density currents in the zone of confluence of two rivers." *Journal of Hydrology*, 508, 328-342.

Martin, J. L., and Wool, T. (2002). "A Dynamic One-Dimensional Model of Hydrodynamics and Water Quality-EPD-RIV1 User's Manual." *Georgia Environmental Protection Division*.

Mellor, G. L., and Yamada, T. (1982). "Development of a turbulence closure model for geophysical fluid problems." *Reviews of geophysics and space physics*, 20(4), 851-875.

Mohseni, O., Stefan, H. G., and Erickson, T. R. (1998). "A nonlinear regression model for weekly stream temperatures." *Water Resources Research*, 34(10), 2685-2692.

Mohseni, O., and Stefan, H. (1999). "Stream temperature/air temperature relationship: a physical interpretation." *Journal of Hydrology*, 218(3), 128-141.

Morin, G., and Couillard, D. (1990). "Predicting river temperatures with a hydrological model." *Encyclopedia of Fluid Mechanics: Surface and groundwater flow phenomena*, 10, 171-209.

Morrill, J. C., Bales, R. C., and Conklin, M. H. (2005). "Estimating stream temperature from air temperature: implications for future water quality." *Journal of Environmental Engineering*, 131(1), 139-146.

Morse, W. L. (1972). "Steam Temperature Prediction under Reduced Flow." *Journal of the Hydraulics Division*, 98(6), 1031-1047.

Nash, J. E., and Sutcliffe, J. V. (1970). "River flow forecasting through conceptual models part I - a discussion of principles." *Journal of Hydrology*, 10(3), 282-290.

Owens, E. M., Effler, S. W., Prestigiacomo, A. R., Matthews, D. A., and O'Donnell, S. M. (2012). "Observations and modeling of stream plunging in an urban lake." *Journal of the American Water Resources Association*, 48(4), 707-721.

Petts, G. E. (1984). "Impounded rivers: perspectives for ecological management." 329pp.

Petts, G. E., Foulger, T. R., Gilvear, D. J., Pratts, J. D., and Thoms, M. C. (1985). "Wave-movement and water-quality variations during a controlled release from Kielder Reservoir, North Tyne River, UK." *Journal of Hydrology*, 80(3-4), 371-389, doi:10.1016/0022-1694(85)90129-5.

Pilgrim, J. M., Fang, X., and Stefan, H. G. (1998). "Stream temperature correlations with air temperatures in Minnesota: Implications for climate warming." *Journal of the American Water Resources Association*, 34(5), 1109-1121.

Railsback, S. (1997). "Design guidance for short-term control of flow releases for temperature management." Rep. 009-97.10, Pac. Gas and Electr. Res. and Dev., San Ramon, CA.

Raphael, J. M. (1962). "Prediction of temperature in rivers and reservoirs." *JOURNAL OF THE POWER DIVISION, VOL 88, NO P 02, JULY, 1962, P 157.*

Reicosky, D., Winkelman, L., Baker, J., and Baker, D. (1989). "Accuracy of hourly air temperatures calculated from daily minima and maxima." *Agricultural and Forest Meteorology*, 46(3), 193-209.

Rueda, F. J., and MacIntyre, S. (2010). "Modelling the fate and transport of negatively buoyant storm–river water in small multi-basin lakes." *Environmental Modelling & Software*, 25(1), 146-157.

Savage, S., and Brimberg, J. (1975). "Analysis of plunging phenomena in water reservoirs." *Journal of Hydraulic Research*, 13(2), 187-205.

Serruya, S. (1974). "The mixing patterns of the Jordan River in Lake Kinneret." *Limnol. Oceanogr*, 19(2), 175-181.

Shen, J., and Lin, J. (2006). "Modeling study of the influences of tide and stratification on age of water in the tidal James River." *Estuarine, Coastal and Shelf Science*, 68(1-2), 101-112.

Shlychkov, V. A., and Krylova, A. I. (2014). "A numerical model of density currents in estuaries of Siberian rivers." *Numerical Analysis and Applications*, 7(3), 255-261.

Singh, B., and Shah, C. (1971). "Plunging phenomenon of density currents in reservoirs." *La Houille Blanche*(1), 59-64.

Sinokrot, B., and Stefan, H. (1993). "Stream Temperature Dynamics: Measurements and Modeling " *Water Resources Research*, 29(7), 2299-2312, doi:10.1029/93WR00540.

Sinokrot, B., Stefan, H. G., and McCormick, M. J. (1995). "Modeling of climate change effects on stream temperatures and fish habitats below dams and near groundwater inputs." *Climatic Change*, 30, 181-200.

Sinokrot, B. A., and Gulliver, J. S. (2000). "In-stream flow impact on river water temperatures." *Journal of Hydraulic Research*, 38(5), 339-349.

Smagorinsky, J. (1963). "General circulation experiments with the primitive equations." *Monthly weather review*, 91(3), 99-164.

Smith, P. C. (1975). "A streamtube model for bottom boundary currents in the ocean." *Deep Sea Research and Oceanographic Abstracts*, Elsevier, v.22, 853-873.

Soliman, M., Ushijima, S., and Kantouch, S. (2014). "Density current propagation in a tidal river." *River Flow 2014*, 197.

Stefan, H. G., and Preud'homme, E. B. (1993). "Stream temperature estimation from air temperature." *Journal of the American Water Resources Association*, 29(1), 27-45.

Texas Water Development Board. (1970). "Reconnaissance of water temperature of selected streams in southern Texas." Report 105, Austin, TX, 12.

Thomann, R. V., and Mueller, J. A. (1987). *Principles of surface water quality modeling and control*, Harper & Row, New York, xii, 644 p.

Toffolon, M., Siviglia, A., and Zolezzi, G. (2010a). "Thermal wave dynamics in rivers affected by hydropeaking." *Water Resources Research*, 46, doi:10.1029/2009wr008234.

Toffolon, M., Siviglia, A., and Zolezzi, G. (2010b). "Thermal wave dynamics in rivers affected by hydropeaking." *Water Resources Research*, 46(W008536), doi:10.1029/2009wr008234.

Wang, Y., Shen, J., and He, Q. (2010). "A numerical model study of the transport timescale and change of estuarine circulation due to waterway constructions in the Changjiang estuary, China." *Journal of Marine Systems*, 82(3), 154-170.

Weems, T. B. (2013). "Water balance analysis using WARMF in support of an EFDC hydrodynamic Model," Department of Civil Engineering, Auburn University, Auburn, AL.

Wells, M., and Nadarajah, P. (2009). "The intrusion depth of density currents flowing into stratified water bodies." *Journal of Physical Oceanography*, 39(8), 1935-1947.

Wool, T. A., Ambrose, R. B., Martin, J. L., Comer, E. A., and Tech, T. (2001). "Water Quality Analysis Simulation Program (WASP)." *User's Manual, Version*, 6.

Wunderlich, W. O., and Shiao, M. C. (1984). "Long-range reservoir outflow temperature planning." *Journal of Water Resources Planning and Management*, 110(3), 285-295.

Xie, R., Wu, D.-A., Yan, Y.-X., and Zhou, H. (2010). "Fine silt particle pathline of dredging sediment in the Yangtze River deepwater navigation channel based on EFDC model." *Journal of Hydrodynamics, Ser. B*, 22(6), 760-772.